

University of Ljubljana
Faculty of Mathematics and Physics
Physics Department

Marko Žnidarič

STABILITY OF QUANTUM DYNAMICS

Dissertation

advisor: Prof. Tomaž Prosen

external advisor: Prof. Thomas H. Seligman

Ljubljana, 2004

Abstract

The stability of quantum systems to perturbations of the Hamiltonian is studied. This stability is quantified by the fidelity, an overlap of an ideal state obtained by the unperturbed evolution, and a perturbed state obtained by the perturbed evolution, both starting from the same initial state. Dependence of fidelity on the initial state as well as on the dynamical properties of the system is considered. In particular, systems having a chaotic or regular classical limit are analysed. The fidelity decay rate is given by an integral of the correlation function of the perturbation and is thus smaller the faster correlation function decays. Quantum systems with a chaotic classical limit can therefore be more stable than regular ones. If the perturbation can be written as a time derivative of another operator, meaning that the time averaged perturbation vanishes, fidelity freezes at a constant value and starts to decay only after a long time inversely proportional to the perturbation strength. In composite systems stability of entanglement to perturbations of the Hamiltonian is analysed in terms of purity. For regular systems purity decay is shown to be independent of Planck's constant for coherent initial states in the semiclassical limit. The accelerated decoherence of macroscopic superpositions is also explained. The theory of fidelity decay is applied to the stability of quantum computation and an improved quantum Fourier transform algorithm is designed and shown to be more stable against random perturbations.

Keywords: quantum stability, fidelity, purity, quantum chaos, decoherence, entanglement, quantum computation, quantum Fourier transformation, the kicked top, Jaynes-Cummings model.

PACS numbers:

- 03.65.Sq Semiclassical theories and applications
- 03.65.Yz Decoherence; open systems; quantum statistical methods
- 03.67.Lx Quantum computation
- 03.67.Mn Entanglement production, characterization, and manipulation
- 03.67.Pp Quantum error correction and other methods for protection against decoherence
- 05.45.-a Nonlinear dynamics and nonlinear dynamical systems
- 05.45.Mt Quantum chaos; semiclassical methods
- 05.45.Pq Numerical simulations of chaotic systems
- 42.50.Ct Quantum description of interaction of light and matter; related experiments

Acknowledgement

I would like to thank my advisor Prof. Tomaž Prosen for giving me the opportunity to work in his group, guiding me and showing me the way. It has been a great pleasure to work with him, sharing the excitement of new discoveries. Initially small project gradually grew, eventually surpassing all our expectations and resulting in the present thesis.

Thanks also go to Prof. Thomas H. Seligman for cooperation on parts of this thesis and for warm hospitality during my stay in Cuernavaca. In particular, he has been a very careful reader of the final manuscript, pointing out english mistakes and confusing statements.

Contents

1	Introduction	1
1.1	Historical Overview	3
1.1.1	Quantum Fidelity	3
1.1.2	Classical Fidelity	7
1.1.3	Entanglement	9
1.2	Outline	10
2	Fidelity	11
2.1	Models for numerics	15
2.1.1	The Kicked Top	15
2.1.2	The Jaynes-Cummings model	17
2.2	Average Fidelity	18
2.2.1	Time Averaged Fidelity	18
2.2.2	State Averaged Fidelity	21
3	General Perturbation	23
3.1	Mixing Dynamics	23
3.1.1	Long Time Behaviour	26
3.2	Regular Dynamics	29
3.2.1	Action-angle Operators	31
3.2.2	Coherent Initial States	32
3.2.3	Random Initial State	35
3.3	Time Scales	38
3.3.1	Illustration with Wigner Functions	41
3.3.2	Coupled Kicked Tops	42
4	Special Case: Zero Time Averaged Perturbation	47
4.1	Mixing Dynamics	49
4.1.1	The Plateau	49
4.1.2	Beyond the Plateau	52
4.2	Regular Dynamics	55
4.2.1	The Numerical Model	58
4.2.2	Coherent Initial State	59
4.2.3	Echo Resonances for Coherent Initial States	64
4.2.4	Random Initial States	69
5	Coupling with the Environment	75
5.1	Reduced Fidelity, Purity Fidelity	75
5.1.1	Inequality Between Fidelity, Reduced Fidelity and Purity Fidelity	76

vi		CONTENTS
	5.1.2	Uncoupled Unperturbed Dynamics 78
	5.1.3	Linear Response Expansion 80
	5.1.4	Numerical Illustration 83
5.2		Mixing Dynamics 84
5.3		Regular Dynamics 84
	5.3.1	Beyond Linear Response 87
	5.3.2	The Jaynes-Cummings Model 90
5.4		Separation of Time Scales 92
	5.4.1	Fast Mixing Environment 94
	5.4.2	Fast Regular Environment 96
5.5		Freeze in a Harmonic Oscillator 98
	5.5.1	The Plateau 101
	5.5.2	Beyond the Plateau 102
5.6		Decoherence for Cat States 107
6		Application: Quantum Computation 107
	6.1	General Framework 108
	6.1.1	Time Dependent Perturbations 109
	6.2	Quantum Fourier Transformation 115
7		Conclusion 116
		Appendices 117
A		Spin Wigner functions 119
B		Coherent State Expectation Values 119

Chapter 1

Introduction

In science one tries to tell people, in such a way as to be understood by everyone, something that no one ever knew before. But in poetry, it's the exact opposite.

—Paul Dirac

Irreversibility of macroscopic behaviour has attracted attention ever since Boltzmann introduced his H -theorem in a seminal paper in 1872 (Boltzmann, 1872), together with the equation bearing his name. The H -theorem is a precursor of what is today known as the second law of thermodynamics, stating that entropy can not decrease in the course of time. The problem was how to reconcile this “arrow of time” with the underlying *reversible* microscopic laws. How come that macroscopic systems always seem to develop in one direction whether the underlying dynamics is symmetric in time? This so called reversibility paradox is usually attributed to Josef Loschmidt. He mentioned it briefly at the end of a paper published in 1876 (Loschmidt, 1876) discussing the thermal equilibrium of a gas subjected to a gravitational field, in an attempt to refute Maxwell’s distribution of velocities for a gas at constant temperature. He also questioned Boltzmann’s monotonic approach towards the equilibrium. Discussing that, if one would reverse all the velocities, one would go from equilibrium towards the initial non equilibrium state, he concludes with : “...*Das berühmte Problem, Geschehenes ungeschehen zu machen, hat damit zwar keine Lösung...*”. Boltzmann was quick to answer Loschmidt’s objections in a paper from 1877 (Boltzmann, 1877), pointing out the crucial importance of the initial conditions and of the probabilistic interpretation of the second law. The fact that for macroscopic systems we always observe a definite “arrow of time” is a consequence of a vast majority of the initial conditions representing an equilibrium state. If we choose the initial state at random it will almost certainly evolve according to the second law of thermodynamics. Of course this probabilistic interpretation still does not solve the problem. Resolution lies in the initial condition, chosen to be a macrostate representing a very small part of the phase space, i.e. having a low entropy. So, provided we start with a low entropy state, the above probabilistic arguments can be used (Lebowitz, 1999) to explain the second law. The question of the initial low entropy state of say the whole universe still remains. For a popular account of this “cosmological” subject see Penrose (1989).

The first written account of the reversibility paradox is actually not due to Loschmidt but due to William Thompson (later Lord Kelvin), although it is possible that Loschmidt mentioned the paradox privately to Boltzmann before. Boltzmann and Loschmidt became good friends while working at the Institute of Physics in Vienna around 1867 (directed at the time by the Slovenian physicist Jožef Stefan). In 1869 Boltzmann moved to Graz, but returned to Vienna in

the period 1873-1876. For a detailed biography of Boltzmann see Cercignani (1998). In a vivid paper (Thompson, 1874) from 1874 Thompson gave a very modern account of irreversibility. When discussing the heat conduction and the equalization of temperature he says: “...*If we allowed this equalization to proceed for a certain time, and then reversed the motions of all the molecules, we would observe a disequalization. However, if the number of molecules is very large, as it is in a gas, any slight deviation from absolute precision in the reversal will greatly shorten the time during which disequalization occurs... Furthermore, if we take account of the fact that no physical system can be completely isolated from its surroundings but is in principle interacting with all other molecules in the universe, and if we believe that the number of these latter molecules is infinite, then we may conclude that it is impossible for temperature-differences to arise spontaneously...*”. The interesting question is then, how short is this *short disequalization time*? The quantity in question is nothing but the fidelity or the Loschmidt echo as it is sometimes called. We evolve the system forward in time with the *unperturbed* evolution, then backward in time with the *perturbed* evolution, and look at the overlap with the initial state. It can be considered in classical mechanics as well as in quantum mechanics. The decay time of the fidelity will then be the time of disequalization in question. Despite its importance for thermodynamics the fidelity was not considered until some years ago, with motivation coming from quantum rather than classical theory.

Quantum theory is arguably the greatest achievement in 20th century physics. There are estimates (Tegmark & Wheeler, 2001) that up to 30% of the gross national product of the US relies on quantum devices. Alone the semiconductor industry is of enormous importance. Still, all these quantum devices do not manipulate individual quanta but rather exploit macroscopic phenomena involving many particles. Experiments involving individual quantum systems became possible only in the '80 with the progress made in e.g. manipulation of cold atoms in traps, single electron devices, entangled photons etc.. This was so to say the experimental birth of what is now called quantum information theory (Nielsen & Chuang, 2001). Quantum information theory married quantum mechanics with information theory and with computer science. It deals with means of processing and transmitting information, and by using quantum systems can achieve things not feasible in any classical way. For instance, one can teleport a quantum state, or perform secure communication over a public channel or do a quantum computation. By using quantum resources to do a computation one is able for instance to factorize a number in a polynomial time, which is presently not known to be possible by classical computer. Also, quantum computers are very efficient in simulating other quantum systems, answering the problem posed by Feynman (1982). Namely, he asked whether it is possible to build a computing machine whose size will grow only linearly with the size of a quantum system simulated on it. With classical computers this is not possible since the size of the Hilbert space needed merely to describe the system grows exponentially with the number of particles. We do not know yet if it is possible to build a quantum computer that will achieve that goal, but on paper quantum computer will be able to do the trick. We say on paper because presently one is able to perform laboratory computations only on a few qubit (less than 10) quantum computer. The main obstacle are errors in the evolution, either due to unwanted coupling with the environment or due to internal errors. Therefore, the main goal is to build a stable quantum computer, resistant to such perturbations. The usual benchmark for stability is fidelity and therefore one ought to understand the behaviour of fidelity in different situations to know how to maximise it. Yet again, the original push to study fidelity came neither from quantum information theory nor from thermodynamics, but from the field of quantum chaos.

The exponential instability of classical systems is a well known and much studied subject. As the underlying laws of nature are quantum mechanical the obvious question arises how this “chaoticity” manifests itself in quantum systems whose classical limit is chaotic. The field

of quantum chaos mainly dealt with stationary properties of classically chaotic systems, like spectral and eigenvector statistics. Despite classical chaos being defined in a dynamical way it was easier to pinpoint the “signatures” of classical chaos in stationary properties (Haake, 1991; Stöckmann, 1999). There were not as many studies of the dynamical aspects of quantum evolution in chaotic systems, some examples being studies of the reversibility of quantum evolution (Shepelyansky, 1983; Casati *et al.*, 1986), the dynamical localization (Fishman *et al.*, 1982; Grempel *et al.*, 1984), energy spreading (Cohen, 2000), wave-packet evolution (Heller, 1991). Classical instability is usually defined as an exponential separation of two nearby trajectories in time. In quantum mechanics the state of a system is completely described by a wave function and so one could be tempted to look at the sensitivity of quantum mechanics to variations of the initial wave function. But quantum evolution is unitary and therefore preserves the dot product (i.e. the distance) between two states and so there is no exponential sensitivity with respect to the variation of the initial state. This, at first sight perplexing, conclusion has been reached because we compared two different things. Classical mechanics can also be stated in terms of a Liouville propagation of phase space densities and this is also unitary. If we want to compare quantum and classical mechanics we have to compare them on the same footing. Quantum mechanics is a probabilistic theory, the wave function just gives the probabilities of measurement outcomes. Therefore we should also formulate classical mechanics in a probabilistic way as a propagation of probability densities in phase space. The idea, first proposed by Peres (1984), was to study not the sensitivity to the variation of the initial condition but with respect to the variation of the *evolution*. He compared two slightly different evolutions starting from the same initial state – the quantum fidelity. For classical systems fidelity gives the same exponential sensitivity to perturbations of the evolution as to perturbations of initial conditions; the two things are equivalent. The quantum fidelity though can behave in a very different way, as we will see in the present work.

The fidelity lies at the crossroad of three very basic areas of physics: thermodynamics, quantum information theory and quantum chaos. The features of the fidelity turned out to be very interesting, as one would expect for such a crossroad.

1.1 Historical Overview

1.1.1 Quantum Fidelity

The quantum fidelity $F(t)$, being the square of the overlap of the state $|\psi(t)\rangle = U_0(t)|\psi(0)\rangle$ obtained by the unperturbed evolution $U_0(t)$ and the state $|\psi_\delta(t)\rangle = U_\delta(t)|\psi(0)\rangle$ obtained by the perturbed evolution $U_\delta(t)$,

$$F(t) := |\langle\psi(t)|\psi_\delta(t)\rangle|^2 = |\langle\psi(0)|U_0^\dagger(t)U_\delta(t)|\psi(0)\rangle|^2, \quad (1.1)$$

has been first used as a measure of quantum stability by Peres (1984), see also his book (Peres, 1995). The fidelity can also be interpreted as an overlap of the initial state and the *echo* state obtained after forward unperturbed evolution followed by a backward perturbed evolution, i.e. after evolution with $U_\delta^\dagger(t)U_0(t)$. Quite generally we can imagine unperturbed evolution being governed by an unperturbed Hamiltonian H_0 and the perturbed evolution by slightly perturbed Hamiltonian $H_\delta = H_0 + \delta V$, with δ a dimensionless perturbation strength and V the perturbation operator. Peres reached non-general conclusion that the decay of fidelity is faster and has a lower asymptotic value for chaotic than for regular classical dynamic. As we will see the general situation can be exactly the opposite. Non decay of the fidelity for regular dynamics in Peres’s work was due to a very special choice of the initial condition, namely that a coherent wave packet was placed in the centre of a stable island. Such a choice is special in two

ways, first the centre of an island is a stationary point and second the number of constituent eigenstates of the initial state is very small. After Peres's work the subject lay untouched for about a decade. In 1996 Ballentine & Zibin (1996) numerically studied a quantity similar to fidelity. Instead of perturbing the backward evolution (i.e. the Hamiltonian), they took the same backward evolution but instead perturbed the state after forward evolution by some instantaneous perturbation, like shifting the whole state by some δx . They also looked at the corresponding classical quantity. The conclusion they reached was that for chaotic dynamics quantum stability was much higher than the classical one, while for regular dynamics the two agreed. All these results were left mainly unexplained. Gardiner *et al.* (1997, 1998) proposed an experimental scheme for measuring the fidelity in an ion trap. Somehow related to the studies of stability was also a work by Schack & Caves (1992, 1993, 1996), where they studied how much information about the environment is needed to prevent the entropy of the system to increase. Fidelity studies received new impetus by a series of NMR experiments carried out by the group of Pastawski.

In NMR echo experiments are a standard tool. The so called spin echo experiment of Hahn (1950) refocuses free induction decay in liquids due to dephasing of the individual spins caused by slightly different Larmour frequencies experienced due to magnetic field inhomogeneities. By an appropriate electromagnetic pulse the Zeeman term is reversed and thus the dynamics of *non-interacting* spins is reversed. The first real *interacting* many-body echo experiment was done in solids by Rhim *et al.* (1970). Time reversal, i.e. changing the sign of the interaction, is achieved for a dipolar interaction whose angular dependence can change sign for a certain “magic” angle, that causes the method to be called magic echo. Still, the magic echo showed strong irreversibility. Much later, Zhang *et al.* (1992) devised a sequence of pulses enabling a *local* detection of polarisation (i.e. magnetic moment). They used a molecular crystal, ferrocene $\text{Fe}(\text{C}_5\text{H}_5)_2$, in which the naturally abundant isotope ^{13}C is used as an “injection” point and a probe, while a ring of protons ^1H constitutes a many-body spin system interacting by dipole forces. The experiment proceeds in several steps: first the ^{13}C is magnetised, then this magnetisation is transferred to the neighbouring ^1H . We thus have a single polarised spin, while others are in “equilibrium”. The system of spins then evolves freely, i.e. spin diffusion takes place, until at time t the dipolar interaction is reversed and by this also spin diffusion. After time $2t$ the echo is formed and we transfer the magnetisation back to our probe ^{13}C enabling the detection of the *polarisation echo*. Note that in the polarisation echo experiments the total polarisation is conserved as the dipole interaction has only “flip-flop” terms like $S_+^j S_-^{j+1}$, which conserve the total spin. To detect the spin diffusion one therefore needs a local probe. With the increase of the reversal time t the polarisation echo – the fidelity – decreases and Zhang *et al.* obtained approximately exponential decay. The nature of this decay has been furthermore elaborated in Pastawski *et al.* (1995). The group of Pastawski then performed a series of NMR experiments where they studied in more detail the dependence of the polarisation echo on various parameters (Levstein *et al.*, 1998; Usaj *et al.*, 1998; Pastawski *et al.*, 2000). They were able to control the size of the residual part of the Hamiltonian, which was not reversed in the experiment and is assumed to be responsible for the polarisation echo decay. For small residual interactions they obtained a Gaussian decay while for a larger ones the decay rate saturated and was independent of the perturbation strength, i.e. of the size of the residual interaction. While there is still no complete consensus on the interpretation of these experimental results they triggered a number of theoretical and even more numerical investigations. We will briefly list them in chronological order.

Using the semiclassical expansion of the quantum propagator Jalabert & Pastawski (2001) derived a *perturbation independent* fidelity decay for localised initial states and chaotic dynamics, $F(t) \sim e^{-\lambda t}$, also called a Lyapunov decay due to its dependence on the Lyapunov exponent λ .

Perturbation independent fidelity decay obtained for strong perturbations has also been studied numerically in a Lorentz gas (Cucchietti *et al.*, 2002a), the perturbation being in the mass of the particle. In the same paper the authors also studied the asymptotic fidelity saturation value which, for the strong perturbations considered, is independent of the perturbation strength, but becomes perturbation dependent for smaller perturbations (see Section 2.2.1). Studying fidelity turned out to be particularly fruitful in terms of the *correlation function* (Prosen, 2002), see also (Prosen & Žnidarič, 2001). For coherent initial states, the fidelity of regular systems decays as a Gaussian while for chaotic systems we have different regimes, the most prominent being the perturbation *dependent* exponential decay. The decay of quantum fidelity in chaotic systems has also been studied by Jacquod *et al.* (2001) and by Cerruti & Tomsovic (2002). For sufficiently small perturbations one gets a Gaussian decay (also called a perturbative regime), for intermediate ones the so-called Fermi golden rule regime of exponential, perturbation dependent decay, while for still stronger perturbations we get the Lyapunov decay. All these regimes, including the fidelity decay for regular dynamics, and for different initial states, were carefully discussed using the correlation function approach in Prosen & Žnidarič (2002). Several interesting results were obtained, perhaps the most surprising one being that in a certain range of parameters we can, by *increasing* chaoticity of the corresponding classical system, *increase* quantum fidelity, i.e. improve the *stability* of quantum dynamics. Different time and perturbation scales were discussed as well as their dependence on the number of degrees of freedom. It is well known that the quantization of classical system is not unique, i.e. there are different quantizations leading to the same semiclassics. Kaplan (2002) compared the quantization ambiguity in chaotic and regular systems, reaching a conclusion that in chaotic systems the quantization ambiguity is *suppressed* as compared with regular ones. Karkuszewski *et al.* (2002) connected the fidelity decay with the decay of the off-diagonal matrix elements of the reduced density matrix, and therefore with decoherence. They claimed that quantum systems, whose classical limit is chaotic, are particularly sensitive to perturbations due to small scale structures in their Wigner functions. Actually, what their results show, was just the dependence of the fidelity decay on the size of the initial state. Fidelity decay is faster for random initial states than for coherent ones and there are no quantum effects in the regime they studied. For related comments see also (Jordan & Srednicki, 2001; Jacquod *et al.*, 2002). The transition between Fermi golden rule and the Lyapunov decay has been further considered in a Bunimovich stadium (Wisniacki *et al.*, 2002), see also (Cucchietti *et al.*, 2002b) for a study of Lyapunov decay. We should stress that the Lyapunov decay of quantum fidelity is purely a consequence of the quantum-classical correspondence. There is nothing “quantum” in it and can be explained in terms of the classical fidelity displaying the same perturbation independent decay as the quantum fidelity (Veble & Prosen, 2004). The fidelity decay can also be connected with the local density of states, although not in a straightforward manner (Wisniacki & Cohen, 2002).

Fidelity decay in mixed systems, having a coexisting regular and chaotic components, is not as well studied as in purely chaotic or regular situation. In (Weinstein *et al.*, 2002a) they studied the fidelity decay for initial states placed at the border between regular and chaotic regions and observed a power-law fidelity decay although over less than an order of magnitude. Jacquod *et al.* (2003) studied averaged fidelity decay in regular systems for perturbations with a zero time average for which they predict a universal power-law decay with a power $3/2$. This does not agree with our findings, see discussion at the end of Section 4.2.2. If the packet after an echo in the chaotic system drifts exponentially away from its position at the beginning, the fidelity can decay also in a super-exponential way (Silvestrov *et al.*, 2003). In the same paper the authors also considered the influence of different averaging procedures on the decay of short-time fidelity. From the correlation function approach one easily sees that

the decay of the fidelity does not only depend on the unperturbed dynamics, say being regular or chaotic, but also on the perturbation. If the correlation function decays to zero sufficiently fast, we can get exponential decay also for regular unperturbed dynamics. Such is the case for instance if the perturbation is modelled by a random matrix (Emerson *et al.*, 2002), but note that such perturbation has no direct classical limit. Instead of the fidelity one can also study the Fourier transformation of the fidelity, see (Wang & Li, 2002). In (Wisniacki, 2003) it was studied how different perturbations of the billiard border influence the short-time fidelity decay. For an attempt to give a uniform approximation of the fidelity decay in the crossover regime between the Gaussian perturbative and the exponential Fermi golden rule decays using random matrix theory see (Cerruti & Tomsovic, 2003b,a) and also (Gorin *et al.*, 2004). The asymptotic saturation level of the fidelity has been studied in (Weinstein *et al.*, 2002c), confirming results of (Prosen & Žnidarič, 2002). Perturbative calculation of the fidelity decay in disordered systems by field theoretical method, i.e. diagrammatic expansion of Green's function, has been done by Adamov *et al.* (2003).

Recently Vaníček & Heller (2003) devised an efficient numerical scheme for a semiclassical evaluation of the quantum fidelity. The method consists of transforming intractable (due to exponentially many contributing orbits) semiclassical expressions in coordinate space into an initial momentum space representation. A surprising quantum phenomenon of a prolonged stability, called freeze of fidelity, has been described in Prosen & Žnidarič (2003b) for regular systems. Later, it has been generalised to arbitrary dynamics, in particular to chaotic systems (Prosen & Žnidarič, 2004). The decay of fidelity in regular one dimensional systems has been studied in (Sankaranarayanan & Lakshminarayan, 2003) and they also numerically observed a very short correspondence between the classical and the quantum fidelity for initial states placed in a rotational part of phase space, where the average perturbation is zero. This is nothing but the freeze of fidelity, not present in classical fidelity. The Lyapunov regime, being of purely classical origin, and its borders of validity have been furthermore elaborated in (Cucchietti *et al.*, 2003b), see also (Prosen & Žnidarič, 2002) for a detailed discussion of borders within which different regimes are valid. They also stressed the importance of non-commutativity of the limits $\hbar \rightarrow 0$ and $\delta \rightarrow 0$ in recovering the classical behaviour, as already explained in (Prosen & Žnidarič, 2002). A nontrivial question, addressed by Hiller, Kottos, Cohen and Geisel (Hiller *et al.*, 2004) concerns the optimal time of the unperturbed evolution, i.e. we fix the duration of the unperturbed evolution and seek the duration of the perturbed evolution for which the fidelity will be maximal. The quantum fidelity decay in weakly chaotic systems when one might not get the Lyapunov or the Fermi golden rule decay has been explored in (Wang *et al.*, 2004). The fidelity for various random matrix models has been analysed by Gorin *et al.* (2004), see also (Cerruti & Tomsovic, 2003b,a). For further random matrix results and their relevance for quantum computation see also (Frahm *et al.*, 2004). In (Iomin, 2003) the fidelity of a nonlinear time-dependent chaotic oscillator with respect to the time-dependent perturbation of its frequency has been studied analytically. Most of the studies so far focused on a few degrees of freedom systems, the exception being (Prosen, 2002). For additional results on the stability of many-body systems see (Izrailev & Castañeda-Mendoza, 2004).

There has also been a large number of papers dealing with the stability of quantum computation, i.e. studies of the fidelity for specific quantum algorithms and perturbations, mainly relying on numerical simulations. Some of these include (Miquel *et al.*, 1996, 1997; Gea-Banacloche, 1998, 1999, 2000). The group of Berman studied in detail the stability of the Ising quantum computer, see for instance (Berman *et al.*, 2001, 2002a,b) and references therein and also (Celardo *et al.*, 2003). The group of Shepelyansky studied the stability of many different quantum algorithms (Georgeot & Shepelyansky, 2000; Song & Shepelyansky, 2001; Benenti *et al.*,

2002; Terraneo & Shepelyansky, 2003), see also (Benenti *et al.*, 2003c) and (Bettelli, 2004). The scaling of errors with various parameters is easily explained by our correlation function approach.

With the advances in experiments manipulating individual quantum systems it has become possible to actually measure quantum fidelity. Apart from NMR echo experiments already mentioned, one is able to measure the quantum fidelity on a few qubit NMR quantum computer (Weinstein *et al.*, 2002b). Particularly promising candidates are ion traps Gardiner *et al.* (1997, 1998), ultra cold atoms in optical traps (Andersen *et al.*, 2003; Schlunk *et al.*, 2003). Experiments with microwave resonators in billiards are also under way (Schäfer *et al.*, 2003).

1.1.2 Classical Fidelity

Classical fidelity can be defined in an analogous way as quantum fidelity and has been first used in (Prosen & Žnidarič, 2002). It is an overlap integral of two classical densities in phase space, obtained by unperturbed and perturbed evolutions,

$$F_{\text{clas}}(t) := \int d\mathbf{x} \rho_0(\mathbf{x}, t) \rho_\delta(\mathbf{x}, t), \quad (1.2)$$

where $\rho_\delta(\mathbf{x}, t)$ is the density in phase space obtained by a perturbed evolution $\phi_\delta(\mathbf{x})$, where $\phi_\delta(\mathbf{x})$ is a volume preserving flow in phase space. The density at time t can be obtained by backward propagating phase space point \mathbf{x} , $\rho_\delta(\mathbf{x}, t) = \rho(\phi_\delta^{-1}(\mathbf{x}), 0)$. Note that in order for fidelity to be normalized to 1, the classical density has to be square normalized, $\int d\mathbf{x} \rho^2(\mathbf{x}, 0) = 1$.

Classical fidelity behaves markedly different from quantum fidelity. For chaotic systems and localized initial states the classical fidelity agrees with quantum only up to the short Ehrenfest time, logarithmic in Planck's constant, when the quantum-classical correspondence breaks down. For regular systems and if the time average perturbation is nonzero though, classical fidelity follows quantum fidelity. On the other hand, if the time averaged perturbation is zero, quantum fidelity exhibits the so called freezing (Chapter 4), while classical fidelity does not, except in the non-generic case of a harmonic oscillator (Section 5.5). The classical fidelity will depend on the stability of orbits in phase space. Linear response will therefore depend on the stability of the flow and this involves the derivatives of the flow, a derivative being an unbounded operator. For chaotic systems for instance, the derivatives grow exponentially in time due to orbit separation, a simple consequence of the famous Lyapunov instability. In a phase space picture, the classical dynamics can produce structures on an arbitrary small scales, even if we start from a smooth density. Resolution of the quantum mechanics on the other hand is limited by a finite Planck constant.

We will give a brief overview of the known results about classical fidelity. This will help us to understand the differences with quantum fidelity which will be the object of study in the present work. The literature on classical fidelity is not nearly as extensive as on quantum fidelity. Linear response calculation has been done in (Prosen & Žnidarič, 2002). Numerical results on the classical fidelity and its correspondence with the quantum fidelity in chaotic systems and in systems exhibiting diffusion have been presented in (Benenti & Casati, 2002). Classical fidelity in regular and chaotic systems has also been theoretically discussed in (Eckhardt, 2003). A detailed explanation of the asymptotic decay in chaotic systems has been given in (Benenti *et al.*, 2003b) and a theoretical explanation of the Lyapunov decay for short times in (Veble & Prosen, 2004). Classically regular systems on the other hand have been worked out in (Benenti *et al.*, 2003a).

Chaotic Systems

The classical fidelity in chaotic systems will go through different decay regimes as time increases. We will consider a localized initial state of size ν . Starting from $t = 0$ fidelity stays close to 1 until time t_ν (Benenti & Casati, 2002; Benenti *et al.*, 2003b),

$$t_\nu \sim \frac{1}{\lambda} \ln \frac{\nu}{\delta}, \quad (1.3)$$

where λ is the Lyapunov exponent. The time t_ν can be thought of as the time in which the initial perturbation is “amplified” to the size of the initial packet and ρ_δ starts to differ from ρ_0 . For a rigorous derivation of t_ν as well as for a discussion of multi-degree of freedom systems, where there is a cascade of times t_ν , see (Veble & Prosen, 2004). After t_ν the so called Lyapunov decay $F(t) = \exp\{-\lambda(t - t_\nu)\}$ sets in and lasts until time t_δ determined by the spreading of the packet over the whole phase space. The Lyapunov decay has been explained by Veble & Prosen (2004) and for systems with more than one degree of freedom there is a whole cascade of Lyapunov decays determined by the Lyapunov spectrum*. If we have a classical system with diffusion, such that the phase space is much larger in one direction, say $q, p \in [0, 2\pi] \times [0, L]$, with $L \gg 2\pi$, time t_δ will be given by (Benenti *et al.*, 2003b)

$$t_\delta \sim \frac{1}{\lambda} \ln \frac{2\pi}{\delta}. \quad (1.4)$$

After t_δ fidelity will decay diffusively $F(t) \sim 1/\sqrt{Dt}$ with the diffusion constant D , until the diffusive process reaches the phase space boundary also in p -direction, i.e. at $t_D \sim L^2/D$. Note that this diffusive regime is present only if $L \gg 2\pi$. After t_D the asymptotic decay of classical fidelity begins. This asymptotic decay is determined by the largest Ruelle-Pollicott resonance (Benenti *et al.*, 2003b), i.e. the eigenvalue of the Perron-Frobenius operator, and is thus the same as the asymptotic decay of classical correlations. If there is a gap in the spectrum of the Perron-Frobenius operator, this decay will be exponential, otherwise it can be power law. Note that this asymptotic decay rate does not depend on the perturbation strength δ but only on the phase space size L . For large times fidelity will decay towards the asymptotic value $\bar{F} = F(t \rightarrow \infty)$ determined by the ratio of the initial packet size and the phase space size. In order to see the asymptotic regime of fidelity decay one has to look at $F(t) - \bar{F}$. Furthermore, for the fidelity at the end of the Lyapunov decay t_δ to be larger than \bar{F} we must have $\delta > \bar{F}$.

The decay rate for classical fidelity in chaotic systems, apart from the non-decaying “shoulder” until t_ν , does not depend on the perturbation strength δ (decay time borders do depend though) and is therefore independent of the perturbation itself. This must be contrasted with quantum fidelity, which as we will see does depend strongly on perturbation strength and type.

Regular Systems

The classical fidelity decay for regular systems has been explained (Benenti *et al.*, 2003a) by studying changes in the action-angle variables caused by the perturbation. There is a competition between two contributions to the fidelity decay. It can decay as a consequence of the ballistic separation of the perturbed and unperturbed packets caused by different frequencies of the perturbed and unperturbed tori on which the initial packet is placed, or it can decay due to different shapes of unperturbed and perturbed tori. In the latter case the decay is caused by predomions of the perturbed packet between unperturbed tori. Therefore, if the perturbation predominantly changes the *frequency* of tori, the classical fidelity will exhibit a *ballistic* decay.

*In case of drift of packets one can get a super-exponential instead of exponential decay of fidelity. For sufficiently small times quantum fidelity will show the same phenomena, see (Silvestrov *et al.*, 2003).

The shape of this ballistic decay is determined by the shape of the initial packet. If the packet is a coherent state having a Gaussian shape, the decay will be Gaussian. On the other hand, if the perturbation predominantly changes the *shape* of the packet the decay will be *algebraic* $F(t) \sim 1/(\delta t)^d$, in a system with d degrees of freedom. Which type of decay one gets, depends on the shape of the perturbation but not on its strength δ , provided it is small enough. The type of the decay can also depend on the position of the initial packet.

Note that the above results were derived under the assumption that the angles across the packet are spread over 2π , i.e. $t > 2\pi/(\Delta_j \partial \omega / \partial \mathbf{j})$, where Δ_j is the width of the initial packet in the action direction. Incidentally, this time is equal to the time t_1 (4.50) after which quantum fidelity freezes at a constant value if the time averaged perturbation is zero (see Section 4.2). Furthermore, the change of the actions across the packet caused by the perturbation must be small, i.e. $\Delta_j \gg \delta$. This last condition translates for coherent packets into $\delta \ll \hbar^{1/2}$, also being the upper limit of validity of approximations used in the calculation of the quantum fidelity plateau (4.61).

Comparing to quantum fidelity, the case of ballistic decay of classical fidelity corresponds to perturbations having a nonzero time average, discussed in Chapter 3. For such perturbations quantum fidelity agrees with the classical one under certain conditions. The case of the algebraic decay corresponds to the perturbation with a vanishing time average. In this case though, the quantum and the classical fidelity do not agree. What is more, quantum fidelity displays an intriguing new feature called freezing (see Section 4.2) and decays only on a much longer time scale $\sim 1/\delta^2$. Whereas only the functional dependence of the classical fidelity decay changes depending on the perturbation type, always decaying on a time scale $\sim 1/\delta$, the decay of quantum fidelity drastically changes if one has a perturbation with a zero time average.

1.1.3 Entanglement

The literature on decoherence is exhaustive and we will here list only those more or less directly related to our work.

Time independent perturbative expansion has been used by Kübler & Zeh (1973) to study the eigenvalues of the reduced density matrix. A similar expansion was used much later for the purity (Kim *et al.*, 1996). Note that these perturbative approaches are not equivalent to our linear response expressions presented in Chapter 5 as they correspond only to the short time regime in which the correlation function is constant. Among the early studies of entropy growth and its relation to the chaoticity of the underlying system is the one by Alicki *et al.* (1996). Miller & Sarkar (1999) observed a linear entropy growth with the slope given by the Lyapunov exponent. Gorin & Seligman (2002, 2003) studied the purity decay for random matrix models. Random matrix asymptotic value of the purity (or of linear entropy) was later re-derived in (Bandyopadhyay & Lakshminarayan, 2002b) and numerically observed in chaotic systems. Prosen & Seligman (2002) first defined the purity fidelity, generalising the purity to echo dynamics. The purity fidelity and its relation with the fidelity in chaotic and regular systems was studied also in (Prosen *et al.*, 2003b) using a correlation function approach which was used also by Tanaka *et al.* (2002) for studying chaotic systems. The connection between the purity and the fidelity was put on a firm ground by a rigorous inequality between the two (Žnidarič & Prosen, 2003; Prosen *et al.*, 2003a). The classical analog of decoherence has been studied in (Gong & Brumer, 2003c,b,a). Using a perturbative approach the influence of the type of the perturbation and of the dynamics on the quantum-classical correspondence were explored, see also (Angelo *et al.*, 2004) for a study of quantum-classical correspondence of entanglement. The entanglement in weakly coupled composite systems was studied in (Žnidarič & Prosen, 2003) as well as (Fujisaki *et al.*, 2003), reaching the same conclusion, namely that the increase of chaos can inhibit the production of entanglement. Subsequently

the inequality between fidelity and purity was used in (Cucchietti *et al.*, 2003a). Entanglement production in a coupled baker's map has been studied in (Scott & Caves, 2003) and in coupled kicked tops in (Bandyopadhyay & Lakshminarayan, 2002a). Similar semiclassical methods as for the evaluation of the fidelity have been used also for the purity (Jacquod, 2004), predicting an exponential decay in chaotic systems, confirming prediction in (Žnidarič & Prosen, 2003), and algebraic decay in regular systems. The predicted power of the algebraic decay though does not agree with our theory and numerical results presented in Section 5.3.1. The entanglement under echo situation during a quantum computation has been studied in (Rossini *et al.*, 2003). Entanglement in weakly coupled kicked tops has been studied also in (Demkowicz-Dobrzański & Kuś, 2004), among other things also for random initial states.

1.2 Outline

In Chapter 2 we introduce the quantum fidelity and briefly review numerical models used for the illustration of the theory. The material in sections dealing with the average fidelity has been mainly published in (Prosen & Žnidarič, 2002) and (Prosen *et al.*, 2003c). The core of Chapter 3 has been published in (Prosen & Žnidarič, 2002), which is the main paper presenting the correlation function approach to fidelity. New, unpublished material consists of numerical demonstration of a Gaussian distribution of diagonal matrix elements in chaotic systems, relevant for a Gaussian perturbative decay of fidelity. New is also the discussion about the average fidelity in regular systems as well as the last part of Section 3.3 with the illustration of the fidelity decay in terms of Wigner functions and some additional figures hopefully clarifying the relations between different decay regimes. The material of Chapter 4 has been published in (Prosen & Žnidarič, 2003b) and (Prosen & Žnidarič, 2004). We unified the approach in mixing and regular situation making the exposition of a regular case more concise. New material is the explanation of the average fidelity decay in regular systems with zero time average perturbation. About half of the contents of Chapter 5 has been published in (Prosen *et al.*, 2003b; Žnidarič & Prosen, 2003; Prosen *et al.*, 2003a). The new material consists of the purity fidelity and the reduced fidelity calculation in regular systems beyond linear response, most of the discussion about the Jaynes-Cummings model, the section describing the freeze in a harmonic oscillator and the last section explaining the accelerated decoherence of cat states. The application of the fidelity theory to the improvement of the quantum Fourier transformation has been published in (Prosen & Žnidarič, 2001) and an extension to the Ising model of quantum computer, not presented in the present work, in (Celardo *et al.*, 2003).

Chapter 2

Fidelity

Basic research is what I am doing when I don't know what I am doing.

—Werner von Braun

Quantum fidelity F between two general density matrices ρ and σ , representing either a pure or a mixed state, has been used by Uhlmann (Uhlmann, 1976),

$$F(\rho, \sigma) = \left(\text{tr} \sqrt{\rho^{1/2} \sigma \rho^{1/2}} \right)^2. \quad (2.1)$$

He called it a transition probability and the name fidelity was introduced by Jozsa (Jozsa, 1994). It is symmetric with respect to the exchange of ρ and σ and in the case of one density matrix being a pure one, the general expression for fidelity simplifies into $F = \langle \psi | \sigma | \psi \rangle$ and if both are pure it is

$$F(\psi, \varphi) = |\langle \psi | \varphi \rangle|^2, \quad (2.2)$$

where obviously $\rho := |\psi\rangle\langle\psi|$ and $\sigma := |\varphi\rangle\langle\varphi|$. We will always deal with pure states and the latter definition (2.2) will be sufficient for us. Note that sometimes the name fidelity is used for a quantity without a square, i.e. for a fidelity amplitude.

We will study stability of quantum dynamics with respect to the perturbation of evolution and the quantity studied will be the fidelity between states obtained by *unperturbed* and *perturbed* evolutions, starting from the same initial state. Let us denote the initial state by $|\psi(0)\rangle$, and the states at time τ as

$$|\psi(\tau)\rangle = U_0(\tau)|\psi(0)\rangle, \quad |\psi_\delta(\tau)\rangle = U_\delta(\tau)|\psi(0)\rangle, \quad (2.3)$$

where $U_0(\tau)$ is a unitary propagator from time 0 to time τ and $U_\delta(\tau)$ is a perturbed propagator. The overlap between the perturbed and unperturbed states, denoted by $F(\tau)$, will serve us as a criterion of stability,

$$F(\tau) = |\langle \psi_\delta(\tau) | \psi(\tau) \rangle|^2 = |f(\tau)|^2, \quad f(\tau) = \langle \psi(0) | M_\delta(\tau) | \psi(0) \rangle, \quad (2.4)$$

where we introduced a complex fidelity amplitude $f(\tau)$ and the unitary *echo operator*

$$M_\delta(\tau) = U_0^\dagger(\tau) U_\delta(\tau). \quad (2.5)$$

The fidelity as defined in (2.4) is a real quantity between 0 for orthogonal states and 1 iff the two states are equal (up to a phase) and is a standard measure of stability.

Up to now we have not specified the propagators $U_0(\tau)$ and $U_\delta(\tau)$ and to simplify the matter we will limit ourselves to the case where a propagator for time τ can be written as a power of some basic single-step propagator U_0 . That is, we will use time index t measuring the number of basic units of duration τ_0 , $\tau = t\tau_0$. We therefore write a single step propagator $U_0 \equiv U_0(\tau_0)$ and similarly for the perturbed evolution $U_\delta \equiv U_\delta(\tau_0)$. The propagator for t steps is now simply the t -th power of a basic propagator $U_0(\tau_0 t) = U_0^t$. These discrete time formalism allows us to treat two interesting cases at once: the case of time-independent Hamiltonian and the case when the Hamiltonian is time periodic function $H(\tau) = H(\tau + \tau_0)$ with a period τ_0 . The latter case includes the so-called kicked systems which will be used for the numerical demonstration of our theory. Note that the theory can be easily generalised also to time-dependent Hamiltonians, only notation becomes more cumbersome. For an example see Section 6.2 describing the application of fidelity theory to the quantum Fourier transformation algorithm. The general perturbed evolution can be written in terms of the perturbation generator V as

$$U_\delta = U_0 \exp(-iV\delta\tau_0/\hbar), \quad (2.6)$$

where δ is a dimensionless perturbation strength. The above equation (2.6) can be considered as a definition of a hermitian operator V , given the unperturbed and perturbed one time step propagators U_0 and U_δ , respectively. In the case of Hamiltonian dynamics with H_0 generating unperturbed evolution as $U_0^t = \exp(-iH_0 t\tau_0/\hbar)$ and with the perturbed Hamiltonian of the form $H_\delta = H_0 + H'\delta$ we have $V = H' + \mathcal{O}(\tau_0\delta)$. The difference between H' and V therefore goes to zero in the limit of either small perturbation strength δ or in the limit of small time step τ_0 . The latter limit, namely $\tau_0 \rightarrow 0$, corresponds to the case of time-independent Hamiltonians, where the time step τ_0 can be chosen arbitrarily small. From now on we will drop the irrelevant parameter τ_0 (i.e. take a unit of time to be τ_0) in all equations, so that the discrete time index t has units of time. We will use the same letter t for a discrete time index as well as for a continuous time (limit $\tau_0 \rightarrow 0$) on few occasions. Whether t is a discrete time index or a continuous will be clear from the context. Our definition of fidelity (2.4) is in discrete time formulation

$$F(t) = |\langle\psi(0)|M_\delta(t)|\psi(0)\rangle|^2, \quad M_\delta(t) := U_0^{-t}U_\delta^t. \quad (2.7)$$

The fidelity is just the expectation value of the echo operator. It can be equivalently expressed in terms of the initial pure density matrix $\rho(0)$ and the *echo* density matrix $\rho^M(t)$ (sometimes referred to as the Loschmidt echo) obtained from $\rho(0)$ by evolving it with the echo operator $M_\delta(t)$

$$\rho(0) = |\psi(0)\rangle\langle\psi(0)|, \quad \rho^M(t) := M_\delta(t)\rho(0)M_\delta^\dagger(t), \quad (2.8)$$

as

$$F(t) = \text{tr}[\rho(0)\rho^M(t)], \quad f(t) = \text{tr}[\rho(0)M_\delta(t)]. \quad (2.9)$$

On several occasions we will be interested in the fidelity averaged over some ensemble of initial states. In such a case the density matrix $\rho(0)$ in the above definitions of fidelity and fidelity amplitude $f(t)$ (2.9) must be replaced by appropriate mixed density matrix. We will frequently use a uniform average over whole Hilbert space of dimension \mathcal{N} , $\rho(0) = 1/\mathcal{N}$, see Section 2.2.2 for details.

Using our definition (2.6) of perturbed dynamics in terms of the perturbation generator V , the echo operator can be rewritten in a more useful way by writing V in the interaction picture*, i.e. for an arbitrary operator A its interaction picture $A(t)$ is

$$A(t) = U_0^{-t}AU_0^t, \quad (2.10)$$

*It can also be considered as the Heisenberg picture of the unperturbed dynamics.

and so the echo operator is

$$M_\delta(t) = \exp(-iV(t-1)\delta/\hbar) \cdots \exp(-iV(0)\delta/\hbar) = \mathcal{T} \exp(-i\Sigma(t)\delta/\hbar), \quad (2.11)$$

where \mathcal{T} is a time-ordering operator and $\Sigma(t)$ is the sum of operators $V(j)$,

$$\Sigma(t) := \sum_{j=0}^{t-1} V(j). \quad (2.12)$$

In the case of the time-independent Hamiltonian one has $\Sigma(t) = \int_0^t V(t')dt'$. The form of the echo operator (2.11) is nothing but the interaction picture of the perturbed propagator, familiar in quantum field theory. Methods of quantum field theory have been actually used by Adamov, Gornyi and Mirlin (Adamov *et al.*, 2003) to calculate the fidelity in a disordered system. Remember that the time dependence of $V(t)$ comes from the interaction picture (2.10) and so $V(t)$ is time dependent even if original perturbation V (2.6) is not, which is the case throughout our derivations. The same definition of fidelity, just by replacing density matrices with the densities in phase space, can be used for classical fidelity, see Veble & Prosen (2004).

The echo operator $M_\delta(t)$ can be written as an exponential function of a single operator by using the Baker-Campbell-Hausdorff (BCH) formula

$$e^A e^B = \exp\left(A + B + \frac{1}{2}[A, B] + \frac{1}{12}[A, [A, B]] + \frac{1}{12}[B, [B, A]] + \cdots\right). \quad (2.13)$$

Applying the BCH formula on the product form of $M_\delta(t)$ (2.11) gives to the order δ^2 in the argument of the exponential function

$$M_\delta(t) = \exp\left\{-\frac{i}{\hbar}\left(\Sigma(t)\delta + \frac{1}{2}\Gamma(t)\delta^2 + \cdots\right)\right\}, \quad (2.14)$$

with the hermitian operator $\Gamma(t)$ being

$$\Gamma(t) = \frac{i}{\hbar} \sum_{j=0}^{t-1} \sum_{k=j}^{t-1} [V(j), V(k)]. \quad (2.15)$$

Both operators $\Sigma(t)$ and $\Gamma(t)$ standing in the expression for the echo operator have a well defined classical limit, provided V has a classical limit. The classical limit of $\Gamma(t)$ can be obtained by replacing commutator with the Poisson bracket $\{\bullet, \bullet\}$, $(-i/\hbar)[\bullet, \bullet] \rightarrow \{\bullet, \bullet\}$. The BCH form (2.14) of the echo operator will be particularly useful in the case of regular dynamics. For now let us list three different possible fidelity decays depending on the behaviour of operator $\Sigma(t)$. For mixing dynamics the fluctuations of $\Sigma(t)$ give the dominant contribution, i.e. terms like $\langle \Sigma^2(t) \rangle$ grow linearly with time as $\sim t$. For regular dynamics second moment $\langle \Sigma^2(t) \rangle \sim t^2$ grows quadratically with time, corresponding to the existence of a nontrivial time-averaged perturbation $V(t)$. In certain cases we can have even $\langle \Sigma^2(t) \rangle \sim t^0$ which results in the so-called freeze of fidelity. Only in this last case is the fidelity decay caused by the operator $\Gamma(t)$.

If we want the fidelity expressed as a power series to all orders in δ the BCH formula becomes too cumbersome. An easier approach is to just expand the product form of the echo operator $M_\delta(t)$ (2.11), giving the fidelity amplitude

$$f(t) = 1 + \sum_{m=1}^{\infty} \frac{(-i)^m \delta^m}{m! \hbar^m} \sum_{j_1, \dots, j_m=0}^{t-1} \mathcal{T} \langle V(j_1) V(j_2) \cdots V(j_m) \rangle, \quad (2.16)$$

where we introduced the notation $\langle \bullet \rangle = \langle \psi(0) | \bullet | \psi(0) \rangle$. One can see, that the fidelity is expressed in terms of m -point quantum correlation functions of the perturbation generator V .

In the semiclassical limit one is able to replace quantum correlation functions with the classical ones and therefore the quantum fidelity is expressed in terms of classical quantities. One should keep in mind that the classical fidelity behaves distinctively different from quantum fidelity (see Chapter 1.1.2) and therefore it is not obvious that quantum fidelity can be expressed in terms of classical quantities. Power series expansion of the classical fidelity for example does not yield a fruitful result (for chaotic systems) due to unboundedness of the classical operators and the classical fidelity can not be expressed in a similar way as the quantum fidelity (2.16).

Fidelity $F(t)$ is now obtained by taking absolute value square of $f(t)$ (2.16). Only even orders in δ survive as odd orders just rotate the phase of the fidelity amplitude $f(t)$, the lowest order being quadratic in δ

$$F(t) = 1 - \frac{\delta^2}{\hbar^2} \sum_{j,k=0}^{t-1} C(j,k) + \mathcal{O}(\delta^4) = 1 - \frac{\delta^2}{\hbar^2} \left\{ \langle \Sigma^2(t) \rangle - \langle \Sigma(t) \rangle^2 \right\} + \mathcal{O}(\delta^4), \quad (2.17)$$

with $C(j,k)$ being the quantum correlation function

$$C(j,k) = \langle V(j)V(k) \rangle - \langle V(j) \rangle \langle V(k) \rangle. \quad (2.18)$$

The second order expansion of the fidelity (2.17) is one of the central theoretical results. Although it is very simple and is just the lowest order expansion it contains most of the essential physics of fidelity decay. Furthermore, there is one very pragmatic reason why it is sufficient and higher orders are not needed. In all practical and experimental applications where the fidelity is the relevant quantity, one is mainly interested in a regime of high fidelity, i.e. of high stability. If the interesting range is say $F(t) > 0.9$, higher orders will give only corrections of order 0.01. To see this, let us denote the second order term with $x = (\delta/\hbar)^2 \sum_{j,k} C(j,k)$. From the expansion (2.16) one can see that the term with δ^{2m} will be at most of the order $(\delta t/\hbar)^{2m} \sim x^{2m}$. So if $1 - F(t) \approx x^2 \ll 1$ one can safely neglect higher orders in δ , i.e. terms of order x^{2m} with $m > 1$, irrespective of the values of individual parameters like δ , \hbar or time t . The range of validity of the lowest order expansion in (2.17) is limited only by the value of $1 - F(t)$. Furthermore, in certain cases such as mixing dynamics (Section 3.1), regular dynamics (Section 3.2) or in the so-called freeze of fidelity (Chapter 4) the series (2.16) can be resummed to all orders in δ and one gets an expression for the fidelity valid in the whole range from 1 to its asymptotic value.

Let us now discuss in more detail the lowest order term in the expansion of fidelity which can be in the case of continuous time-independent Hamiltonian written as

$$1 - F(t) = \frac{\delta^2}{\hbar^2} \int_0^t \int_0^t C(t', t'') dt' dt''. \quad (2.19)$$

This *linear response* expression is reminiscent of Green-Kubo like formulas. It says that the “dissipation of quantum information” $1 - F(t)$ equals the double integral of the correlation function of the perturbation V . An interesting and somehow counterintuitive conclusion can be drawn from it, namely, the *smaller* the integral of time correlation function the higher fidelity will be. In the semiclassical limit the quantum correlation function approaches the classical one, provided the initial state $|\psi(0)\rangle$ also has a well defined classical limit, and one will see a fast decay of the correlation function for chaotic systems while for regular systems the correlation function typically will not decay. The double integral of the correlation function will therefore grow as $\propto t$ for chaotic systems and like $\propto t^2$ for regular systems. The fidelity will in turn decay *more slowly* for chaotic systems than for regular ones. Or in other words, the more chaotic the systems is, the slower decay of quantum fidelity it will have, i.e. the more stable it is to perturbations. This must be contrasted with the behaviour of the classical fidelity (see Section 1.1.2) which is just the opposite. The more chaotic the system is, the faster classical fidelity will decay.

2.1 Models for numerics

We will always use numerical simulations to compare with the theoretical derivations. Two classes of systems will be used. One group will be the so-called kicked top models, describing dynamics of a spin “kicked” by some external field. In the case of a kicked top the Hamiltonian is time periodic and the propagator U_0 or U_δ represent a Floquet map over the period of one kick. The second example will be a Jaynes-Cummings system familiar in quantum optics. The Jaynes-Cummings model is a time-independent model with two degrees of freedom representing a harmonic oscillator (boson) coupled with a spin (fermion). In the following two subsections we will present both models and briefly describe their properties, while the actual numerical results will be presented in each chapter as needed.

2.1.1 The Kicked Top

The kicked top has been introduced by Haake, Kuś and Scharf (Haake *et al.*, 1987) and has served as a numerical model in numerous studies since then (Haake, 1991; Shack *et al.*, 1994; Fox & Elston, 1994; Alicki *et al.*, 1996; Miller & Sarkar, 1999; Breslin & Milburn, 1999). In addition the kicked top might also be experimentally realizable (Haake, 2000).

In Chapter 3, discussing the fidelity decay for general perturbations, we will use a unitary one step propagator

$$U_0 = U(\gamma, \alpha) = \exp(-i\gamma S_y) \exp\left(-i\alpha \frac{S_z^2}{2S}\right), \quad (2.20)$$

where $S_{x,y,z}$ are standard spin operators $[S_k, S_l] = i\epsilon_{klm} S_m$ and α, γ are two parameters determining dynamical properties. The propagator for t steps is U_0^t . Half-integer (integer) spin S determines the size of the Hilbert space $\mathcal{N} = 2S + 1$ and the value of the effective Planck constant $\hbar = 1/S$. The perturbed propagator U_δ is obtained by perturbing the parameter α

$$U_\delta = U(\gamma, \alpha + \delta), \quad (2.21)$$

so that the perturbation generator V is

$$V = \frac{1}{2} \left(\frac{S_z}{S} \right)^2. \quad (2.22)$$

In the classical limit $S \rightarrow \infty$ the area preserving map corresponding to U_0 can be obtained from the Heisenberg equations for spin operators, $\mathbf{S}(1) = U_0^\dagger \mathbf{S} U_0$. The classical map is most easily written in terms of a unit vector on a sphere $\mathbf{r} = (x, y, z) = \mathbf{S}/S$ as

$$\begin{aligned} x' &= \cos \gamma (x \cos(\alpha z) - y \sin(\alpha z)) + z \sin \gamma \\ y' &= y \cos(\alpha z) + x \sin(\alpha z) \\ z' &= z \cos \gamma - \sin \gamma (x \cos(\alpha z) - y \sin(\alpha z)). \end{aligned} \quad (2.23)$$

The classical perturbation generator (2.22) is simply $^\dagger V \rightarrow v = z^2/2$. The angle γ in the propagator is usually set to $\pi/2$ whereas we will use two different values, $\gamma = \pi/2$ and $\gamma = \pi/6$. For these two values of γ the classical correlation function displays two different decays towards zero, a monotonic decay for $\gamma = \pi/6$ and an oscillatory decay for $\gamma = \pi/2$.

The phase space of the classical map (2.24) is regular for small values of α , at $\alpha \sim 3$ (see e.g. (Peres, 1995)) most of tori disappear and for still larger α the system is fully chaotic.

[†]We will use lowercase letters for classical quantities.

For $\gamma = \pi/2$ the unperturbed propagator U_0 (as well as the perturbed one) commutes with the operator R_y of a π rotation around y-axis, $R_y = \exp(-i\pi S_y)$. In addition there is an antiunitary symmetry so that the Hilbert space is reducible to three invariant subspaces. Following notation in Peres's book (Peres, 1995) we denote them with EE, OO and OE with the basis states (here we assume S to be even)

$$\begin{aligned} \text{EE} : & \quad |0\rangle, \{|2m\rangle + |-2m\rangle\} / \sqrt{2} & \mathcal{N}_{\text{EE}} = S/2 + 1 \\ \text{OO} : & \quad \{|2m-1\rangle - |-(2m-1)\rangle\} / \sqrt{2} & \mathcal{N}_{\text{OO}} = S/2 \\ \text{OE} : & \quad \{|2m\rangle - |-2m\rangle\} / \sqrt{2}, \{|2m-1\rangle + |-(2m-1)\rangle\} / \sqrt{2} & \mathcal{N}_{\text{OE}} = S, \end{aligned} \quad (2.24)$$

where m runs from 1 to $S/2$ and $|m\rangle$ are standard eigenstates of S_z . For $\gamma \neq \pi/2$ the subspaces EE and OO coalesce as R_y is the only symmetry left and we have just two invariant subspaces. Except if stated otherwise the initial state will always be chosen from subspace OE (i.e. initial coherent state will be projected onto OE subspace) so that the size of the relevant Hilbert space will be $\mathcal{N} = S$.

In Chapter 4, dealing with the so-called freeze of fidelity, we will take a slightly different form of the propagator which will be presented in the mentioned chapter. Apart from the one dimensional kicked top we will also use a system of two coupled kicked tops to demonstrate the dependence of the fidelity decay on the number of degrees of freedom. The one step propagator for two coupled kicked tops is chosen to be

$$U_\delta = U_1(\gamma, \alpha) U_2(\gamma, \alpha) \exp(-i(\delta + \varepsilon)V/\hbar). \quad (2.25)$$

Propagators U_1 and U_2 are the usual single kicked top propagators (2.20) acting on the first and the second top, respectively, and the last term with operator V is responsible for the coupling of strength ε for unperturbed evolution and $\varepsilon + \delta$ for perturbed one. The operator V will be left unspecified for now as we will use different V 's.

The initial state $|\psi(0)\rangle$ used for fidelity evaluation will be either a random state with the expansion coefficients $c_m = \langle m|\psi(0)\rangle$ being independent Gaussian complex numbers or a coherent state. A random state might be the most relevant for quantum computations for instance as it contains the most information and the states used in quantum computation are expected to be "random". Coherent state centred at the position $\mathbf{r}^* = (\sin \vartheta^* \cos \varphi^*, \sin \vartheta^* \sin \varphi^*, \cos \vartheta^*)$ is given by expansion

$$|\vartheta^*, \varphi^*\rangle = \sum_{m=-S}^S \binom{2S}{S+m}^{1/2} \cos^{S+m}(\vartheta^*/2) \sin^{S-m}(\vartheta^*/2) e^{-im\varphi^*} |m\rangle. \quad (2.26)$$

Equivalently, it can be written in terms of a complex parameter τ as

$$|\vartheta^*, \varphi^*\rangle = \frac{e^{-i\varphi^* S}}{(1 + |\tau|^2)^S} \exp(\tau S_-) |S\rangle, \quad \tau = e^{i\varphi^*} \tan(\vartheta^*/2), \quad (2.27)$$

with $S_\pm = S_x \pm iS_y$. In the semiclassical limit of large spin S the expansion coefficients of coherent state c_m go towards $c_m \asymp \exp(-S(m/S - z^*)^2/2(1 - z^{*2})) e^{-im\varphi^*}$. Coherent states have a well defined classical limit and this enables to compare the quantum fidelity for coherent initial states with the corresponding classical fidelity. The initial classical phase space density corresponding to a coherent state is (Fox & Elston, 1994)

$$\rho_{\text{clas}}(\vartheta, \varphi) = \sqrt{\frac{2S}{\pi}} \exp\{-S[(\vartheta - \vartheta^*)^2 + (\varphi - \varphi^*)^2 \sin^2 \vartheta]\}. \quad (2.28)$$

The above density is normalised as $\int \rho_{\text{clas}}^2 d\Omega = 1$.

2.1.2 The Jaynes-Cummings model

The Jaynes-Cummings model (Jaynes & Cummings, 1963; Tavis & Cummings, 1968), see also (Meystre & Sargent III, 1990, p. 336), is a system of a coupled harmonic oscillator and a spin. It can be realized experimentally in the cavity electrodynamics experiments (QED) by sending a beam of atoms through a cavity. The electromagnetic field in the cavity is quantized with the Hamiltonian $\hbar\omega a^\dagger a$, and the spin degree of freedom $\hbar\varepsilon S_z$ of atoms interacts with the electromagnetic field. The dominant interaction is a dipolar $\mathbf{d} \cdot \mathbf{E}$, with the monochromatic field $\mathbf{E} = \varepsilon E_0 (ae^{ikr} - a^\dagger e^{-ikr})$. For two level atoms only y-component of the dipole moment \mathbf{d} is nonzero and is proportional to $S_y = -\frac{1}{2}(S_+ - S_-)$. All this results in the Hamiltonian

$$H = \hbar\omega a^\dagger a + \hbar\varepsilon S_z + \frac{\hbar}{\sqrt{2S}} \{G(aS_+ + a^\dagger S_-) + G'(a^\dagger S_+ + aS_-)\}, \quad (2.29)$$

with boson lowering/raising operators a, a^\dagger , $[a, a^\dagger] = 1$. Planck's constant is chosen as $\hbar = 1/S$ so that the semiclassical limit is reached for $S \rightarrow \infty$. If we are close to a resonance $\omega = \varepsilon$ the rotating-wave approximation can be made in which the fast oscillating term G' can be neglected and only the G -term is retained (oscillating with small $\omega - \varepsilon$). In our discussion we will predominantly focus on this situation of $G' = 0$. In addition, frequencies ω and ε are usually in a GHz regime, while the coupling G is of the order of kHz and is therefore small. If either $G = 0$ or $G' = 0$ the model is integrable with an additional invariant being the difference or the sum of the spin and boson (harmonic oscillator) quanta.

The initial state will be always chosen as a product state of spin and boson coherent states. The spin coherent state is the same as above (2.26), while the coherent state for a boson is

$$|\alpha\rangle = e^{\alpha a^\dagger - \alpha^* a} |0\rangle = \exp(-|\alpha|^2/2) \sum_{k=0}^{\infty} \frac{\alpha^k}{\sqrt{k!}} |k\rangle, \quad (2.30)$$

with α being a complex parameter determining the position of the coherent state and $|k\rangle$ is an eigenstate of operator $a^\dagger a$ having k boson quanta. The classical density corresponding to the boson coherent initial state with a complex parameter $\alpha = \alpha_r + i\alpha_i$ is

$$\rho_{\text{class}}(q, p) = \sqrt{\frac{2S}{\pi}} \exp \left\{ -S \left[(q - \sqrt{2/S} \alpha_r)^2 + (p - \sqrt{2/S} \alpha_i)^2 \right] \right\}. \quad (2.31)$$

The normalisation is as usual $\int \rho_{\text{class}}^2 dq dp = 1$.

The classical Hamiltonian is obtained by taking the limit $S \rightarrow \infty$ and defining new canonical quantum operators, q_1 and p_1 for a boson and q_2 and p_2 for a spin

$$a = \sqrt{\frac{S}{2}}(q_1 + ip_1), \quad \sqrt{1 - p_2^2} e^{iq_2} = S_+/S. \quad (2.32)$$

They satisfy commutation relations $[q_1, p_1] = i\hbar$ and $[q_2, p_2] = i\hbar$. In the limit $S \rightarrow \infty$ they commute and can be replaced by the classical variables resulting in the classical Hamiltonian

$$H_{\text{class}} = \frac{\omega}{2}(p_1^2 + q_1^2) + \varepsilon p_2 + G_+ \sqrt{1 - p_2^2} q_1 \cos q_2 - G_- \sqrt{1 - p_2^2} p_1 \sin q_2 - \frac{\omega}{2S}, \quad (2.33)$$

with $G_\pm = G \pm G'$.

2.2 Average Fidelity

Sometimes the average fidelity is of interest, i.e. the fidelity averaged over some ensemble of initial states. Such an average fidelity is also more amenable to theoretical treatment. Easier to calculate is the average fidelity amplitude $f(t)$ which is of second order in the initial state $|\psi\rangle$ while the fidelity $F(t)$ is of fourth order in $|\psi\rangle$. We will show that the difference between the average fidelity amplitude and the average fidelity is semiclassically small.

In a finite Hilbert space the fidelity will not decay to zero but will instead fluctuate around some small plateau value. The value of this plateau equals to a time averaged fidelity. For ergodic systems this time averaged value equals to the phase space averaged one.

2.2.1 Time Averaged Fidelity

We want to calculate the value of fidelity in the limit $t \rightarrow \infty$ that is its asymptotic value for large time. For a finite Hilbert space size \mathcal{N} the fidelity will start to fluctuate for long times due to a discreteness of the spectrum of the evolution operator. The size of this fluctuations can be calculated by evaluating a time average fidelity \bar{F}

$$\bar{F} = \lim_{m \rightarrow \infty} \frac{1}{m} \sum_{t=0}^m F(t). \quad (2.34)$$

This is easily done if we expand the initial state in eigenbasis of the unperturbed propagator U_0 and denote the matrix elements between unperturbed and perturbed eigenstates by P_{kl}

$$U_0|\phi_l\rangle = \exp(-i\phi_l)|\phi_l\rangle, \quad U_\delta|\phi_l^\delta\rangle = \exp(-i\phi_l^\delta)|\phi_l^\delta\rangle, \quad P_{kl} = \langle\phi_k|\phi_l^\delta\rangle. \quad (2.35)$$

We denoted the eigenphases of unperturbed and perturbed one-step propagator with ϕ_l and ϕ_l^δ , respectively. The matrix P is unitary and in the case when both eigenvectors can be chosen to be real it is orthogonal. This happens if U_0 and U_δ commute with an antiunitary[‡] operator T whose square is identity[§]. The fidelity amplitude can now be written

$$f(t) = \sum_{lm} (P^\dagger \rho)_{lm} P_{ml} \exp(-i(\phi_l^\delta - \phi_m)t), \quad (2.36)$$

with $\rho_{lm} = \langle\phi_l|\rho(0)|\phi_m\rangle$ being the matrix elements of the initial density matrix in the unperturbed eigenbasis. To calculate the average fidelity \bar{F} we have to take the absolute value square of $f(t)$. Averaging over time t we will assume that the phases are nondegenerate

$$\overline{\exp(i(\phi_l^\delta - \phi_{l'}^\delta + \phi_m - \phi_{m'})t)} = \delta_{mm'}\delta_{ll'}. \quad (2.37)$$

This results in the average fidelity

$$\bar{F} = \sum_{ml} |(\rho P)_{ml}|^2 |P_{ml}|^2. \quad (2.38)$$

The time averaged fidelity therefore understandably depends on the initial state ρ as well as on the “overlap” matrix P .

[‡]Antiunitary operator must satisfy $\langle T\psi|T\phi\rangle = \langle\psi|\phi\rangle^*$.

[§]Square of an arbitrary antiunitary operator is $T^2 = \pm\mathbb{1}$. Time reversal operator for a system with spin is $T = \exp(-i\pi S_y)K$, with a complex conjugation operator K . If the system has an integer spin (or half-integer spin and an additional rotational invariance symmetry) we have $T^2 = \mathbb{1}$.

For *small perturbation* strengths, say δ smaller than some critical δ_{rm} , the unitary matrix P will be close to identity. Using $P \rightarrow \mathbb{1}$ for $\delta \ll \delta_{\text{rm}}$ (2.38) gives us

$$\bar{F}_{\text{weak}} = \sum_l \rho_{ll}^2. \quad (2.39)$$

One should keep in mind that for the above result \bar{F}_{weak} we needed eigenphases to be nondegenerate, $\phi_l^\delta \neq \phi_m$ (2.37), and at the same time $P \rightarrow \mathbb{1}$. This approximation is justified in the lowest order in δ , when off diagonal matrix elements are $|P_{ml}|^2 \propto \delta^2$.

On the other hand, for sufficiently *large* $\delta \gg \delta_{\text{rm}}$ and complex perturbations V one might assume P to be close to a random matrix with independent real or complex matrix elements P_{ml} . Then we can average expression (2.38) over a Gaussian distribution $\propto \exp(-\beta \mathcal{N} |P_{ml}|^2 / 2)$ of matrix elements P_{ml} , where we have $\beta = 1$ for orthogonal P and $\beta = 2$ for unitary P . This averaging gives $\langle |P_{ml}|^4 \rangle = (4 - \beta) / \mathcal{N}^2$ and $\langle |P_{ml}|^2 \rangle = 1 / \mathcal{N}$ for the variance of P_{ml} (brackets $\langle \bullet \rangle$ denote here averaging over the distribution of matrix elements and not over the initial state). The average fidelity for strong perturbation can therefore be expressed as

$$\bar{F}_{\text{strong}} = \frac{4 - \beta}{\mathcal{N}} \sum_l \rho_{ll}^2 + \frac{1}{\mathcal{N}} \sum_{l \neq m} |\rho_{lm}|^2. \quad (2.40)$$

The point of crossover δ_{rm} from weak (2.39) to strong (2.40) perturbation regime is system dependent and can not be discussed in general apart from expecting it to scale with \hbar similarly as a mean level spacing $\delta_{\text{rm}} \sim \hbar^d$. We will discuss the value of \bar{F} for three different initial states:

- (i) First, let us consider the simplest case when the initial state is an *eigenstate* of U_0 say, $\rho = |\phi_1\rangle\langle\phi_1|$ with matrix elements $\rho_{lm} = \delta_{l,1}\delta_{m,1}$. For *weak perturbations* this gives (2.39) $\bar{F}_{\text{weak}} = 1$, therefore the fidelity does not decay at all. This result can be generalised to the case when ρ is a superposition of a number of eigenstates, say K of them, all with approximately the same weight, so that one has diagonal density matrix elements of order $\rho_{ll} \sim 1/K$, resulting in $\bar{F}_{\text{weak}} \sim 1/K$. On the other hand, for *strong perturbation* $\delta \gg \delta_{\text{rm}}$ we get $\bar{F}_{\text{strong}} = (4 - \beta) / \mathcal{N}$ for an initial eigenstate. Summarising, for an initial eigenstate we have time averaged values of fidelity

$$\bar{F}_{\text{weak}} = 1, \quad \bar{F}_{\text{strong}} = (4 - \beta) / \mathcal{N}. \quad (2.41)$$

With this simple result we can easily explain the numerical result of Peres (Peres, 1995) where no-decay of fidelity was found for a coherent initial state sitting in the centre of an elliptic island, thus being a superposition of a very small number of eigenstates (it is almost an eigenstate). The behaviour in generic case may be drastically different as described in the present work.

- (ii) Second, consider the case of a *random pure* initial state $|\psi\rangle = \sum_m c_m |\phi_m\rangle$, giving $\rho_{ml} = c_m c_l^*$. The coefficients c_m are independent random complex Gaussian variables with variance $1/\mathcal{N}$, resulting in averages $\langle |\rho_{lm}|^2 \rangle = 1/\mathcal{N}^2$ for $m \neq l$ and $\langle \rho_{ll}^2 \rangle = 2/\mathcal{N}^2$ (average is over Gaussian distribution of c_m). Using this in expressions for average fidelity (2.39) and (2.40) we get

$$\bar{F}_{\text{weak}} = 2/\mathcal{N}, \quad \bar{F}_{\text{strong}} = 1/\mathcal{N}. \quad (2.42)$$

For random initial state there is therefore only a factor of 2 difference between finite size fluctuating plateau for weak and for strong perturbation. The result for weak perturbation agrees with the case (i) where we had $\bar{F}_{\text{weak}} \sim 1/K$ if there were K participating eigenvectors.

- (iii) Third, for a *uniform average* over the whole Hilbert space, i.e. taking a non-pure initial density matrix $\rho = \mathbb{1}/\mathcal{N}$, we have

$$\bar{F}_{\text{weak}} = 1/\mathcal{N}, \quad \bar{F}_{\text{strong}} = (4 - \beta)/\mathcal{N}^2. \quad (2.43)$$

As expected, the fluctuating plateau is the smallest for an uniform average over the whole Hilbert space and strong perturbation.

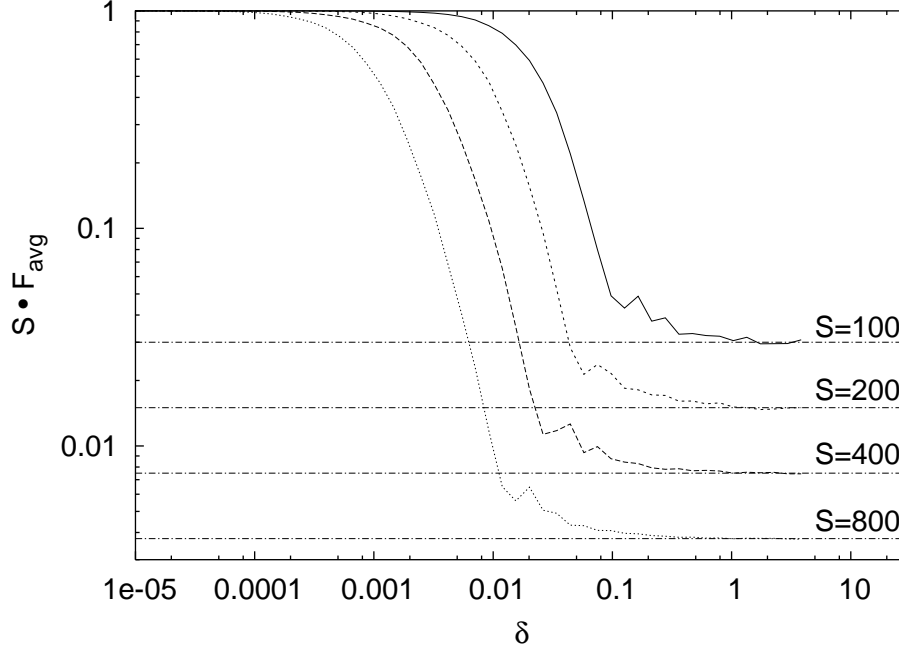


Figure 2.1: Dependence of time averaged fidelity (multiplied by the Hilbert space size $\mathcal{N} = S$) \bar{F} on δ is shown for a chaotic kicked top system and Hilbert space average $\rho = \mathbb{1}/\mathcal{N}$, i.e. our case (iii). The transition from weak to strong perturbation regime is seen (2.43). Horizontal full lines are the theoretical predictions \bar{F}_{strong} (2.43), while the theoretical result for the weak regime corresponds to 1.

Observe that the average fidelity \bar{F} (2.38) is of fourth order in matrix elements of P , the same as the inverse participation ratio (IPR) of the perturbed eigenstates. Actually, in the case of initial eigenstate, our case (i), the average fidelity (2.38) can be rewritten as $\bar{F} = \sum_m |P_{1m}|^4$, exactly the IPR. The inverse of the IPR is a number between 1 and \mathcal{N} which can be thought of as giving the approximate number of unperturbed eigenstates represented in the expansion of a given perturbed eigenstate. For an average over the whole space, case (iii), we have instead $\bar{F} = \sum_{l,m} |P_{lm}|^4 / \mathcal{N}^2$, i.e. the average IPR divided by \mathcal{N} . The time averaged fidelity is thus directly related to the *localisation* properties of eigenstates of U_δ in terms of eigenstates of U_0 . However, except for the pathological case of the initial state being a small combination of eigenstates of U_0 with weak perturbation, the fidelity fluctuation is always between the limiting values $2/\mathcal{N}$, and $3/\mathcal{N}^2$. Therefore, the fidelity will decay only until it reaches the value of finite size fluctuations and will fluctuate around \bar{F} thereafter. The time t_∞ when this happens, $F(t_\infty) = \bar{F}$, depends on the decay of fidelity and will be discussed in subsequent chapters.

To illustrate the above theory we have calculated the average fidelity (2.38) for a kicked top with a propagator (2.20). As an initial state we used $\rho = \mathbb{1}/\mathcal{N}$, i.e. the case (iii), where the Hilbert space size is determined by the spin value, $\mathcal{N} = S$ (OE subspace). We calculated the

dependence of \bar{F} on δ for two cases: a chaotic one for kicked top parameters $\alpha = 30$, $\gamma = \pi/2$ shown in Figure 2.1 and a regular one for $\alpha = 0.1$, $\gamma = \pi/2$ shown in Figure 2.2. In both cases one can see a transition from the weak perturbation regime $\bar{F}_{\text{weak}} = 1/\mathcal{N}$ to the strong regime $\bar{F}_{\text{strong}} = 3/\mathcal{N}^2$ for large δ . In the chaotic case the critical δ_{rm} can be seen to scale as $\delta_{\text{rm}} \sim \hbar = 1/S$. In the regular situation, the strong perturbation regime is reached only for a strong perturbation $\delta \sim 4$, where the propagator U_δ itself becomes chaotic. Namely, the transition from the regular to chaotic regime in the kicked top happens at around $\alpha = 3$, see e.g. (Peres, 1995). Still, if one defines δ_{rm} as the points where the deviation from the weak regime starts (point of departure from 1 in Figure 2.2) one has scaling $\delta_{\text{rm}} \sim 1/S$ also in the regular regime.

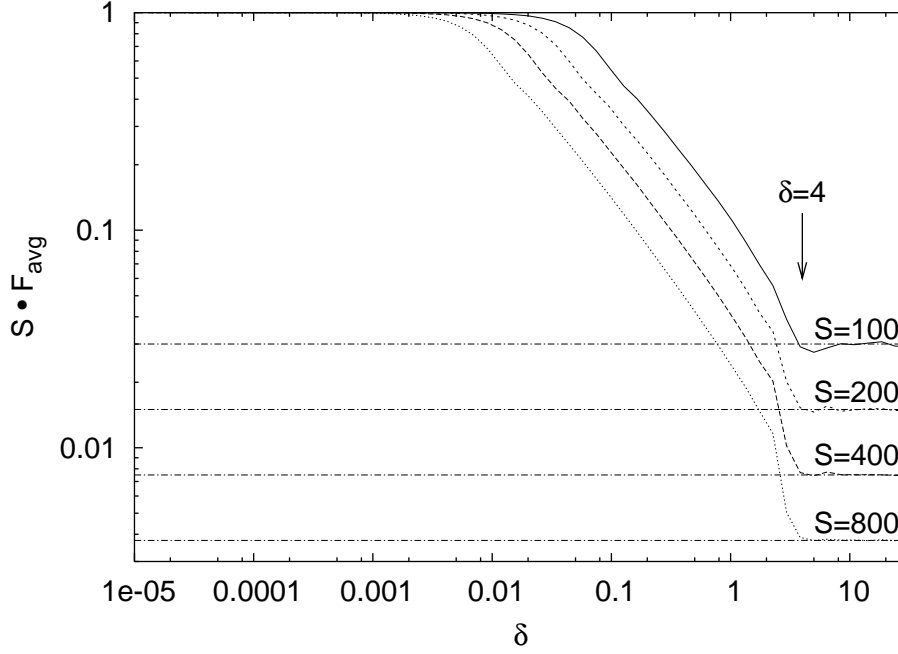


Figure 2.2: The same as Figure 2.1 but for a regular kicked top.

2.2.2 State Averaged Fidelity

In previous section we used the initial density matrix $\rho(0) = \mathbb{1}/\mathcal{N}$ in expression (2.9) for the fidelity amplitude to calculate the average fidelity over the whole Hilbert space. As the fidelity is of fourth order in the initial state $|\psi(0)\rangle$, whereas the fidelity amplitude is bilinear in $|\psi(0)\rangle$ the average fidelity is not equal to the quantity obtained by first averaging fidelity amplitude and subsequently squaring it. In general the difference between the two depends on the ensemble of states over which we average.

Let us look only at the simplest case of averaging over random initial states, denoted by $\langle\langle \bullet \rangle\rangle$. In the asymptotic limit of large Hilbert space size $\mathcal{N} \rightarrow \infty$ the averaging is simplified by the fact that the expansion coefficients c_m of a random initial state in an arbitrary basis become independent Gaussian variables with variance $1/\mathcal{N}$. Quantities bilinear in the initial state, like the fidelity amplitude or the correlation function, result in the following expression

$$\langle\langle \psi | A | \psi \rangle\rangle =: \langle\langle A \rangle\rangle = \langle\langle c_m^* A_{ml} c_l \rangle\rangle = \frac{1}{\mathcal{N}} \text{tr} A, \quad (2.44)$$

where A is an arbitrary operator. The averaging is done simply by means of a trace over the

whole Hilbert space. For the fidelity $F(t)$ which is of fourth order in $|\psi\rangle$ we get

$$\langle\langle F(t) \rangle\rangle = \langle\langle c_m^* [M_\delta(t)]_{ml} c_l c_p [M_\delta(t)]_{pr}^* c_r^* \rangle\rangle = |\langle\langle f(t) \rangle\rangle|^2 + \frac{1}{N}. \quad (2.45)$$

The difference between the average fidelity and the average fidelity amplitude is therefore semi-classically small (Prosen *et al.*, 2003c).

There are two reasons why averaging over random initial states is of interest. First, in the field of quantum information processing this are the most interesting states as they have the least structure, i.e. can accomodate the largest amount of information. Second, for ergodic dynamics and sufficiently long times one can replace expectation values in a specific generic state $|\psi\rangle$ by an ergodic average. If the system is ergodic on the whole space one can calculate the correlation function $C(j, k)$ (2.18) by means of a simple trace (2.44), so that it does not depend on the initial state, or even calculate it classically in the leading semiclassical order, which greatly simplifies theoretical derivations[¶]. For regular systems, where the decay of fidelity depends on the initial state, the ergodic averaging differs from the average in a specific initial state, although one can still be interested in the behaviour of the average fidelity. Such an averaging will be discussed in the section describing the decay of fidelity in regular systems.

We have seen that for sufficiently large Hilbert spaces there is no difference between averaging the fidelity amplitude or the fidelity or taking a single random initial state. For mixing dynamics the long time fidelity decay is independent of the initial state even if it is a non-random, whereas in the regular regime it is state dependent. For instance, the long time Gaussian decay (Section 3.2.2) depends on the position of the initial coherent state. The fidelity averaged over this position of the initial coherent state might be of interest and will not be equal to the fidelity averaged over random initial states. We will discuss averaging over coherent states at the end of Section 3.2.2 describing long time fidelity decay for coherent initial states.

[¶]In the case of autonomous systems the canonical or micro-canonical averaging should be used instead.

Chapter 3

General Perturbation

An expert is a person who has made all the mistakes that can be made in a very narrow field.

—Niels Bohr

3.1 Mixing Dynamics

Here we assume that the system is mixing such that the correlation function of the perturbation V decays sufficiently fast; this typically (but not necessarily) corresponds to globally chaotic classical motion. Due to *ergodicity* we will assume the initial density matrix to be $\rho(0) = \mathbb{1}/\mathcal{N}$, so that all averages over a specific initial state can be replaced by a full Hilbert space average, $\langle . \rangle = \text{tr}(.)/\mathcal{N}$ (Section 2.2.2). For any other initial state (e.g. in the worst case for the minimal wave packet – coherent state) one obtains identical results on $F(t)$ for sufficiently long times*, i.e. longer than the *Ehrenfest* time $t_E \approx \ln(1/\hbar)/\lambda$ (for a classically chaotic system with maximal Lyapunov exponent λ) needed for a minimal wave packet to spread effectively over the accessible phase space (Berman & Zaslavsky, 1978). The state averaged quantum correlation function is homogeneous in time, i.e. $C(j, k) = C(k - j)$, so we simplify the second order linear response formula for the fidelity (2.17)

$$F(t) = 1 - \frac{\delta^2}{\hbar^2} \left\{ tC(0) + 2 \sum_{j=1}^{t-1} (t-j)C(j) \right\} + \mathcal{O}(\delta^4). \quad (3.1)$$

If the decay of the correlation function $C(j)$ is sufficiently fast, namely if its integral converges on a certain characteristic *mixing time* scale t_{mix} , then the above formula can be further simplified. For times $t \gg t_{\text{mix}}$ we can neglect the second term under the summation in (3.1) and obtain a linear fidelity decay in time t (in the linear response)

$$F(t) = 1 - 2(\delta/\hbar)^2 \sigma t, \quad (3.2)$$

with the transport coefficient σ being

$$\sigma = \frac{1}{2}C(0) + \sum_{j=1}^{\infty} C(j) = \lim_{t \rightarrow \infty} \frac{\langle \Sigma^2(t) \rangle - \langle \Sigma(t) \rangle^2}{2t}. \quad (3.3)$$

*The exception might be systems with localized states.

In the continuous time case σ is just the integral of the correlation function. Note that σ has a well defined classical limit obtained from the classical correlation function and in the semiclassical limit this classical σ_{cl} will agree with the quantum one.

We can make a stronger statement in a non-linear-response regime if we make an additional assumption on the factorisation of higher order time-correlations, n -point mixing. This implies that $2m$ -point correlation $\langle V(j_1) \cdots V(j_{2m}) \rangle$ is appreciably different from zero for $j_{2m} - j_1 \rightarrow \infty$ only if all (ordered) time indices $\{j_k, k = 1 \dots 2m\}$ are *paired* with the time differences within each pair, $j_{2k} - j_{2k-1}$, being of the order or less than t_{mix} . Then we can make a further reduction, namely if $t \gg m t_{\text{mix}}$ the terms in the expansion of the fidelity amplitude $f(t)$ (2.16) are

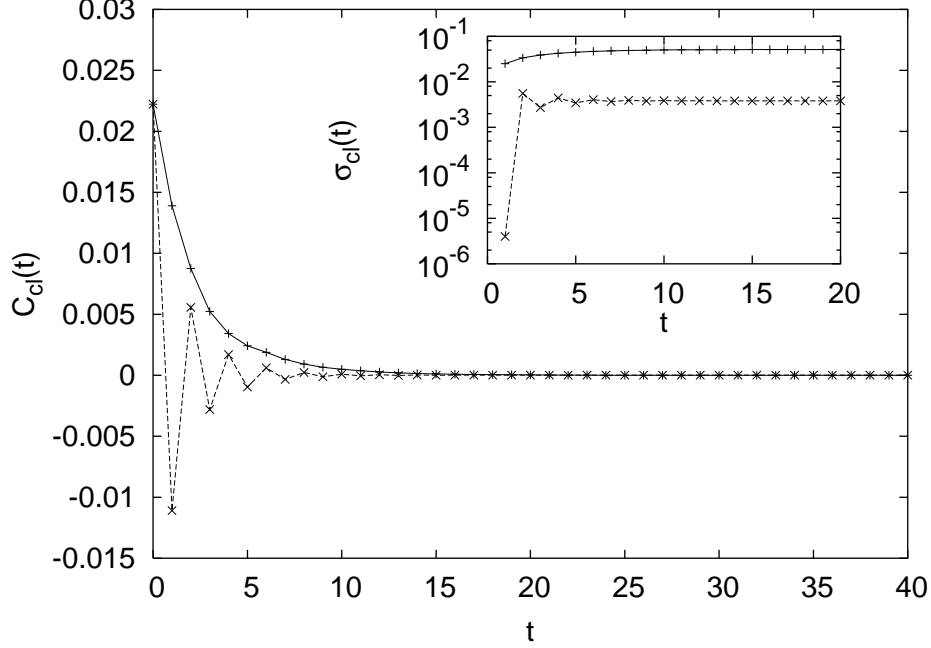


Figure 3.1: The classical correlation function (2.18) of perturbation V (3.6) for chaotic kicked top and $\gamma = \pi/6$ (top solid curve) and $\gamma = \pi/2$ (bottom broken curve). The finite time integrated correlation function is shown in the inset.

$$\begin{aligned}
 & \mathcal{T} \sum_{j_1, \dots, j_{2m}=0}^{t-1} \langle V(j_1) V(j_2) \cdots V(j_{2m}) \rangle \rightarrow \\
 & \rightarrow \mathcal{T} \sum_{j_1, \dots, j_{2m}=0}^{t-1} \langle V(j_1) V(j_2) \rangle \cdots \langle V(j_{2m-1}) V(j_{2m}) \rangle \rightarrow \frac{(2m)!}{m! 2^m} (2\sigma t)^m.
 \end{aligned} \tag{3.4}$$

The fidelity amplitude is therefore $f(t) = \exp(-\delta^2 \sigma t / \hbar^2)$ and the fidelity is

$$F(t) = \exp(-t/\tau_m), \quad \tau_m = \frac{\hbar^2}{2\delta^2 \sigma_{\text{cl}}}, \tag{3.5}$$

with a mixing decay time-scale $\tau_m = \mathcal{O}(\delta^{-2})$ and a classical limit of the transport coefficient σ_{cl} . We should stress again that the above result (3.5) has been derived under the assumption of true quantum mixing which can be justified only in the limit $\mathcal{N} \rightarrow \infty$, e.g. either in the semiclassical or the thermodynamic limit. Thus for the true quantum-mixing dynamics the fidelity will decay exponentially. The same result has been derived also by a quite different

approach, using a Fermi golden rule (Jacquod *et al.*, 2001; Cerruti & Tomsovic, 2002). That is why this regime of exponential fidelity decay is sometimes called a Fermi golden rule regime.

To numerically check the above exponential decay, we will use the kicked top (2.20) with parameter $\alpha = 30$, giving a totally chaotic classical dynamics. As argued before, one can calculate the transport coefficient σ (3.3) by using the classical correlation function of the perturbation (2.22),

$$V_{\text{cl}} = v = \frac{1}{2}z^2. \quad (3.6)$$

We consider two different values of kicked top parameter γ , namely $\gamma = \pi/2$ and $\gamma = \pi/6$. The classical correlation functions can be seen in Figure 3.1. The correlation function (obtained by averaging over 10^5 initial conditions on a sphere) is shown in the main frame. The correlation functions have qualitatively different decay towards zero for the two chosen γ 's. In the inset the convergence of classical σ (3.3) is shown, where one can see that the mixing time is $t_{\text{mix}} \sim 5$. The values of σ_{cl} are $\sigma_{\text{cl}} = 0.00385$ for $\gamma = \pi/2$ and $\sigma_{\text{cl}} = 0.0515$ for $\gamma = \pi/6$. These values

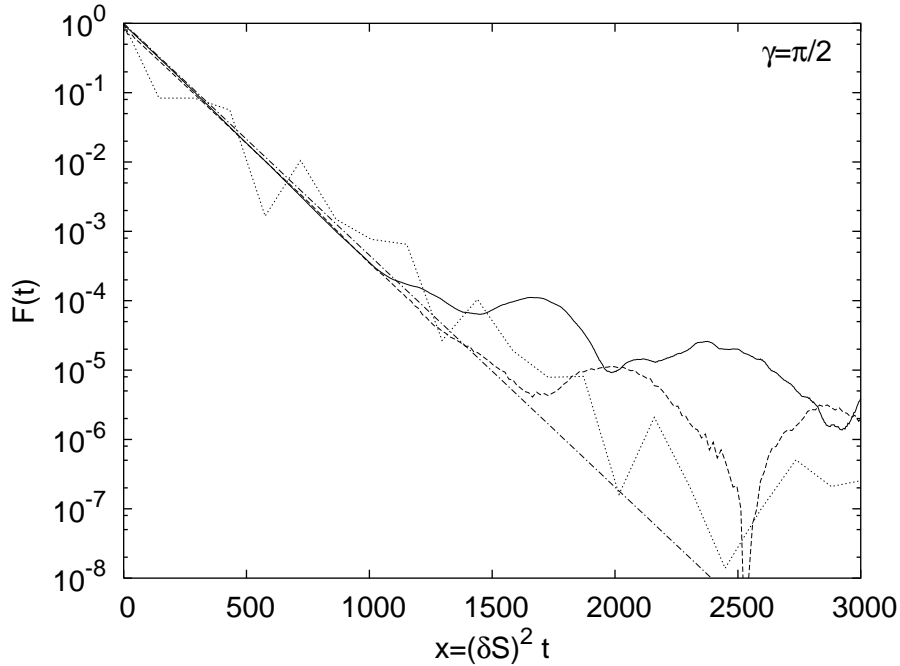


Figure 3.2: Quantum fidelity decay in the chaotic regime for $\gamma = \pi/2$ and three different perturbation strengths $\delta = 5 \times 10^{-4}$, 1×10^{-3} and 3×10^{-3} (solid, dashed and dotted curves, respectively) is shown. The chain line gives theoretical decay (3.5) with the classically calculated σ seen in Figure 3.1.

are used to calculate the theoretical decay of fidelity $F(t) = \exp(-\delta^2 S^2 2\sigma_{\text{cl}} t)$ (3.5) which is compared with the numerical simulation in Figures 3.2 and 3.3. We used averaging over the whole Hilbert space, $\rho(0) = \mathbb{1}/\mathcal{S}$ and checked that that due to ergodicity there was no difference for large S if we choose a fixed initial state, say a coherent state. As fidelity will decay only until it reaches its finite size fluctuating value \bar{F} (2.43) we choose a large $S = 4000$ in order to be able to check exponential decay over as many orders of magnitude as possible. In Figure 3.2 the decay of quantum fidelity is shown for $\gamma = \pi/2$. The agreement with the theory is excellent. Note that the largest δ shown corresponds to $\tau_m \sim 1$ so the condition for n -point mixing $t \gg t_{\text{mix}}$ is no longer satisfied. The agreement with theory is still good due to the oscillatory nature of the correlation decay (see Figure 3.1) fulfilling the factorisation assumption (3.4) on

average. In Figure 3.3 for $\gamma = \pi/6$ a similar decay can be seen. In both cases fidelity starts to

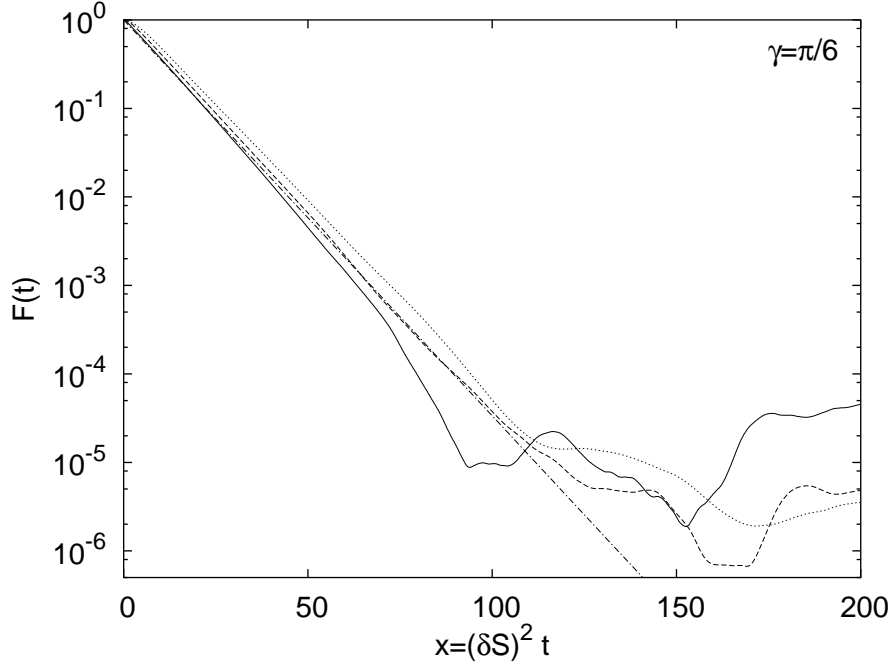


Figure 3.3: Similar figure as 3.2, only for $\gamma = \pi/6$ and perturbation strengths $\delta = 1 \times 10^{-4}$, 2×10^{-4} and 3×10^{-4} (solid, dashed and dotted curves, respectively).

fluctuate around \bar{F} calculated in the section 2.2.1 for times larger than t_∞ .

3.1.1 Long Time Behaviour

We assumed that the quantum correlation function $C(j)$ decays to zero and its integral converges to σ . For a system having a finite Hilbert space of size \mathcal{N} , the correlation function asymptotically does not decay but has a non-vanishing plateau \bar{C} due to finite \mathcal{N} , similarly as we have a finite asymptotic value of the fidelity \bar{F} . This will cause the double correlation sum to grow quadratically with time. Because this plateau \bar{C} is small, the quadratic growth will overtake linear growth $2\sigma_{\text{cl}}t$ only for large times. The time averaged correlation function $C(j, k)$ (2.18) can be calculated assuming a nondegenerate unperturbed spectrum ϕ_k as

$$\bar{C} = \lim_{t \rightarrow \infty} \frac{1}{t^2} \sum_{j,k=0}^{t-1} C(j, k) = \sum_k \rho_{kk} (V_{kk})^2 - \left(\sum_k \rho_{kk} V_{kk} \right)^2, \quad (3.7)$$

where ρ_{kk} are diagonal matrix elements of the initial density matrix $\rho(0)$ and V_{kk} are diagonal matrix elements of the perturbation V in the eigenbasis of the unperturbed propagator U_0 . One can see that \bar{C} depends only on the diagonal matrix elements[†], in fact it is equal to the variance of the diagonal matrix elements. Since the classical system is ergodic and mixing, we will use a version of the *quantum chaos conjecture* (Feingold & Peres, 1986; Wilkinson, 1987; Feingold *et al.*, 1989; Prosen & Robnik, 1993; Prosen, 1994) saying that V_{mn} are independent Gaussian random variables with a variance given by the Fourier transformation $S(\omega)$ (divided by \mathcal{N}) of the corresponding classical correlation function $C_{\text{cl}}(j)$ at frequency $\omega = \phi_m - \phi_n$. On

[†]The case when diagonal matrix elements are zero is the subject of Chapter 4.

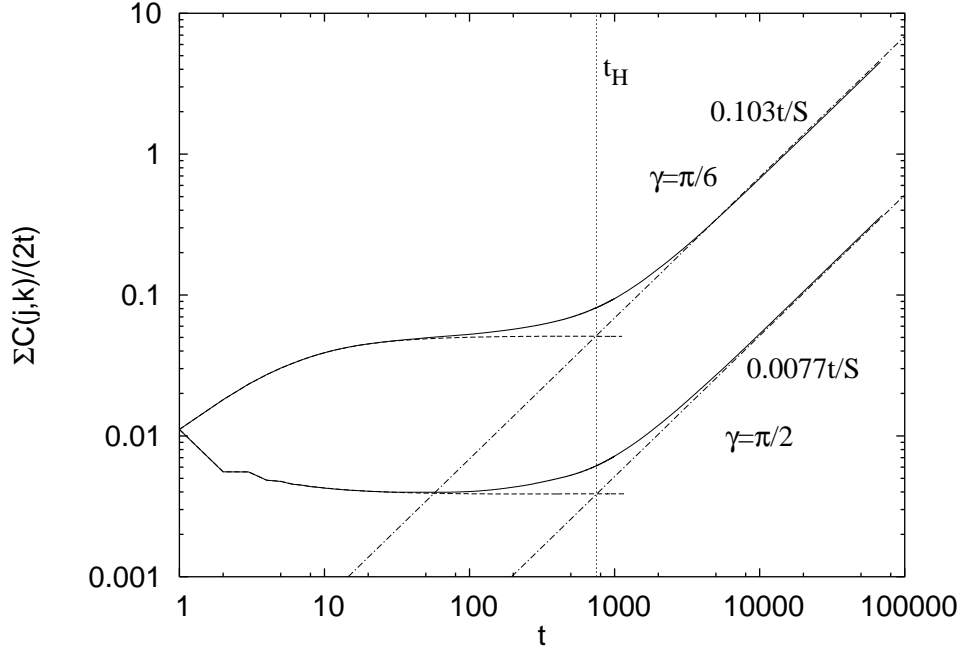


Figure 3.4: The finite time quantum correlation sum $\sigma(t) = \sum_{j,k=0}^{t-1} C(j,k)/2t$ (solid curves) together with the corresponding classical sum $\sigma_{cl}(t) = \sum_{j,k=0}^{t-1} C_{cl}(j,k)/2t$ (dashed curves saturating at σ_{cl} and ending at $t \sim 1000$) is shown for the chaotic kicked top. Quantum data are for a full trace $\rho = \mathbb{1}/\mathcal{N}$ with $S = 1500$. Upper curves are for $\gamma = \pi/6$ while lower curves are for $\gamma = \pi/2$. Chain lines are best fits for asymptotic linear functions corresponding to $\bar{C}t/2 = 0.0077t/S$ for $\gamma = \pi/2$ and $0.103t/S$ for $\gamma = \pi/6$.

the diagonal we have $\omega = 0$ and an additional factor of 2 due to random matrix measure on the diagonal. Using $2\sigma_{cl}t = \sum_{j,k}^t C(j,k) = S(0)t$ we can write

$$\bar{C} = \frac{2S(0)}{\mathcal{N}} = \frac{4\sigma_{cl}}{\mathcal{N}}. \quad (3.8)$$

Because of ergodicity, for large \mathcal{N} , \bar{C} does not depend on the statistical operator ρ used in the definition of the correlation function, provided we do not take some non generic state like a single eigenstate $|\phi_k\rangle$ for instance. Note that Equation (3.8) is valid on a single quantum invariant subspace. If U_0 has symmetries, so that its Hilbert space is split into s components of sizes \mathcal{N}_j , the average \bar{C} will be different on different subspaces, $\bar{C}_j = 4\sigma_{cl}/\mathcal{N}_j$. Averaging over all invariant subspaces then gives

$$\bar{C} = \frac{4s\sigma_{cl}}{\mathcal{N}}, \quad (3.9)$$

so that \bar{C} is increased by a factor s compared to the situation with only a single subspace. The fidelity decay will start to be dominated by the average plateau (3.8) at time t_H when the quadratic growth takes over, $\bar{C}t_H^2 \approx 2\sigma_{cl}t_H$,

$$t_H = \frac{1}{2}\mathcal{N} \propto \hbar^{-d}, \quad (3.10)$$

which is nothing but the *Heisenberg time* associated with the inverse density of states. Again, if one has s invariant subspaces, the Heisenberg time is $t_H = \mathcal{N}/2s$. This crossover time agrees with the result of Cerruti & Tomsovic (2002) and for random matrix models with Gorin *et al.* (2004).

In Figure 3.4 we show numerical calculation of the correlation sum for the chaotic kicked top at $\alpha = 30$. We compare the classical correlation sum (the same data as in Figure 3.1) and quantum correlation sum. One can nicely see the crossover from linear growth of quantum correlation sum $2\sigma_{\text{cl}}t$ for small times $t < t_H$, to the asymptotic quadratic growth due to correlation plateau \bar{C} . In addition, numerically fitted asymptotic growth $0.103t/S$ and $0.0077t/S$ nicely agree with formula for \bar{C} , using $\mathcal{N} = S$ and classical values of transport coefficients $\sigma_{\text{cl}} = 0.0515$ and 0.00385 for $\gamma = \pi/6$ and $\gamma = \pi/2$, respectively.

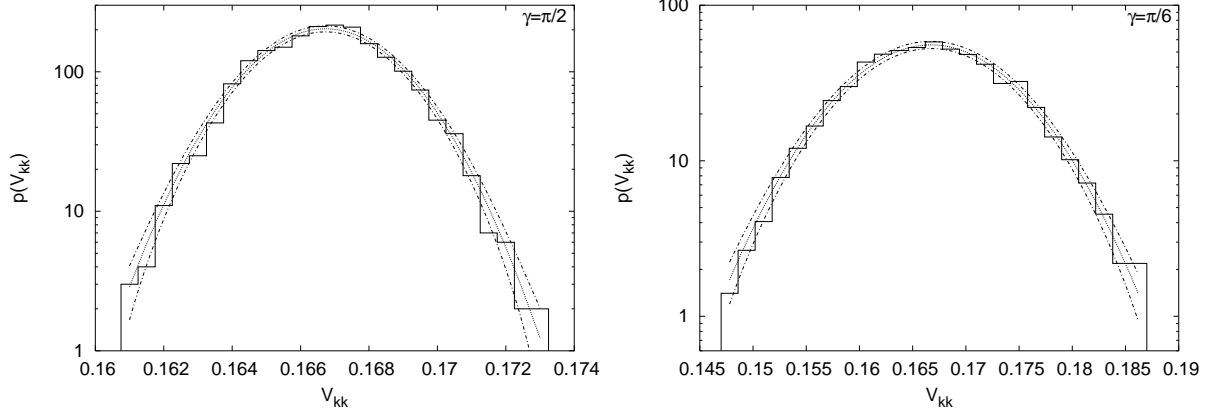


Figure 3.5: Histogram of the normalised distribution of the diagonal matrix elements V_{kk} for the chaotic kicked top and $S = 4000$ on OE subspace (2.24). The dotted line is the theoretical Gaussian distribution with the second moment \bar{C} and the two chain lines are expected $\sqrt{N_i}$ statistical deviations if there are N_i elements in the i -th bin. Note the different x -ranges in two figures due to different σ_{cl} for the two chosen γ .

For times $t > t_H$, and provided δ is sufficiently small, the correlation sum will grow quadratically and the linear response fidelity reads

$$F(t) = 1 - \frac{\delta^2}{\hbar^2} \frac{4\sigma_{\text{cl}}}{\mathcal{N}} t^2. \quad (3.11)$$

To derive the decay of fidelity beyond the linear response regime one needs higher order moments of diagonal elements of perturbation V . If we use the BCH form of the echo operator (2.14) and discard the term involving $\ddagger \Gamma(t)$, we have the fidelity amplitude $f(t) = \sum_k \exp(-iV_{kk}\delta t/\hbar)/\mathcal{N}$, where we choose an ergodic average $\rho = 1/\mathcal{N}$. In the limit $\mathcal{N} \rightarrow \infty$ we can replace the sum with an integral over the probability distribution of diagonal matrix elements $p(V_{kk}) = p(V)$,

$$f(t) = \int dV p(V) \exp(-iV\delta t/\hbar). \quad (3.12)$$

For long times the fidelity amplitude is therefore a Fourier transformation of the distribution of diagonal matrix elements. For classically mixing systems the distribution is conjectured to be Gaussian with the second moment equal to \bar{C} (3.8). This is confirmed by numerical data in Figure 3.5. The mean value of diagonal matrix elements is perturbation specific and is for our choice of the perturbation (2.22) $\sum_k V_{kk}/(2S+1) = (2S+1)(S+1)/12S^2$. From the figure we can see that the distribution is indeed Gaussian with the variance agreeing with the theoretically predicted $\bar{C} = 4\sigma_{\text{cl}}/S$. The Fourier transformation of a Gaussian is readily calculated and we

[‡]in Chapter 4 we will see that the size of $\Gamma(t)$ term grows at most linearly with time and so can be neglected because of δ^2 prefactor.

get a Gaussian fidelity decay

$$F(t) = \exp\left(-(t/\tau_p)^2\right), \quad \tau_p = \sqrt{\frac{\mathcal{N}}{4\sigma_{\text{cl}}}} \frac{\hbar}{\delta}. \quad (3.13)$$

In order to see a Gaussian fidelity decay for mixing systems the perturbation strength δ must be sufficiently small. If it is not, the fidelity will decay exponentially (3.5) to its fluctuating plateau \bar{F} before time t_H when the Gaussian decay starts. Demanding that the mixing decay time τ_m is smaller than $t_H = \mathcal{N}/2$ gives the critical perturbation strength δ_p ,

$$\delta_p = \frac{\hbar}{\sqrt{\sigma_{\text{cl}}\mathcal{N}}}. \quad (3.14)$$

For $\delta < \delta_p$ we will have a Gaussian decay (3.13) otherwise the decay will be exponential (3.5), for details see Section 3.3.

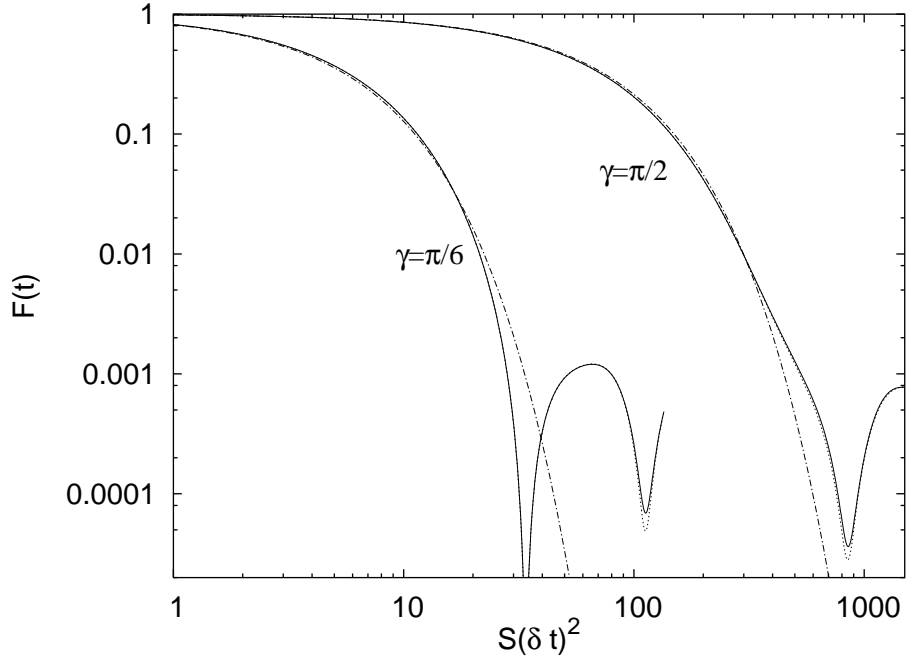


Figure 3.6: Quantum fidelity decay for $\delta < \delta_p$ in the chaotic regime. For $\gamma = \pi/2$ data for $\delta = 1 \cdot 10^{-6}$ (solid curve) and $5 \cdot 10^{-6}$ (dotted curve) are shown. For $\gamma = \pi/6$, $\delta = 3 \cdot 10^{-7}$ (solid) and $1 \cdot 10^{-6}$ (dotted) are shown. Note that for both γ the curves for both δ practically overlap. The chain curves are theoretical predictions (3.13) with classically computed σ_{cl} .

Again we numerically checked the predicted Gaussian decay for the chaotic kicked top with $\alpha = 30$ and $S = 1500$ and a full trace average over Hilbert space. The results of numerical simulation, together with the theory are shown in Figure 3.6.

The regime of Gaussian decay is sometimes referred to as the perturbative regime (Cerruti & Tomsovic, 2002; Jacquod *et al.*, 2001) because it can be derived using the lowest order perturbation theory. Writing first order corrections in phases $\phi_k^\delta = \phi_k + V_{kk}\delta/\hbar$ and for overlap matrix $P_{kl} = \delta_{kl} + \mathcal{O}(\delta)$ (2.36) one gets the Fourier transform formula (3.12).

3.2 Regular Dynamics

As opposed to mixing dynamics which was characterised by a linear growth of the double sum of the correlation function, the regular regime will typically exhibit *quadratic* growth. By a

regular regime we again refer to the behaviour of the correlation function. Typically, its double sum will exhibit quadratic growth for integrable or mixed (KAM) systems. In such case, we can define a time average correlation function, denoted by \bar{C}

$$\bar{C} = \lim_{t \rightarrow \infty} \frac{1}{t^2} \sum_{j,k=0}^{t-1} C(j,k). \quad (3.15)$$

For nonzero \bar{C} we will call this a “regular regime”. Of course, we have \mathcal{N} -dependent nonzero value of \bar{C} also in mixing systems (3.8), as discussed in Section 3.1.1. Here we consider only systems where \bar{C} exists in the limit of $\mathcal{N} \rightarrow \infty$, i.e. nonzero \bar{C} is a consequence of the dynamics and not of the finite Hilbert space size. Due to non-ergodicity all expectation values (like \bar{C}) depend on the initial state, and we can not use ergodic average over the whole Hilbert space as for mixing dynamics. The time in which time averaging of the correlation function converges will be denoted by t_{ave} . For times $t \gg t_{\text{ave}}$ the linear response fidelity decays quadratically in time

$$F(t) = 1 - \frac{\delta^2}{\hbar^2} \bar{C} t^2. \quad (3.16)$$

In contrast to the mixing regime one does not need any further assumptions in order to go beyond the linear response formula. Namely, for times $t \gg t_{\text{ave}}$ we can define a time average perturbation \bar{V}

$$\bar{V} = \lim_{t \rightarrow \infty} \frac{1}{t} \sum_{k=0}^{t-1} V(k) = \lim_{t \rightarrow \infty} \frac{\Sigma(t)}{t}. \quad (3.17)$$

Observe that \bar{V} is by construction a constant of motion, $[\bar{V}, U_0] = 0$. In a mixing regime \bar{V} is trivial (in the limit $\mathcal{N} \rightarrow \infty$), i.e. proportional to the identity[§], whereas for regular dynamics nontrivial \bar{V} exists. The special case of $\bar{V} = 0$ will be considered in Chapter 4. In the case of nondegenerate spectrum of the unperturbed propagator U_0 , the time average is simply the diagonal part of V in the eigenbasis $|\phi_k\rangle$ of the unperturbed propagator, namely

$$\bar{V} = \sum_k V_{kk} |\phi_k\rangle \langle \phi_k|, \quad (3.18)$$

where as usual $V_{kk} = \langle \phi_k | V | \phi_k \rangle$. Note that the average correlation function is

$$\bar{C} = \langle \bar{V}^2 \rangle - \langle \bar{V} \rangle^2. \quad (3.19)$$

For times $t \gg t_{\text{ave}}$ the operator $\Sigma(t)$ is dominated by the linearly growing term $\bar{V}t$ and one can neglect contributions not growing with time. The BCH form of the echo operator can therefore be simply written as

$$M_\delta(t) = \exp(-i\bar{V}\delta t/\hbar), \quad t \gg t_{\text{ave}}, \quad (3.20)$$

where we neglected the term $\sim \Gamma(t)\delta^2$ as it becomes important only at large times $\sim 1/\delta^2$, whereas the first term will cause the fidelity to decay already in time $\sim 1/\delta$. The above form of the echo operator will be the main ingredient of theoretical calculation of the fidelity decay in the regular regime.

As the operator \bar{V} commutes with the unperturbed propagator it is diagonal in the eigenbasis $|\phi_k\rangle$. In integrable systems the basis states $|\phi_k\rangle$ can be ordered in a very special way. Namely, there exist quantum numbers which are eigenvalues of canonical action operators having a very simple algebra. Using action-angle operators will make derivations easier and will furthermore enable us to use classical action-angle variables in the leading semiclassical order, thereby approximating quantum fidelity in classical terms. So before proceeding with the evaluation of $f(t)$ for various initial states, let us have a look at action-angle operators.

[§] Actually it can be made zero by subtracting from V the identity operator which only rotates a phase of the fidelity amplitude and does not affect the fidelity itself.

3.2.1 Action-angle Operators

Since we assume the classical system to be completely integrable (at least locally, by KAM theorem, in the phase space part of interest) we can employ action-angle variables, $\{j_k, \theta_k, k = 1 \dots d\}$, in d degrees of freedom system. In the present section, dealing with the regular regime as well as in Section 4.2.1 describing quantum freeze of fidelity in regular systems, we shall use lowercase letters to denote *classical variables* and capital letters to denote the corresponding *quantum operators*. For instance, the quantum Hamiltonian will be given as $H(\mathbf{J}, \boldsymbol{\Theta})$ whereas its classical limit will be written as $h(\mathbf{j}, \boldsymbol{\theta})$.

As our unperturbed Hamiltonian is integrable, it is a function of actions only, i.e. $h_0 = h_0(\mathbf{j})$. The solution of classical equations of motion is very simple,

$$\begin{aligned} \mathbf{j}(t) &= \mathbf{j}, \\ \boldsymbol{\theta}(t) &= \boldsymbol{\theta} + \boldsymbol{\omega}(\mathbf{j})t \pmod{2\pi} \end{aligned} \quad (3.21)$$

with a dimensionless frequency vector

$$\boldsymbol{\omega}(\mathbf{j}) := \frac{\partial h_0(\mathbf{j})}{\partial \mathbf{j}}. \quad (3.22)$$

The classical limit $v(\mathbf{j}, \boldsymbol{\theta})$ of our perturbation generator V can be written as a Fourier series

$$v(\mathbf{j}, \boldsymbol{\theta}) = \sum_{\mathbf{m} \in \mathbb{Z}^d} v_{\mathbf{m}}(\mathbf{j}) e^{i\mathbf{m} \cdot \boldsymbol{\theta}}, \quad (3.23)$$

where a multi-index \mathbf{m} has d components. The classical limit of the time-averaged perturbation \bar{V} is $\bar{v} = v_0(\mathbf{j})$, i.e. just the zeroth Fourier mode of the perturbation.

In quantum mechanics, one quantises the action-angle variables using the famous EBK procedure (see e.g. (Berry, 1977)) where one defines the action (momentum) operators \mathbf{J} and angle operators $\exp(i\mathbf{m} \cdot \boldsymbol{\Theta})$ satisfying the canonical commutation relations,

$$[J_k, \exp(i\mathbf{m} \cdot \boldsymbol{\Theta})] = \hbar m_k \exp(i\mathbf{m} \cdot \boldsymbol{\Theta}), \quad k = 1, \dots, d. \quad (3.24)$$

As the action operators are mutually commuting they have a common eigenbasis $|\mathbf{n}\rangle$ labelled by d -tuple of quantum numbers $\mathbf{n} = (n_1, \dots, n_d)$,

$$\mathbf{J}|\mathbf{n}\rangle = \hbar(\mathbf{n} + \boldsymbol{\alpha})|\mathbf{n}\rangle \quad (3.25)$$

where $0 \leq \alpha_k \leq 1$ are the Maslov indices which are irrelevant for the leading order semiclassical approximation we will use. It follows from (3.24) that the angle operators act as shifts

$$\exp(i\mathbf{m} \cdot \boldsymbol{\Theta})|\mathbf{n}\rangle = |\mathbf{n} + \mathbf{m}\rangle. \quad (3.26)$$

The Heisenberg equations of motion can be trivially solved in the leading semiclassical order by simply disregarding the operator ordering,

$$\begin{aligned} \mathbf{J}(t) &= e^{iH_0 t/\hbar} \mathbf{J} e^{-iH_0 t/\hbar} = \mathbf{J}, \\ e^{i\mathbf{m} \cdot \boldsymbol{\Theta}(t)} &= e^{iH_0 t/\hbar} e^{i\mathbf{m} \cdot \boldsymbol{\Theta}} e^{-iH_0 t/\hbar} \cong e^{i\mathbf{m} \cdot \boldsymbol{\omega}(\mathbf{J})t} e^{i\mathbf{m} \cdot \boldsymbol{\Theta}}, \end{aligned} \quad (3.27)$$

in terms of the frequency operator $\boldsymbol{\omega}(\mathbf{J})$. Throughout this paper we use the symbol \cong for 'semiclassically equal', i.e. asymptotically equal in the leading order in \hbar . Similarly, time evolution of the perturbation observable is obtained in the leading order by substitution of classical with quantal action-angle variables in the expression (3.23)

$$V(t) = e^{iH_0 t/\hbar} V e^{-iH_0 t/\hbar} \cong \sum_{\mathbf{m}} v_{\mathbf{m}}(\mathbf{J}) e^{i\mathbf{m} \cdot \boldsymbol{\omega}(\mathbf{J})t} e^{i\mathbf{m} \cdot \boldsymbol{\Theta}}. \quad (3.28)$$

Operator $\bar{V}(\mathbf{J})$ is diagonal in the eigenbasis $|\mathbf{n}\rangle$ and therefore the expectation value of the echo operator (3.20) in the initial density matrix ρ is

$$f(t) = \sum_{\mathbf{n}} \exp(-i\delta t \bar{V}(\hbar\{\mathbf{n} + \boldsymbol{\alpha}\})/\hbar) D_{\rho}(\hbar\mathbf{n}), \quad D_{\rho}(\hbar\mathbf{n}) = \langle \mathbf{n} | \rho | \mathbf{n} \rangle. \quad (3.29)$$

For pure initial states D_{ρ} is just $D_{\rho} = |\langle \psi | \mathbf{n} \rangle|^2$. This is still the exact quantum mechanical expression of the fidelity amplitude. Now we make a leading order semiclassical approximation by replacing quantum \bar{V} with its classical limit \bar{v} and replacing the sum over quantum numbers \mathbf{n} with the integral over classical actions \mathbf{j} . The replacement of the sum with the action space integral (ASI) is valid up to classically long times t_a , such that the variation of the argument in the exponential across one Planck cell is small,

$$t_a = \frac{1}{|\partial_{\mathbf{j}} \bar{v}| \delta} \sim \hbar^0 / \delta. \quad (3.30)$$

Subsequently we will see that the fidelity decays on shorter times and so the approximation is justifiable. By denoting with $d_{\rho}(\mathbf{j})$ the classical limit of $D_{\rho}(\hbar\mathbf{n})$ we arrive at the fidelity amplitude

$$f(t) \cong \hbar^{-d} \int d^d \mathbf{j} \exp\left(-i \frac{\delta}{\hbar} t \bar{v}(\mathbf{j})\right) d_{\rho}(\mathbf{j}). \quad (3.31)$$

This expression will be used to evaluate the fidelity for different initial states.

3.2.2 Coherent Initial States

We proceed to evaluate fidelity amplitude (3.31) for coherent initial state centred at $(\mathbf{j}^*, \boldsymbol{\theta}^*)$ in action-angle phase space. The expansion coefficients of the initial density matrix $\rho = |\mathbf{j}^*, \boldsymbol{\theta}^*\rangle \langle \mathbf{j}^*, \boldsymbol{\theta}^*|$ for a general coherent state in d degrees of freedom system can be written as

$$\langle \mathbf{n} | \mathbf{j}^*, \boldsymbol{\theta}^* \rangle = \left(\frac{\hbar}{\pi}\right)^{d/4} |\det \Lambda|^{1/4} \exp\left\{-\frac{1}{2\hbar} (\mathbf{J}_{\mathbf{n}} - \mathbf{j}^*) \cdot \Lambda (\mathbf{J}_{\mathbf{n}} - \mathbf{j}^*) - i \mathbf{n} \cdot \boldsymbol{\theta}^*\right\}, \quad (3.32)$$

where Λ is a positive symmetric $d \times d$ matrix of squeezing parameters and $\mathbf{J}_{\mathbf{n}} = \hbar(\mathbf{n} + \boldsymbol{\alpha})$ is an eigenvalue of operator \mathbf{J} in eigenstate $|\mathbf{n}\rangle$. The classical limit of D_{ρ} (3.29) is therefore

$$d_{\rho}(\mathbf{j}) = (\hbar/\pi)^{d/2} |\det \Lambda|^{1/2} \exp(-(\mathbf{j} - \mathbf{j}^*) \cdot \Lambda (\mathbf{j} - \mathbf{j}^*)/\hbar). \quad (3.33)$$

The ASI for the fidelity amplitude can now be evaluated by the stationary phase method. To lowest order in δt the stationary point \mathbf{j}_s , i.e. the zero of $[-i\delta t \bar{v} - (\mathbf{j} - \mathbf{j}^*) \cdot \Lambda (\mathbf{j} - \mathbf{j}^*)]$, is at

$$\mathbf{j}_s = \mathbf{j}^* + \frac{i t \delta}{2} \Lambda^{-1} \bar{\mathbf{v}}' + \mathcal{O}(\delta^2), \quad (3.34)$$

where the derivative of the average perturbation is

$$\bar{\mathbf{v}}' = \frac{\partial \bar{v}(\mathbf{j}^*)}{\partial \mathbf{j}}. \quad (3.35)$$

For $\delta t \ll 1$ the stationary point is simply at \mathbf{j}^* and the fidelity is

$$F(t) = \exp\left\{-(t/\tau_r)^2\right\}, \quad \tau_r = \frac{1}{\delta} \sqrt{\frac{2\hbar}{\bar{\mathbf{v}}' \cdot \Lambda^{-1} \bar{\mathbf{v}}'}}. \quad (3.36)$$

The fidelity amplitude on the other hand has an additional phase,

$$f(t) = \exp\left\{-(t/\tau_r)^2/2\right\} \exp(-i \bar{v}(\mathbf{j}^*) \delta t / \hbar). \quad (3.37)$$

Comparing the fidelity (3.36) with the linear response formula (3.16) we see that the average correlation function for a coherent initial state is $\bar{C} = \frac{1}{2}\hbar(\bar{\mathbf{v}}' \cdot \Lambda^{-1}\bar{\mathbf{v}}')$.

We have already briefly explained the behaviour of classical fidelity in Section 1.1.2, for details see (Benenti *et al.*, 2003a). For regular dynamics one gets a ballistic decay of classical fidelity for perturbations predominantly changing frequencies of tori or power-law decay for perturbations predominantly changing the shape of tori. In the ballistic case, provided one is allowed to replace the perturbation v with its time average $\bar{v}(\mathbf{j})$, one gets the same Gaussian decay of the classical fidelity as for the quantum one (3.36). Therefore, in the regime where \bar{v} determines the decay of classical fidelity, classical and quantum fidelity agree. From the expression for the echo operator (3.20) one can in this case interpret the fidelity as the overlap between the initial coherent state and the state obtained after the evolution with the Hamiltonian $\delta\bar{v}$. Because \bar{v} is a function of actions only, the classical equations of motion are very simple, namely only the frequency of classical motion is changed by the amount $\Delta\omega = \bar{\mathbf{v}}'\delta$. This change in frequency causes the “echo” packet $M_\delta(t)|\psi(0)\rangle$ to move *ballistically* away from its initial position and as a consequence fidelity decays. For coherent state the shape of the packet is Gaussian and therefore fidelity decay is also Gaussian. For other forms of localized initial packets the functional form of the fidelity will be different but with the same dependence on the ballistic separation “speed” $\bar{\mathbf{v}}'$. If $\bar{V} \equiv 0$ we obviously have $\bar{\mathbf{v}}' = 0$, this situation will be discussed in Chapter 4 describing a freeze of fidelity.

In one dimensional systems ($d = 1$) another phenomena should be observable. After long time the echo packet will make a whole revolution around the torus causing the fidelity to be large again. This will happen after the so-called beating time t_b determined by $\delta\bar{v}'(j^*)t_b = 2\pi$,

$$t_b = \frac{2\pi}{\bar{v}'\delta}. \quad (3.38)$$

This beating phenomena is particular to one dimensional systems as in general the incommensurability of frequencies will suppress the revivals of fidelity.

Let us now illustrate the above theory with numerical experiment. We again take the kicked top (2.20), but this time with $\gamma = \pi/2$ and $\alpha = 0.1$ resulting in regular classical dynamics. The perturbation is the same as for mixing situation, i.e. a perturbation in α resulting in a classical perturbation $v = z^2/2$ (2.22). Let us denote by $\vartheta, \tilde{\varphi}$ the spherical angular coordinates measured with respect to the y -axis. For $\alpha = 0$ the action-angle variables are ($j = \cos \tilde{\vartheta} = y, \theta = \tilde{\varphi}$) and we can use the preceding theory. The squeezing parameter for spin coherent states is (2.26)

$$\Lambda = 1/\sin^2 \tilde{\vartheta} = 1/(1 - y^2). \quad (3.39)$$

To calculate the decay time τ_r we need the derivative of the average perturbation. For $\alpha = 0$ the evolution is very simple, just a rotation by $\pi/2$ around the y -axis, resulting in

$$\bar{v} = \frac{1}{4}(1 - j^2), \quad \bar{v}' = -\frac{j}{2}. \quad (3.40)$$

Theoretical decay of fidelity is therefore

$$F(t) = \exp\left(-\delta^2 S t^2 y^2 (1 - y^2)/8\right), \quad (3.41)$$

where we used $\hbar = 1/S$. In Figure 3.7 we show the results of numerical calculation for a coherent packet placed at spherical coordinates (with respect to z -axis) $(\vartheta^*, \varphi^*) = \pi(1/\sqrt{3}, 1/\sqrt{2})$ resulting in action $y = 0.77$ (note that we projected the initial state onto the invariant OE subspace (2.24)). Spin number is chosen $S = 100$. Excellent agreement with the theoretical Gaussian decay can be seen. In addition, we can observe a revival of the fidelity at t_b . For our OE subspace the initial state is composed of two symmetrically positioned images, so that the beating time is $t_b = 2\pi/y\delta$, which nicely agrees with the numerics.

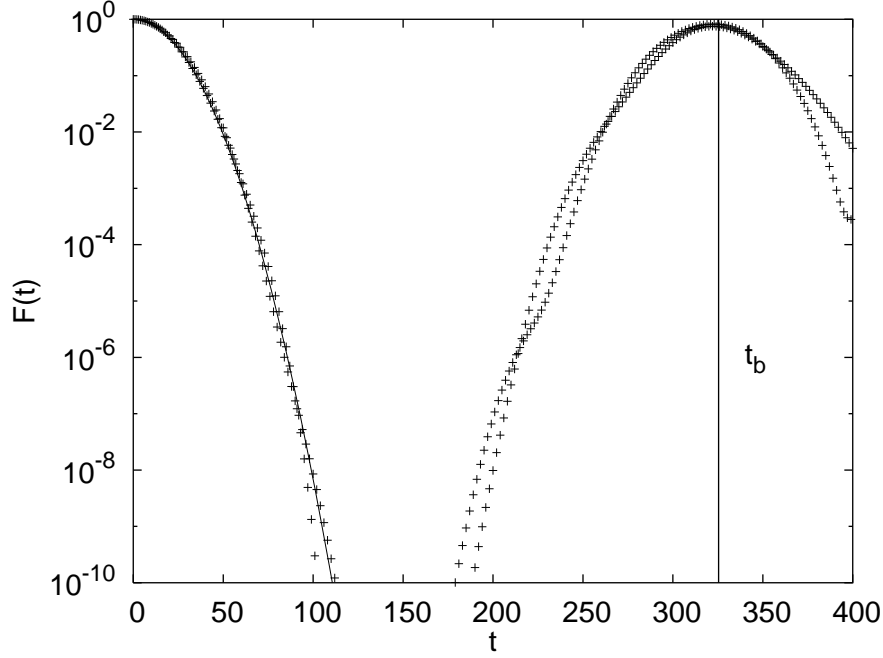


Figure 3.7: Quantum fidelity for a coherent state of the regular kicked top, $\alpha = 0.1$, $S = 100$, $\gamma = \pi/2$ and $\delta = 0.0025$. The full curve is the theoretical decay (3.41) and the vertical line indicates the theoretical beating time (3.38).

Average Fidelity

If $F(t, \mathbf{j})$ is Gaussian fidelity decay (3.36) for a coherent initial state centred at \mathbf{j} , we can define the average fidelity

$$\langle F(t) \rangle_{\mathbf{j}} := \frac{(2\pi)^d}{\mathcal{V}} \int d^d \mathbf{j} F(t, \mathbf{j}). \quad (3.42)$$

Packing all \mathbf{j} dependent terms in a non-negative scalar function $g(\mathbf{j})$, the fidelity decay for a single coherent state can be written as $F(t, \mathbf{j}) := \exp(-\delta^2 t^2 g(\mathbf{j})/\hbar)$. For large $\delta^2 t^2/\hbar$ the main contribution to the average will come from regions of small $g(\mathbf{j})$ where the fidelity decay is slow. In general the function $g(\mathbf{j})$ will have zeros in action space, for simplicity let us assume there is a single zero at \mathbf{j}^* of order η . The asymptotic decay can then be calculated and scales as

$$\langle F(t) \rangle_{\mathbf{j}} \asymp \left(\frac{\hbar}{\delta^2 t^2} \right)^{d/\eta}, \quad (3.43)$$

where the sign \asymp will denote “in the asymptotic limit” throughout the work. For infinite phase space the order of a zero η can only be an even number, whereas for a finite space η can also be odd.

To illustrate the theory, we calculated the average decay for the kicked top and the perturbation in α used before. The function g is $g(j) = j^2(1 - j^2)/8$. We have three zeros, two of order $\eta = 1$ at the boundary of the phase space $j = \pm 1$ and one of order $\eta = 2$ at $j = 0$. Asymptotically the zero with $\eta = 2$ will dominate, giving the decay

$$\langle F(t) \rangle_{\mathbf{j}} \asymp \frac{\sqrt{2\pi}}{\delta t \sqrt{S}}. \quad (3.44)$$

Figure 3.8 shows that we indeed get asymptotic $\sim t^{-1}$ decay. If one averages the fidelity

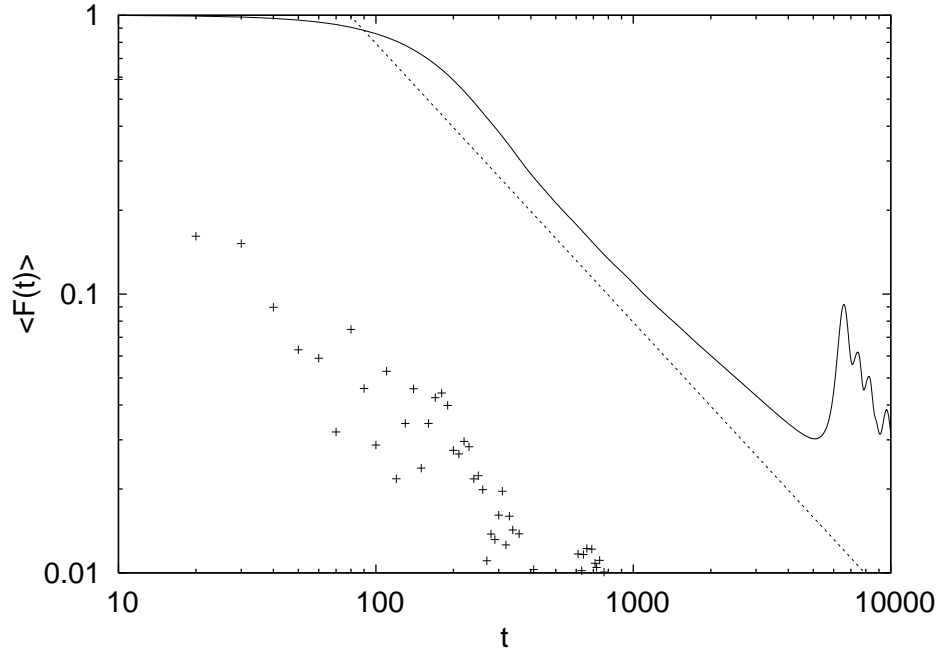


Figure 3.8: Average fidelity decay $\langle F(t) \rangle_j$ (3.42) for a regular kicked top with $\alpha = 0.1$, $\gamma = \pi/2$ and perturbation of strength $\delta = 10^{-3}$ in the parameter α . The averaging is done over 200 coherent initial states randomly placed on a sphere and projected onto OE subspace (2.24). The Dotted line is the theoretical power law decay (3.44). Pluses show the absolute value square of the average fidelity amplitude.

amplitude, the result is close to zero (pluses in the figure) because the phase present in the fidelity amplitude (3.37) averages to zero[¶].

As a second example, we take the same regular kicked top system and parameters, only the perturbation is now in rotation angle γ , i.e. $U_\delta := U(\gamma + \delta, \alpha)$. The function g is in this case $g(j) = (1 - j^2)/2$. As opposed to the previous case, now we have only two zeros of order $\eta = 1$ at $j = \pm 1$. The asymptotic decay is therefore

$$\langle F(t) \rangle_j \asymp \frac{1}{\delta^2 t^2 S}. \quad (3.45)$$

Denominator is now quadratic in time, whereas for the perturbation S_z^2 it was linear. The theoretical decay law is again confirmed by the numerical experiment shown in Figure 3.9. The asymptotic power law decay of average fidelity is therefore *system dependent*.

An entirely analogous method will be used in the next section to calculate the asymptotic decay for a random initial state. The only difference is that for *a random initial state* the zeros of \bar{v} are the relevant quantity, whereas for an *average* fidelity decay of *a coherent state* the zeros of τ_r , i.e. zeros of \bar{v}' are important. Therefore, in a regular system the asymptotic decay for a random initial state is usually not the same as the average decay for a coherent state.

3.2.3 Random Initial State

In the previous section we have seen that for localized packets the fidelity decay is dictated by the separation of two packets due to the perturbation. The opposite possible choice of

[¶]One would have to have zeros of \bar{v} and \bar{v}' at the same position j^* to get a nonzero average, which is generally not the case.

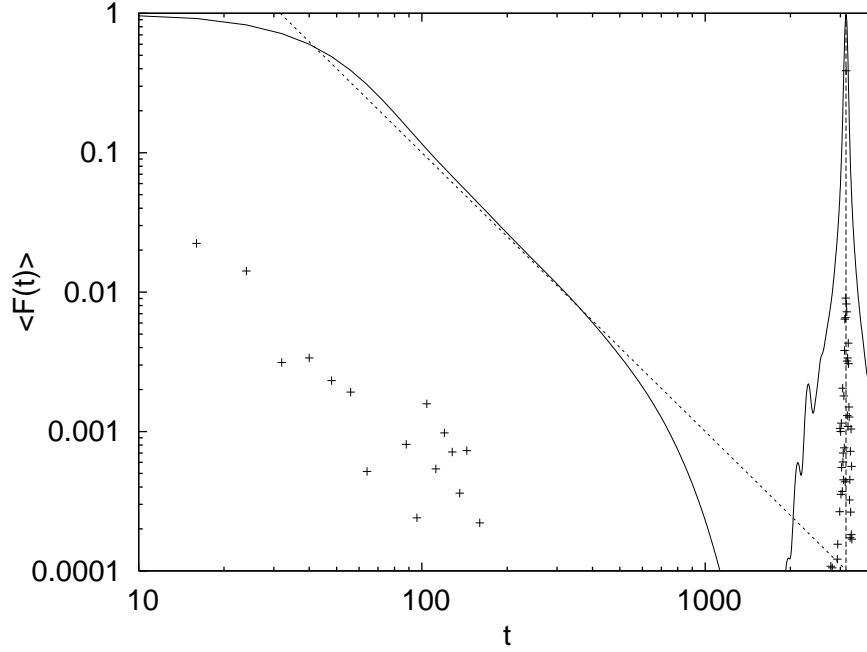


Figure 3.9: Average fidelity decay $\langle F(t) \rangle_j$ (3.42) for a regular kicked top. Everything is the same as in Figure 3.8 apart from the perturbation being in the angle γ . Dotted line is the theoretical power law decay (3.45) without any fitting parameter. Note that we have different power law decay as in Figure 3.8. The vertical dotted line shows the position of the beating time $t_b = \pi/\delta$ (3.38) which is in this case independent of j . If t_b depends on j (as in Figure 3.8) such recovery is absent in the average fidelity.

initial condition is to take completely *delocalised* state, a uniform mixture of all states $\rho = \mathbb{1}/\mathcal{N}$ being the extreme case. For uniform initial density matrix $\rho = \mathbb{1}/\mathcal{N}$, the D_ρ takes the form $D_\rho(\mathbf{J}) = 1/\mathcal{N}$. The classical limit of D_ρ is obtained by calculating the number of states \mathcal{N} using the Thomas-Fermi rule, resulting in the classical limit $d_\rho(\mathbf{j}) = (2\pi\hbar)^d/\mathcal{V}$, where \mathcal{V} is the size of the classical phase space. While for small times fidelity will decay quadratically (3.16), for large $\delta t/\hbar$ the integral in $f(t)$ (3.31) can again be calculated using the method of stationary phase. In contrast to a coherent state case, now one can have more than one stationary point. If we have p stationary points, $\mathbf{j}_\eta, \eta = 1, \dots, p$, where the phase is stationary, $\partial \bar{v}(\mathbf{j}_\eta)/\partial \mathbf{j} = \mathbf{0}$, the integral results in

$$f(t) = \frac{(2\pi)^{3d/2}}{\mathcal{V}} \left| \frac{\hbar}{t\delta} \right|^{d/2} \sum_{\eta=1}^p \frac{\exp\{-it\bar{v}(\mathbf{j}_\eta)\delta/\hbar - i\nu_\eta\}}{|\det \bar{\mathbf{V}}_\eta|^{1/2}}, \quad (3.46)$$

where $\{\bar{\mathbf{V}}_\eta\}_{kl} := \partial^2 \bar{v}(\mathbf{j}_\eta)/\partial j_k \partial j_l$ is a matrix of second derivatives at the stationary point η , and $\nu_\eta = \pi(m_+ - m_-)/4$ where m_\pm are the numbers of positive/negative eigenvalues of the matrix $\bar{\mathbf{V}}_\eta$. We also assumed that the phase space is infinite. In a finite phase space we will have diffractive oscillatory corrections in the stationary phase formula, see end of Section 4.2.4 or numerical results below. Note also that for a large Hilbert space dimension \mathcal{N} the fidelity for a *single initial random state* will also decay according to the asymptotic formula (3.46). The decay time of the quantum fidelity for random initial states scales therefore as $\tau_r \sim \hbar/\delta$ and is by a factor $\sqrt{\hbar}$ shorter than for coherent initial states. We repeat that the stationary phase formula (3.46) is expected to be correct in the range $\text{const } \hbar/\delta < t < \text{const}'/\delta$ so it will give asymptotic decay of fidelity. Most interesting to note is the power-law dependence on time

and perturbation strength, $F(t) \asymp [\hbar/(t\delta)]^d$. With increasing dimensionality d of a system the decay gets faster. This allows for a possible crossover to a Gaussian decay when approaching the thermodynamic limit $d \rightarrow \infty$, observed in a class of kicked spin chains by Prosen (2002). Agreement beyond linear response with the Gaussian decay is frequently observed also for a finite d , e.g. in a spin model of quantum computation (Prosen & Žnidarič, 2001) or even in a one dimensional kicked top seen in Figure 3.10.

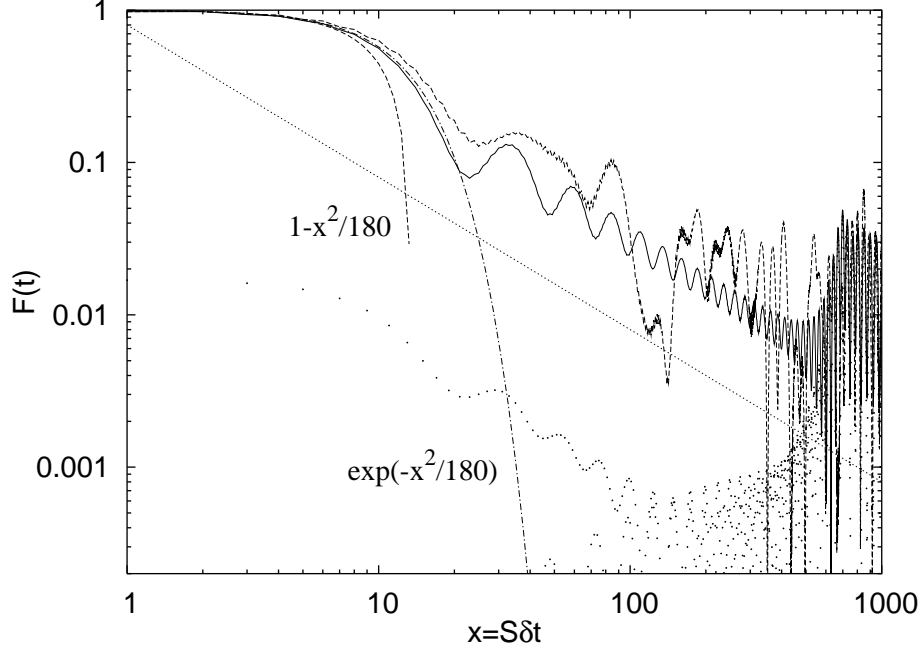


Figure 3.10: Fidelity decay for the regular kicked top, $\alpha = 0.1$, $\gamma = \pi/2$, $\delta = 0.01$, $S = 100$. The solid curve gives the results of a numerical simulation for $\rho = \mathbb{1}/N$ on the OE subspace (2.24). Isolated dots denote the difference between numerical calculation and analytic formula (3.48) for $\alpha \rightarrow 0$, $|F_{\text{num.}}(t) - F_{\text{anali.}}(t)|$. The dotted line gives a predicted asymptotic decay $\propto t^{-1}$, and the dashed/chain curves are the predicted fidelity decays at small times, namely the second order expansion $F(t) = 1 - (St\delta)^2/180$, and 'improved' one by an exponential. The wiggling dashed curve represents the numerics for a single random state.

For numerical demonstration we take the same kicked top system as for the case of coherent initial states, $\alpha = 0.1$, $\gamma = \pi/2$ and $S = 100$ and perturbation in parameter α , giving $\bar{v} = (1 - j^2)/4$. Rather than comparing the numerical results with the asymptotic formula (3.46) we will try to directly calculate the fidelity decay in order to demonstrate oscillatory corrections due to a finite Hilbert space. We start with the quantum expression for the fidelity amplitude (3.29), using the eigenvalues $(2m - 1)^2$ of operator S_y^2 on OE subspace,

$$F(t) = \left| \frac{2}{S} \sum_{m=1}^{S/2} \exp(-i\delta t(2m - 1)^2/4S) \right|^2. \quad (3.47)$$

For large S we can replace the sum with an integral and get

$$F(t) = \frac{\pi}{\delta St} \left| \text{erfi}\left(\frac{1}{2}e^{i\pi/4}\sqrt{\delta St}\right) \right|^2, \quad (3.48)$$

where $\text{erfi}(z) = \frac{2}{i\sqrt{\pi}} \int_0^{iz} e^{-t^2} dt$ is a complex error function with the limit $\lim_{x \rightarrow \infty} |\text{erfi}(\frac{1}{2}e^{i\pi/4}\sqrt{x})| = 1$ to which it approaches by oscillating around 1. We therefore have an analytic expression for

the fidelity (3.48) in the case of an uniform average over the whole Hilbert space or, equivalently, over one random initial state. Its asymptotic decay is proportional to t^{-1} which agrees with the general semiclassical asymptotic (3.46) but in addition we have an oscillatory erfi correction due to a finite space. For small times we can get initial quadratic linear response decay by expanding the full theoretical formula (3.48) or more easily by simply calculating \bar{C} according to formula (3.19). One can even use the classical calculation. For $\alpha = 0$ we have $\bar{v} = (1 - y^2)/4$, so the classical average correlation functions is

$$\bar{C}_{\text{cl}} = \frac{1}{16}(\overline{y^4} - \overline{y^2}^2) = \frac{1}{180}, \quad (3.49)$$

where the averages are performed over a uniform distribution on a sphere. In Figure 3.10 we compare theoretical decay (3.48) with the numerical as well as with the linear response formula $F(t) = 1 - (\delta S)^2 \bar{C}_{\text{cl}} t^2$. Also, beyond the linear response there is a significant agreement with the Gaussian approximation $F(t) = \exp(-\delta^2 S^2 \bar{C}_{\text{cl}} t^2)$ obtained by exponentiating the linear response expression.

3.3 Time Scales

Let us close the present chapter with an overview of time scales of different fidelity decays depending on parameters δ and \hbar and on the initial state.

For regular dynamics we have only three relevant time scales, the classical averaging time t_{ave} in which the average perturbation operator converges to \bar{V} , the quantum fidelity decay time τ_{r} and the time t_{∞} when the fidelity reaches a fluctuating plateau due to a finite dimension of Hilbert space. For times smaller than t_{ave} decay is system and state specific and can not be discussed in general. After t_{ave} the fidelity decay is first quadratic in time as dictated by the linear response formula (3.16). The decay time τ_{r} scales as $\sim \sqrt{\hbar}/\delta$ (3.36) for coherent initial states and as $\sim \hbar/\delta$ (3.46) for random initial states. Beyond linear response the functional dependence of the decay is Gaussian for coherent initial states and power law for random initial states with the before mentioned decay time τ_{r} . This decay persists until the finite size plateau \bar{F} (2.38) is reached at time t_{∞} . The time t_{∞} again depends on the initial state as well as on the Hilbert space dimension \mathcal{N} . For random initial states the power law decay gets faster with increasing dimensionality d of the system, and is conjectured to approach a Gaussian decay in the thermodynamic limit.

For mixing dynamics we have a more complicated situation. There are five relevant time scales (even six for coherent initial states): The classical mixing time t_{mix} on which correlation functions decay; the quantum decay time of the fidelity τ_{m} ; the Heisenberg time t_{H} after which the system starts for “feel” finiteness of Hilbert space; the decay time τ_{p} of perturbative Gaussian decay present after t_{H} ; the time t_{∞} when the fidelity reaches finite size plateau; for coherent initial states we have in addition the Ehrenfest time t_{E} up to which we have quantum-classical correspondence. Depending on the interrelation of these time scales, i.e. depending on the perturbation strength δ , Planck’s constant \hbar and the dimensionality d , we will also have different decays of fidelity. All different regimes can be reached by fixing \hbar and increasing δ . Let us follow different decay regimes as we increase δ (shown in Figure 3.11):

- (a) For $\delta < \delta_{\text{p}}$ we will have $t_{\text{H}} < \tau_{\text{m}}$. This means that at the Heisenberg time, the fidelity due to exponential decay (3.5) will still be close to 1, $F(t_{\text{H}}) \approx 1$, and we will see only a Gaussian decay due to finite Hilbert space (3.13). The critical δ_{p} below which we will see this regime has already been calculated (3.14) and is

$$\delta_{\text{p}} = \frac{\hbar}{\sqrt{\sigma_{\text{cl}} \mathcal{N}}} = \hbar^{d/2+1} \frac{(2\pi)^{d/2}}{\sqrt{\sigma_{\text{cl}} \mathcal{V}}}. \quad (3.50)$$

For $\delta < \delta_p$ the fidelity will have Gaussian decay with the decay time τ_p (3.13)

$$\tau_p = \frac{\hbar^{1-d/2}}{\delta} \sqrt{\frac{\mathcal{V}}{4\sigma_{cl}(2\pi)^d}}. \quad (3.51)$$

As we increase δ , we will eventually reach a regime in which we will see initial exponential decrease and then at t_H crossover into a Gaussian decay until the plateau is reached at t_∞ .

- (b) For $\delta_p < \delta < \delta_s$ we will have a crossover from the initial exponential decay (3.5) to the asymptotic Gaussian decay (3.13) at time t_H . This regime will take place if $\tau_m < t_H < t_\infty$. With increasing perturbation, t_∞ will decrease and the upper border δ_s is determined by the condition $t_\infty = t_H$. Denoting a finite size plateau by $\bar{F} \sim 1/\mathcal{N}^\mu$, with μ lying between 1 and 2, depending on the initial state (see Section 2.2.1), we have the condition $\exp(-(t_H/\tau_p)^2) = \bar{F}$ which gives

$$\delta_s = \frac{\hbar}{\sqrt{\sigma_{cl}\mathcal{N}}} \sqrt{\mu \ln \mathcal{N}} = \delta_p \sqrt{\mu \ln \mathcal{N}}. \quad (3.52)$$

Further increasing the perturbation, we reach perhaps the most interesting regime, in which quantum fidelity can decay faster the more chaotic the systems is. In this regime the exponential decay persists until the plateau is reached.

- (c) For $\delta_s < \delta < \delta_{\text{mix}}$ (δ_E) we will have an exponential decay until t_∞ . The upper border δ_{mix} is determined by the condition $\tau_m = t_{\text{mix}}$ which is a point where the argument leading to the factorisation of n -point correlation function breaks down. For random initial states δ_{mix} does not depend on \hbar and we get

$$\delta_{\text{mix}} = \frac{\hbar}{\sqrt{2\sigma_{cl}t_{\text{mix}}}} = \delta_p \sqrt{\frac{\mathcal{N}}{2t_{\text{mix}}}}. \quad (3.53)$$

Note that the relative size of this window $\delta_{\text{mix}}/\delta_s = \sqrt{\mathcal{N}/2\mu t_{\text{mix}} \ln \mathcal{N}}$ increases both in the semiclassical $\hbar \rightarrow 0$ and in the thermodynamic $d \rightarrow \infty$ limit.

For coherent initial states the quantum correlation function relaxes on a slightly longer time scale, namely on the Ehrenfest time $t_E \sim -\ln \hbar/\lambda$. Until t_E quantum packet follows the classical trajectory and afterwards interferences start to build leading to the breakdown of quantum-classical correspondence. Equating $\tau_m = t_E$ gives the upper border for coherent states

$$\delta_E = \frac{\hbar}{\sqrt{-\ln \hbar}} \sqrt{\frac{\lambda}{2\sigma_{cl}}} = \delta_{\text{mix}} \sqrt{\frac{\lambda t_{\text{mix}}}{-\ln \hbar}}. \quad (3.54)$$

- (d) For $\delta > \delta_{\text{mix}}$ the perturbation is so strong that the quantum fidelity decays before t_{mix} , i.e. perturbed and unperturbed dynamics are essentially unrelated and fidelity decays almost instantly.

For coherent initial states the upper border of regime (c) is at δ_E which is smaller than the lower border of regime (d) δ_{mix} which opens up the possibility of another regime between (c) and (d), namely for $\delta_E < \delta < \delta_{\text{mix}}$ the fidelity will decay within the Ehrenfest time. In this regime the decay of quantum fidelity is the same as the decay of classical fidelity and can be explained in terms of classical Lyapunov exponents (Veble & Prosen, 2004). Note that the relative width of this regime $\delta_{\text{mix}}/\delta_E = \sqrt{\ln(1/\hbar)/\lambda t_{\text{mix}}}$ grows only logarithmically in $1/\hbar$, i.e. much slower than the width of regime (c).

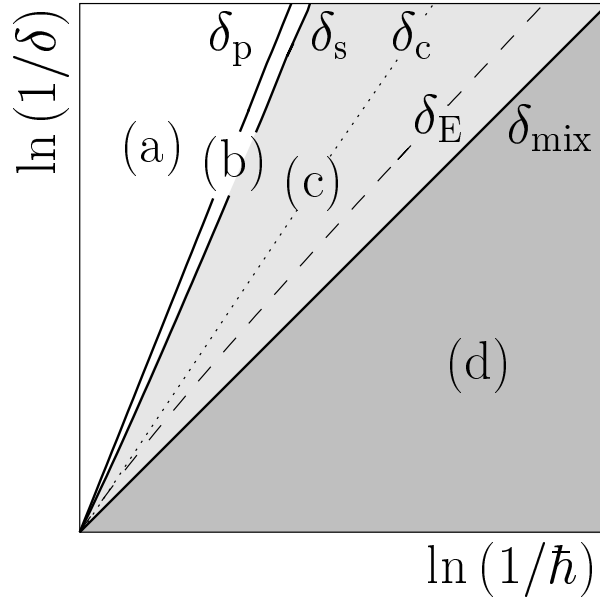


Figure 3.11: Schematic view of different fidelity decay regimes for mixing dynamics. For details see text.

The fidelity decay time scales as $\sim 1/\delta$ for regular systems, while it is $\sim 1/\delta^2$ for mixing dynamics. This opens up an interesting possibility: is it possible that the fidelity would decay *faster* for regular systems than for chaotic ones? The answer is yes. Demanding $\tau_r < \tau_m$ we find that for sufficiently small δ one will indeed have faster fidelity decay in regular systems. This will happen for

$$\delta < \begin{cases} \delta_r = \hbar \bar{C}^{1/2} / 2\sigma_{cl} \propto \hbar & \text{random init.state} \\ \delta_c = \hbar^{3/2} \sqrt{\bar{\mathbf{v}}' \cdot \Lambda^{-1} \bar{\mathbf{v}}' / 8\sigma_{cl}^2} \propto \hbar^{3/2} & \text{coherent init.state} \end{cases} \quad (3.55)$$

We explicitly wrote the result for regular initial states δ_r and coherent initial states δ_c as the two have different scaling with \hbar . We can see that for random initial states δ_r scales in the same way as δ_{mix} and so one has faster decay of fidelity in regular systems just provided $\delta < \delta_r \sim \delta_{mix}$. For a coherent initial state this can be satisfied above the perturbative border $\delta > \delta_p$ only in more than one dimension $d > 1$. In one dimensional systems δ_p and δ_c have the same scaling with \hbar and whether we can observe faster decay of fidelity in regular systems than in chaotic ones depends on the values of σ_{cl} and $\bar{\mathbf{v}}'$. We stress that our result does not contradict any of the existing findings on quantum-classical correspondence. For example, a growth of quantum dynamical entropies (Alicki *et al.*, 1996; Miller & Sarkar, 1999) persists only up to logarithmically short Ehrenfest time t_E , which is also the upper bound for the so-called “Lyapunov” decay of the fidelity (Jalabert & Pastawski, 2001; Cucchietti *et al.*, 2002a) and within which one would always find $F^{reg}(t) > F^{mix}(t)$ (for coherent states) above the perturbative border $\delta > \delta_p$, whereas our theory reveals new nontrivial quantum phenomena with a semiclassical prediction (but not correspondence!) much beyond that time. If we let $\hbar \rightarrow 0$ first, and then $\delta \rightarrow 0$, i.e. we keep $\delta \gg \delta_{r,c}(\hbar)$, then we recover the result supported by classical intuition, namely that the regular (non-ergodic) dynamics is more stable than the chaotic (ergodic and mixing) dynamics. On the other hand, if we let $\delta \rightarrow 0$ first, and only after that $\hbar \rightarrow 0$, i.e. satisfying (3.55), we find somewhat counterintuitive result saying that chaotic (mixing) dynamics is more stable than the regular one. We can conclude the section by saying that we have *three non-commuting limits*, namely the *semiclassical limit* $\hbar \rightarrow 0$, the

perturbation strength limit $\delta \rightarrow 0$, and the *thermodynamic limit* $d \rightarrow \infty$, such that no pair of these limits commutes.

Similar regimes as for the fidelity decay were also obtained by Cohen (1999, 2000); Cohen & Kottos (2000) when studying parametrically driven systems and energy dissipation.

3.3.1 Illustration with Wigner Functions

In order to demonstrate faster decay of fidelity for a regular than for a chaotic system we did a numerical simulation on the kicked top. For chaotic situation we choose $\alpha = 30$, while for regular one we take $\alpha = 0.1$ as before. Other parameters are the same for the chaotic and the regular case, $\gamma = \pi/2$, $S = 100$ and a coherent initial state at $(\vartheta^*, \varphi^*) = \pi(1/\sqrt{3}, 1/\sqrt{2})$. Perturbation of strength $\delta = 1.5 \cdot 10^{-2}$ is in parameter α . In Figure 3.12 we show the fidelity decay for both cases and an illustration of states in terms of Wigner functions. Spin Wigner function is a distribution on a sphere with a nice property that if we have two states ρ_1 and ρ_2 and their corresponding Wigner functions W_{ρ_1} and W_{ρ_2} the following equality holds,

$$\text{tr}(\rho_1 \rho_2) = \int W_{\rho_1} W_{\rho_2} d\Omega. \quad (3.56)$$

For an exact definition of a spin Wigner function see Appendix A. Wigner functions enable us to represent fidelity, which is an overlap of the initial state $\rho(0)$ with the echo state $\rho^M(t)$ (2.8), as a phase space overlap integral of two Wigner functions. Also, the classical quantity analogous to Wigner function is just the classical density in phase space. But note that Wigner function is not necessarily positive whereas the classical density is, so the positivity of a Wigner function is a necessary condition (but not sufficient) for the classicality of a state. In Figure 3.12 we show for the chaotic (triangles in the fidelity plot and pictures above) and the regular case (pluses in the fidelity plot and pictures below) two series of Wigner functions at different times ($t = 0, 60, 120$): the Wigner function after the unperturbed forward evolution (row labeled “forward”) and the Wigner function after the echo (row labeled “echo”). We also show the structure of the classical phase space. In the inset the same data for the fidelity decay is shown on a longer time scale and the vertical line shows the theoretical position of t_b . The fidelity is the overlap between the echo Wigner function and the initial Wigner function. For our choice of coherent initial states, the initial Wigner function is a Gaussian in the semiclassical limit (2.28). For chaotic dynamics the forward Wigner function develops negative values around the Ehrenfest time after which the quantum-classical correspondence is lost. For the regular dynamics this correspondence persists much longer, namely until the “integrable” Ehrenfest time $\sim \hbar^{-1/2}$ after which the initial wave packet of size $\sim \hbar^{1/2}$ spreads over the phase space. For a detailed study of Wigner functions in chaotic systems see (Horvat & Prosen, 2003; Lombardi & Seligman, 1993) and references therein. The echo Wigner function for regular dynamics moves ballistically from the initial position, causing the Gaussian decay of fidelity. But note that for regular dynamics the echo Wigner function does not have negative values even if they occur in the forward Wigner function. In our case the quantum fidelity agrees with the classical one for regular dynamics. In a chaotic case on the other hand, the echo image stays at the initial position and diffusively decays in amplitude, causing the fidelity to decay slower than in regular case. Classical fidelity follows quantum fidelity in the chaotic regime only up to the chaotic Ehrenfest time.

Finally, we would like to illustrate the dimensional dependence of the fidelity decay. We have seen that in $d > 1$ border δ_c is above the perturbative border and so one can get faster regular decay in a wider range of δ . In addition, strong revivals of fidelity in one dimensional regular systems for coherent initial states should be absent for $d > 1$.

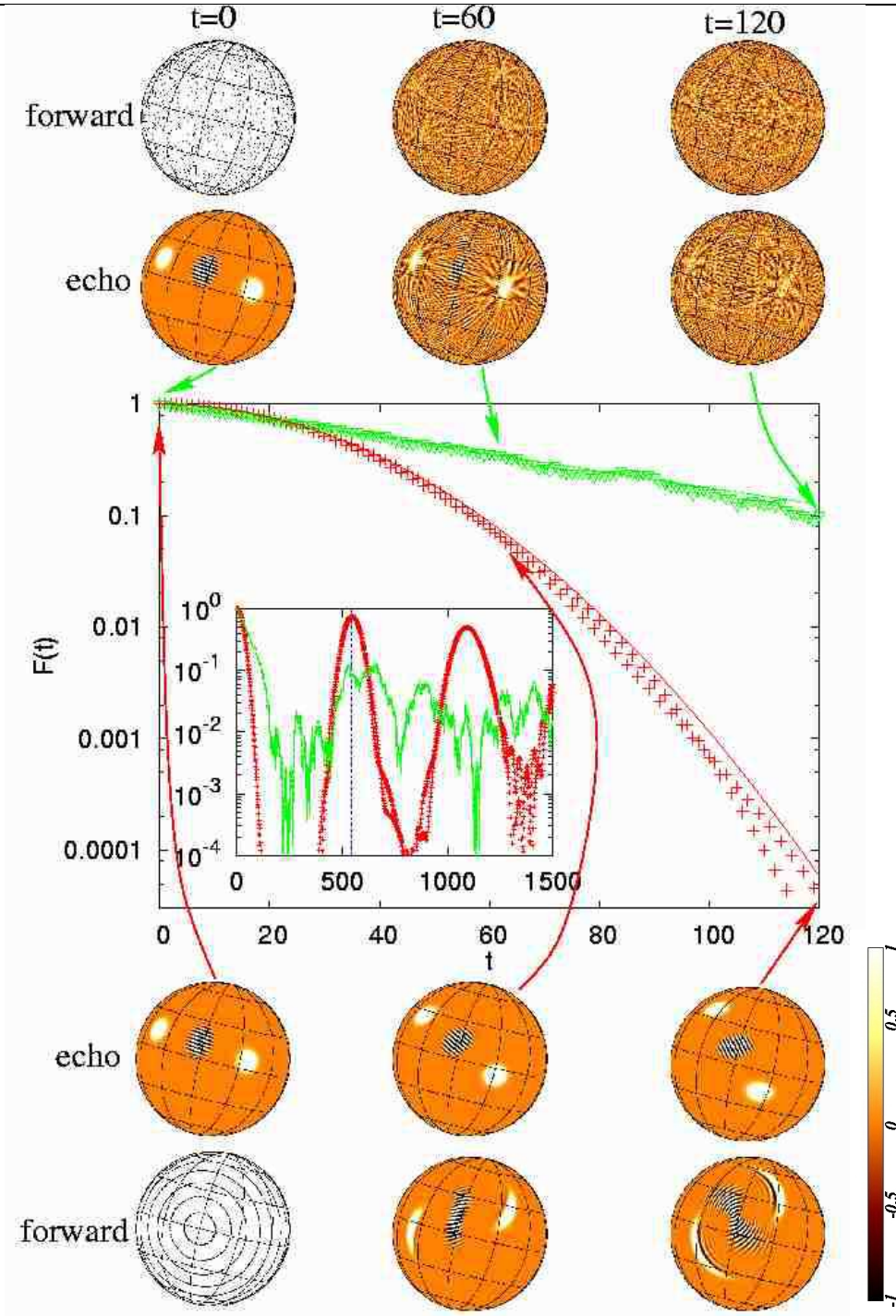


Figure 3.12: Fidelity decay for chaotic (top curve and pictures) and regular (bottom curve and pictures) kicked top. Initial conditions and the perturbation are the same in both cases (see text for details). Wigner functions after forward and echo evolution are shown.

3.3.2 Coupled Kicked Tops

As already remarked, for a one dimensional system ($d = 1$), the ‘surprising’ behaviour of the regular decay time being smaller than the mixing one, $\tau_r < \tau_m$, is for coherent initial states possible only around the border (3.50) δ_p (unless σ_{cl} is very small) where the exponential decay

in the mixing regime goes over to a Gaussian decay due to a finite \mathcal{N} . However, for more than one degree of freedom, such behaviour is generally possible well above the finite size perturbative border δ_p . In order to illustrate this phenomenon we will now briefly consider a numerical example of a pair of coupled kicked tops where $d = 2$.

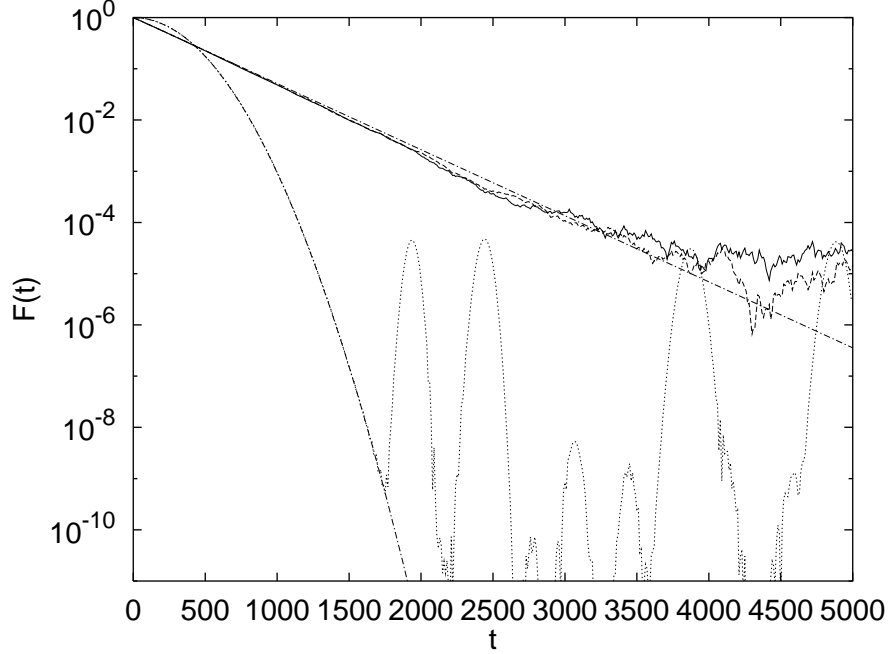


Figure 3.13: Fidelity decay for two coupled kicked tops, $\delta = 8 \cdot 10^{-4}$ and $S = 200$. The upper curves are for $\epsilon = 20$ (mixing regime), the solid curve for a coherent initial state and the dashed curve for a random one. The lower dotted curve is for $\epsilon = 1$ (regular regime) and a coherent initial state. The exponential and Gaussian chain curves give, respectively, the expected theoretical decays (3.5) and (3.36), with the Gaussian decay time determined by the best fit.

We take a simplified version of coupled kicked tops (2.25) with a unitary propagator

$$U(\epsilon) = e^{-i\frac{\pi}{2}S_{1y}} e^{-i\frac{\pi}{2}S_{2y}} e^{-i\epsilon S_{1z}S_{2z}/S}. \quad (3.57)$$

where \mathbf{S}_1 and \mathbf{S}_2 are two independent quantum angular momentum vectors. The perturbed propagator is obtained by perturbing the parameter ϵ , so that $U_\delta = U(\epsilon + \delta)$. The perturbation generator is therefore

$$V = \frac{1}{S^2} S_{1z} S_{2z}, \quad (3.58)$$

with $\hbar = 1/S$. We have used the propagator (3.57) over the full $(2S + 1)^2$ dimensional Hilbert space, without taking into account the symmetry classes of the double kicked top.

The classical limit is obtained by $S \rightarrow \infty$ and writing the classical angular momentum vectors in terms of two unit vectors on the sphere $\mathbf{r}_{1,2} = \mathbf{S}_{1,2}/S$. In component notation we get the classical map

$$\begin{aligned} x'_{1,2} &= z_{1,2} \\ y'_{1,2} &= y_{1,2} \cos(\epsilon z_{2,1}) + x_{1,2} \sin(\epsilon z_{2,1}) \\ z'_{1,2} &= -x_{1,2} \cos(\epsilon z_{2,1}) + y_{1,2} \sin(\epsilon z_{2,1}) \end{aligned} \quad (3.59)$$

We have chosen two regimes, non-ergodic (KAM) regime for $\epsilon = 1$ where a vast majority of classical orbits are stable, and mixing regime for $\epsilon = 20$ where no significant traces of stable classical orbits were found and where the correlation sum was to a very good accuracy given by the first term only

$$\sigma \approx \frac{1}{2}C(0) = \frac{1}{2S^4\mathcal{N}} \text{tr} S_{1z}^2 S_{2z}^2 = \frac{1}{18} \left(1 + \frac{1}{S}\right)^2. \quad (3.60)$$

The value of σ if the whole correlation sum is calculated is $\sigma = 0.058$, only slightly larger than $1/18$ given by $C(0)$. Our motivation here was to compare the regular and mixing fidelity decays for the coherent initial state which is here the product of spin coherent states (2.26) for each top

$$|\vartheta, \varphi\rangle = |\vartheta_2, \varphi_2\rangle \otimes |\vartheta_1, \varphi_1\rangle. \quad (3.61)$$

In Figure 3.13 we show the fidelity decay at $S = 200$ and $\delta = 8 \cdot 10^{-4}$ in regular and mixing

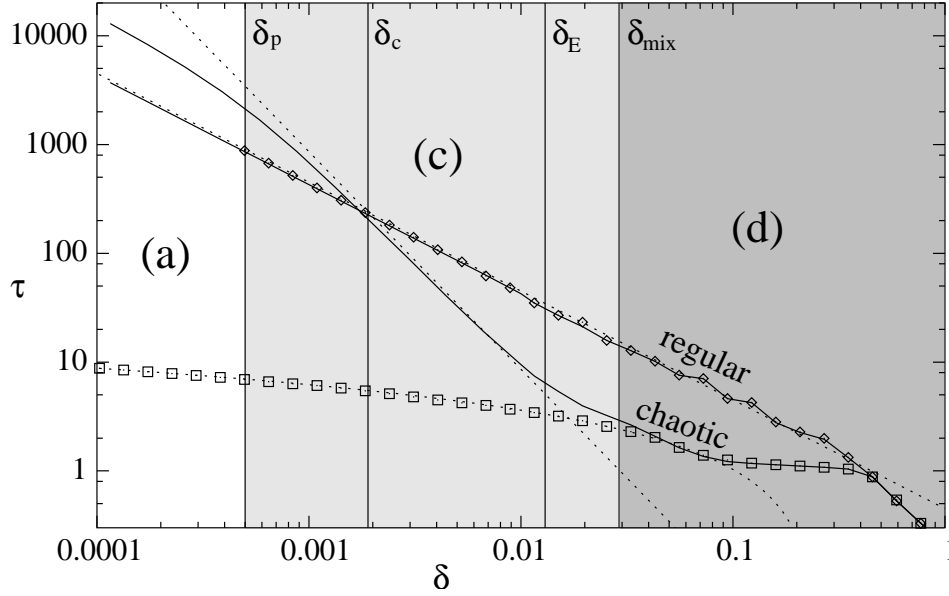


Figure 3.14: Numerically calculated decay time of the quantum and classical fidelity for the double kicked top. The two full curves show quantum fidelity, the one with a higher slope for the chaotic regime and the other for the regular regime. Symbols are decay times of classical fidelity, diamonds for the regular and squares for the chaotic regime. The two dotted straight lines are theoretical decay time predictions for the regular (3.63) and chaotic (3.62) regimes. The dotted curve (overlapping with squares) is the theoretical classical decay time $\tau_{\text{clas}} = \ln(0.25/\delta)/\lambda$. Vertical lines show the theoretical position of perturbation borders (3.64). The shading and the letters (a),(c) and (d) correspond to the regimes described in Figure 3.11. The Zeno regime corresponds to very short times $\tau < 1$ (i.e. strong perturbations $\delta > 0.4$).

cases starting from the coherent state (3.61) with $(\vartheta_1, \varphi_1) = (\vartheta_2, \varphi_2) = \pi(1/\sqrt{3}, 1/\sqrt{2})$. We find excellent agreement between the theoretical predictions (3.5) and (3.36) and the numerics. Note that we are here already in the regime $\delta < \delta_c$ where the fidelity decay in the mixing regime is slower than in regular regime. In mixing regime ($\epsilon = 20$) we show for comparison also the fidelity decay for a random initial state for which the decay is (due to ergodicity) almost identical to the one for coherent initial state. Overall the fidelity decay here is similar as in a one-dimensional case, however, the scaling of various time and perturbation scales on $\hbar = 1/S$ is different as discussed in Section 3.3. Observe also that in the regular regime the revivals of

fidelity (quantum recurrences at t_b) are much less pronounced in $d = 2$ than in $d = 1$ (e.g. in Figure 3.7).

To furthermore illustrate theoretical regimes of the fidelity decay as explained in the previous section (Figure 3.11) we numerically calculated the dependence of the time τ at which the fidelity falls to value 0.37 on the perturbation strength δ for the double kicked top model (3.57). The initial state is the same product coherent state as before. We also computed the decay time for the classical fidelity in order to compare the quantum and the classical fidelity. The results for $S = 100$ are on Figure 3.14. For both the classical and the quantum fidelity we calculated two sets of data, one for regular regime at $\varepsilon = 1$ and one for chaotic regime at $\varepsilon = 5$. Numerical data is then compared with the theoretical predictions. For the chaotic decay time we use previously calculated $\sigma = 0.058$ (3.60) to get τ_m (3.5)

$$\tau_m = \frac{8.6}{\delta^2 S^2}. \quad (3.62)$$

In the regular case we used fitting of the decay in Figure 3.13 to get the theoretical prediction (3.36), i.e. to obtain $\sqrt{\bar{v}'\Lambda^{-1}\bar{v}'}$,

$$\tau_r = \frac{4.5}{\delta\sqrt{S}}, \quad \sqrt{\bar{v}'\Lambda^{-1}\bar{v}'} = 0.31. \quad (3.63)$$

Note that the coefficient $\sqrt{\bar{v}'\Lambda^{-1}\bar{v}'}$ has been obtained by numerical fitting only for convenience. In principle it could be obtained from classical dynamics, but we would again have to resort to numerical calculations as the system at $\varepsilon = 1$ is in a mixed KAM-like regime. The values of σ and $\sqrt{\bar{v}'\Lambda^{-1}\bar{v}'}$ can then be used to calculate various perturbation borders as discussed in the beginning of Section 3.3. For our choice of $S = 100$ we get (3.50,3.55,3.54,3.53)

$$\delta_p = 0.0005, \quad \delta_c = 0.0019, \quad \delta_E = 0.013, \quad \delta_{\text{mix}} = 0.029. \quad (3.64)$$

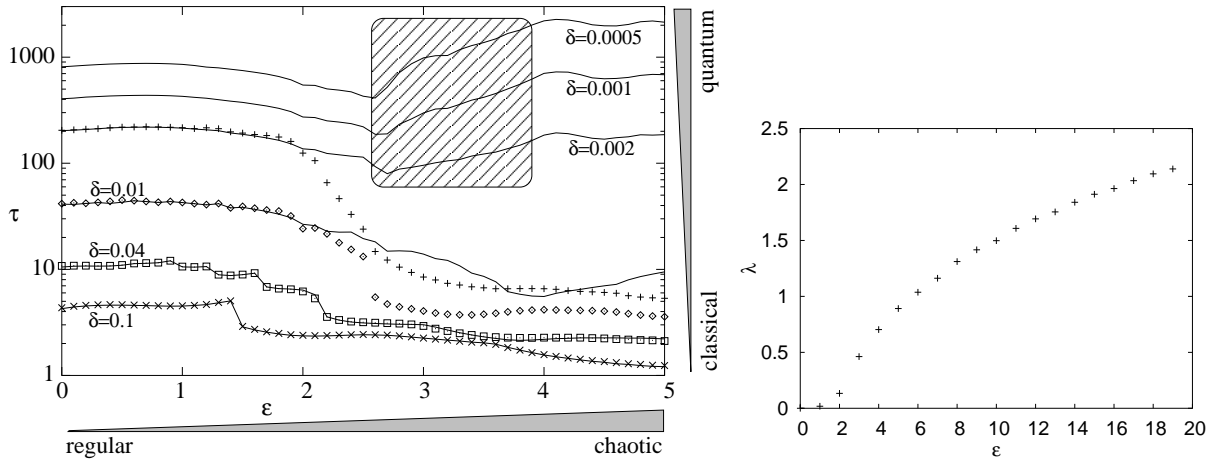


Figure 3.15: Numerically calculated dependence of quantum (solid lines) and classical (symbols) fidelity decay times on the parameter ε for the double kicked top. Different curves are for different perturbation strengths δ . By increasing ε the classical dynamics goes from regular to mixing regime, see also right figure showing the dependence on ε of numerically calculated Lyapunov exponents. By decreasing δ on the other hand, we go from the regime of quantum-classical correspondence for $\delta > \delta_E$ towards a genuinely quantum regime, where in a chaotic regime we can *increase* the decay time by *increasing* chaoticity – shaded region for the three smallest δ .

These theoretical borders are denoted with vertical lines in Figure 3.14. We can see, that in regular regime the quantum and the classical fidelity agree in the whole range of δ and furthermore agree with the theoretical τ_r . In the chaotic regime things are a bit more complicated. By decreasing perturbation from $\delta = 1$ we are at first in regime of very strong perturbation where the fidelity decay happens faster than any dynamical scale and it does not depend on whether we look at chaotic or regular system or quantum or classical fidelity. This is the so-called Zeno regime. For smaller δ the regular and chaotic regimes start to differ but in the chaotic regime we still have quantum-classical correspondence. This correspondence breaks down around δ_{mix} where the quantum fidelity starts to follow the theoretical τ_m , while the classical fidelity decay is $\tau_{\text{clas}} = \log(0.25/\delta)/\lambda$, with 0.25 being a fitting parameter (depending on the width of the initial packet) and $\lambda = 0.89$ is the Lyapunov exponent, read from Figure 3.15. For a brief explanation of this classical decay see Section 1.1.2. Incidentally, in our system at $\varepsilon = 5$ the classical mixing time is very short^{||}, $t_{\text{mix}} \sim 1$, and we see that the correspondence breaks already slightly before δ_E . The quantum fidelity decay time τ_m is valid until a perturbative border δ_p is reached, when a finite Hilbert space dimension effects become important and the decay time becomes equal to τ_p . Note that for $\delta < \delta_c$ we indeed have a faster fidelity decay for a *chaotic* dynamics than for a *regular* one.

Another interesting aspect of our correlation function formalism is that the decay rate of the fidelity in a mixing situation is proportional to the integral of the correlation function σ . As stronger chaoticity will usually result in a *faster decay* of $C(t)$ and therefore in smaller σ , this means that *increasing* chaoticity (of the classical system) will *increase* quantum fidelity, i.e. stabilise quantum dynamics. Of course, for this to be observable we have to be out of the regime of quantum-classical correspondence. All this is illustrated in Figure 3.15, where we show similar decay times as in Figure 3.14, i.e. the same system, initial condition and $S = 100$, but depending on the parameter ε for six different perturbation strengths δ . Parameter ε controls the chaoticity of the classical dynamics. At $\varepsilon = 1$ we are in the regular regime and for larger ε we get into the chaotic regime, also seen from the dependence of the Lyapunov exponent. We can see that in the regular regime ($\varepsilon < 2$) the classical fidelity agrees with the quantum one regardless of δ . In the chaotic regime though, the agreement is present only for the two largest δ shown, where we have $\delta > \delta_{\text{mix}}$ (3.64). For $\delta < \delta_c$ and for chaotic dynamics (three smallest δ) we get into the non-intuitive regime (shaded region in Figure 3.15) where the quantum fidelity will increase if we increase chaoticity. Note that this growth of the decay time stops at around $\varepsilon \sim 4$ because the classical mixing time t_{mix} gets so small that the transport coefficient is given by its time independent term $\sigma = C(0)/2$ alone.

^{||}This is the reason why σ (3.60) is almost entirely given by $C(0)$.

Chapter 4

Special Case: Zero Time Averaged Perturbation

One should always keep an open mind, but not so open that one's brains fall out.

—*Bertrand Russell*

In the previous chapter we considered general perturbations, for which the double correlation sum was growing with time either linearly for mixing dynamics or quadratically for regular systems. What about the third possibility, namely if it *does not* grow with time. This situation will be the subject of the present chapter. We will demand that $\langle \Sigma^2(t) \rangle \sim t^0$ for any initial state, i.e. all matrix elements of Σ^2 must be $\mathcal{O}(t^0)$,

$$\Sigma_{jk}^2(t) \propto t^0, \quad j, k = 1, \dots, \mathcal{N}. \quad (4.1)$$

We will write the perturbation V as the sum of its time average \bar{V} and the rest, called the *residual* part V_{res}

$$V =: \bar{V} + V_{\text{res}}. \quad (4.2)$$

For a nondegenerate* spectrum of the unperturbed propagator U_0 we have seen that the time averaged perturbation equals to the diagonal part of V (3.18) therefore, the residual V_{res} is just the off-diagonal part of V and has zeros on the diagonal, $(V_{\text{res}})_{kk} \equiv 0$. The operator $\Sigma(t)$ can then be written as $\Sigma(V, t) = \bar{V}t + \mathcal{O}(t^0)$, where the second part depends just on V_{res} and does not grow with time. One can conclude that to satisfy condition (4.1) the time averaged perturbation must be zero, $\bar{V} \equiv 0$. The subject of the present chapter are perturbations with $\bar{V} = 0$, also called *residual* perturbations because $V = V_{\text{res}}$. For non-residual perturbations all essential physics was contained in the operator $\Sigma(t)$. For residual perturbations on the other hand, the second term involving $\Gamma(t)$ in the BCH form (2.14) of the echo operator will also be important. Matrix elements of $\Gamma(t)$ in the eigenbasis of U_0 are

$$\begin{aligned} \frac{\langle \phi_j | \Gamma(t) | \phi_j \rangle}{t} &= \frac{1}{\hbar} \sum_{k \neq j} |V_{jk}|^2 \cot\left[\frac{1}{2}(\phi_k - \phi_j)\right] + \mathcal{O}(t^{-1}), \\ \frac{\langle \phi_j | \Gamma(t) | \phi_k \rangle}{t} &= \frac{1}{\hbar} (V_{jj} - V_{kk}) V_{jk} \frac{e^{-i\frac{1}{2}(\phi_j - \phi_k)} + e^{-i(\phi_j - \phi_k)(\frac{1}{2} - t)}}{2 \sin[\frac{1}{2}(\phi_k - \phi_j)]} + \mathcal{O}(t^{-1}), \quad j \neq k. \end{aligned} \quad (4.3)$$

*For degenerate spectra we have $\bar{V} = \sum_{k,l} \delta(\phi_k - \phi_l) V_{kl} |\phi_k\rangle \langle \phi_l|$.

Note that the matrix elements of $\Gamma(t)$ can not grow faster than linearly with t , despite the double sum over time in the definition of Γ . We see that, provided the perturbation is residual, the limit of *time-averaged* $\Gamma(t)$ defined as

$$\bar{\Gamma} = \lim_{t \rightarrow \infty} \frac{\Gamma(t)}{t} = \frac{i}{\hbar} \lim_{t \rightarrow \infty} \frac{1}{t} \sum_{t'=0}^{t-1} \sum_{t''=t'}^{t-1} [V(t'), V(t'')] \quad (4.4)$$

exists and is *diagonal* in the eigenbasis of U_0 :

$$\bar{\Gamma} = \sum_j \bar{\Gamma}_{jj} |\phi_j\rangle \langle \phi_j|, \quad \bar{\Gamma}_{jj} = \frac{1}{\hbar} \sum_{k \neq j} |V_{jk}|^2 \cot[\frac{1}{2}(\phi_k - \phi_j)]. \quad (4.5)$$

The operator $\bar{\Gamma}$ is again a constant of motion, $[U_0, \bar{\Gamma}] = 0$.

Any residual perturbation can be defined in terms of another operator W by the following prescription

$$V = W(1) - W(0), \quad W(t) := U_0^{-t} W U_0^t. \quad (4.6)$$

In the continuous time case we would have definition $V =: (d/dt)W = \frac{i}{\hbar}[H_0, W]$. Indeed, given a residual perturbation one easily determines the matrix elements of W as

$$W_{jk} := \frac{V_{jk}}{\exp(i(\phi_j - \phi_k)) - 1}. \quad (4.7)$$

Note that instead of the unperturbed evolution operator U_0 one could use any other unitary operator that has the same degeneracy and eigenvectors as U_0 in the definition of V in terms of W (4.6). With the newly defined operator W , the expression for $\Sigma(t)$ is extremely simple,

$$\Sigma(t) = W(t) - W(0). \quad (4.8)$$

Similarly, the expression for $\Gamma(t)$ is also considerably simplified,

$$\Gamma(t) = \Sigma_R(t) - \frac{i}{\hbar}[W(0), W(t)], \quad R := \frac{i}{\hbar}[W(0), W(1)], \quad (4.9)$$

and

$$\Sigma_R(t) := \sum_{t'=0}^{t-1} R(t'), \quad R(t) := U_0^{-t} R U_0^t. \quad (4.10)$$

The operator $\Gamma(t)$ is, apart from the term $\frac{i}{\hbar}[W, W(1)]$, similarly as $\Sigma(t)$ the sum of $R(t)$. In the continuous time case we have $R := \frac{i}{\hbar}[W, (d/dt)W] = \hbar^{-2}[W, [W, H_0]]$ and $\Gamma(t) = \int_0^t dt' R(t') - \frac{i}{\hbar}[W, W(t)]$. The fidelity decay will be given by the echo operator

$$M_\delta(t) = \exp \left\{ -\frac{i}{\hbar} \left(\Sigma(t)\delta + \frac{1}{2}\Gamma(t)\delta^2 + \dots \right) \right\}, \quad (4.11)$$

with $\Sigma(t)$ (4.8) and $\Gamma(t)$ (4.10) expressed in terms of the operator W . We see that for small times $t < t_2$, with $t_2 \sim 1/\delta$, the second term involving $\Gamma(t)$ can be neglected. Therefore, for $t < t_2$ the fidelity amplitude is simply

$$f(t) = \langle \exp(-i\delta(W(t) - W(0))/\hbar) \rangle. \quad (4.12)$$

Expanding $f(t)$ to the second order in δ , we find $F(t) = 1 - \frac{\delta^2}{\hbar^2}(\kappa_0^2 + \kappa_t^2 - C(t) - C(t)^*)$ where $\kappa_k^2 := \langle W^2(k) \rangle - \langle W(k) \rangle^2$, $C(t) := \langle W(t)W(0) \rangle - \langle W(t) \rangle \langle W(0) \rangle$. Using the Cauchy-Schwartz

inequality $|C(t)| \leq \kappa_0 \kappa_t$ and the fact that for a bounded operator W the sequence κ_t is bounded, say by r , we find a *freeze of fidelity*

$$1 - F(t) \leq 4 \frac{\delta^2}{\hbar^2} r^2, \quad t < t_2 \quad (4.13)$$

for *arbitrary* quantum dynamics, irrespective of the existence and the nature of the classical limit. For residual perturbation the fidelity therefore stays high up to a classically long time t_2 and only then starts to decay again. After t_2 the second term $\Gamma(t)$ will become important and this will cause the fidelity to decay. We have to stress that the freeze of fidelity is of purely quantum origin. The classical fidelity does not exhibit such behaviour.

Although residual perturbations might seem artificial at first sight, there are two possibilities how they can arise. First, the average perturbation \bar{V} commutes with the Hamiltonian H_0 generating U_0 and can sometimes be put together with the original H_0 into the unperturbed Hamiltonian, thereby resulting in a residual perturbation. This moving of \bar{V} into H_0 just changes the eigenenergies and is often done in various mean field approaches. Another possibility to have $\bar{V} = 0$ is due to symmetries. For instance, having a unitary symmetry P commuting with the unperturbed evolution, $[U_0, P] = 0$, and perturbation V anticommuting with the symmetry, $VP = -PV$, will result in a residual perturbation. But note that in order to have a well defined operator W (4.7) with no singularities near the diagonal, so that our theory can be applied, the matrix elements of V must increase smoothly away from the diagonal.

In the next two sections we will discuss two examples for which one can use the echo operator (4.11) to calculate fidelity decay to all orders in δ . This can be done for completely mixing dynamics and for the opposite extreme of regular dynamics. In both cases we will also assume the operators V , W , and therefore also R , to have well defined classical limits, so we will be able to use semiclassical arguments. For small times $t < t_2$ the fidelity will freeze to a constant value - the plateau. The value of the plateau will be determined by the non-increasing $\Sigma(t)$,

$$F_{\text{plat}}(t) = \left| \left\langle \exp \left(-i \frac{\delta}{\hbar} \{W(t) - W(0)\} \right) \right\rangle \right|^2. \quad (4.14)$$

For large times $t > t_2$ instead, the fidelity decay will be determined by the operator R in $\Gamma(t)$.

4.1 Mixing Dynamics

4.1.1 The Plateau

We begin with the linear response evaluation of the fidelity plateau (4.14). For classically mixing dynamics we can assume that for times larger than some mixing time t_1 the time correlations vanish in leading semiclassical order, $C(t) \rightarrow \mathcal{O}(\hbar)$. Also, quantum expectation values become time independent and equal to their classical values in leading order. We will denote by $\langle A \rangle_{\text{cl}} := \int d\mu A_{\text{cl}}$ the classical average value of observable A . Therefore, for times $t_1 < t < t_2$ the linear response expression for fidelity plateau, i.e. its time-independent value is

$$F_{\text{plat}} \cong 1 - \frac{\delta^2}{\hbar^2} (\kappa_0^2 + \kappa_{\text{cl}}^2), \quad \kappa_t^2 := \langle W^2(t) \rangle - \langle W(t) \rangle^2, \quad (4.15)$$

where $\kappa_{\text{cl}}^2 := \langle w^2 \rangle_{\text{cl}} - \langle w \rangle_{\text{cl}}^2$ is time-independent classical limit of κ_t^2 with the classical limit $w(\mathbf{q}, \mathbf{p})$ of operator W . We will consider two kinds of initial states, namely coherent states and random states. For coherent initial states (CIS) the mixing time t_1 is equal to the Ehrenfest time, $t_1 \sim -\ln \hbar / \lambda$. As the initial state variance of W is proportional to the spread of the CIS, $\kappa_0^2 \propto \hbar$, it can be neglected with respect to κ_{cl}^2 . The fidelity plateau for CIS is therefore

$F_{\text{plat}}^{\text{CIS}} \cong 1 - (\delta/\hbar)^2 \kappa_{\text{cl}}^2$. For random initial states (RIS), the mixing time is \hbar independent, $t_1 \propto \hbar^0$. Also initial state average for RIS is equal to ergodic average and the fidelity plateau is in this case $F_{\text{plat}}^{\text{RIS}} \cong 1 - 2(\delta/\hbar)^2 \kappa_{\text{cl}}^2$. Summarising, the linear response value of the fidelity plateau is for CIS and RIS

$$1 - F_{\text{plat}}^{\text{CIS}} \cong \frac{\delta^2}{\hbar^2} \kappa_{\text{cl}}^2, \quad 1 - F_{\text{plat}}^{\text{RIS}} \cong 2 \frac{\delta^2}{\hbar^2} \kappa_{\text{cl}}^2, \quad (4.16)$$

i.e. it is twice as large for RIS than for CIS.

One can go beyond linear response in approximating (4.14) using a simple fact that in the leading order in \hbar quantum observables commute, and as before, that for $t > t_1$ the time correlations vanish, namely $\langle \exp(-i\frac{\delta}{\hbar}(W(t) - W)) \rangle \cong \langle \exp(-i\frac{\delta}{\hbar}W(t)) \rangle \langle \exp(i\frac{\delta}{\hbar}W) \rangle$. For $t > t_1$ expectation values become time independent and so

$$F_{\text{plat}} \cong |\langle \exp(-i\omega\delta/\hbar) \rangle_{\text{cl}} \langle \exp(iW\delta/\hbar) \rangle|^2. \quad (4.17)$$

Note that the the right average is an average over initial state whereas the left average is the classical average over the invariant measure. The fidelity plateau can be compactly expressed in terms of a generating function $G(\delta/\hbar)$

$$G(z) := \langle \exp(-izw) \rangle_{\text{cl}} = \frac{1}{\mathcal{V}} \int d^d \mathbf{q} d^d \mathbf{p} \exp \{-iz w(\mathbf{q}, \mathbf{p})\}. \quad (4.18)$$

For CIS one can neglect the initial state average over a localized packet, i.e. the second term, and gets

$$F_{\text{plat}}^{\text{CIS}} \cong |G(\delta/\hbar)|^2. \quad (4.19)$$

For RIS on the other hand, initial state average is equal to the classical average in the leading order and we have

$$F_{\text{plat}}^{\text{RIS}} \cong |G(\delta/\hbar)|^4. \quad (4.20)$$

We have a universal relation between the plateau for CIS and RIS, namely $F_{\text{plat}}^{\text{RIS}} \cong (F_{\text{plat}}^{\text{CIS}})^2$. If the argument $z = \delta/\hbar$ of the generating function is large, the analytic function $G(z)$ can be calculated generally by the method of stationary phase. In the simplest case of a single isolated stationary point \mathbf{x}^* in N dimensions we obtain

$$|G(z)| \asymp \left| \frac{\pi}{2z} \right|^{N/2} \left| \det \partial_{x_j} \partial_{x_k} w(\mathbf{x}^*) \right|^{-1/2}. \quad (4.21)$$

This expression gives an asymptotic power law decay of the plateau height independent of the perturbation details. Note that for a finite phase space we will have oscillatory *diffraction corrections* to Eq. (4.21) due to a finite range of integration $\int d\mu$ which in turn causes an interesting situation for specific values of z , namely that by increasing the perturbation strength δ we can actually increase the value of the plateau.

We tested the above theory by numerical experiments. For the system we choose the kicked top, with slightly different order of factors as before (2.20). One step propagator is

$$U_0 := \exp \left(-i\alpha \frac{S_z^2}{2S} \right) \exp \left(-i\frac{\pi}{2} S_y \right). \quad (4.22)$$

We take $\alpha = 30$ ensuring fully chaotic classical dynamics whereas spin size is taken $S = 1000$ giving effective Planck's constant $\hbar = 1/S = 1 \cdot 10^{-3}$. Again we choose two initial states, a random one and a coherent one centred at $(\vartheta^*, \varphi^*) = (1, 1)$ and both are projected onto OE subspace (2.24). To get a residual perturbation we take $W := S_z^2/2S^2$ so that $W(1) = S_x^2/2S^2$ giving the perturbation generator

$$V := \frac{S_x^2 - S_z^2}{2S^2}. \quad (4.23)$$

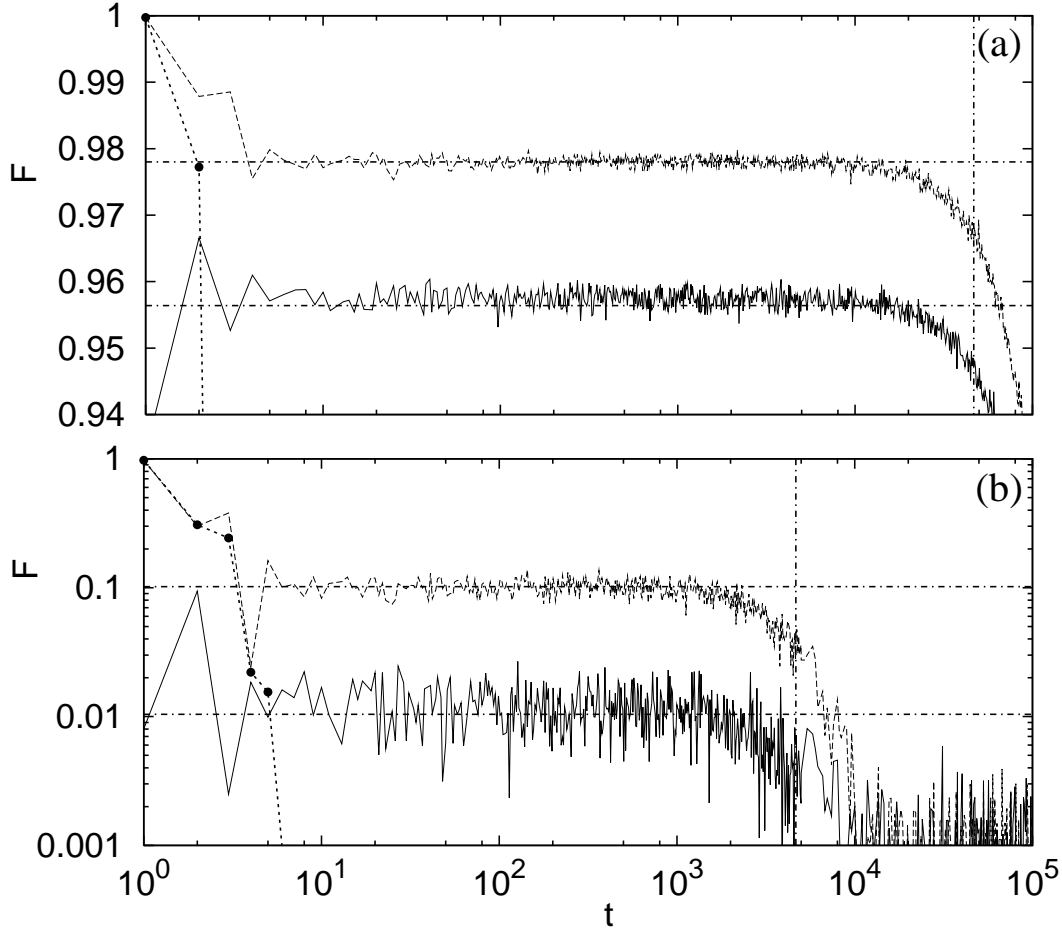


Figure 4.1: $F(t)$ for the kicked top with perturbations $\delta = 10^{-3}$ (a), and $\delta = 10^{-2}$ (b). In each plot the upper curve is for CIS and the lower for RIS. Horizontal chain lines are theoretical plateau values, linear response (4.16) in (a) and full (4.20,4.19) in (b). Vertical chain lines are theoretical values of t_2 (4.29). The full circles represent calculation of corresponding classical fidelity for the CIS which follows quantum fidelity up to the Ehrenfest ($\log \hbar$) barrier and exhibits no freezing.

The perturbed propagator is as always $U_\delta = U_0 \exp(-i\delta V/\hbar)$. We choose two perturbation strengths. A weak $\delta = 10^{-3}$ to check the linear response expressions (4.16). The results are seen in Figure 4.1a. The classical value of κ_{cl}^2 used in theoretical formulas is easily calculated for $w = z^2/2$ and one gets $\kappa_{\text{cl}}^2 = 1/45$. In Figure 4.1b we show numerical results for larger $\delta = 10^{-2}$ where the plateau is very low and full formulas must be used. Generating function (4.18) can be calculated exactly without stationary phase approximation, resulting in

$$G(\delta S) = \sqrt{\frac{\pi}{2\delta S}} \operatorname{erfi} \left(e^{i\pi/4} \sqrt{\delta S/2} \right). \quad (4.24)$$

We have an asymptotic power law decay as predicted by the general stationary phase formula[†] (4.21). In addition, due to a finite phase space we have a diffractive oscillatory erfi correction. Theoretical prediction for the plateau using $G(\delta S)$ (4.24) agrees well with the numerical results shown in the figure. Small quantum fluctuations around the theoretical plateau values lie beyond

[†]Note that $w = z^2/2$ has one stationary point in $N = 1$ dimension, despite the phase space being two-dimensional.

the leading semiclassical approximation used in our theoretical derivations. Note also that the quantum fidelity and its plateau values have been expressed (in the leading order in \hbar) in terms of classical quantities only. Yet, the freezing of fidelity is a purely quantum phenomenon as one can also see in Figure 4.1 where the classical fidelity does not exhibit freezing.

4.1.2 Beyond the Plateau

Next we shall consider the regime of long times $t > t_2$. Then the second term in the exponential of the echo operator (4.11) dominates the first one, however even the first term may not be negligible for large δ . Up to terms of order $\mathcal{O}(t\delta^3)$ we can factorize Eq. (4.11) as $M_\delta(t) \approx \exp(-i\frac{\delta}{\hbar}(W(t) - W)) \exp(-i\frac{\delta^2}{2\hbar}\Gamma(t))$. When computing the expectation value we again use the fact that in leading semiclassical order operator ordering is irrelevant and that, since $t \gg t_1$, any time-correlation can be factorized thus the second term $\frac{i}{\hbar}[W, W(t)]$ of $\Gamma(t)$ (4.9) vanishes and we have

$$F(t) \cong F_{\text{plat}} \left| \left\langle \exp \left(-i\frac{\delta^2}{2\hbar} \Sigma_R(t) \right) \right\rangle \right|^2, \quad t > t_2. \quad (4.25)$$

This result is quite intriguing. It tells us that apart from a pre-factor F_{plat} , the decay of the fidelity due to a residual perturbation is formally the same (in the leading semiclassical order when time ordering is not important) as the fidelity decay with a generic non-residual perturbation, eq. (2.11), when one substitutes the operator V with R and the perturbation strength δ with $\delta_R = \delta^2/2$. Thus we can directly apply the semiclassical theory of fidelity decay for general perturbations explained in Section 3.1, using a renormalised perturbation R of renormalised strength δ_R . Here we simply rewrite the key results in the 'non-Lyapunov' perturbation-dependent regime, $\delta_R < \hbar$. Using the classical transport rate σ_R ,

$$\sigma_R := \lim_{t \rightarrow \infty} \frac{\langle \Sigma_R^2(t) \rangle_{\text{cl}} - \langle \Sigma_R \rangle_{\text{cl}}^2}{2t}, \quad (4.26)$$

we have either an exponential decay

$$F(t) \cong F_{\text{plat}} \exp \left(-\frac{\delta^4}{2\hbar^2} \sigma_R t \right), \quad t < t_H, \quad (4.27)$$

or a (perturbative) Gaussian decay

$$F(t) \cong F_{\text{plat}} \exp \left(-\frac{\delta^4}{2\hbar^2} \sigma_R \frac{t^2}{t_H} \right), \quad t > t_H. \quad (4.28)$$

The crossover between the two decay regimes happens at the Heisenberg time $t_H = \mathcal{N}/2$ (3.10). Of course, the same consideration regarding the asymptotic saturation value of the fidelity \bar{F} due to a finite \mathcal{N} applies here as well (see discussion of time scales in Section 3.3). The prefactor F_{plat} can be calculated as described in the previous section, Eq. (4.17), and *depends* on the initial state. The exponential terms of (4.27,4.28) on the other hand *do not* depend on the initial state.

From the two possible regimes of long-time fidelity decay we can also more precisely specify time t_2 when the plateau ends. Comparing the two factors in (4.27,4.28) with the plateau value (Eq. 4.16 for $\delta < \hbar$), we obtain a semiclassical estimate of t_2

$$t_2 \approx \min \left\{ \sqrt{\frac{t_H \kappa_{\text{cl}}^2}{\sigma_R}} \frac{1}{\delta}, \frac{\kappa_{\text{cl}}^2}{\sigma_R \delta^2} \right\}. \quad (4.29)$$

In Figure 4.1 we can see nice agreement of theoretical t_2 with the results of the simulation.

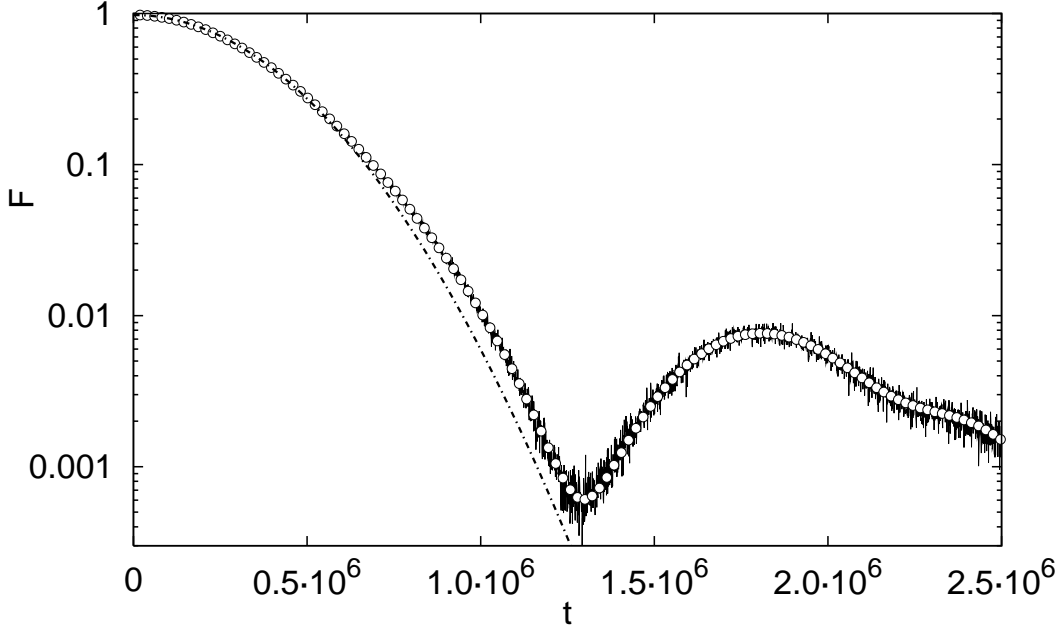


Figure 4.2: Long time Gaussian decay (4.28) for the same CIS and parameters as in Figure 4.1a. The full curve is a direct numerical simulation, empty circles are numerical calculation using a renormalised perturbation R of strength δ_R (4.30), while the chain curve gives the theoretical decay.

Interestingly though, as we have another time scale t_2 , the duration of the plateau, not present for a general case of non-residual perturbation, the exponential regime (4.27) can only take place if $t_2 < t_H$, otherwise we immediately get a Gaussian decay after the plateau. If one wants to keep $F_{\text{plat}} \sim 1$ (i.e. high) and have an exponential decay in the full range until the asymptotic $\bar{F} \sim 1/\mathcal{N}$, the condition on dimensionality is imposed. Namely, demanding high plateau $\delta/\hbar < 1$ for $t < t_2$ and low fidelity in the limit $\hbar \rightarrow 0$ at the Heisenberg time, $F(t_H) = \exp(-(\delta/\hbar)^4 \sigma_R / 4\hbar^{d-2})$, gives condition on dimensionality $d \geq 2$. In one dimensional systems and in the semiclassical limit the exponential decay (4.27) therefore can not be seen.

We again compared theory with numerics. The system is the one dimensional kicked top already used in the previous section describing the plateau. The perturbation generator R for our choice of W is

$$R = -\frac{1}{2S^3}(S_x S_y S_z + S_z S_y S_x), \quad (4.30)$$

having a classical limit $R_{\text{cl}} = r = -xyz$. We numerically calculated the integral of the classical correlation function (4.26) giving the transport coefficient $\sigma_R = 5.1 \cdot 10^{-3}$. In Figure 4.2 we show three different sets of data. Direct numerical calculation, “a renormalised calculation” obtained by taking perturbed dynamics as $U_\delta = U_0 \exp(-i\delta_R R/\hbar)$, i.e. perturbation generator R with the strength $\delta_R = \delta^2/2$ and theoretical Gaussian decay (4.28) where all parameters have been calculated classically. Apart from the plateau prefactor F_{plat} (which is close to 1) the decay does not depend on the initial state.

Double Kicked Top

To demonstrate that for $d > 1$ we can also get an exponential decay of the fidelity, we also consider a two dimensional system. We look at two ($d = 2$) coupled tops \mathbf{S}_1 and \mathbf{S}_2 described

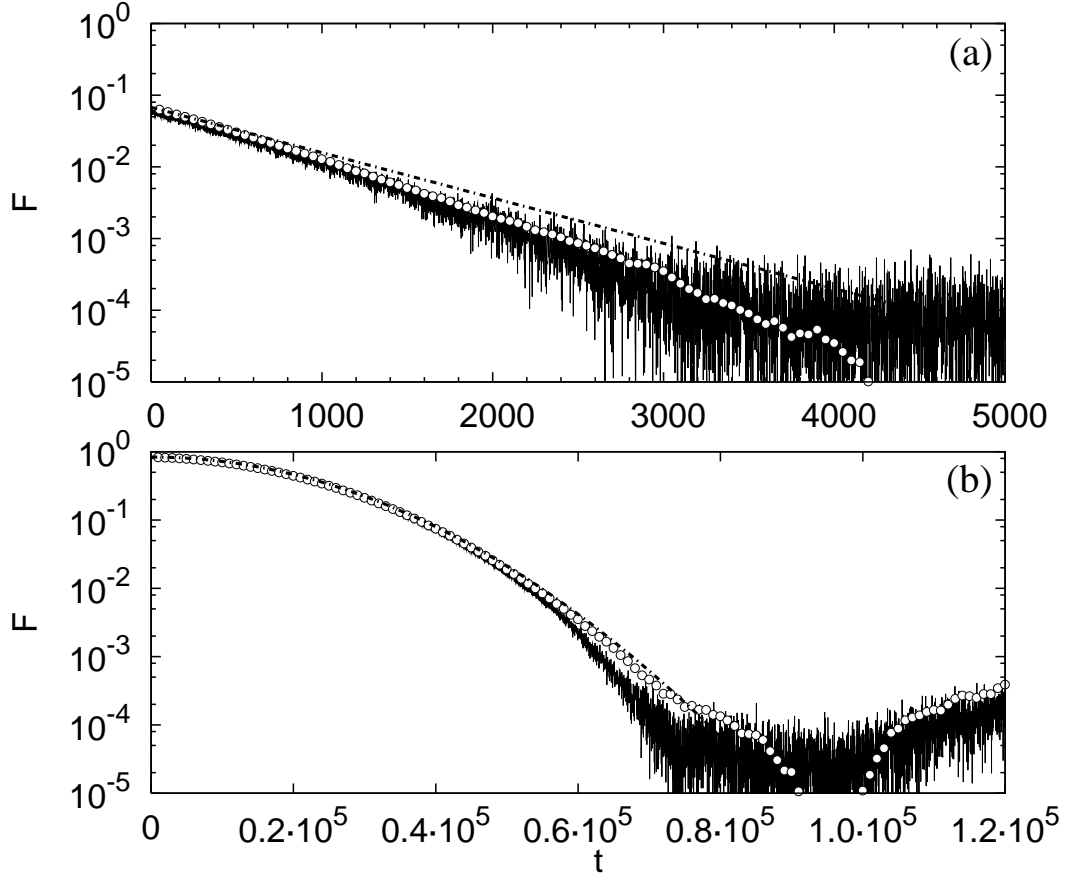


Figure 4.3: Long time fidelity decay for two coupled kicked tops. For strong perturbation $\delta = 7.5 \cdot 10^{-2}$ in (a) we obtain an exponential decay (4.27), and for smaller $\delta = 2 \cdot 10^{-2}$ in (b) we get a Gaussian decay (4.28). The three curves have the same meaning as in Figure 4.2.

by a propagator

$$U_0 = \exp(-i\varepsilon S_{z1} S_{z2}) \exp(-i\pi S_{y1}/2) \exp(-i\pi S_{y2}/2), \quad (4.31)$$

with a perturbation generated by

$$W = A_1 \otimes \mathbb{1} + \mathbb{1} \otimes A_2, \quad A = S_z^2/2S^2. \quad (4.32)$$

We set $S = 1/\hbar = 100$, and $\varepsilon = 20$ in order to be in a fully chaotic regime. The initial state is always a direct product of spin coherent states centred at $(\varphi_{1,2}, \vartheta_{1,2}) = (1, 1)$ which is subsequently projected on an invariant subspace of dimension $\mathcal{N} = S(S+1)$ spanned by $\{\mathcal{H}_{\text{OE}} \otimes \mathcal{H}_r\}_{\text{sym}}$, where $\mathcal{H}_r = \mathcal{H} \setminus \mathcal{H}_{\text{OE}}$ and $\{\cdot\}_{\text{sym}}$ is a subspace symmetric with respect to the exchange of the two tops. The results of numerical simulation are shown in Figure 4.3. We show only the long-time decay, as the situation in the plateau is qualitatively the same as for $d = 1$. For sufficiently large perturbation one obtains an exponential decay shown in Figure 4.3a, while for smaller perturbation we have a Gaussian decay shown in Figure 4.3b. Numerical data have been successfully compared with the theory (4.27,4.28) using a classically calculated $\sigma_R = 9.2 \cdot 10^{-3}$ together with theoretical F_{plat} , and with the “renormalised” numerics using the operator R , similarly as in Figure 4.2 for a one dimensional system.

4.2 Regular Dynamics

The procedure of calculating the fidelity decay for the case of regular dynamics will be similar as for general perturbations in Section 3.2. We will use the classical action-angle variables (for definition see Section 3.2.1) and semiclassical methods to calculate the fidelity plateau as well as its long time decay. The only difference will be that in contrast to the case of a general perturbation, where only $\Sigma(t)$ was important in the BCH form of the echo operator, here the second term involving $\Gamma(t)$ will also be relevant for long times. The same form of the echo operator (4.11) has already been used for the case of a residual perturbation in mixing systems as described in the previous section. The existence of action-angle variables enables us to expand the classical limit v of the quantum perturbation generator V into Fourier series

$$v(\mathbf{j}, \boldsymbol{\theta}) := \sum_{\mathbf{m} \neq \mathbf{0}} v_{\mathbf{m}}(\mathbf{j}) e^{i\mathbf{m} \cdot \boldsymbol{\theta}}. \quad (4.33)$$

The fact that the perturbation is residual is reflected in the zeroth Fourier coefficient which is zero, $v_0 \equiv 0$, so we explicitly excluded this term from the summation. Classically this means that the perturbation only changes the shapes of tori as the average change of the frequency along the unperturbed tori is zero. For the explanation of the decay of classical fidelity in case of a residual perturbation see (Benenti *et al.*, 2003a). Similarly, we can expand the classical limit $w(\mathbf{j}, \boldsymbol{\theta})$ of a quantum observable W ,

$$w(\mathbf{j}, \boldsymbol{\theta}) := \sum_{\mathbf{m} \neq \mathbf{0}} w_{\mathbf{m}}(\mathbf{j}) e^{i\mathbf{m} \cdot \boldsymbol{\theta}}. \quad (4.34)$$

The zeroth Fourier mode w_0 can be set to zero as it cancels in the definition of v in terms of w . Using these expansions we can easily calculate the leading semiclassical forms of $\Sigma(t)$ and $\Gamma(t)$. For $\Sigma(t)$ (4.8) we have

$$\Sigma(t) \cong w(\mathbf{J}, \boldsymbol{\Theta} + \boldsymbol{\omega}(\mathbf{J})t) - w(\mathbf{J}, \boldsymbol{\Theta}) \cong \sum_{\mathbf{m} \neq \mathbf{0}} w_{\mathbf{m}}(\mathbf{J}) (e^{i\mathbf{m} \cdot \boldsymbol{\omega}(\mathbf{J})t} - 1) e^{i\mathbf{m} \cdot \boldsymbol{\Theta}}. \quad (4.35)$$

Note that this is still an operator (capital \mathbf{J} and $\boldsymbol{\Theta}$) and is correct in the leading semiclassical order (the sign \cong). Coefficients $w_{\mathbf{m}}$ can be also expressed in terms of $v_{\mathbf{m}}$ as

$$w_{\mathbf{m}}(\mathbf{j}) = -ie^{-i\mathbf{m} \cdot \boldsymbol{\omega}(\mathbf{j})t/2} \frac{v_{\mathbf{m}}(\mathbf{j})}{2 \sin(\frac{1}{2}\mathbf{m} \cdot \boldsymbol{\omega}(\mathbf{j}))}. \quad (4.36)$$

In the continuous time case we have $w_{\mathbf{m}} = -iv_{\mathbf{m}}/\mathbf{m} \cdot \boldsymbol{\omega}$.

The operator $\Sigma(t)$ will determine the plateau. Long time decay on the other hand will be dictated by the operator $\Gamma(t)$. For long times when this decay will take place we can define an average $\bar{\Gamma}$ (4.4) and approximate $\Gamma(t) \approx \bar{\Gamma}t$. This approximation is justifiable as we will see, because the fidelity decay will happen on a long time scale $\sim 1/\delta^2$, whereas the average of $\Gamma(t)$ converges in a much shorter classical averaging time t_{ave} . As one can see from the definition of $\Gamma(t)$ in Eq. (4.9), the average $\bar{\Gamma}$ is nothing but the time averaged operator R . For R the semiclassical limit r can be calculated using the Poisson brackets instead of commutators, $r = -\{w, w(1)\}$. When we average r over time, only the zeroth Fourier mode survives resulting in

$$\bar{\Gamma}(\mathbf{J}) \cong \bar{r}(\mathbf{J}), \quad \bar{r}(\mathbf{j}) = - \sum_{\mathbf{m} \neq \mathbf{0}} \mathbf{m} \cdot \partial_{\mathbf{j}} \left\{ |w_{\mathbf{m}}(\mathbf{j})|^2 \sin[\mathbf{m} \cdot \boldsymbol{\omega}(\mathbf{j})] \right\}. \quad (4.37)$$

In the continuous time case we would have $\bar{r} = - \sum_{\mathbf{m} \neq \mathbf{0}} \mathbf{m} \cdot \partial_{\mathbf{j}} \{ |w_{\mathbf{m}}|^2 \mathbf{m} \cdot \boldsymbol{\omega} \}$.

From the equation for $w_{\mathbf{m}}$ (4.36) in terms of $v_{\mathbf{m}}$ we see that the denominator $\sin(\mathbf{m} \cdot \boldsymbol{\omega}/2)$ could cause problems at points of vanishing $\mathbf{m} \cdot \boldsymbol{\omega}(\mathbf{j}) = 0$. This divergence carries over to all

operators like $\bar{\Gamma}$ or $\Sigma(t)$. In classical perturbation theory this so-called “small denominator” problem is well known and cannot be avoided. For our quantum mechanical calculation though, there is an easy remedy. It is sufficient to remember that we are dealing with a residual perturbation, i.e. the one for which all matrix elements V_{jk} are zero if the corresponding eigenphases are equal, $\phi_j = \phi_k$. But the term $\mathbf{m} \cdot \boldsymbol{\omega}$ is nothing else than the semiclassical approximation for $\phi_j - \phi_k$. Therefore, one can see that actually all the diverging terms have to be excluded when evaluating expectation values. This is furthermore confirmed if we compare the semiclassical expression for $\bar{\Gamma}$ (4.37) with the matrix elements of operator $\Gamma(t)$ (4.3). An example of such a calculation will be presented when describing the decay for random initial states.

Using semiclassical expressions for $\Sigma(t)$ and $\bar{\Gamma}$ we can write the echo operator as

$$M_\delta(t) = \exp \left\{ -\frac{i}{\hbar} \left(\Sigma(t)\delta + \frac{1}{2}\bar{\Gamma}t\delta^2 \right) \right\}, \quad (4.38)$$

with $\Gamma(t)$ and $\bar{\Gamma}$ given in Eqs. (4.35,4.37). The third order term in the BCH form of the echo operator (4.38) can be shown to grow no faster than $\delta^3 t$ and can therefore be neglected. For times smaller than t_2 (specified later) the term involving $\bar{\Gamma}$ can be neglected and the fidelity will exhibit freeze. The fidelity amplitude of the plateau is $f(t)_{\text{plat}} \cong \langle \exp(-i\delta\Sigma(t)/\hbar) \rangle$ with semiclassical $\Sigma(t)$. Furthermore, for $t > t_1$ the fidelity plateau is time independent and can be calculated by averaging the fidelity amplitude over time

$$f_{\text{plat}} \cong \lim_{t \rightarrow \infty} \frac{1}{t} \sum_{t'=0}^t f(t'). \quad (4.39)$$

Time averaging the classical version of $\Sigma(t) = \Sigma(\mathbf{j}, \boldsymbol{\theta}(t))$ (4.35) is equivalent to averaging over the angle $\boldsymbol{\theta}$, resulting in the fidelity plateau

$$f_{\text{plat}} \cong \left\langle \exp \left(i \frac{\delta}{\hbar} w(\mathbf{J}, \boldsymbol{\Theta}) \right) \int \frac{d^d \mathbf{x}}{(2\pi)^d} \exp \left(-i \frac{\delta}{\hbar} w(\mathbf{J}, \mathbf{x}) \right) \right\rangle, \quad (4.40)$$

where we assumed ergodicity of $\mathbf{m} \cdot \boldsymbol{\omega} t$ so we could replace a sum over t with an integral over angles.

For long times $t > t_2$ the second term in the echo operator becomes dominant. If the plateau is small ($\delta < \hbar$), the first term with $\Sigma(t)$ can be neglected and the fidelity is

$$F(t) = \left| \left\langle \exp \left\{ -i \frac{\delta^2 t}{2\hbar} \bar{\Gamma}(\mathbf{J}) \right\} \right\rangle \right|^2. \quad (4.41)$$

For strong perturbations, when the plateau is not negligible, both terms should be retained. But as opposed to the mixing situation where we could factorize the two contributions, here one can not make any general statements. In the following theoretical calculations we will focus on the case when the plateau can be neglected in comparison with the long time decay. The formula (4.41) is completely analogous to the long time fidelity decay for a non-residual perturbation and we can use the same ASI representation in terms of an integral over classical actions. The role of \bar{V} is played by $\bar{\Gamma}$ and the perturbation is here $\delta^2/2$. The fidelity amplitude in the ASI formulation is therefore

$$f(t) \cong \hbar^{-d} \int d^d \mathbf{j} \exp \left(-i \frac{\delta^2 t}{2\hbar} \bar{r}(\mathbf{j}) \right) d_\rho(\mathbf{j}), \quad (4.42)$$

with $d_\rho(\mathbf{j})$ being the classical limit of $D_\rho(\hbar\mathbf{n}) = \langle \mathbf{n} | \rho | \mathbf{n} \rangle$ and recall that \bar{r} is the classical limit of $\bar{\Gamma}$ (4.37). The ASI representation is valid in a time range $t_1 < t < t_a$, where the upper limit t_a is determined by the variation of the phase over one Planck's cell,

$$t_a = \frac{2}{|\partial_j \bar{r}|_{\text{ef}}} \frac{1}{\delta^2} \sim \hbar^0 \delta^{-2}. \quad (4.43)$$

Before going on with the evaluation of the plateau (4.40) or of the long time decay (4.42) for random and coherent initial states, let us justify why we were allowed to time average the plateau.

Justification of Time Average Plateau

By expanding the echo operator into power series over δ , the calculation of the plateau is turned into calculation of expectation values of moments $\Sigma^k(t)$,

$$\Sigma^k(t) \cong \sum_{\mathbf{m}_1, \dots, \mathbf{m}_k \neq \mathbf{0}} \prod_{l=1}^k w_{\mathbf{m}_l}(\mathbf{J}) (e^{i\mathbf{m}_l \cdot \boldsymbol{\omega}(\mathbf{J})t} - 1) e^{i\mathbf{m}_l \cdot \boldsymbol{\Theta}}. \quad (4.44)$$

We can average over the initial density matrix ρ with matrix elements $\rho_{\mathbf{n}, \mathbf{n}'}$ in the action eigenbasis. Taking into account that the exponential of operator $\boldsymbol{\Theta}$ acts like a shift operator (3.26) and that eigenvalues of \mathbf{J} are $\hbar(\mathbf{n} + \boldsymbol{\alpha})$, we see that the expectation value will be a sum of terms of the form

$$\sum_{\mathbf{m}_1, \dots, \mathbf{m}_k \neq \mathbf{0}} \sum_{\mathbf{n}} g(\hbar\mathbf{n}) e^{i\mathbf{m} \cdot \boldsymbol{\omega}(\hbar\mathbf{n})t} \rho_{\mathbf{n}, \mathbf{n} + \mathbf{m}'}, \quad (4.45)$$

where the function g depends on indices \mathbf{m}_l , index $\mathbf{m}' := \sum_l^k \mathbf{m}_l$ and $\mathbf{m} := \sum_l^k s_l \mathbf{m}_l$ with $s_l = 0$ or 1 depending on which terms we take from the product in Eq. (4.44). We also neglected Maslov indices as they are negligible in the leading semiclassical order. For our derivation only the inner sum over \mathbf{n} is important. Let us consider two cases of initial states ρ , random initial state and coherent initial state.

For a random initial state we average over a random ensemble, resulting in $\rho_{\mathbf{n}, \mathbf{m}} \rightarrow \delta_{\mathbf{n}, \mathbf{m}}/\mathcal{N}$. From this we immediately conclude that index \mathbf{m}' in Eq. (4.45) must be zero, and as a consequence also $\mathbf{m} = \mathbf{0}$ is zero. Therefore, for random initial states only terms with all $\mathbf{m}_l \equiv \mathbf{0}$ survive the averaging over random ensemble (which is the same as if we would average over time instead of over random ensemble). The time scale t_1 after which approximation with a time average is permissible is determined just by frequencies, $t_1 \sim 1/|\mathbf{m} \cdot \boldsymbol{\omega}|$ and does not depend on \hbar or perturbation strength δ , i.e. for random initial states we have

$$t_1 \sim \delta^0 \hbar^0. \quad (4.46)$$

For localized initial states a little more work is needed to show that the expectation value equals the time average. For definiteness we will consider coherent initial states, for which the matrix elements have a Gaussian distribution (3.32). Furthermore, we will assume that the number of relevant Fourier modes is smaller than the width (in \mathbf{n}) of the initial packet. As the width of the packet grows as $\hbar^{-1/2}$ this is justifiable in the semiclassical limit provided $w(\mathbf{j}, \boldsymbol{\theta})$ is sufficiently smooth, so that its Fourier coefficients decrease sufficiently fast. In this approximation we have

$$\rho_{\mathbf{n}, \mathbf{n} + \mathbf{m}'} \cong d_\rho(\hbar\mathbf{n}) e^{i\mathbf{m}' \cdot \boldsymbol{\theta}^*}, \quad (4.47)$$

with d_ρ a classical limit of the quantum structure function (3.33). The inner summation over quantum actions $\hbar\mathbf{n}$ in Eq. (4.45) can now be replaced with an integral over the classical action

\mathbf{j} and the method of stationary phase can be used to calculate the resulting integral. Expanding frequencies around the centre of the packet \mathbf{j}^* , $\omega(\mathbf{j}^* + \mathbf{x}) = \omega(\mathbf{j}^*) + \Omega\mathbf{x} + \dots$, where

$$\Omega_{jk} := \frac{\partial \omega_j(\mathbf{j}^*)}{\partial j_k}, \quad (4.48)$$

is a matrix of frequency derivatives, we can calculate the sum

$$\begin{aligned} \sum_{\mathbf{n}} g(\hbar \mathbf{n}) e^{i\mathbf{m} \cdot \omega(\hbar \mathbf{n})t} d_\rho(\hbar \mathbf{n}) &\cong \hbar^{-d} \int d^d \mathbf{j} g(\mathbf{j}) e^{i\mathbf{m} \cdot \omega(\mathbf{j})t} d_\rho(\mathbf{j}) \\ &\cong g(\mathbf{j}^*) e^{i\mathbf{m} \cdot \omega(\mathbf{j}^*)t} \left(\frac{\hbar}{\pi} \right)^{d/2} |\det \Lambda|^{1/2} \int d^d \mathbf{x} \exp \left(-\frac{1}{\hbar} \mathbf{x} \cdot \Lambda \mathbf{x} + i\mathbf{t} \mathbf{m} \cdot \Omega \mathbf{x} \right) \\ &= g(\mathbf{j}^*) e^{i\mathbf{m} \cdot \omega(\mathbf{j}^*)t} \exp \left(-\frac{\hbar t^2}{4} \mathbf{m} \cdot \Omega \Lambda^{-1} \Omega^T \mathbf{m} \right). \end{aligned} \quad (4.49)$$

We see that all terms with $\mathbf{m} \neq \mathbf{0}$ decay to zero. The longest decay time scale of Gaussian envelopes is estimated as

$$t_1 = \left(\frac{\hbar}{4} \min_{\mathbf{m} \neq \mathbf{0}} \left(\mathbf{m} \cdot \Omega \Lambda^{-1} \Omega^T \mathbf{m} \right) \right)^{-1/2} \propto \hbar^{-1/2}. \quad (4.50)$$

This means that for times longer than t_1 only term with zero \mathbf{m} will survive which is equivalent to time averaging the classical expression. Note that the Gaussian decay (4.49) is absent if $\Omega = 0$, *e.g.* in the case of a d -dimensional harmonic oscillator. Fidelity decay for a residual perturbation in a harmonic oscillator will be discussed for a Jaynes-Cummings model in Section 5.5. There may also be a general problem with the formal existence of the scale t_1 (4.50) if the derivative matrix Ω is singular, but this may not actually affect the fidelity for sufficiently fast converging or finite Fourier series (3.23). Time t_1 can be interpreted as the *integrable Ehrenfest time*, up to which quantum-classical correspondence will hold. After t_1 a quantum wave packet of size $\sim \sqrt{\hbar}$ will spread over a classically large region of size $\sim \hbar^0$ and interference phenomena will become important. This will also be reflected in the fidelity. As the perturbation $w_{\mathbf{m}}$ will couple different tori, the echo packet will also start to exhibit interferences after t_1 and therefore we can expect agreement between quantum and classical fidelity only up to time t_1 . This must be contrasted with the case of a general non-residual perturbation, where there were no upper limits on the correspondence between quantum and classical fidelity for localized initial packets under certain conditions.

4.2.1 The Numerical Model

For the sake of numerical demonstration in the present section of residual perturbations in a regular dynamics we take an integrable kicked top model with a slightly different unperturbed one step propagator

$$U_0 = \exp \left(-i \frac{\alpha}{2} S \left\{ \frac{S_z}{S} - \beta \right\}^2 \right), \quad (4.51)$$

where we introduced a second parameter β . The classical map corresponding to U_0 is simply a twist around z-axis

$$\begin{aligned} x_{t+1} &= x_t \cos(\alpha(z_t - \beta)) - y_t \sin(\alpha(z_t - \beta)) \\ y_{t+1} &= y_t \cos(\alpha(z_t - \beta)) + x_t \sin(\alpha(z_t - \beta)) \\ z_{t+1} &= z_t. \end{aligned} \quad (4.52)$$

Unperturbed evolution represents a continuous time system with the classical Hamiltonian h_0 generating a frequency field $\omega(j)$

$$h_0(j) = \frac{1}{2}\alpha(j - \beta)^2, \quad \omega(j) = \alpha(j - \beta). \quad (4.53)$$

Here we used a canonical transformation from a unit-sphere to an action-angle pair $(j, \theta) \in [-1, 1] \times [0, 2\pi)$, namely

$$x = \sqrt{1 - j^2} \cos \theta, \quad y = \sqrt{1 - j^2} \sin \theta, \quad z = j. \quad (4.54)$$

We perturb the Hamiltonian by periodic kicking with a transverse pulsed field in x direction,

$$h_\delta(j, \theta, \tau) = \frac{1}{2}\alpha(j - \beta)^2 + \delta\sqrt{1 - j^2} \cos \theta \sum_{k=-\infty}^{\infty} \delta(\tau - k). \quad (4.55)$$

Perturbed quantum evolution is given by a product of two unitary propagators

$$U_\delta = U_0 \exp(-i\delta S_x), \quad (4.56)$$

so the perturbation generator is

$$V = S_x/S. \quad (4.57)$$

The classical perturbation has only one Fourier component, namely

$$v(j, \theta) = \sqrt{1 - j^2} \cos \theta, \quad v_{\pm 1}(j) = \frac{1}{2}\sqrt{1 - j^2}, \quad (4.58)$$

whereas zeroth Fourier component is zero, $v_0 \equiv 0$, indicating that we have a residual perturbation, $\bar{v} = 0$ and $\bar{V} = 0$. The classical limit w of W is also readily calculated, giving

$$w(j, \theta) = \frac{1}{2}\sqrt{1 - j^2} \frac{\sin(\theta - \omega/2)}{\sin(\omega/2)}, \quad (4.59)$$

with $\omega = \alpha(j - \beta)$. The reason we introduced parameter β is to be able to control a possible singularity in $w(j, \theta)$ at points where $\omega = 0$.

4.2.2 Coherent Initial State

The Plateau

For times $t < t_1$ quantum fidelity will follow the classical fidelity and will be system specific. For times $t_1 < t < t_2$ quantum fidelity will exhibit the plateau while the classical fidelity will continue to decay. To calculate the quantum plateau we have to evaluation the time-average formula for the plateau (4.40). We shall make use of the fact that for coherent states we have the expectation value

$$\langle \exp(-(i\delta/\hbar)g(\mathbf{J}, \boldsymbol{\Theta})) \rangle \cong \exp(-(i\delta/\hbar)g(\mathbf{j}^*, \boldsymbol{\theta}^*)). \quad (4.60)$$

for some smooth function g , provided that the size of the wave-packet $\sim \sqrt{\hbar}$ is smaller than the oscillation scale of the exponential $\sim \hbar/\delta$, *i.e.* provided $\delta \ll \hbar^{1/2}$. Then the squared modulus of f_{plat} (4.40) reads

$$F_{\text{plat}}^{\text{CIS}} \cong \frac{1}{(2\pi)^{2d}} \left| \int d^d \boldsymbol{\theta} \exp\left(-\frac{i\delta}{\hbar}w(\mathbf{j}^*, \boldsymbol{\theta})\right) \right|^2. \quad (4.61)$$

It is interesting to note that the angle θ^* does not affect the probability F_{plat} as it only rotates the phase of the amplitude f_{plat} . Note the similarity of this result with the plateau for coherent initial states and mixing dynamics, Eq. (4.19). In the mixing case we had an equilibrium average of w in $2d$ dimensional phase space, whereas for regular dynamics we have an average over only d dimensional angle-space of θ . For weak perturbation $\delta < \hbar$ only the linear response expression for the plateau is needed. Expanding general F_{plat} we obtain

$$1 - F_{\text{plat}}^{\text{CIS}} = \frac{\delta^2}{\hbar^2} \nu_{\text{CIS}}, \quad \nu_{\text{CIS}} = \sum_{\mathbf{m} \neq \mathbf{0}} |w_{\mathbf{m}}(\mathbf{j}^*)|^2. \quad (4.62)$$

Results of the numerical simulation for $\beta = 0$, $\alpha = 1.1$ are shown in Figure 4.4. For our choice of the perturbation (4.59) the integral in the semiclassical expression of the plateau (4.61) is readily calculated. Actually, the calculation of F_{plat} can be analytically carried out for any perturbation with a single nonzero Fourier mode $\pm \mathbf{m}_0$, with the result

$$F_{\text{plat}}^{\text{CIS}} = J_0^2 \left(2 \frac{\delta}{\hbar} |w_{\mathbf{m}_0}(\mathbf{j}^*)| \right), \quad (4.63)$$

where J_0 is the zero order Bessel function. For a more general multi-mode perturbations we have to evaluate the integral (4.61) numerically. For our single mode perturbation w (4.59) we have

$$F_{\text{plat}}^{\text{CIS}} = J_0^2 \left(\delta S \frac{\sqrt{1 - j^{*2}}}{2 \sin(\alpha j^*/2)} \right). \quad (4.64)$$

The linear response expansion of this general result reads

$$1 - F_{\text{plat}}^{\text{CIS}} = (\delta S)^2 \nu_{\text{CIS}}, \quad \nu_{\text{CIS}} = \frac{1 - j^{*2}}{8 \sin^2(\alpha j^*/2)}. \quad (4.65)$$

For numerical illustration in Figure 4.4 the initial coherent packet has been placed at $(\vartheta^*, \varphi^*) = (1, 1)$. We can see that until time t_1 (4.50) quantum fidelity follows the classical one (circles in Figure 4.4). After t_1 quantum fidelity freezes at the plateau, whose value nicely agrees with the linear response formula (4.65) or with the full expression (4.64) for strong perturbation. Vertical chain lines show theoretical values of t_2 , which is the time when the plateau ends. Also, at certain times the quantum fidelity exhibits resonances, i.e. strong revivals of fidelity. These “spikes” occurring at regular intervals are prominent also in a long time decay of fidelity in Figure 4.5. These will be called the *echo resonances* and are particular to one-dimensional systems.

Long Time Decay

To obtain long time decay of quantum fidelity one has to evaluate the ASI in Eq.(4.42). Everything is analogous to the case of general non-residual perturbation described in Section 3.2. In the formula for $F(t) = \exp(-(t/\tau_r)^2)$ (3.36) we only have to replace the perturbation δ with $\delta^2/2$ and \bar{v} with \bar{r} , so that the fidelity decay is

$$F(t) \cong \exp \left\{ -(t/\tau_{\text{rr}})^2 \right\}, \quad \tau_{\text{rr}} = \frac{1}{\delta^2} \sqrt{\frac{8\hbar}{\bar{\mathbf{r}}' \cdot \Lambda^{-1} \bar{\mathbf{r}}'}}, \quad (4.66)$$

with the semiclassical \bar{r} given in Eq. (4.37) and its derivative $\bar{\mathbf{r}}' := \partial_{\mathbf{j}} \bar{r}$. The decay time scales as $\tau_{\text{rr}} \sim \hbar^{1/2} \delta^{-2}$ and is thus smaller than the upper limit $t_a \sim \hbar^0 \delta^{-2}$ of the validity of the stationary phase approximation used in deriving the Gaussian decay. Remember that the

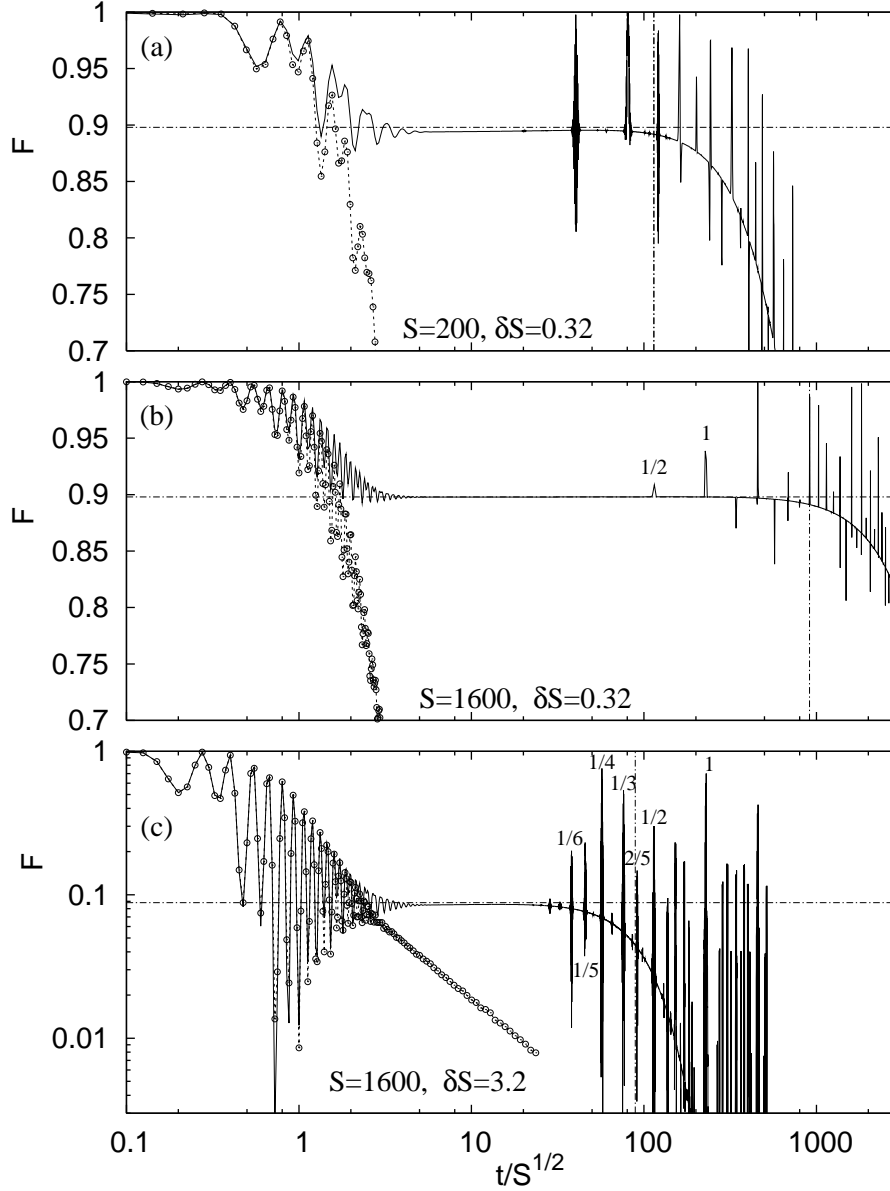


Figure 4.4: Short time decay of the fidelity for a quantized top is shown for the coherent initial state, for $S = 200$ (a), and $S = 1600$ (b), with a fixed product $\delta S = 0.32$, where the plateau is well described by linear response. In (c) we show $S = 1600$ and a stronger perturbation with $\delta S = 3.2$. Note that the time axis is rescaled as t/t_1 . Symbols connected with dashed lines denote the corresponding classical fidelity. The horizontal chain line denotes the theoretical value of the plateau (4.64), while the vertical chain line denotes the estimated theoretical value for t_2 (4.67). In (b,c) we also indicate fractional $2\pi k/p$ resonances with k/p marked on the figure (see text for details).

above formula is valid only if the plateau is small and the $\Sigma(t)$ term can be neglected, i.e. for $\delta < \nu_{\text{CIS}}^{-1/2}\hbar$. For such small δ the crossover time t_2 from the plateau to the long time decay can be estimated by comparing the linear response plateau (4.65) with the long time decay (4.66), $(\delta/\hbar)^2 \nu_{\text{CIS}} \approx (t_2/\tau_{\text{tr}})^2$, resulting in $t_2 \approx \tau_{\text{tr}} \delta \sqrt{\nu_{\text{CIS}}}/\hbar \sim \hbar^{-1/2} \delta^{-1}$. For stronger perturbations,

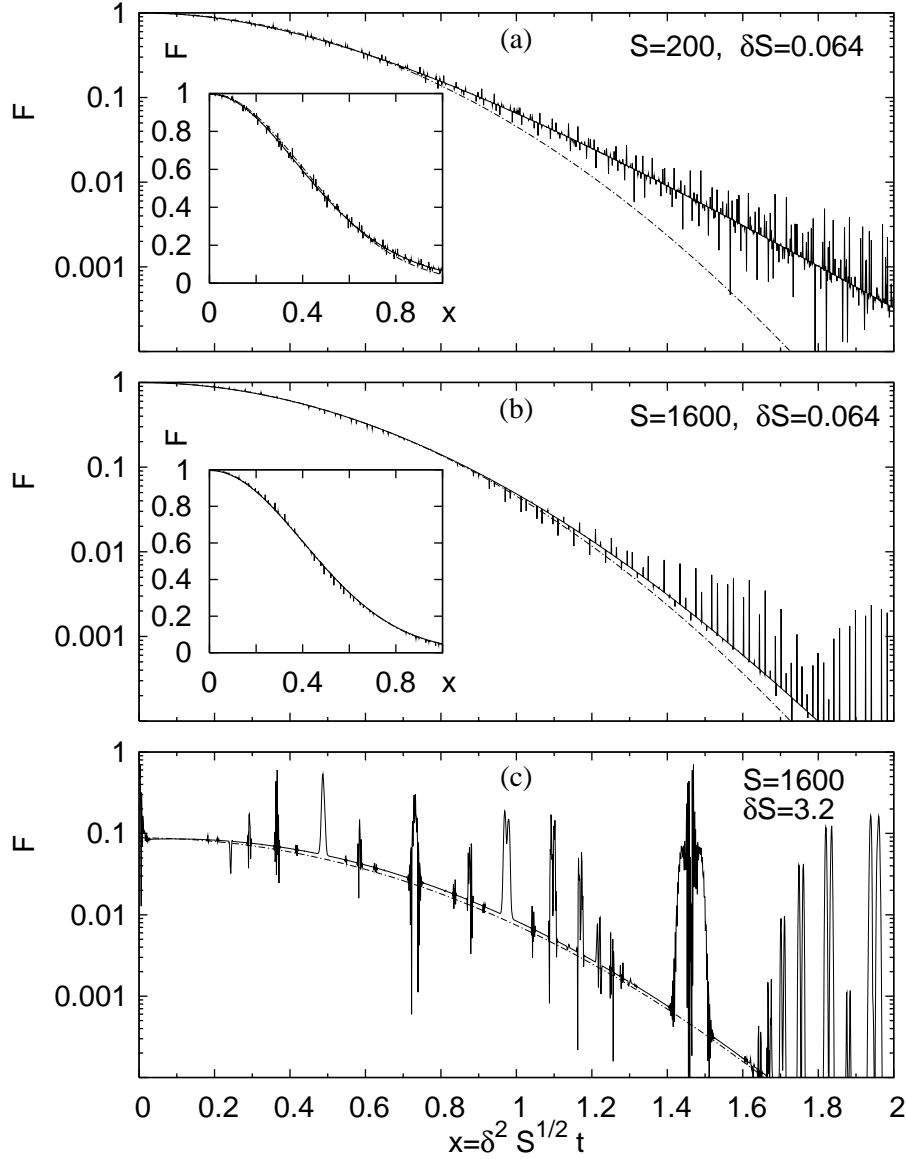


Figure 4.5: Long time ballistic decay of the fidelity for the kicked top with coherent initial state is shown for cases $S = 200$ (a), and $S = 1600$ (b), of weak perturbation $\delta S = 0.064$, and for strong perturbation $S = 1600, \delta S = 3.2$ (c). Chain curves indicate a theoretical Gaussian (4.66) with analytically computed coefficients, except in case (c), where we multiply the theoretical Gaussian decay by a prefactor 0.088 being equal to the theoretical value of the plateau (4.64), and re-scale the exponent of the Gaussian by a factor 0.8 taking into account the effect of a non-small first term in the exponent of (4.38). Note that in the limit $S \rightarrow \infty$ the agreement with semiclassical theory improves and that the size of the resonant spikes is of the same order as the drop in the linear response plateau. The insets show the data and the theory on the normal scale.

namely up to $\delta \sim \sqrt{\hbar}$ time t_2 can be simply estimated by τ_{rr} . We therefore have

$$t_2 = \min\left\{1, \frac{\delta}{\hbar} \nu_{\text{CIS}}^{1/2}\right\} \tau_{\text{rr}} = \min\{\text{const } \hbar^{1/2} \delta^{-2}, \text{const } \hbar^{-1/2} \delta^{-1}\}. \quad (4.67)$$

Time scale t_2 can be seen in Figure 4.4 as the point of departure of fidelity from the plateau value. Using our model with $\alpha = 1.1$ and $\beta = 0$ and the position of the initial coherent state

at $(\vartheta^*, \varphi^*) = (1, 1)$ this can be calculated to be $t_2 = \min\{0.57\sqrt{S}/\delta, 0.57/(\delta^2\sqrt{S})\}$ (similarity of numerical prefactors is just a coincidence). These theoretical positions of t_2 are shown with vertical chain lines in Figure 4.4 and are given by $\tau_{\text{rr}}\nu_{\text{CIS}}^{1/2}\delta/\hbar$ in Figures 4.5a,b while it is τ_{rr} for a strong perturbation $\delta S = 3.2$ in Figure 4.4c. Long time decay of fidelity is shown in figure 4.5. Theoretical Gaussian decay (4.66), shown with a chain curve, is again confirmed by numerical results. The average $\bar{\Gamma}$ given by classical \bar{r} is (4.37)

$$\bar{r} = \frac{1}{8\sin^2(\alpha j/2)} \left\{ \alpha(1 - j^2) + 2j \sin(\alpha j) \right\}. \quad (4.68)$$

The derivative \bar{r}' is

$$\bar{r}' = \frac{1}{8} \left\{ 4 \cot(\alpha j/2) - \alpha \left[4j + \alpha(1 - j^2) \cot(\alpha j/2) \right] / \sin^2(\alpha j/2) \right\}, \quad (4.69)$$

which gives using $\Lambda = 1/(1 - j^2)$ for spin coherent states the decay time (4.66) $\tau_{\text{rr}} = 0.57\delta^{-2}\hbar^{1/2}$. Note that we do not have any fitting parameters, except in the case of a strong perturbation ($\delta S \gg 1$, Figure 4.5c) where the prefactor and the exponent of a Gaussian had to be slightly adjusted due to the non-negligible effect of the first term in (4.38) [see caption for details].

Average fidelity

We should remark that, although we obtain asymptotically Gaussian decay of fidelity for a single coherent initial state, one may be interested in an *effective fidelity* averaged with respect to phase-space positions of the initial coherent state, similarly as for the case of general perturbations (3.42). For times $t < t_2$ when we have a plateau, the average fidelity $\langle F(t) \rangle_j$ will also have a plateau of the same height as the plateau for a random initial state calculated in Section 4.2.4, Equation (4.82). In the linear response regime this plateau is just twice as large as for a single coherent state. Long time decay of the average fidelity $\langle F(t) \rangle_j$ will be given by the phase space average of the regular decay time τ_{rr} . The calculation is very similar to the one for a general perturbation described at the end of Section 3.2.2 so we won't repeat it here. Asymptotically we will have a power law decay with the power determined by the order η of zeros of $\bar{\mathbf{r}}' \cdot \Lambda^{-1}\bar{\mathbf{r}}'$ and dimensionality d (see Eq. 3.43) which is not universal as claimed by some authors (Jacquod *et al.*, 2003). To demonstrate asymptotic power law decay (3.43) we take the same regular kicked top model (4.51) as used throughout this section with parameter $\alpha = 1.1$, $\beta = 0$ and spin size $S = 1000$. We take perturbation (4.57) of strength $\delta = 5 \cdot 10^{-4}$ and average fidelity over 200 coherent initial states placed randomly over sphere. The results are in Figure 4.6. The τ_{rr}^2 , i.e. $\bar{\mathbf{r}}' \cdot \Lambda^{-1}\bar{\mathbf{r}}'$ has for our $\bar{\mathbf{r}}'$ (4.69) two zeros of the first order, $\eta = 1$, at $j = \pm 1$. The derivative (i.e. the first nonzero term in the expansion around zero) of the term $\bar{\mathbf{r}}' \cdot \Lambda^{-1}\bar{\mathbf{r}}'$ evaluated at $j = -1$ is

$$c = \frac{2\alpha - \sin \alpha}{2\sin^2(\alpha/2)}. \quad (4.70)$$

The asymptotic theoretical decay (3.43) should then be

$$\langle F(t) \rangle_j \asymp \frac{8}{\delta^4 S t^2 c}, \quad (4.71)$$

where for $\alpha = 1.1$ the coefficient is $c = 2.4$. This theoretical decay agrees with numerics in Figure 4.6. The theoretical value of the plateau according to the Equation (4.84) for a random initial state should be 0.58 which also agrees with numerics.

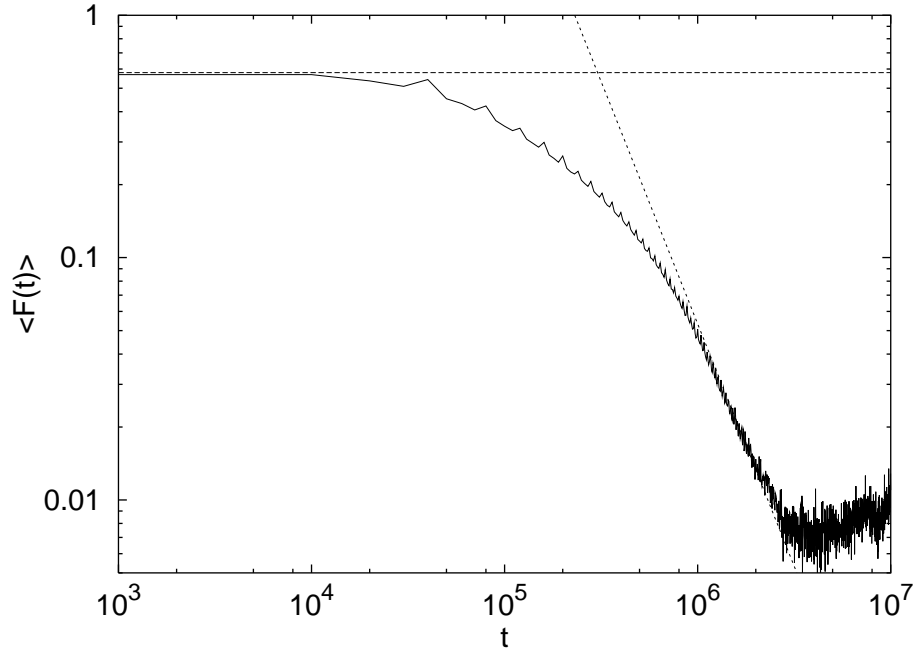


Figure 4.6: Average fidelity decay $\langle F(t) \rangle_j$ (4.71) for the regular kicked top with freezing (no fitting parameters!). The dotted line is the theoretical power law decay (4.71). The horizontal line gives the theoretical value of the plateau (4.84).

Illustration in Terms of Wigner Function

All the phenomena described theoretically in the preceding subsections can be nicely illustrated in terms of the *echoed Wigner function* — the Wigner function $W_{\rho_M}(\cos \vartheta, \varphi)$ of the echo-dynamics. For details regarding the spin Wigner functions see Appendix A and the discussion at the end of Section 3.3. The fidelity $F(t)$ is given simply by the overlap of the echoed Wigner function and the Wigner function of the initial state. Therefore, the phase-space chart of the echoed Wigner function contains the most detailed information on echo-dynamics and illustrates the essential differences between different regimes of fidelity decay. This is shown in Figure 4.7 for the quantized top, see also online movies (Prosen & Žnidarič, 2003a). In the initial *classical regime*, $t < t_1$, the echoed Wigner function has not yet developed negative values and is in point-wise agreement with the Liouville density of the classical echo-dynamics. In the *plateau regime*, $t_1 < t < t_2$, the echoed Wigner function decomposes into several pieces, one of which freezes at the position of the initial packet providing significant and constant overlap — the plateau. At very particular values of time, namely at the echo resonances, different pieces of the echoed Wigner function somehow magically recombine back into the initial state. In the asymptotic, *ballistic regime*, $t > t_2$, even the frozen piece starts to drift ballistically away from the position of the initial packet, thus explaining a fast Gaussian decay of fidelity.

4.2.3 Echo Resonances for Coherent Initial States

Let us now discuss the behaviour of the fidelity for initial wave-packets in the regime of linear response approximation in some more detail. We shall consider possible deviations from the time average plateau (4.40). Specifically we will explain the resonances observed *e.g.* in Figure 4.4.

For such a resonance to occur the phases of terms $\langle \Sigma^k(t) \rangle$ (4.44) have to build up in a constructive way and this is clearly impossible in a generic case, unless:

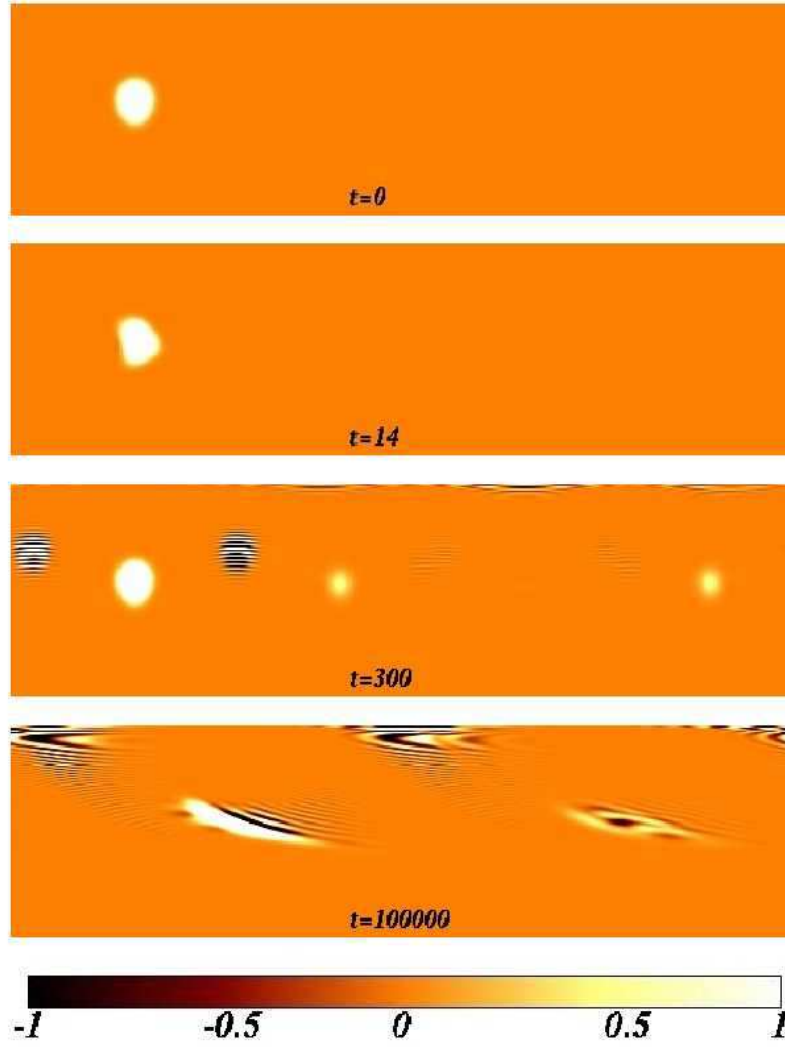


Figure 4.7: [Movies online (Prosen & Žnidarič, 2003a)] Snapshots of the Wigner function of echo-dynamics for a quantized top $\alpha = 1.1, \beta = 0, \gamma = 0$ with $S = 200$ and for $\delta = 1.6 \cdot 10^{-3}$ (same as in Figures 4.4a, 4.8a). The upper hemisphere is shown with $j = \cos \vartheta \in [0, 1]$ on the vertical axis and $\theta = \varphi \in [0, 2\pi]$ on the horizontal axis. From top to bottom we show: the initial state at $t = 0$, the state at $t = 14 \approx t_1$ when we are around the regular Ehrenfest time, at $t = 300$ in the middle of the plateau, and at $t = 100000$ in the ballistic regime.

- (i) We have one dimension $d = 1$, so we sum up over a one-dimensional array of integers n in action space[‡].
- (ii) The wave-packet is localized over a classically small region of the action space/lattice such that a variation of the frequency derivative $d\omega(j)/dj$ over this region is sufficiently small.

In this subsection we thus consider a one-dimensional case, $d = 1$. For simplicity we will focus on a linear response regime, so we will study time-dependent terms $\langle \Sigma^2(t) \rangle$ and $\langle \Sigma(t) \rangle$ with $\Sigma(t)$ given in Eq. (4.35). In the justification of the time average plateau, Section 4.2, we replaced a sum over n with an integral over action space. Here the time is not small enough

[‡]In more than one dimension we would clearly need a strong condition on commensurability of frequency derivatives over the entire region of the action lattice where the initial state is supported.

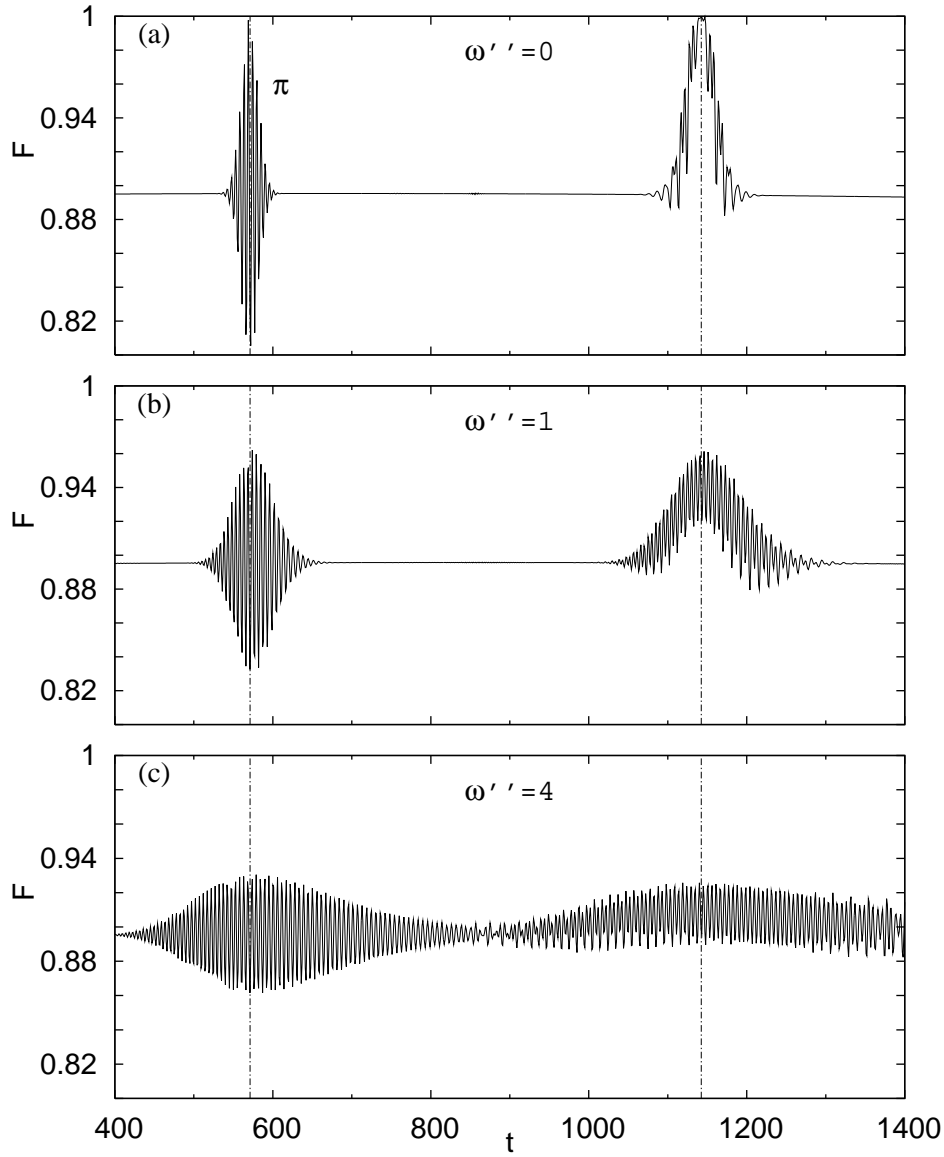


Figure 4.8: Structure of echo resonances for coherent initial states of the modified quantum top $U_0 = \exp(-iS[\alpha(S_z/S)^2/2 + \gamma(S_z/S - j^*)^3/6])$, $S = 200$, $\delta = 1.6 \cdot 10^{-3}$, for increasing values of $\omega'' = \gamma = 0$ (a), $\omega'' = 1$ (b), and $\omega'' = 4$ (c), which weakens and broadens the resonances. Note that in (a), $\omega'' = 0$ we have the same data as in Figure 4.4a. Vertical chain lines show theoretical times $t_r/2$ for π , and t_r for 2π resonances.

and furthermore the very graininess of quantum actions is the source of resonances and we will have to explicitly consider sums over n . We seek a condition, such that consecutive phases in the exponential build up an interference pattern.

2π -resonance:

Let us expand the frequency around the centre of the packet

$$\omega(j) = \omega^* + (j - j^*)\omega' + \frac{1}{2}(j - j^*)^2\omega'' + \dots \quad (4.72)$$

where $\omega^* = \omega(j^*)$, $\omega' = d\omega(j^*)/dj$ and $\omega'' = d^2\omega(j^*)/dj^2$. The phases in the sums of the form (4.49) with factors $e^{im\omega(\hbar n)}$ come into resonance, for $m = 1$ and hence for any higher $m \geq 1$, when they change by 2π per quantum number, which happens at time t_r ,

$$\hbar\omega't_r = 2\pi, \quad t_r = \frac{2\pi}{\hbar\omega'}, \quad (4.73)$$

and its integer multiples. It is interesting to note that these resonant times correspond precisely to the condition for *revivals* of the wave-packet in the *forward* evolution (apart from a phase-space translation) studied in (Braun & Savichev, 1996) and (Leichtle *et al.*, 1996). In addition, we need that the coherence of linearly increasing phases is not lost along the size of the wave-packet, *i.e.*

$$\zeta := m\omega''t\Delta_j^2 = \frac{\hbar m\omega''t}{2\Lambda} < 2\pi, \quad (4.74)$$

where we denoted by $\Delta_j := \langle (j - j^*)^2 \rangle^{1/2} = \sqrt{\frac{\hbar}{2\Lambda}}$ the action-width of the initial wave-packet. Therefore, if $\zeta \ll 2\pi$ we will observe echo resonances at integer multiples of 2π -resonance time t_r .

The shape of the echo resonance can also be derived. Let time t be *close* to kt_r , $k \in \mathbb{Z}$, and write $t = kt_r + t'$ where $t' \ll t_r$, so that $\hbar\omega't' \ll 2\pi$. We can estimate the general time dependent sum over n in entirely analogous fashion to Eq. (4.49) by: (i) shifting the time variable to t' , (ii) incorporating the resonance condition, and (iii) approximating the resulting sum by an integral, due to the smallness of t' ,

$$\begin{aligned} \sum_n g(\hbar n) e^{im\omega(\hbar n)t} d_\rho(\hbar n) &\cong \sum_n g(\hbar n) e^{im(\omega^* + (\hbar n - j^*)\omega' + \frac{1}{2}(\hbar n - j^*)^2\omega'')(t_r + t')} d_\rho(\hbar n) \\ &= e^{im\omega^*t} \sum_n g(\hbar n) e^{im((\hbar n - j^*)\omega't' + \frac{1}{2}(\hbar n - j^*)^2\omega''t)} d_\rho(\hbar n) \\ &\cong e^{im\omega^*t} g(j^*) \sqrt{\frac{\Lambda}{\pi\hbar}} \int dj e^{im((j - j^*)\omega't' + \frac{1}{2}(j - j^*)^2\omega''t) - \frac{\Lambda}{\hbar}(j - j^*)^2} \\ &= e^{im\omega^*t} g(j^*) \frac{1}{\sqrt{1 - i\zeta}} \exp\left(-\frac{\hbar m^2\omega'^2 t'^2}{4\Lambda} \frac{1 + i\zeta}{1 + \zeta^2}\right). \end{aligned} \quad (4.75)$$

We see that the resonance has a Gaussian envelope, modulated with an oscillation frequency $\approx \omega^*$. At the resonance centre $t' = 0$, and assuming $\zeta \ll 1$, we can easily calculate the linear response terms in the fidelity, getting $\langle \Sigma^2(t) \rangle = \langle \Sigma(t) \rangle^2$. Therefore, for small ζ the fidelity at a 2π echo resonance is 1. We get a perfect revival of fidelity. For non-negligible ζ , the resonance height dies as $(1 + \zeta^2)^{-1/2}$. As ζ depends on time t , the resonances will decrease in height with the increasing order k of the resonance. That is, for the k -th resonance occurring at $t = kt_r$ we have

$$\zeta = k \frac{\pi m \omega''}{\Lambda \omega'}, \quad (4.76)$$

and the magnitude of the resonances therefore falls as $\sim 1/k$. We will get strong and numerous resonances, *i.e.* small ζ , provided that either the second derivative ω'' is small, or the initial state is squeezed such that $\Lambda \gg 1$. For example, if the second derivative vanishes everywhere, $\omega'' \equiv 0$, then the resonances may appear even for extended states. This is the case for our numerical model, where resonances can be seen also for a random state in Figure 4.10. The Gaussian envelope of the resonance has an effective width

$$\Delta_r = \frac{m\omega'}{\Delta_j} \sqrt{1 + \zeta^2} \sim k/\sqrt{\hbar}. \quad (4.77)$$

In the semiclassical limit, the resonance positions scale as $t_r \propto \hbar^{-1}$, while their widths grow only as $\Delta_r \propto \hbar^{-1/2}$, so they are well separated. On the other hand, with increasing order k the resonance width grows, and they eventually start to overlap at $k \sim 1/\sqrt{\hbar}$. This overlapping takes place at time $\sim \hbar^{-3/2}$ and is smaller than t_2 provided $\delta < \nu_{\text{CIS}}^{-1/2} \hbar$.

The structure of 2π -resonance is nicely illustrated in a numerical example in Figure 4.8, where we consider a slightly modified model with

$$U_0 = \exp(-iS[\alpha(S_z/S)^2/2 + \gamma(S_z/S - j^*)^3/6]), \quad (4.78)$$

corresponding to $h_0(j) = \alpha j^2/2 + \gamma(j - j^*)^3/6$ and a coherent initial state at $(\vartheta, \varphi) = (1, 1)$. For such a system $\omega'' = \gamma$ may not be identically vanishing and $\omega' = \alpha$.

π - and

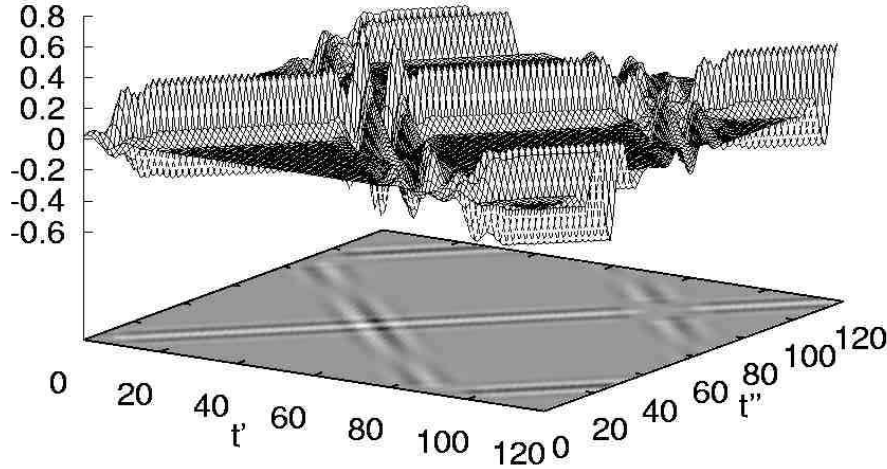


Figure 4.9: Two-time correlation function $C(t', t'')$ (2.18) for the quantized top with $\alpha = 1.1$, $\gamma = 0$, $S = 16$, and coherent initial state at $(\vartheta, \varphi) = (1, 1)$. The structures giving rise to a π and 2π resonance can be seen.

We note that one may obtain a resonance condition for a single time-dependent term (4.75) with fixed m even at a shorter time, namely for $t = t_r/m$. This is trivially the case for perturbations with many, or at least more than one Fourier components with $|m| > 1$. However, in such cases only selected time-dependent terms of the moment will be affected, so the fidelity will generically *not come back to 1*, even in the linear response regime and in the strongly resonant case $\zeta \ll 1$. Such (incomplete) resonances at fractional times $(k/m)t_r$ will be called $2\pi/m$ -resonances.

However, we may obtain a resonant condition at $t = t_r/2$ even for the first Fourier component $m = 1$ of the perturbation, as taking the square of the operator $\Sigma(t)$ produces Fourier components $m + m' = \pm 2$. Such a resonant behaviour at times $(k + \frac{1}{2})t_r$ will be called a π -resonance.

So for perturbations with a *single* Fourier mode $m = \pm 1$, or more generally with only odd-numbered Fourier modes $m = 2l + 1$, the π -resonance can affect only the term having $e^{i(m+m')\omega(\hbar n)t}$ in the expression for the second moment. All other terms (having a single m in the phase) result in their time-averaged values. To see this, we observe that the time dependent

parts of the form $g(\hbar n)e^{im\omega t}$ are proportional to $\sum_n d_\rho(\hbar n)g(\hbar n)(-1)^{mn}$. As m is an odd number and $d_\rho(\hbar n)g(\hbar n)$ is a smooth function of n , this sum averages to zero. This allows us to again compute explicitly the fidelity in linear response close to the peak in a strongly resonant case. We find

$$\begin{aligned}\langle \Sigma(t) \rangle &\cong - \sum_{m=2l+1} w_m(j^*) e^{im\theta^*}, \quad \text{for } |t - (k + \frac{1}{2})t_r| \ll \Delta_t, \text{ and } \zeta \ll 1, \\ \langle \Sigma^2(t) \rangle &\cong \left(\sum_{m=2l+1} w_m(j^*) e^{im\theta^*} \right)^2 + \left(\sum_{m=2l+1} w_m(j^*) e^{im(\theta^* + \omega^* t)} \right)^2, \\ 1 - F(t) &\cong \frac{\delta^2}{\hbar^2} \left(\sum_{m=2l+1} |w_m(j^*)| \cos(m\omega^* t + \beta_m) \right)^2,\end{aligned}\tag{4.79}$$

where β_m are phases of complex numbers $w_m(j^*)e^{im\theta^*}$. So we have learned that the fidelity at the peak of a π -resonance displays an oscillatory pattern, oscillating precisely around the plateau value $F_{\text{plat}}^{\text{CIS}}$ (4.62) with an amplitude of oscillations equal to $1 - F_{\text{plat}}^{\text{CIS}}$ so that the fidelity comes back to 1 close to the peak of the resonance.

Again, our numerical example illustrates such an oscillatory structure of π -resonance in Figure 4.8. The resonances can also be nicely seen in ‘short-time’ Figure 4.4, and because $\zeta = 0$ also in the ‘long-time’ Figure 4.5. In Figure 4.9 we depict the structure of π - and 2π -resonance as reflected in the two-time correlation function $C(t', t'')$. Note that the first intersection of the soliton-like-trains for $t' - t'' = \text{const}$ and $t + t' = \text{const}$ happens at $t_r/2$ and produces a π -resonance, while the second intersection at t_r produces a 2π -resonance.

In analogy to the emergence of a π -resonance as a consequence of the contribution from the *second* moment of $\Sigma(t)$, even for the first Fourier mode $m = 1$, we shall eventually obtain also fractional $2\pi/p$ -resonances at times $(k/p)t_r$ in the non-linear-response regimes where higher moments $\langle \Sigma^p(t) \rangle$ contribute to $F(t) \sim \langle \exp(-i\Sigma(t)\delta/\hbar) \rangle$. This is illustrated numerically in Figure 4.4c showing the case of strong perturbation $\delta S = 3.2$ so that higher orders are important. One indeed obtains fractional resonances, some of which have been marked on the figure.

4.2.4 Random Initial States

The second specific case of interest is that of random initial states. Here we shall assume that our Hilbert space has a finite dimension \mathcal{N} , like e.g. in the case of the kicked top or a general quantum map with a finite classical phase space, or it is determined by some large classically invariant region of phase space, e.g. we may consider all states $|\mathbf{n}\rangle$ between two energy surfaces $E_1 < h_0(\hbar \mathbf{n}) < E_2$ of an autonomous system. In any case we have the scaling

$$\mathcal{N} \cong \frac{\mathcal{V}}{(2\pi\hbar)^d},\tag{4.80}$$

where \mathcal{V} is the volume of the relevant classical phase space. Throughout this section we will assume that the Hilbert space size \mathcal{N} is sufficiently large, so that the difference between the expectation value in a single random state and an average over the whole space can be neglected. Also, as discussed in Section 2.2.2, the difference between the average fidelity amplitude squared and the average fidelity is semiclassically small.

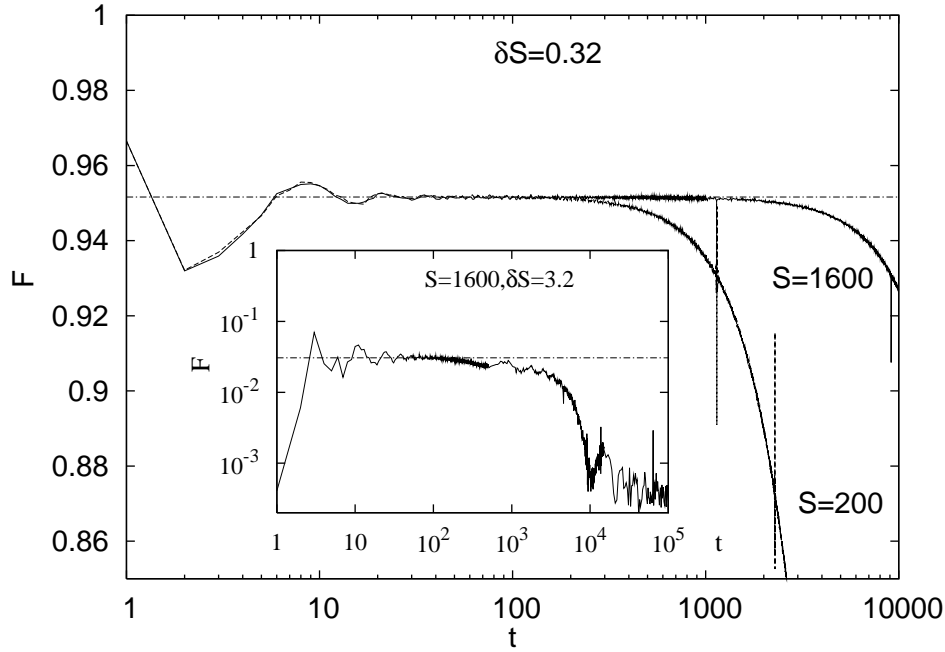


Figure 4.10: Short time fidelity for a quantized top with $\beta = 1.4$ (having no singularities) and a random initial state. In order to reduce statistical fluctuations, averaging over 20 random initial states is performed for $S = 1600$, and over 100 initial states for $S = 200$. The horizontal chain line shows the semiclassical theory (4.82). Echo resonances (two spikes for $S = 200$) are here present due to the special property $\omega''(j) = 0$ and will be absent for a more generic unperturbed system. The main figure shows the case of the weak perturbation $\delta S = 0.32$, whereas the inset is for the strong perturbation $\delta S = 3.2$.

The Plateau

To calculate the plateau we replace the quantum expectation value $\langle \bullet \rangle$ with a classical phase space average, resulting in a fidelity amplitude

$$f_{\text{plat}}^{\text{RIS}} \cong \frac{(2\pi)^d}{\mathcal{V}} \int d^d \mathbf{j} \left| \int \frac{d^d \boldsymbol{\theta}}{(2\pi)^d} \exp \left(-\frac{i\delta}{\hbar} w(\mathbf{j}, \boldsymbol{\theta}) \right) \right|^2. \quad (4.81)$$

Interestingly, the plateau for a random initial state is just the *average* plateau for a coherent state squared, where averaging is done over the position of the initial coherent state. If we denote the plateau for a coherent initial state centred at \mathbf{j}^* by $F_{\text{plat}}^{\text{CIS}}(\mathbf{j}^*)$ (Eq. 4.61), then the plateau for a random initial state $F_{\text{plat}}^{\text{RIS}}$ is simply

$$F_{\text{plat}}^{\text{RIS}} \cong \left| \frac{(2\pi)^d}{\mathcal{V}} \int d^d \mathbf{j} F_{\text{plat}}^{\text{CIS}}(\mathbf{j}) \right|^2. \quad (4.82)$$

Similarly as in mixing dynamics there is a square relationship between the plateau for RIS and CIS. In the mixing case the plateau for CIS does not depend on the position of the initial state due to ergodicity, here though the plateau for CIS does depend on \mathbf{j}^* and one has to take a square of the average plateau for CIS. In the linear response approximation one has a simple formula for the plateau

$$1 - F_{\text{plat}}^{\text{RIS}} \cong \frac{\delta^2}{\hbar^2} \nu_{\text{RIS}}, \quad \nu_{\text{RIS}} = 2 \frac{(2\pi)^d}{\mathcal{V}} \int d^d \mathbf{j} \sum_{\mathbf{m} \neq 0} |w_{\mathbf{m}}(\mathbf{j})|^2. \quad (4.83)$$

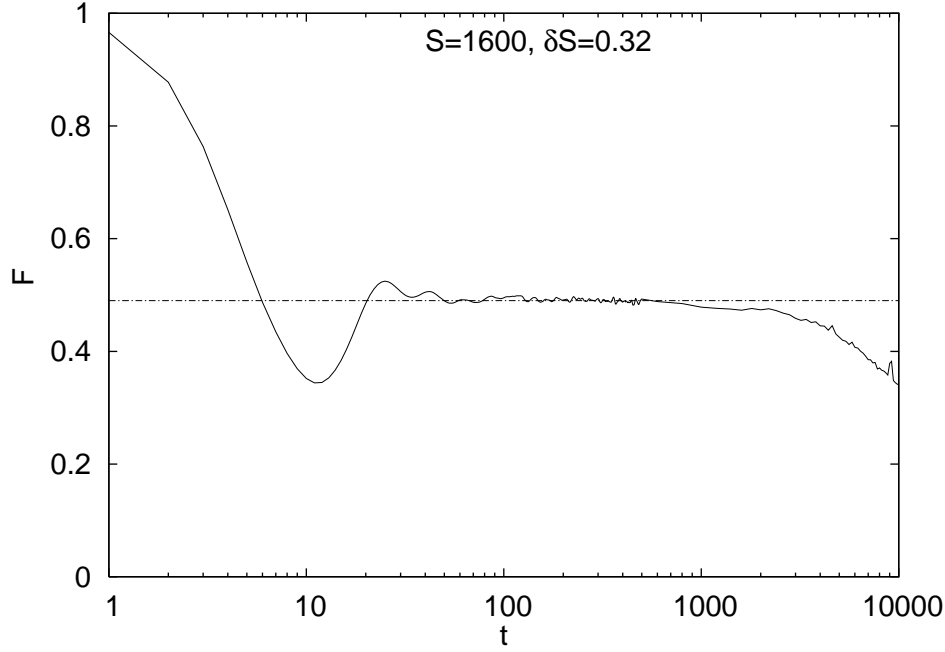


Figure 4.11: Short time fidelity decay for $\beta = 0$ (we have singularities) and a random initial state. The chain line shows the theoretical value of the plateau as computed from Eq. (4.84).

In Section 4.2 we already discussed possible divergence problems in $w_{\mathbf{m}}$. If we express $w_{\mathbf{m}}$ in terms of $v_{\mathbf{m}}$, Eq. (4.36), we have denominators $\sin(\mathbf{m} \cdot \boldsymbol{\omega}(\mathbf{j})/2)$. We therefore have divergences at points in phase space where $\mathbf{m} \cdot \boldsymbol{\omega}(\mathbf{j}) = 2\pi k$ with k an integer. For a coherent initial state this was not a real problem as it would occur only if we placed initial packet at such a point. For random initial state though, there is an average over the whole action space in the plateau formula and if there is a single diverging point somewhere in the phase space it will cause divergence. The solution is very simple as explained in Section 4.2. The integral is actually an approximation for a sum over $\hbar \mathbf{n}$ and so we have to retain the original sum over the eigenvalues of the action operator and exclude possible diverging terms. The formula for the plateau in the case of such divergences is

$$F_{\text{plat}}^{\text{RIS}} \cong \left| \frac{1}{\mathcal{N}} \sum_{\mathbf{n}}^{\mathbf{m} \cdot \boldsymbol{\omega}(\hbar \mathbf{n}) \neq 2\pi k} F_{\text{plat}}^{\text{CIS}}(\hbar \mathbf{n}) \right|^2, \quad (4.84)$$

where in the summation over \mathbf{n} we exclude all terms for which for any constituent Fourier mode \mathbf{m} we would have $\mathbf{m} \cdot \boldsymbol{\omega}(\hbar \mathbf{n}) = 2\pi k$.

Again we find an excellent confirmation of our theoretical predictions in the numerical experiment for the same system as for a coherent initial state (4.51). In the first calculation we choose the shift $\beta = 1.4$ so that we have no singular frequency in the action space. In Figure 4.10 we demonstrate the plateau, which in the case of random states starts earlier than for coherent states, namely at $t_1 \propto \hbar^0 \delta^0$ (4.46). The value of the plateau can be immediately written in terms of the result for coherent states,

$$F_{\text{plat}}^{\text{RIS}} \cong \left[\frac{1}{2} \int_{-1}^1 dj J_0^2 \left(\delta S \frac{\sqrt{1-j^2}}{2 \sin \{\alpha(j-\beta)/2\}} \right) \right]^2. \quad (4.85)$$

The integral has to be calculated numerically. Horizontal chain lines in Figure 4.10 correspond to this theoretical values and agree with numerics, both for the weak perturbation $\delta S = 0.32$ and

the strong perturbation $\delta S = 3.2$ (inset). Small echo resonances visible in the figures are due to the fact that the Hamiltonian is a quadratic function of the action and therefore $\omega'' \equiv 0$, so that the resonance condition (4.73) is satisfied also for extended states (4.74). For a more generic Hamiltonian these narrow resonant spikes will be absent. In Figure 4.11 we also demonstrate the plateau in the fidelity for the zero-shift case $\beta = 0$ with a singular-frequency, $\omega(j = 0) = 0$, where we again find an excellent agreement with the theoretical prediction (4.84). In this case the theoretical value has been obtained by replacing an integral in (4.85) with a sum as implied by Eq. (4.84) and summing over all quantum numbers except $n = 0$. Observe that the value of the plateau is much lower than in the case of a non-zero shift $\beta = 1.4$ in Figure 4.10 as quantum numbers around $n = 0$ will be close-to resonant.

Long Time Decay

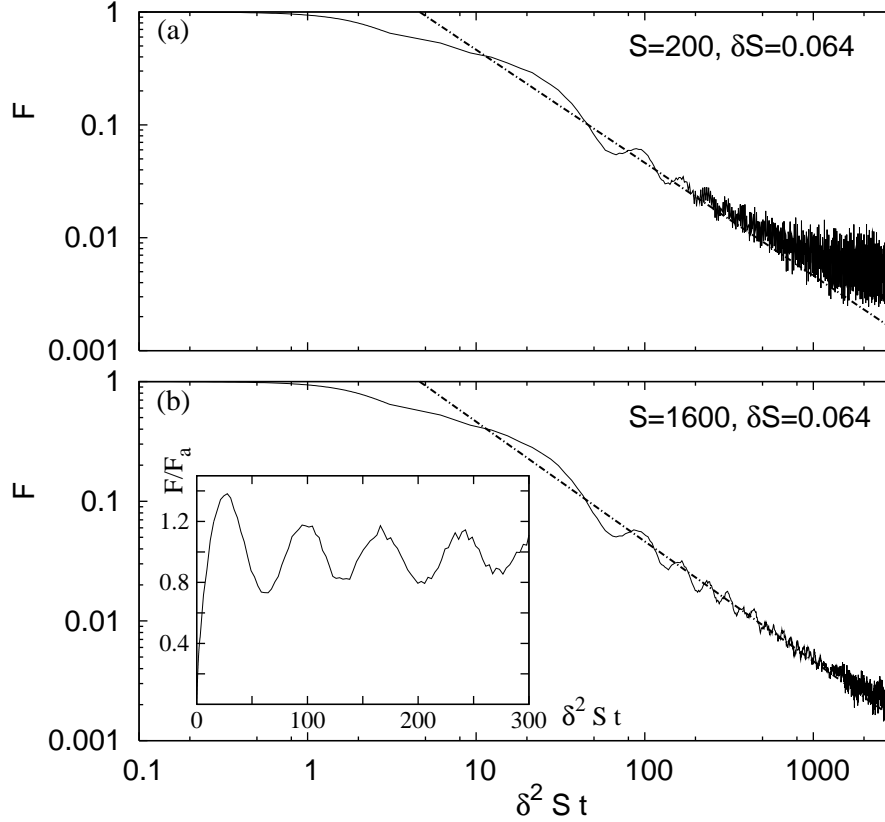


Figure 4.12: Long time power law fidelity decay for random states in the kicked top with $\beta = 0$ and $\alpha = 1.1$, for $S = 200$ (a), and $S = 1600$ (b). Here averaging for $S = 200$ is performed over 1000 initial random states, otherwise all is the same as for Figure 4.10. The heavy chain line shows the theoretical asymptotic decay (4.87) with an analytically computed prefactor (no fitting parameters). The inset in the bottom figure shows the diffractive quotient between the numerical fidelity and the asymptotic formula (4.86) (chain line in the main figure).

After a sufficiently long time $t > t_2$ fidelity will start to decay. To calculate this decay we have to evaluate the ASI formula (4.42). For a uniform average over Hilbert space we have $D_\rho = 1/\mathcal{N}$ with the classical limit $d_\rho(\mathbf{j}) = (2\pi\hbar)^d/\mathcal{V}$. The fidelity amplitude is therefore

$$f(t) \cong \frac{(2\pi)^d}{\mathcal{V}} \int d^d \mathbf{j} \exp \left(-i \frac{\delta^2 t}{2\hbar} \bar{r}(\mathbf{j}) \right). \quad (4.86)$$

The stationary phase procedure is completely analogous to the situation for the case of non-residual perturbation, described in Section 3.2.3, Eq. (3.46). We will only write the asymptotic result,

$$F(t) \asymp \left(\frac{t_{\text{ran}}}{t} \right)^d, \quad t_{\text{ran}} = \text{const} \times \frac{\hbar}{\delta^2}. \quad (4.87)$$

Here we should remember that the asymptotic formula (4.87) has been obtained as a stationary phase approximation of an integral in the limit of an infinite action space. If we have a finite region of the action space, as is the case for the kicked top, the stationary phase approximation gives an additional oscillating prefactor, whose amplitude is damped as $(\hbar/t)^{1/2}$ for $\hbar \rightarrow 0$ and/or $t \rightarrow \infty$, and which can be interpreted as a *diffraction*. This oscillating prefactor can be seen in numerical data for the fidelity in the inset of Figure 4.12. For random states the time t_2 when the plateau ends is independent of \hbar and is determined by the ratio of two competing terms in the BCH form or the echo operator, $t_2 \sim |\delta \Sigma(t)/\hbar|/|\delta^2 \bar{\Gamma}/2\hbar|$, therefore we have

$$t_2 \sim 1/\delta. \quad (4.88)$$

This agrees with the numerical results shown in Figures 4.10 and 4.11.

Chapter 5

Coupling with the Environment

When a man tells you that he got rich through hard work, ask him: 'Whose?'

—Don Marquis

The fidelity might not always be the relevant measure of stability. Coupling with the environment is usually unavoidable so that the evolution of our system is no longer Hamiltonian. To preserve the Hamiltonian formulation we have to include the environment in our description. We therefore have a “central system”, denoted by a subscript “c”, and an environment, denoted by subscript “e”. The names *central system* and *environment* will be used just to denote two pieces of a composite system, without any connotation on their properties, dimensionality etc. The central system will be that part which is of interest and the environment the rest. The Hilbert space is a tensor product $\mathcal{H} = \mathcal{H}_c \otimes \mathcal{H}_e$ and the evolution of a whole system is determined by a Hamiltonian or a propagator on the whole Hilbert space \mathcal{H} of dimension $\mathcal{N} = \mathcal{N}_c \mathcal{N}_e$. The unperturbed state $|\psi(t)\rangle$ and the perturbed one $|\psi_\delta(t)\rangle$ are obtained with propagators $U(t)$ and $U_\delta(t)$ (2.3). Fidelity would in this case be the overlap of two wave functions on the *whole space*. But if we are not interested in the environment, this is clearly not the relevant quantity. Namely, the fidelity will be low even if the two wave functions are the same on the subspace of the central system and differ only on the environmental part.

5.1 Reduced Fidelity, Purity Fidelity

We can define a quantity analogous to the fidelity, but which will measure the overlap just on the subspace of interest, i.e. on the subspace of the central system. Let us define a reduced density matrix of a central subsystem

$$\rho_c(t) := \text{tr}_e[\rho(t)], \quad \rho_c^M(t) := \text{tr}_e[\rho^M(t)], \quad (5.1)$$

where $\text{tr}_e[\bullet]$ denotes a trace over the environment and $\rho^M(t) = M_\delta(t)\rho(0)M_\delta(t)^\dagger$ is the so-called echo density matrix. Throughout this chapter we will assume that the initial state is a pure product state, i.e. a direct product,

$$|\psi(0)\rangle = |\psi_c(0)\rangle \otimes |\psi_e(0)\rangle =: |\psi_c(0); \psi_e(0)\rangle, \quad (5.2)$$

where we also introduced a short notation $|\psi_c; \psi_e\rangle$ for pure product states. The resulting initial density matrix $\rho(0) = |\psi(0)\rangle\langle\psi(0)|$ is of course also pure. The fidelity was defined as $F(t) =$

$\text{tr}[\rho(0)\rho^M(t)]$ (2.9) and in a similar fashion we will define a *reduced fidelity* (Žnidarič & Prosen, 2003) denoted by $F_R(t)$,

$$F_R(t) := \text{tr}_c[\rho_c(0)\rho_c^M(t)]. \quad (5.3)$$

The reduced fidelity measures the distance between the initial reduced density matrix and the reduced density matrix after the echo. Note that our definition of the reduced fidelity agrees with the information-theoretic fidelity (2.1) on a central subspace \mathcal{H}_c only if the initial state is a pure product state, so that $\rho_c(0)$ is also a pure state.

One of the weirdest features of quantum mechanics is entanglement. Of some interest is therefore also whether the coupling with the environment will produce entanglement and how fast. Due to the coupling between the central system and the environment the initial product state will evolve after an echo into the pure entangled state $M_\delta(t)|\psi(0)\rangle$ and therefore the reduced density matrix $\rho_c^M(t)$ will be a mixed one. For a pure state $|\psi(t)\rangle$ the criterion for entanglement is very simple. It is quantified by a *purity* $I(t)$, defined as

$$I(t) := \text{tr}_c[\rho_c^2(t)], \quad \rho_c(t) := \text{tr}_e[|\psi(t)\rangle\langle\psi(t)|]. \quad (5.4)$$

Purity, or equivalently von Neumann entropy $-\text{tr}(\rho \ln \rho)$, is a standard quantity used in decoherence studies (Zurek, 1991). If the purity is less than one, $I < 1$, then the state $|\psi\rangle$ is entangled (between the environment and the central system), otherwise it is a product state. Similarly, one can define a purity after an echo, called *purity fidelity* (Prosen & Seligman, 2002) $F_P(t)$,

$$F_P(t) := \text{tr}_c[\{\rho_c^M(t)\}^2]. \quad (5.5)$$

All three quantities, the fidelity $F(t)$, the reduced fidelity $F_R(t)$ and the purity fidelity $F_P(t)$ measure stability to perturbations. If the perturbed evolution is the same as the unperturbed one, they are all equal to one, otherwise they are less than one. The fidelity $F(t)$ measures the stability of a whole state, the reduced fidelity gives the stability on \mathcal{H}_c and the purity fidelity measures separability of $\rho^M(t)$. One expects that fidelity is the most restrictive quantity of the three - $\rho(0)$ and $\rho^M(t)$ must be similar for $F(t)$ to be high. For $F_R(t)$ to be high, only the reduced density matrices $\rho_c(0)$ and $\rho_c^M(t)$ must be similar, and finally, the purity fidelity $F_P(t)$ is high if only $\rho^M(t)$ factorizes. It looks though as fidelity is the strongest criterion for stability.

5.1.1 Inequality Between Fidelity, Reduced Fidelity and Purity Fidelity

Actually, one can prove the following inequality for an arbitrary *pure* state $|\psi\rangle$ and an arbitrary *pure product* state $|\phi_c; \phi_e\rangle$ (Žnidarič & Prosen, 2003; Prosen *et al.*, 2003a),

$$|\langle\phi_c; \phi_e|\psi\rangle|^4 \leq |\langle\phi_c|\rho_c|\phi_c\rangle|^2 \leq \text{tr}_c[\rho_c^2], \quad (5.6)$$

where $\rho_c := \text{tr}_e[|\psi\rangle\langle\psi|]$.

Proof. Uhlmann's theorem (Uhlmann, 1976), i.e. noncontractivity of the fidelity, states that tracing over an arbitrary subsystem can not decrease the fidelity,

$$\text{tr}[|\phi_c; \phi_e\rangle\langle\phi_c; \phi_e||\psi\rangle\langle\psi|] \leq \text{tr}[|\phi_c\rangle\langle\phi_c|\rho_c]. \quad (5.7)$$

Then, squaring and applying the Cauchy-Schwartz inequality $|\text{tr}[A^\dagger B]|^2 \leq \text{tr}[AA^\dagger] \text{tr}[BB^\dagger]$ we immediately obtain the wanted inequality (5.6).

The rightmost quantity in the inequality $I = \text{tr}[\rho_c^2]$ is nothing but the purity of state $|\psi\rangle$ and so does not depend on $|\phi_c; \phi_e\rangle$. One can think of inequality (5.6) as giving us a *lower bound* on purity. An interesting question for instance is, which state $|\phi_c; \phi_e\rangle$ optimises this bound for a given $|\psi\rangle$, i.e. what is the maximal attainable overlap $|\langle\phi_c; \phi_e|\psi\rangle|^4$ (fidelity) for a

given purity. The rightmost inequality is optimised if we choose $|\phi_c\rangle$ to be the eigenstate of the reduced density matrix ρ_c corresponding to its largest eigenvalue λ_1 , $\rho_c|\phi_c\rangle = \lambda_1|\phi_c\rangle$. To optimise the left part of the inequality, we have to choose $|\phi_e\rangle$ to be the eigenstate of $\rho_e := \text{tr}_c[\rho]$ corresponding to the same largest eigenvalue λ_1 , $\rho_e|\phi_e\rangle = \lambda_1|\phi_e\rangle$. The two reduced matrices ρ_e and ρ_c have the same eigenvalues (Araki & Lieb, 1970), $\lambda_1 \geq \lambda_2 \geq \dots \geq \lambda_{N_c}$. For such choice of $|\phi_c; \phi_e\rangle$ the left inequality is actually an equality, $|\langle\phi_c; \phi_e|\psi\rangle|^4 = |\langle\phi_c|\rho_c|\phi_c\rangle|^2 = \lambda_1^2$ and the right inequality is

$$\lambda_1^2 \leq \text{tr}[\rho_c^2] = \sum_{j=1}^{N_c} \lambda_j^2, \quad (5.8)$$

with equality iff $\lambda_1 = 1$. In the case when the largest eigenvalue is close to one, $\lambda_1 = 1 - \epsilon$, the purity will be $I = (1 - \epsilon)^2 + \mathcal{O}(\epsilon^2) \sim 1 - 2\epsilon$ and the difference between the purity and the overlap will be of the *second order* in ϵ , $I - |\langle\phi_c; \phi_e|\psi\rangle|^4 \sim \epsilon^2$. Therefore, for high purity the optimal choice of $|\phi_c; \psi_s\rangle$ gives a sharp lower bound, i.e. its deviation from I is of second order in the deviation of I from unity.

For our purpose of studying stability to perturbations, a special case of the general inequality (5.6) is especially interesting. Namely, taking for $|\psi\rangle$ the state after the echo evolution $M_\delta(t)|\psi(0)\rangle$ and for a product state $|\phi_c; \phi_e\rangle$ the initial state $|\psi(0)\rangle$ (5.2), we obtain

$$F^2(t) \leq F_R^2(t) \leq F_P(t). \quad (5.9)$$

Immediate consequence of this inequality is that if the fidelity is high, the reduced fidelity and the purity fidelity will also be high. In the case of perturbations with a zero time average in Chapter 4, the fidelity freezes at the plateau and from the inequality we immediately know that the same phenomenon will be present for the reduced fidelity and the purity fidelity.

5.1.2 Uncoupled Unperturbed Dynamics

Special, but very important case is when the unperturbed dynamics U_0 represents two uncoupled systems, so that we have

$$U_0 = U_c \otimes U_e. \quad (5.10)$$

This is a frequent situation if the coupling with the environment is “unwanted”, so that our ideal evolution U_0 would be an uncoupled one. The reduced fidelity $F_R(t)$ and the purity fidelity $F_P(t)$ have especially nice forms in such case.

The reduced fidelity (5.3) can be rewritten as

$$F_R(t) = \text{tr}_c[\rho_c(0)\rho_c^M(t)] = \text{tr}_c[\rho_c(t)\rho_c^\delta(t)], \quad (5.11)$$

where $\rho_c(t)$ is the unperturbed state of the central system and $\rho_c^\delta(t) := \text{tr}_e[U_\delta(t)\rho(0)U_\delta^\dagger(t)]$ the corresponding state obtained by perturbed evolution. Whereas for a general unperturbed evolution the reduced fidelity was an overlap of the initial state with an echo state, for a factorized unperturbed evolution it can also be interpreted as the overlap of the (reduced) unperturbed state at time t with a perturbed state at time t , similarly as the fidelity.

The purity fidelity can also be simplified for uncoupled unperturbed evolution. As the U_0 is in factorized form, we can bring it out of the innermost trace in the definition of the purity fidelity and use the cyclic property of the trace, finally arriving at

$$F_P(t) = \text{tr}_c[\{\rho_c^M(t)\}^2] = \text{tr}_c[\{\rho_c^\delta(t)\}^2] = I(t). \quad (5.12)$$

The purity fidelity is therefore equal to the purity of the forward evolution. The general inequality gives in this case

$$F^2(t) \leq F_R^2(t) \leq I(t), \quad (5.13)$$

and so the fidelity and the reduced fidelity give a lower bound on the decay of purity. Because the purity is frequently used in studies of decoherence this connection is especially appealing.

In all our theoretical derivations regarding the purity fidelity we will assume a general unperturbed evolution, but one should keep in mind that the results immediately carry over to purity in the case of uncoupled unperturbed dynamics. Also a large part of our numerical demonstration in next two sections will be done on systems with an uncoupled unperturbed dynamics as this is usually the more interesting case.

5.1.3 Linear Response Expansion

We proceed with the linear response expansion of the reduced fidelity (5.3) and the purity fidelity (5.5). We will use notation $\rho_c := |\psi_c(0)\rangle\langle\psi_c(0)|$ for initial pure density matrix on a central system and $\rho_e := |\psi_e(0)\rangle\langle\psi_e(0)|$ for the environment. The perturbed propagator is defined in exactly the same way as for the fidelity (2.6) in terms of the perturbation generator V . To order $\mathcal{O}(\delta^4)$ we get,

$$\begin{aligned} 1 - F(t) &= \left(\frac{\delta}{\hbar}\right)^2 \langle \Sigma(t)(\mathbb{1} \otimes \mathbb{1} - \rho_c \otimes \rho_e) \Sigma(t) \rangle \\ 1 - F_R(t) &= \left(\frac{\delta}{\hbar}\right)^2 \langle \Sigma(t)(\mathbb{1} - \rho_c) \otimes \mathbb{1} \Sigma(t) \rangle \\ 1 - F_P(t) &= 2 \left(\frac{\delta}{\hbar}\right)^2 \langle \Sigma(t)(\mathbb{1} - \rho_c) \otimes (\mathbb{1} - \rho_e) \Sigma(t) \rangle, \end{aligned} \quad (5.14)$$

where $\langle \bullet \rangle = \text{tr}[(\rho_c \otimes \rho_e) \bullet]$ denotes the quantum expectation value in the initial product state and $\Sigma(t)$ is the sum of $V(t)$ (2.12). If the expectation values are written explicitly in terms of expectations in the base states $|j; \nu\rangle$, $j = 1, \dots, \mathcal{N}_c$, $\nu = 1, \dots, \mathcal{N}_e$, with the convention that the first base state $|1; 1\rangle := |\psi_c; \psi_e\rangle$ is the initial state, we have

$$\begin{aligned} 1 - F(t) &= \left(\frac{\delta}{\hbar}\right)^2 \left\{ \langle 1; 1 | \Sigma^2(t) | 1; 1 \rangle - \langle 1; 1 | \Sigma(t) | 1; 1 \rangle^2 \right\} \\ 1 - F_R(t) &= \left(\frac{\delta}{\hbar}\right)^2 \left\{ \langle 1; 1 | \Sigma^2(t) | 1; 1 \rangle - \sum_{\nu=1}^{\mathcal{N}_e} |\langle 1; \nu | \Sigma(t) | 1; 1 \rangle|^2 \right\} \\ 1 - F_P(t) &= 2 \left(\frac{\delta}{\hbar}\right)^2 \left\{ \langle 1; 1 | \Sigma^2(t) | 1; 1 \rangle - \sum_{\nu=1}^{\mathcal{N}_e} |\langle 1; \nu | \Sigma(t) | 1; 1 \rangle|^2 - \sum_{j=2}^{\mathcal{N}_c} |\langle j; 1 | \Sigma(t) | 1; 1 \rangle|^2 \right\}. \end{aligned} \quad (5.15)$$

As one can see, the linear response expansion of course also satisfies the general inequality (5.9). The difference between $F_R(t)$ and $F(t)$ as well as between $F_P(t)$ and $F(t)$ is in *off-diagonal* matrix elements of operator $\Sigma(t)$. Somehow reminiscent perturbative expansion, although without time dependence, has been obtained in studying the eigenvalues of the reduced density matrix (Kübler & Zeh, 1973). Depending on the growth of linear response terms with time we will again have two general categories, that of mixing dynamics and that of regular dynamics.

Mixing Dynamics

For mixing dynamics the correlations decay and the linear response term will grow linearly with time. For large times one can argue that $\Sigma(t)$ should look like a random matrix and the terms giving the difference between the fidelity and the purity fidelity and the reduced fidelity can be estimated as

$$\frac{\sum_{j=2}^{\mathcal{N}_c} |\langle j; 1 | \Sigma(t) | 1; 1 \rangle|^2}{\langle 1; 1 | \Sigma^2(t) | 1; 1 \rangle} \sim \frac{\sum_j |[\Sigma(t)]_{(j;1),(1;1)}|^2}{\sum_{j,\nu} |[\Sigma(t)]_{(1;1),(j,\nu)}|^2} \sim \frac{1}{\mathcal{N}_e}, \quad (5.16)$$

because there are more terms in the sum for fidelity. Therefore we can estimate the difference $F_P(t) - F^2(t) \sim 1/\mathcal{N}_c + 1/\mathcal{N}_e$ and $F_R(t) - F(t) \sim 1/\mathcal{N}_c$. Provided both dimensions $\mathcal{N}_{c,e}$ are large and for sufficiently long times, so the “memory” of the initial state is lost and the correlations decay, we can expect the decay of all three quantities to be the same.

Regular Dynamics

For regular dynamics on the other hand, $\Sigma(t)$ will not approach a random matrix but will grow with time with a well defined long time limit $\Sigma(t) \rightarrow \bar{V}t$. This will happen for times larger than the averaging time t_{ave} (3.17). Expectation value of $\Sigma^2(t)$ will then grow quadratically with time. In a similar way as we defined the average correlation function \bar{C} (3.15), we can also define a time average of the correlation functions occurring in the linear response expressions for $F_R(t)$ and $F_P(t)$,

$$\begin{aligned}\bar{C}_R &:= \lim_{t \rightarrow \infty} \frac{\langle \Sigma(t)(\mathbb{1} - \rho_c) \otimes \mathbb{1} \Sigma(t) \rangle}{t^2} = \langle \bar{V}(\mathbb{1} - \rho_c) \otimes \mathbb{1} \bar{V} \rangle \\ \bar{C}_P &:= \lim_{t \rightarrow \infty} \frac{\langle \Sigma(t)(\mathbb{1} - \rho_c) \otimes (\mathbb{1} - \rho_e) \Sigma(t) \rangle}{t^2} = \langle \bar{V}(\mathbb{1} - \rho_c) \otimes (\mathbb{1} - \rho_e) \bar{V} \rangle.\end{aligned}\quad (5.17)$$

In the linear response regime purity fidelity and reduced fidelity will therefore decay quadratically with time, if \bar{C}_R and \bar{C}_P are nonzero.

For coherent initial states the average correlation function \bar{C} is proportional to \hbar (3.36) provided $\bar{v}(\mathbf{j})$ is sufficiently smooth. In the semiclassical limit we can make an expansion around the centre of the wave packet $\bar{v}(\mathbf{j}) \approx \bar{v}(\mathbf{j}^*) + \bar{\mathbf{v}}'(\mathbf{j}^*)\{\mathbf{j} - \mathbf{j}^*\} + \dots$. The second moment $\langle \bar{v}^2 \rangle_{\text{cl}} - \langle \bar{v} \rangle_{\text{cl}}^2$ is then proportional to the dispersion in \mathbf{j} of the initial packet (3.33), i.e. to \hbar . As we take a product initial coherent packet we have a $d_c + d_e$ dimensional squeezing matrix Λ

$$\Lambda = \begin{pmatrix} \Lambda_c & 0 \\ 0 & \Lambda_e \end{pmatrix}, \quad (5.18)$$

and we can write derivatives of classical \bar{v} as

$$\bar{\mathbf{v}}' =: (\bar{\mathbf{v}}'_c, \bar{\mathbf{v}}'_e), \quad \bar{\mathbf{v}}'_c := \frac{\partial \bar{v}(\mathbf{j}^*)}{\partial \mathbf{j}_c}, \quad \bar{\mathbf{v}}'_e := \frac{\partial \bar{v}(\mathbf{j}^*)}{\partial \mathbf{j}_e}, \quad (5.19)$$

where we split actions \mathbf{j} into two components $\mathbf{j} =: (\mathbf{j}_c, \mathbf{j}_e)$. The formula for \bar{C} (3.36) can then be written as

$$\bar{C} = \frac{1}{2} \hbar \left(\bar{\mathbf{v}}'_c \Lambda_c^{-1} \bar{\mathbf{v}}'_c + \bar{\mathbf{v}}'_e \Lambda_e^{-1} \bar{\mathbf{v}}'_e \right), \quad (5.20)$$

By a similar method one can calculate also \bar{C}_R (5.17) and gets

$$\bar{C}_R = \frac{1}{2} \hbar \left(\bar{\mathbf{v}}'_c \Lambda_c^{-1} \bar{\mathbf{v}}'_c \right). \quad (5.21)$$

For \bar{C}_P on the other hand, the lowest order expansion of $\bar{\mathbf{v}}'$ used for \bar{C} and \bar{C}_R gives zero. To get \bar{C}_P we must expand \bar{v} to the *second* order in $(\mathbf{j} - \mathbf{j}^*)$

$$\bar{v}(\mathbf{j}) \approx \bar{v}(\mathbf{j}^*) + \bar{\mathbf{v}}'(\mathbf{j}^*)\{\mathbf{j} - \mathbf{j}^*\} + \frac{1}{2} \{\mathbf{j} - \mathbf{j}^*\} \cdot \bar{v}''(\mathbf{j}^*)\{\mathbf{j} - \mathbf{j}^*\} + \dots, \quad (5.22)$$

where $\bar{v}''(\mathbf{j}^*)$ is a symmetric matrix of second derivatives evaluated at the position of initial packet \mathbf{j}^* ,

$$\bar{v}'' = \begin{pmatrix} \bar{v}''_{cc} & \bar{v}''_{ce} \\ \bar{v}''_{ec} & \bar{v}''_{ee} \end{pmatrix}, \quad \bar{v}''_{lk}(\mathbf{j}^*) := \frac{\partial^2 \bar{v}(\mathbf{j}^*)}{\partial j_l \partial j_k}. \quad (5.23)$$

The only nonzero contribution to \bar{C}_P comes from off-diagonal terms \bar{v}_{ce}'' and $\bar{v}_{ec}'' = (\bar{v}_{ce}'')^T$, with the final result being

$$\bar{C}_P = \left(\frac{1}{2}\hbar\right)^2 \text{tr}[u], \quad u := \Lambda_c^{-1} \bar{v}_{ce}'' \Lambda_e^{-1} \bar{v}_{ec}''. \quad (5.24)$$

The result for \bar{C}_P is very interesting as it means that the purity fidelity in regular systems will decay as $F_P(t) = 2(\delta/\hbar)^2 \bar{C}_P t^2$ on \hbar -independent time scale because of $\bar{C}_P \propto \hbar^2$. Note that to reach this conclusion of \hbar -independent decay, we need only the existence of a smooth classical limit of $\Sigma(t)$, therefore $F_P(t)$ will decay on \hbar -independent time scale even before \bar{V} converges, i.e. for $t < t_{\text{avg}}$.

A simple special case of time averaged perturbation \bar{V} is the tensor product form $\bar{V} = \bar{V}_c \otimes \bar{V}_e$. Then we have $\bar{v}_{ce}'' = \bar{v}_c' \otimes \bar{v}_e' / \bar{v}$ (note that in order to comply with our previous notation we have $\bar{v}_c' = (\partial_c \bar{v}_c) \bar{v}_e$). If in addition $\Lambda_{c,e}$ are diagonal, then the average \bar{C}_P is

$$\bar{C}_P = \left(\frac{1}{2\bar{v}}\hbar\right)^2 \left(\bar{v}_c' \Lambda_c^{-1} \bar{v}_c'\right) \left(\bar{v}_e' \Lambda_e^{-1} \bar{v}_e'\right). \quad (5.25)$$

As we can see, for a tensor product forms of the time averaged perturbation there is a relation between \bar{C} , \bar{C}_R and \bar{C}_P ,

$$\bar{v}^2 \bar{C}_P \equiv \bar{C}_R (\bar{C} - \bar{C}_R). \quad (5.26)$$

The purity fidelity will be high, i.e. decoherence will be slow, if we either make \bar{C}_R small or make \bar{C}_R close to \bar{C} . Note that if \bar{C}_R is small, then the inequality (5.9) already tells that \bar{C}_P will be also small, but here we have a stronger result, that \bar{C}_P is of second order in \hbar whereas \bar{C}_R is only of first order.

5.1.4 Numerical Illustration

Here we would like to briefly demonstrate quadratic decay of the purity fidelity for regular systems and linear decay for chaotic systems. Furthermore, we will show that one can also have a situation where the purity fidelity $F_P(t)$ decays slower for chaotic systems than for regular. We take a Jaynes-Cummings model (Section 2.1.2) which is a two degrees of freedom model of a harmonic oscillator coupled to a spin. As initial state we always take a product state of two coherent states, for the spin the coherent state (2.26) is centred at $(\vartheta^*, \varphi^*) = (1, 1)$ and for the boson coherent state (2.30) we take $\alpha = 1.15$. We take two different sets of parameters. For the chaotic regime we choose $\omega = \epsilon = 0.3$ and $G = G' = 1$, for which the energy of the initial state is $E = 1.0$ and the classical Poincaré section shows a single ergodic component. The second set of parameters is $\omega = \epsilon = 0.3$ and $G = 1$, while $G' = 0$, for which the systems is integrable and the energy is $E = 0.63$. The perturbation is chosen to be in the spin energy ϵ , i.e. a detuning, corresponding to the perturbation generator V

$$V = \hbar S_z. \quad (5.27)$$

Because the simulation is very time consuming for the chaotic case, we choose a small spin size $S = 4$, resulting in an effective Planck's constant $\hbar = 1/4$.

Note that, as opposed to previous kicked top model, here the system is conservative, and the time index t is continuous. First we want to check the growth of linear response terms with time. In Figure 5.1 we show the correlation integral $S_F(t)$ for fidelity and the difference $S_F(t) - S_P(t)$ between the correlation integrals for fidelity $S_F(t)$ and for purity fidelity $S_P(t)$,

$$\begin{aligned} S_F(t) &:= \frac{1}{t} \langle \Sigma(t) (\mathbb{1} \otimes \mathbb{1} - \rho_c \otimes \rho_e) \Sigma(t) \rangle \\ S_P(t) &:= \frac{1}{t} \langle \Sigma(t) (\mathbb{1} - \rho_c) \otimes (\mathbb{1} - \rho_e) \Sigma(t) \rangle. \end{aligned} \quad (5.28)$$

Note that for chaotic systems $S_F(t)$ should converge to 2σ (3.3), where σ is the transport coefficient, i.e. the integral of the correlation function. The difference $S_F(t) - S_P(t)$ should on the other hand be of the order $\sim 2\sigma(1/\mathcal{N}_c + 1/\mathcal{N}_e) \sim \sigma/2$ (due to $1/\mathcal{N}_c + 1/\mathcal{N}_e \approx 1/S$). These two predictions are nicely confirmed by the lower two curves in Figure 5.1. We can see

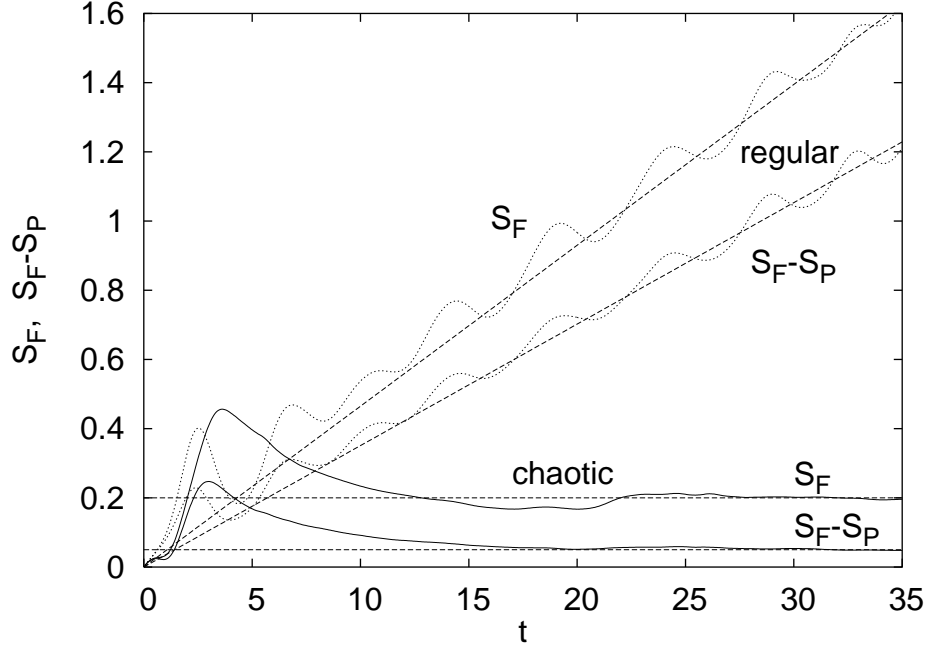


Figure 5.1: The correlation integral $S_F(t)$ and $S_F(t) - S_P(t)$ (5.28) in the Jaynes-Cummings model for regular dynamics (upper curves) and chaotic dynamics (lower curves). The horizontal dashed lines (for the chaotic case) are at $2\sigma = 0.2$ and $0.2/4$. The two linearly increasing dashed lines for regular dynamics have slopes $\bar{C} = 0.046$ and $\bar{C}(1 - 0.98/4)$.

that the correction to the purity fidelity is really of order $1/S$ in the chaotic case and would therefore vanish in the semiclassical limit. For regular dynamics we expect $S_F(t)$ to grow linearly with time, with the slope given by \bar{C} , $S_F(t) \rightarrow \bar{C}t$, with $\bar{C} \propto 1/S$ (5.20). The purity fidelity integral should grow as $S_P(t) \rightarrow \bar{C}_P t$ with $\bar{C}_P \propto 1/S^2$ (5.24). The difference should therefore be $S_F(t) - S_P(t) \sim S_F(1 - \text{const}/S)$. This is again confirmed in Figure 5.1. We checked that $S_P \propto 1/S^2$ also for larger S , up to $S = 24$.

Next, we would like to demonstrate a faster decay of the purity fidelity in the regular regime than in the chaotic one. We set the perturbation strength to $\delta = 0.005$ for which we expect the purity fidelity to become lower in the regular regime at the time determined by $1 - F_P(t) = 2\delta^2 S^2 \bar{C}_P t^2 \approx 1 - F(t) = \delta^2 S^2 2\sigma t$, i.e. at $t \approx 9$, where we used $\sigma = 0.1$ and $\bar{C}_P = 0.011$ as given in Figure 5.1. In Figure 5.2 we show the purity-fidelity for chaotic and regular regimes. We can see the crossover at the predicted time $t \approx 9$. We also illustrate the evolution of the purity fidelity with the square of the Wigner function corresponding to the reduced density matrix $\rho_c^M(t)$ on the central spin subspace. If $W_{\rho_c^M}(\vartheta, \varphi)$ is the Wigner function, purity fidelity can be written as a phase space integral

$$F_P(t) = \int d\Omega W_{\rho_c^M}^2(\vartheta, \varphi). \quad (5.29)$$

For details about the spin Wigner function see Appendix A. Near the top and bottom of Figure 5.2 we see this evolution for the chaotic and the integrable Hamiltonian respectively.

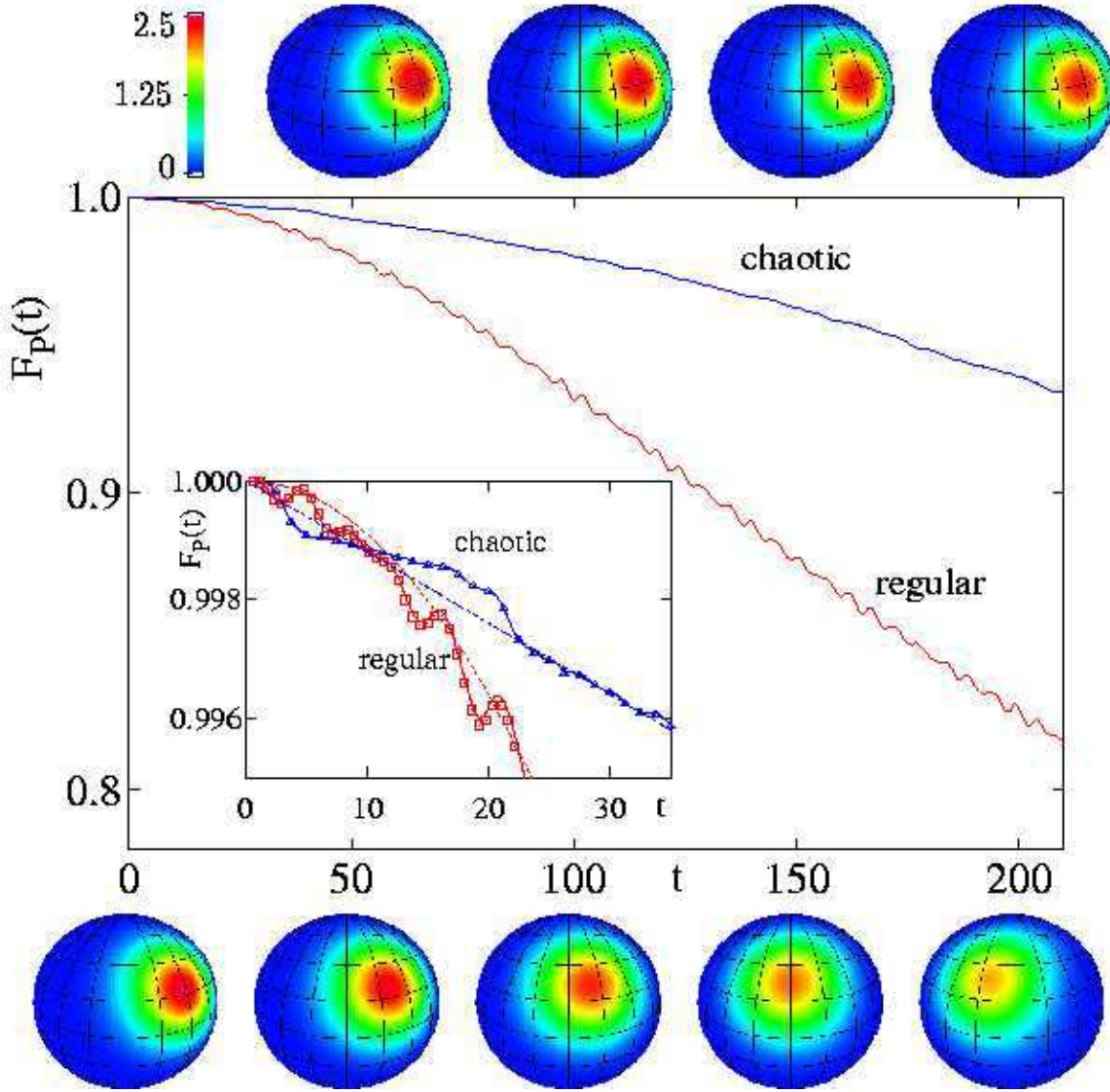


Figure 5.2: Echo dynamics in the Jaynes-Cummings model. The square of the Wigner function for chaotic dynamics (top diagrams) and integrable dynamics (bottom diagrams) is shown as a function of time at times corresponding to the axis. The purity fidelity is shown in the main frame on the same time scale and for short times in the inset. Red curves give the integrable and blue curves the chaotic evolution. In the inset full curves show the complete numerics, symbols the evaluation starting from the numerical correlation integrals of Figure 5.1 and dashed curves the linear or quadratic approximation using σ and \bar{C}_P .

In the centre of the figure we plot the purity fidelity on the same time scale as the Wigner functions in the main frame and an amplification of short times in the inset. We observe detailed agreement of numerics with the results obtained from the numerical values of the correlation integrals $S_F(t)$ and $S_P(t)$, reproducing the oscillatory structure of the decay. From the same correlation integrals we obtained the coefficients for the linear and quadratic decay, which agree well if we discard the oscillations. It is important to remember that the integral over the square of the Wigner function gives the purity fidelity and therefore the fading of the picture will be indicative of the purity fidelity decay. On the other hand the movement of the

centre is an indication of the rapid decay of fidelity (not shown in the figure).

5.2 Mixing Dynamics

Discussing linear response results (Section 5.1.3) in the case of mixing dynamics we have shown that the linear decay is the same for all three quantities. Similar random matrix arguments as for the linear response can be used also for higher order terms and therefore one expects that in the semiclassical limit of small $1/\mathcal{N}_c + 1/\mathcal{N}_e$ we will have the same exponential decay (3.5)

$$F_P(t) \approx F_R^2(t) \approx F^2(t) = \exp(-2t/\tau_m), \quad (5.30)$$

with the decay time $\tau_m = \hbar^2/2\delta^2\sigma_{cl}$ (3.5) independent of the initial state. This result is expected to hold when $\Sigma(t)$ can be approximated with a random matrix for large times (5.16) and V does not contain terms acting on only one subspace. Such terms could cause fidelity to decay while having no influence on purity.

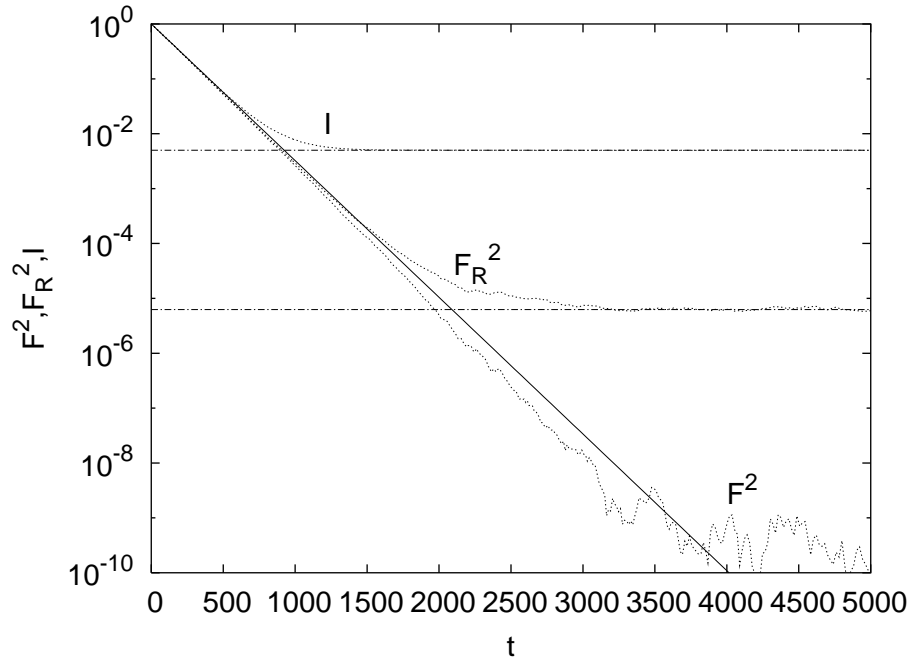


Figure 5.3: Decay of $F^2(t)$, $F_R^2(t)$ and $I(t)$ (dotted curves) in the mixing regime of the double kicked top. The solid line gives the theoretical exponential decay (5.30) with τ_m calculated from the classical $\sigma_{cl} = 0.056$. Horizontal chain lines give the saturation values of the purity and the reduced fidelity, $1/200$ and $1/400^2$, respectively.

For numerical verification of this result we chose a double kicked top system (2.25) with $\varepsilon = 0$, so that the unperturbed evolution is uncoupled. For the double kicked top model we will always have an uncoupled unperturbed evolution in all our numerical demonstrations in this chapter. Other parameters are $\gamma_{c,e} = \pi/2.1$ and $\alpha_{c,e} = 30$, ensuring chaotic classical dynamics. The spin size is chosen to be $S = 200$, so that we have $\mathcal{N}_{c,e} = 2S + 1$. The perturbation is

$$V = \frac{1}{S^2} S_z \otimes S_z, \quad (5.31)$$

with the strength $\delta = 8 \cdot 10^{-4}$. The coherent product initial state is placed at $\vartheta_{c,e}^* = \pi/\sqrt{3}$, $\varphi_{c,e}^* = \pi/\sqrt{2}$. We show in Figure 5.3 the decay of the fidelity $F(t)$, the reduced fidelity $F_R(t)$

and the purity $I(t)$. Clean exponential decay is observed in all three cases, on a time scale τ_m (5.30) given by the classical transport coefficient σ_{cl} . We numerically calculated the classical correlation function

$$C_{cl}(t) = [\langle z_c(t)z_c(0) \rangle_{cl}]^2, \quad (5.32)$$

where we took into consideration that the unperturbed dynamics is uncoupled and is the same for both subsystems and that $\langle z \rangle_{cl} = 0$. Taking only the first term $C_{cl}(0) = 1/9$ would give $\sigma_{cl} = 1/18$ (3.3) while the full sum of $C_{cl}(t)$ gives a slightly larger value $\sigma_{cl} = 0.056$. Exponential decay, of course, persists only up to the saturation value determined by a finite Hilbert space size (see Section 2.2.1).

5.3 Regular Dynamics

5.3.1 Beyond Linear Response

Purity Fidelity

For regular dynamics and coherent initial states one can calculate purity fidelity to all orders in the semiclassical limit and not just the linear response expansion (5.24). For times larger than the averaging time t_{ave} the echo operator goes towards $M_\delta(t) \rightarrow \exp(-i\delta\bar{V}t/\hbar)$. In the semiclassical limit we can use the classical limit \bar{v} instead of \bar{V} . Classical $\bar{v}(\mathbf{J})$ is a function of action operators only and so similarly to the evaluation of fidelity one can use the ASI (3.31) for the evaluation of purity fidelity. A partial trace over the environment gives an integral over \mathbf{j}_e and due to a square in the definition of purity fidelity we end up with an integral over $2(d_c + d_e) = 2d$ dimensions, if d_c is the dimension of \mathbf{j}_c and d_e of \mathbf{j}_e ,

$$F_P(t) \cong \hbar^{-2d} \int d\Gamma \exp \left[-i \frac{\delta}{\hbar} t \{ \bar{v}(\mathbf{j}_c, \mathbf{j}_e) - \bar{v}(\mathbf{j}'_c, \mathbf{j}_e) + \bar{v}(\mathbf{j}'_c, \mathbf{j}'_e) - \bar{v}(\mathbf{j}_c, \mathbf{j}'_e) \} \right] d_\rho(\mathbf{j}) d_\rho(\mathbf{j}'), \quad (5.33)$$

where $d\Gamma = d^d \mathbf{j} d^d \mathbf{j}'$, $\mathbf{j} = (\mathbf{j}_c, \mathbf{j}_e)$, $\mathbf{j}' = (\mathbf{j}'_c, \mathbf{j}'_e)$ and $d_\rho(\mathbf{j})$ is the classical limit of $\langle \mathbf{n} | \rho | \mathbf{n} \rangle$ (3.31). Next we expand $\bar{v}(\mathbf{j})$ around the position of the initial packet (5.22). The constant term $\bar{v}(\mathbf{j}^*)$ and the linear terms cancel exactly as well as the diagonal quadratic terms, regardless of the position of the initial packet. The argument of the exponential function which remains is then

$$-i \frac{\delta t}{\hbar} [(\mathbf{j}_c - \mathbf{j}'_c) \cdot \bar{v}''_{ce}(\mathbf{j}^*)(\mathbf{j}_e - \mathbf{j}'_e)], \quad (5.34)$$

with the matrix \bar{v}'' of second derivatives given in Equation (5.23). The resulting expansion can be used in $F_P(t)$ (5.33) to calculate the purity fidelity for initial states having well defined classical $d_\rho(\mathbf{j})$. For coherent initial states $d_\rho(\mathbf{j})$ are Gaussian (3.33) and so the whole integral is also a Gaussian, giving

$$F_P(t) = \frac{1}{\sqrt{\det(\mathbb{1} - i\delta t L^{-1} \tilde{V}'')}}, \quad (5.35)$$

where L and \tilde{V}'' are $2d$ dimensional matrices

$$L := \begin{pmatrix} \Lambda_c & 0 & 0 & 0 \\ 0 & \Lambda_c & 0 & 0 \\ 0 & 0 & \Lambda_e & 0 \\ 0 & 0 & 0 & \Lambda_e \end{pmatrix}, \quad \tilde{V}'' := \frac{1}{2} \begin{pmatrix} 0 & 0 & \bar{v}''_{ce} & -\bar{v}''_{ce} \\ 0 & 0 & -\bar{v}''_{ce} & \bar{v}''_{ce} \\ \bar{v}''_{ec} & -\bar{v}''_{ec} & 0 & 0 \\ -\bar{v}''_{ec} & \bar{v}''_{ec} & 0 & 0 \end{pmatrix}, \quad (5.36)$$

with matrices of squeezing parameters Λ_c and Λ_e (5.18) of dimensions d_c and d_e , respectively, and $d_c \times d_e$ dimensional matrix \bar{v}''_{ce} (5.23). Note that the determinant is real despite the imaginary

unit. The determinant of the matrix $\mathbb{1} - i\delta t L^{-1} \tilde{V}''$ can be simplified using the following identity for block matrices

$$\det \begin{pmatrix} A & B \\ C & D \end{pmatrix} = \det(A) \det(D - CA^{-1}B) = \det(D) \det(A - BD^{-1}C), \quad (5.37)$$

with $m \times n$ dimensional matrices B and C^T . Noting that the matrix $\mathbb{1} - i\delta t L^{-1} \tilde{V}''$ has $\mathbb{1}$ on the diagonal, we obtain

$$\det(\mathbb{1} - i\delta t L^{-1} \tilde{V}'') = \det(\mathbb{1} + (\delta t)^2 Z), \quad (5.38)$$

with Z being the $2d_c \times 2d_c$ dimensional matrix

$$Z := \frac{1}{2} \begin{pmatrix} \Lambda_c^{-1} \bar{v}_{ce}'' \Lambda_e^{-1} \bar{v}_{ec}'' & -\Lambda_c^{-1} \bar{v}_{ce}'' \Lambda_e^{-1} \bar{v}_{ec}'' \\ -\Lambda_c^{-1} \bar{v}_{ce}'' \Lambda_e^{-1} \bar{v}_{ec}'' & \Lambda_c^{-1} \bar{v}_{ce}'' \Lambda_e^{-1} \bar{v}_{ec}'' \end{pmatrix}. \quad (5.39)$$

To simplify the determinant of $\mathbb{1} + (\delta t)^2 Z$ we use the following identity

$$\det \begin{pmatrix} A & B \\ C & D \end{pmatrix} = \det(DA - BC), \quad (5.40)$$

for square matrices A, B, C and D and commuting B and D , $[B, D] = 0$. Using this finally gives

$$F_P(t) = \frac{1}{\sqrt{\det\{\mathbb{1} + (\delta t)^2 u\}}}, \quad u := \Lambda_c^{-1} \bar{v}_{ce}'' \Lambda_e^{-1} \bar{v}_{ec}''. \quad (5.41)$$

Note that u is the same $d_c \times d_c$ matrix we had in the expression for \bar{C}_P (5.24). This very simple, yet important result deserves a little discussion. It gives the purity fidelity (and thereby as a special case also the purity) decay for regular systems and coherent initial states to all orders in δ . Its validity is limited to times larger than the averaging time t_{ave} in which \bar{V} converges and for sufficiently small \hbar . Planck's constant must be small to allow the replacement of \bar{V} with its classical limit \bar{v} and \bar{v} must be smooth on the scale of the wave packet size $\sqrt{\hbar}$. Furthermore, we replaced a sum over the quantum numbers with an integral over the actions, the validity of this being given by the condition $\delta t |\bar{v}_{ce}''| \hbar^2 / \hbar \ll 1$, i.e. $\delta t_u < 1/\hbar$, if t_u is the upper time limit of validity of the ASI. As we will see, the asymptotic decay of purity fidelity as given by Equation (5.41) is between $1/(\delta t)$ and $1/(\delta t)^{d_c}$, depending on the matrix u . The $F_P(t)$ at the upper border t_u is therefore between \hbar and \hbar^{d_c} . The purity fidelity will for long times saturate at the plateau given by the finite Hilbert space size, $\bar{F}_P \approx 1/\mathcal{N}_c \sim \hbar^{d_c}$. Comparing this, we see that the upper border t_u coincides with the point where the asymptotic saturation \bar{F}_P is reached for one degree of freedom systems. For $d_c > 1$ the ASI break time t_u is only by a constant factor smaller than the time when we reach \bar{F}_P . Summarising, the purity fidelity decay (5.41) is valid from t_{ave} all the way to the asymptotic plateau \bar{F}_P provided \hbar is sufficiently small, without any bound on δ .

Let us now explore the asymptotic decay of $F_P(t)$. To simplify theoretical arguments, we assume that the squeezing parameters are all equal to one*, $L \equiv \mathbb{1}$ so that we have $u = \bar{v}_{ce}'' \bar{v}_{ce}''^T$. In $1 + d_e$ degrees of freedom systems ($d_c = 1$), the matrix u is just a number, and the purity fidelity decays as

$$F_P(t) = \frac{1}{\sqrt{1 + u(\delta t)^2}}, \quad d_c = 1. \quad (5.42)$$

A single parameter u is already fixed by the linear response, i.e. by the value of \bar{C}_P (5.24). Asymptotically we get $F_P(t) \asymp 1/(\delta t)$ decay *regardless* of the second dimension d_e . For general

*Usually this can be achieved by the right choice of actions.

systems with $d_c > 1$ one can see that the determinant $\det \{\mathbb{1} + (\delta t)^2 u\}$ is a polynomial of order at most d_c in $(\delta t)^2$. Furthermore, as the matrix u is symmetric and positive definite, its eigenvalues are positive, meaning that all the coefficients of the polynomial are positive and the $F_P(t)$ is always less than one. In a special case, when the matrix u can be written as a tensor product of two vectors, like $u = \bar{v}_{ce}'' \bar{v}_{ce}''^T =: \mathbf{x} \otimes \mathbf{y}$, the determinant is again simple regardless of the dimensions involved and we get

$$F_P(t) = \frac{1}{\sqrt{1 + (\delta t)^2 \mathbf{x} \cdot \mathbf{y}}}, \quad u = \mathbf{x} \otimes \mathbf{y}. \quad (5.43)$$

In such case we again get the asymptotic $F_P(t) \asymp 1/(\delta t)$ decay, but here *regardless* of *both* dimensions. Matrix u has such a form for instance if all the matrix elements of \bar{v}_{ce}'' are the same (e.g. for the perturbation $\bar{v} = \sum_{k,l} (\mathbf{j}_c \otimes \mathbf{j}_e)_{kl}$). Our result of course applies also to the purity decay in weakly coupled systems and does not agree with the result of Jacquod (2004).

Reduced Fidelity

For the reduced fidelity a similar procedure based on the ASI can be used. In the expansion of $\bar{v}(\mathbf{j})$ around \mathbf{j}^* (5.22) the first non vanishing term is a linear one. The resulting Gaussian integrals are analogous to the ones in the calculation of the fidelity decay for coherent initial states (but there are twice as many), the final result being a Gaussian decay

$$F_R(t) = \exp \left(-\frac{\delta^2}{\hbar^2} \bar{C}_R t^2 \right), \quad (5.44)$$

with a single parameter $\bar{C}_R = \frac{1}{2} \hbar (\bar{\mathbf{v}}_c' \Lambda_c^{-1} \bar{\mathbf{v}}_c')$ given by the linear response alone (5.21).

Numerical Illustration

To numerically confirm the above formulas for the decay of purity fidelity and reduced fidelity we take a double kicked top model (2.25). To be in a regular regime we take $\alpha_{c,e} = 0$ and $\gamma_c = \pi/2.1$ and $\gamma_e = \pi/\sqrt{7}$. Different unperturbed frequencies $\gamma_c \neq \gamma_e$ are chosen in order to have a general situation, i.e. that the subsystems are not in resonance. Unperturbed dynamics is again uncoupled, $\varepsilon = 0$, so that the purity fidelity equals purity. The spin size is chosen $S = 100$ and the initial product coherent state is placed at $(\vartheta^*, \varphi^*)_c = \pi(1/\sqrt{3}, 1/\sqrt{2})$ and $(\vartheta^*, \varphi^*)_e = \pi(1/\sqrt{3}, 3/\sqrt{7})$. The perturbation with strength $\delta = 0.01$ is of the form

$$V = \frac{1}{S^4} S_z^2 \otimes S_z^2. \quad (5.45)$$

Unperturbed classical evolution is very simple, namely rotation around y -axes for angles γ_c and γ_e for the central system and the environment, respectively. The classical limit of \bar{V} is readily calculated and expressed in terms of the actions $j_c = y_c$ and $j_e = y_e$,

$$\bar{v} = \frac{1}{4} (1 - j_c^2) (1 - j_e^2). \quad (5.46)$$

The derivatives of \bar{v} are $\bar{v}_c' = -j_c(1 - j_e^2)/2$ and similarly for \bar{v}_e' . The squeezing parameter for the spin coherent states is $\Lambda = 1/(1 - j^2)$ and the average correlation function \bar{C} (5.20) is

$$\bar{C} = \frac{1}{S} (1 - j_c^2) (1 - j_e^2) \{j_c^2 (1 - j_e^2) + j_e^2 (1 - j_c^2)\}, \quad (5.47)$$

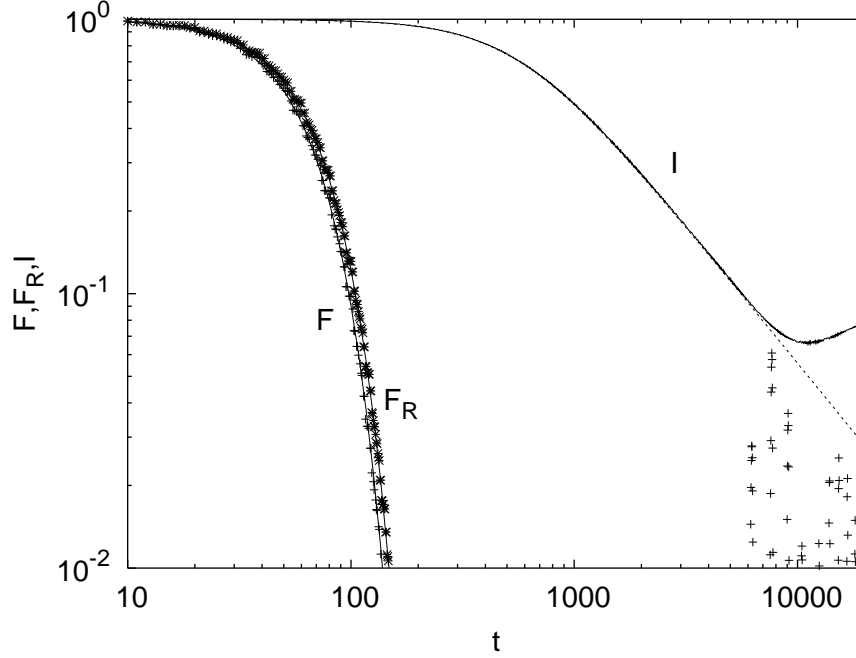


Figure 5.4: Decay of $F(t)$, $F_R(t)$ and $I(t)$ in the regular regime of the double kicked top. For parameters see text. The theoretical Gaussian decay for the fidelity (3.36) and the reduced fidelity (5.44), with the theoretical value of \bar{C} (5.47) and \bar{C}_R (5.48), overlap with the numerics (symbols) within the line width. Theoretical purity decay (5.42) (dotted curve) as determined by the theoretical u (5.49) also nicely agrees with the numerics (full curve) up to the plateau.

which for our choice of the initial coherent packet gives $\bar{C} = 0.024/S$. For the reduced fidelity we get

$$\bar{C}_R = \frac{1}{S} j_c^2 (1 - j_c^2) (1 - j_e^2), \quad (5.48)$$

which evaluates to $\bar{C}_R = 0.021/S$. The above two parameters \bar{C} and \bar{C}_R completely determine the Gaussian fidelity (3.36) and reduced fidelity (5.44) decays. As we have $1 + 1$ degrees of freedom system, the purity is determined by a single parameter u (5.42). For our perturbation we get

$$u = j_c^2 j_e^2 (1 - j_c^2) (1 - j_e^2), \quad (5.49)$$

giving $u = 0.032$ for our initial product coherent state. As our perturbation \bar{V} is of the product form, we could as well use a universal relation between \bar{C}_P , \bar{C}_R and \bar{C} (5.26) to calculate \bar{C}_P (or equivalently u). The numerical results are shown in Figure 5.4, together with the theory. Agreement is excellent.

5.3.2 The Jaynes-Cummings Model

In this section we will consider in detail the stability of a Jaynes-Cummings model, described in Section 2.1.2, under various perturbations. The Jaynes-Cummings system can be experimentally realized and so it is a possible model on which one could experimentally study the quantum stability. In experiments one usually has only a co-rotating term, i.e. G' is zero, therefore we will focus on a situation when we have $G' = 0$ in the unperturbed dynamics and so the classical limit of the unperturbed system is integrable. For the initial state we will always choose a product of coherent states for a harmonic oscillator, given by a real parameter α

(2.30), and a spin, given by the initial position (ϑ, φ) (2.26). In studies of the reduced fidelity and purity fidelity we will consider the spin as a central system, and the harmonic oscillator as an environment. For regular dynamics with coherent initial states the decay of fidelity and reduced fidelity is Gaussian with the decay time determined by a single parameter \bar{C} and \bar{C}_R , while the decay of the purity fidelity is $F_P(t) = 1/\sqrt{1+u(\delta t)^2}$ (5.42) and is again determined by a single parameter u . With this in view, it is sufficient to determine only the linear response parameters \bar{C} (5.20), \bar{C}_R (5.21) and \bar{C}_P (5.24), to get the decay to all orders in δ . Therefore, we will focus only on the calculation of these coefficients. The calculation of the expectation values in the coherent initial state is described in Appendix B.

Our unperturbed system will be

$$H_0 = \hbar\omega a^\dagger a + \hbar\varepsilon S_z + G \frac{\hbar}{\sqrt{2S}}(aS_+ + a^\dagger S_-). \quad (5.50)$$

For the perturbation we will look at four different situations:

- variation of ω , corresponding to $V = \hbar a^\dagger a =: [\delta\omega]$
- variation of ε , corresponding to $V = \hbar S_z =: [\delta\varepsilon]$
- variation of G , corresponding to $V = \frac{\hbar}{\sqrt{2S}}(aS_+ + a^\dagger S_-) =: [\delta G]$
- variation of G' , corresponding to $V = \frac{\hbar}{\sqrt{2S}}(aS_- + a^\dagger S_+) =: [\delta G']$,

where we introduced short notation $V = [\delta\bullet]$ symbolically denoting the perturbation in the parameter \bullet . In the last case of $V = [\delta G']$ and if $G = 0$ all correlations average to zero, corresponding to the residual perturbation (i.e. freezing), and this case will be considered separately in Section 5.5.

As an additional simplifying assumption, we will assume that we have $\omega = \varepsilon$, i.e. spin and an oscillator are in resonance. For $G \neq 0$ we have numerically checked that the average correlation functions are quite insensitive to the resonance condition. The only exception being the $V = [\delta G]$ perturbation, for which \bar{C} , \bar{C}_R and \bar{C}_P vanish if we are out of resonance and have $G = 0$. Because this freezing case will be studied separately, we do not lose generality by taking $\omega = \varepsilon$ but gain in the simpler theoretical calculations. Namely, in resonance the G term commutes with the unperturbed Hamiltonian, $[aS_+ + a^\dagger S_-, H_0] = 0$. In addition, in experimental implementations we are usually close to the resonance condition.

Perturbation of the frequency ω

We will first analyse the case when the perturbation consists of the variation of ω , so that the perturbation generator is

$$V = \hbar a^\dagger a. \quad (5.51)$$

Due to the resonance condition $\omega = \varepsilon$ the unperturbed propagator U_0 factorises into a part proportional to the G term and the rest. The perturbation in the Heisenberg picture is therefore

$$V(t) = e^{iG(a^\dagger S_- + a S_+)t/\sqrt{2S}} (\hbar a^\dagger a) e^{-iG(a^\dagger S_- + a S_+)t/\sqrt{2S}}. \quad (5.52)$$

To calculate the average correlation function one needs an integral of the perturbation $\Sigma(t) = \int_0^t V(\tau) d\tau$ in the limit $t \rightarrow \infty$. As the constant G just re-scales time in the perturbation $V(t)$ (5.52), the \bar{C} 's which are an infinite time limit property of $\Sigma(t)$ will not depend on G , except

$$V = [\delta\varepsilon] = \hbar S_z$$

$$V = [\delta\omega] = \hbar a^\dagger a$$

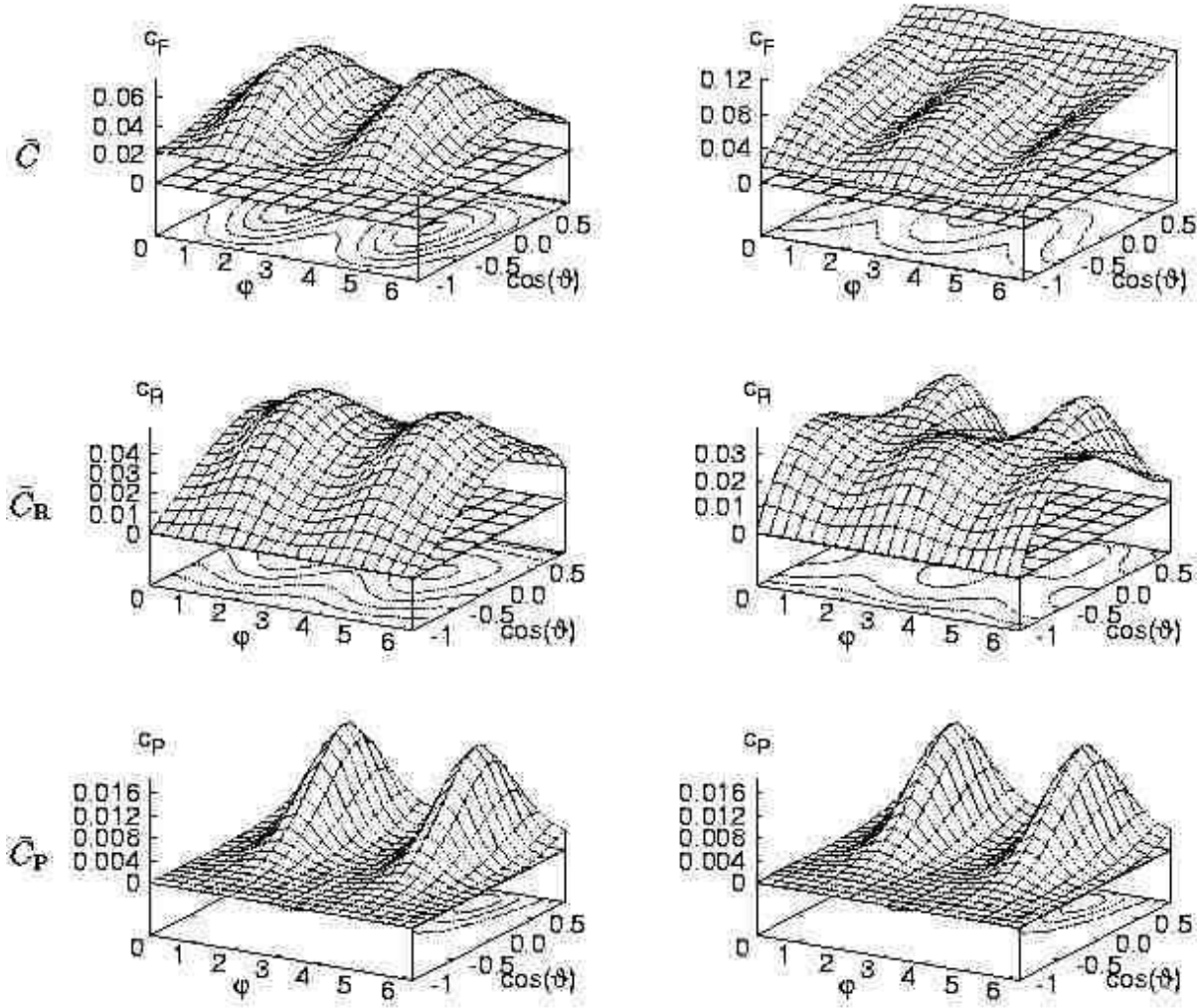


Figure 5.5: Numerically calculated dependence of \bar{C} 's on the position of the spin coherent state φ and $\cos\vartheta$ for $\omega = \varepsilon = 0.3$, $G = 1$ (everything is independent of G provided it is nonzero), $G' = 0$, $\alpha = 1.15$ and $J = 4$. Left column shows the results for ε perturbation and the right for the perturbation in ω .

possibly at $G = 0$ where the symmetry of H_0 changes and we might have an effect due to degeneracies. Direct calculation in this simple case of $G = 0$ gives

$$\bar{C} = \frac{1}{S} \frac{\alpha^2}{S}, \quad \bar{C}_R = \bar{C}_P = 0, \quad (\text{if } G = 0), \quad (5.53)$$

for the initial product coherent state (2.26,2.30). Note that α^2/S has a well defined classical limit, namely the energy of the oscillator. The last two results are expected. The $\bar{C}_P = 0$ because the perturbed dynamics is also uncoupled and $\bar{C}_R = 0$ because the perturbation is only in the oscillator (“environment”) part of H_0 . For $G > 0$ we get an additional angle dependent term of order $\hbar^2 = 1/S^2$ which can be seen in numerically calculated \bar{C} 's in Figure 5.5. Therefore, there is a discontinuous jump in all three \bar{C} 's at $G = 0$, the discontinuity being proportional to

\hbar^2 and thus of higher order for \bar{C} while it is the leading order term for \bar{C}_R and \bar{C}_P . Otherwise the values of the plateaus \bar{C} are independent of the coupling G , but of course the time scale on which we get the convergence of \bar{C} 's scales as $1/G$. For small G the discontinuity will happen at large times.

Perturbation of the spin energy ε

In this case the perturbation generator is

$$V = \hbar S_z. \quad (5.54)$$

Everything is analogous to the previous case and in the simple uncoupled case of $G = 0$ (and $\omega = \varepsilon$) we get

$$\bar{C} = \bar{C}_R = \frac{1}{S} \frac{\sin^2 \vartheta}{2}, \quad \bar{C}_P = 0, \quad (\text{if } G = 0). \quad (5.55)$$

The \bar{C} now does not depend on the oscillator coherent state parameter α but instead depends on the position of the spin coherent state. Also, the \bar{C}_R is now nonzero as we make the perturbation in our central system. At $G = 0$ there is again a discontinuity of order \hbar^2 in all three \bar{C} 's, otherwise they are independent of G . For \bar{C} and \bar{C}_R this discontinuity is of higher order in \hbar and can be neglected in the semiclassical limit. Dependence of numerically calculated \bar{C} 's on the initial position of the spin coherent packet is shown in Figure 5.5. One can see, that \bar{C}_P is equal for $[\delta\omega]$ and $[\delta\varepsilon]$ perturbations. Therefore the decoherence (purity fidelity) is insensitive to which frequency we detune, whereas fidelity and reduced fidelity are not.

Perturbation in the coupling G

The perturbation generator is

$$V = \frac{\hbar}{\sqrt{2S}}(a^+ S_- + a S_+). \quad (5.56)$$

We again take the resonant condition $\omega = \varepsilon$. Now the perturbation is constant in time $V(t) = V(0)$ regardless of the value of G and we can calculate all three \bar{C} 's for an arbitrary G . These are written in Figure 5.6 next to each plot showing its dependence on the initial spin packet position. There is no dependence on G and also no discontinuity at $G = 0$, contrary to previous two examples. Also the \bar{C} and \bar{C}_P are strictly larger than in the case of ω or ε perturbation whereas the \bar{C}_R is of order \hbar and is smaller than for the ε perturbation. Now $\bar{C}_P \propto \hbar^2$ is of course nonzero and gives us the decay time scale of purity fidelity (or purity in the case of $G = 0$).

5.4 Separation of Time Scales

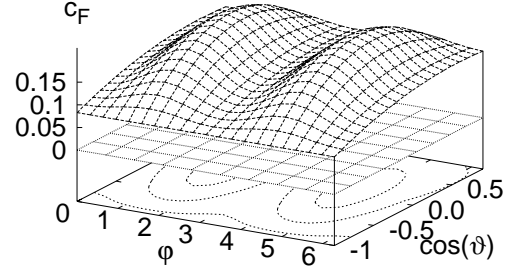
Until now we have discussed two broad categories, mixing systems in which the whole correlation function decays and regular systems where we had a plateau in the correlation function. In this section we will consider situation where the time scale of the environment is much smaller than that of the central system and the correlation function can be considerably simplified. We will furthermore consider perturbations of the product form

$$V = V_c \otimes V_e. \quad (5.57)$$

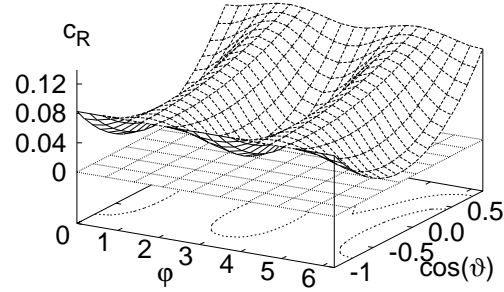
For numerical illustrations we will use a coupled double kicked top with $\varepsilon = 0$, i.e. an uncoupled unperturbed system. To simplify notation we will use $\langle A_c \rangle$ to denote the average of operator A_c

$$V = [\delta G] = \frac{\hbar}{\sqrt{2S}}(a^+ S_- + a S_+)$$

$$\bar{C} = \bar{C}_R + \frac{1}{2S} \sin^2 \vartheta$$



$$\bar{C}_R = \bar{C}_P + \frac{\alpha^2}{S^2} (\sin^2 \vartheta \sin^2 \varphi + \cos^2 \vartheta)$$



$$\bar{C}_P = \frac{1}{S^2} \cos^4 \frac{\vartheta}{2}$$

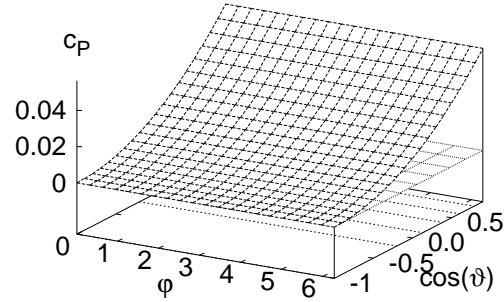


Figure 5.6: Dependence of \bar{C} 's on the position of the spin coherent initial state (φ and $\cos \vartheta$) for $\omega = \varepsilon = 0.3$, $G = 1$ (everything is independent of G), $G' = 0$, $\alpha = 1.15$ and $J = 4$. The left column shows exact theoretical results whereas the right one shows numerical plots of this dependence. All is for the perturbation in the coupling constant G .

acting only on the *central system* in the initial state of the *central system*, $\langle A_c \rangle = \text{tr}_c[A_c \rho_c(0)]$, and similarly for the environment. If the operator acts on the whole system, then $\langle A \rangle$ denotes the expectation in the *whole* initial state, as before. When the time scale of the environmental correlations $\langle V_e(t) V_e(t') \rangle$ is much smaller than the time scale of the central systems' correlations $\langle V_c(t) V_c(t') \rangle$, time averaging over the fast environmental part of the perturbation can be performed. Regarding the environmental correlation function two extreme situations are possible. If the correlations of the environment decay, we will call such a case “fast mixing environment”, and we have a finite integral of the environmental correlation function. If the correlations of the environment do not decay, we will call it a “fast regular environment”, and we have generically a non vanishing average correlation function of the environment.

5.4.1 Fast Mixing Environment

The situation, when the time scale t_e on which the correlation function for the environment decays is much smaller than the time scale t_c of the central system, is of considerable physical interest. This includes various “brownian” like baths, where the correlation times are smaller than the dynamical times of the central system in question. The correlation sums $S_F(t)$, $S_P(t)$ (5.28) and $S_R(t)$,

$$S_R(t) := \frac{1}{t} \langle \Sigma(t) (\mathbb{1} - \rho_c) \otimes \mathbb{1} \Sigma(t) \rangle, \quad (5.58)$$

giving the linear response decay of the fidelity $F(t) = 1 - (\delta/\hbar)^2 t S_F(t)$, the reduced fidelity $F_R(t) = 1 - (\delta/\hbar)^2 t S_R(t)$ and of the purity (or generally purity fidelity) $I(t) = 1 - 2(\delta/\hbar)^2 t S_P(t)$ can be significantly simplified in such situation. We will furthermore assume $\overline{\langle V_e \rangle} = 0$, with $\overline{\langle A \rangle} = \lim_{t \rightarrow \infty} t^{-1} \int_0^t \langle A(\xi) \rangle d\xi$ denoting a time average. This assumption corresponds to an equilibrium situation where the average “force” V_e vanishes. The integration over the fast variable V_e can be carried out and we get for $t \gg t_c \gg t_e$

$$\begin{aligned} S_F(t) &= 2\sigma_e \overline{\langle V_c^2 \rangle} \\ S_R(t) &= 2\sigma_e \left\{ \overline{\langle V_c^2 \rangle} - \overline{\langle V_c \rangle^2} \right\} \\ S_P(t) &= 2\sigma_e \left\{ \overline{\langle V_c^2 \rangle} - \overline{\langle V_c \rangle^2} \right\}, \end{aligned} \quad (5.59)$$

with

$$\sigma_e := \lim_{t \rightarrow \infty} \langle \Sigma_e^2(t) \rangle / 2t, \quad \text{with} \quad \Sigma_e(t) = \int_0^t V_e(\xi) d\xi, \quad (5.60)$$

being the integral of the autocorrelation function for the environmental part of the perturbation V_e alone. The result does not depend on the initial state of the environment. Some interesting conclusions can be drawn from these linear response results (5.59).

We can see that the decay time scale depends only on the time average diagonal correlations of the central system $\langle V_c^2(t) \rangle$ and not on the full correlation function. This is a simple consequence of the separation of time scales and means that the decay of all three stability measures does not depend on the dynamics of the central system (e.g. being mixing or regular). Furthermore, reduced fidelity $F_R(t)$ and the purity $I(t)$ will decay on the same time scale (5.59), meaning that the decay of the reduced fidelity is predominantly caused by the loss of coherence, i.e. entanglement between the two factor spaces. This in turn means that the reduced fidelity, which is a property of echo dynamics, i.e. of comparison of two slightly different Hamiltonian evolutions, is equivalent to the decay of the purity.

If the initial state of the central system $\rho_c(0)$ is a Gaussian wave packet (coherent state) then the dispersion $\overline{\langle V_c^2 \rangle} - \overline{\langle V_c \rangle^2}$ is by factor of order \hbar *smaller* than $\overline{\langle V_c^2 \rangle}$. Thus for coherent initial states of the central system, irrespective of the initial state of the environment, the $F_R(t)$ and $I(t)$ are going to decay on a $1/\hbar$ times *longer* time scale than $F(t)$. We have therefore reached a general conclusion based on the assumption of chaotic fast environment (which is often the case), namely that the coherent states are most robust against decoherence (decay of purity), provided $t_e \ll t_c$ and decoherence time is longer than the correlation time of the environment, $t_e \ll t_{\text{dec}}$. If decoherence is even faster than the time scale of the environment, as is the case for macroscopic superpositions, then formulas (5.59) are not valid any more as one is effectively in a regular regime with $S_P(t) \propto t^2$. Decoherence time is then independent not just of systems dynamics but also of environmental dynamics characterised by σ_e (Braun *et al.*, 2001; Strunz *et al.*, 2003; Strunz & Haake, 2003).

In the regime of fast chaotic environment one can derive a master equation for a reduced density matrix of the central system (Kolovsky, 1994; Meystre & Sargent III, 1990). We take a

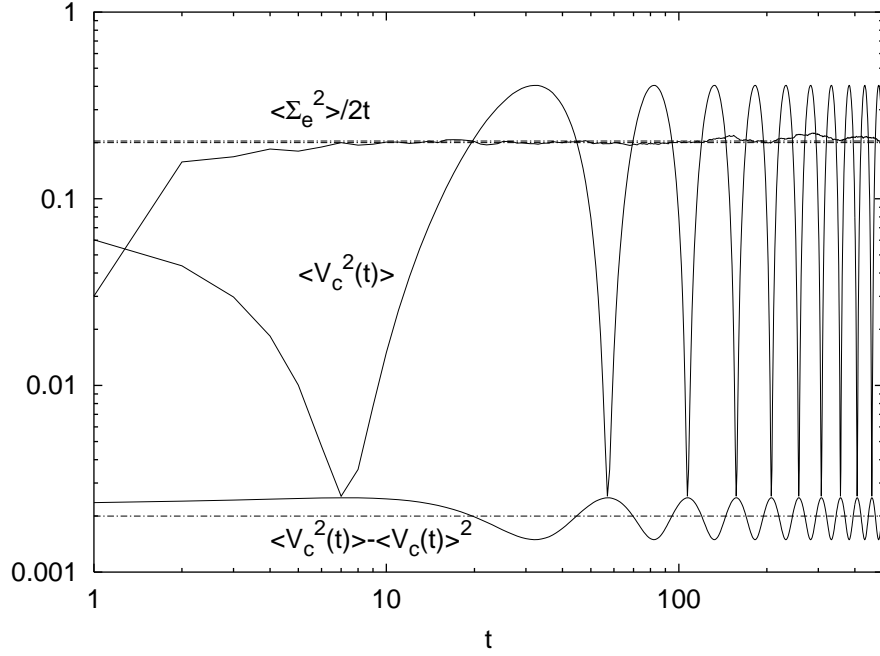


Figure 5.7: Various correlation sums from formulas (5.59) in a fast chaotic regime (solid curves, as indicated in the figure). Chain lines indicate corresponding theoretical time averages. For details see text.

partial trace over the environment of the echo density matrix $\rho^M(t)$ and write it for a small time step Δt . This time step Δt must be larger than the correlation time t_e of the environment and at the same time smaller than the correlation time t_c of the central system. For the environmental part of the correlation function we assume fast exponential decay (particular exponential form is not essential) which is independent of the state $\rho(0)$

$$\text{tr}_e[V_e(t)V_e(t')\rho] \longrightarrow \frac{\sigma_e}{t_e} \exp\{-|t-t'|/t_e\} \text{tr}_e[\rho]. \quad (5.61)$$

Assuming the perturbation to be a product $V(t) = V_c(t) \otimes V_e(t)$ and the average “force” $\text{tr}_e[V_e(t)\rho]$ to vanish together with the exponential decay of environmental correlations of the form (5.61) for an arbitrary state, yields a master equation for the reduced density matrix $\rho_c^M(t) := \text{tr}_e[\rho^M(t)]$,

$$\dot{\rho}_c^M(t) = -\frac{\delta^2}{\hbar^2} \sigma_e[V_c(t), [V_c(t), \rho_c^M(t)]]. \quad (5.62)$$

Master equation is strictly valid in the Markovian limit of the correlation function being a delta function in time or if considered on time scales larger than the correlation time.

For numerical demonstration we use a double kicked top with: $V_{c,e} = S_z/S$, $S = 200$, $\delta = 1.5 \cdot 10^{-3}$, coherent initial state at $(\vartheta, \varphi)_{c,e} = (\pi/\sqrt{3}, \pi/\sqrt{2})$ and parameters $\alpha_c = 0$, $\gamma_c = \pi/50$ for the central system and $\alpha_e = 30$, $\gamma_e = \pi/2.1$ for the environment. Actually, we could take any value of α_c and would get qualitatively similar results. The only advantage of using regular central dynamics $\alpha_c = 0$ is that it is then possible to explicitly calculate averages $\overline{\langle V_c^2 \rangle}$ and $\overline{\langle V_c^2 \rangle} - \overline{\langle V_c \rangle}^2$. Namely, if $\alpha_c = 0$ and $\gamma_c \ll 1$ we get

$$\begin{aligned} \overline{\langle V_c^2 \rangle} &= \frac{1}{2}(1 - y_c^2) + \frac{1}{4S}(1 + y_c^2) \\ \overline{\langle V_c^2 \rangle} - \overline{\langle V_c \rangle}^2 &= \frac{1}{4S}(1 + y_c^2). \end{aligned} \quad (5.63)$$

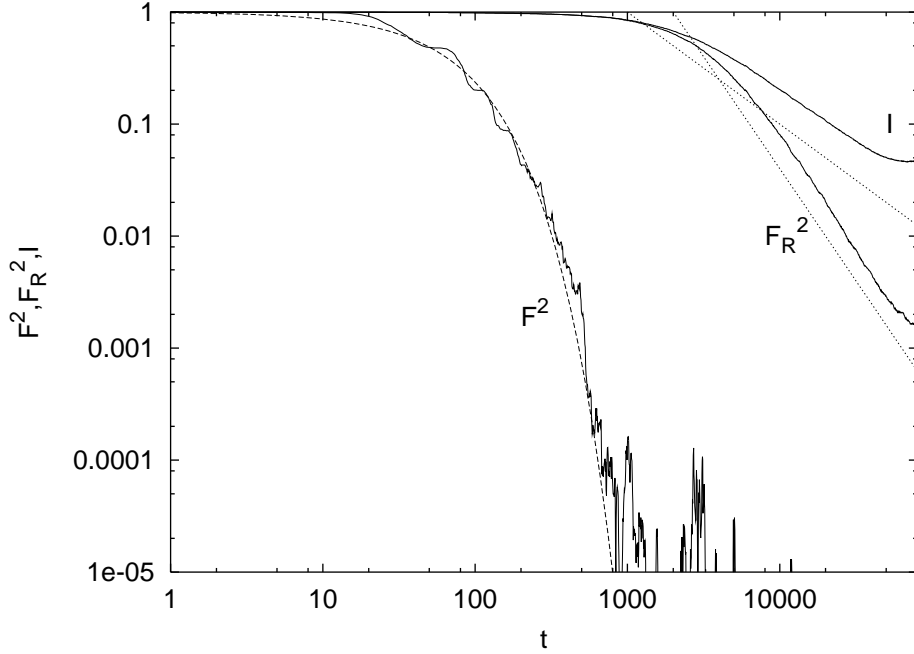


Figure 5.8: Decay of $F^2(t)$, $F_R^2(t)$ and $I(t)$ for fast chaotic environment. The dashed line is an exponential function with the exponent given by the values of σ_e and $\overline{\langle V_c^2 \rangle}$ (5.59) while the two dotted lines have slopes -2 and -1 . For parameters see text.

The values of these two quantities for our initial condition are $\overline{\langle V_c^2 \rangle} = 0.202$ and $\overline{\langle V_c^2 \rangle} - \overline{\langle V_c \rangle}^2 = 0.399/S$, and are shown in Figure 5.7 with two dotted lines (by pure coincidence we have $\sigma_e = 0.20 \approx \overline{\langle V_c^2 \rangle}$), together with numerically calculated time dependent (not yet averaged) $\langle V_c^2(t) \rangle$ and $\langle V_c^2(t) \rangle - \langle V_c(t) \rangle^2$. This time dependent values oscillate on a time scale ≈ 50 , which is much longer than the time ≈ 10 in which σ_e converges and so the assumption $t_e \ll t_c$ is justified. The values of all three quantities are then used in the linear response formulas (5.59) to give us the time scales on which F , F_R and I decay. The results are shown in Figure 5.8. We can see that the fidelity again decays exponentially as predicted, but the reduced fidelity and the purity have a power-law tails. The decay time can be estimated by the lowest order expansions (5.59). Using the values of σ_e and $\overline{\langle V_c^2 \rangle} - \overline{\langle V_c \rangle}^2$ (theoretical expression (5.63)), we get $\tau_F \approx 1/(0.16\delta^2 S^2)$ and $\tau_{R,P} \approx 1/(0.32\delta^2 S)$ (τ_F and τ_R are for F^2 and F_R^2) which agrees with numerics in Figure 5.9. The same general conclusion again holds: the more chaotic the environment is (smaller σ_e), the slower the decay of all three quantities. Purity and reduced fidelity both decay on a $1/\hbar$ longer time scale than the fidelity in accordance with expressions (5.63) for coherent initial states.

5.4.2 Fast Regular Environment

Here we will explore perhaps a less physical situation of a regular environmental dynamics, i.e. one with non-decaying correlation function. The double integral of environmental correlations grows as $\propto t^2$ and we can define the average correlation function

$$\bar{C}_e := \lim_{t \rightarrow \infty} \langle \Sigma_e^2(t) \rangle / t^2. \quad (5.64)$$

If in addition the correlations of the system also do not decay then the correlation sum of the total system will grow as $\propto t^2$ which is just the regular regime already discussed before.

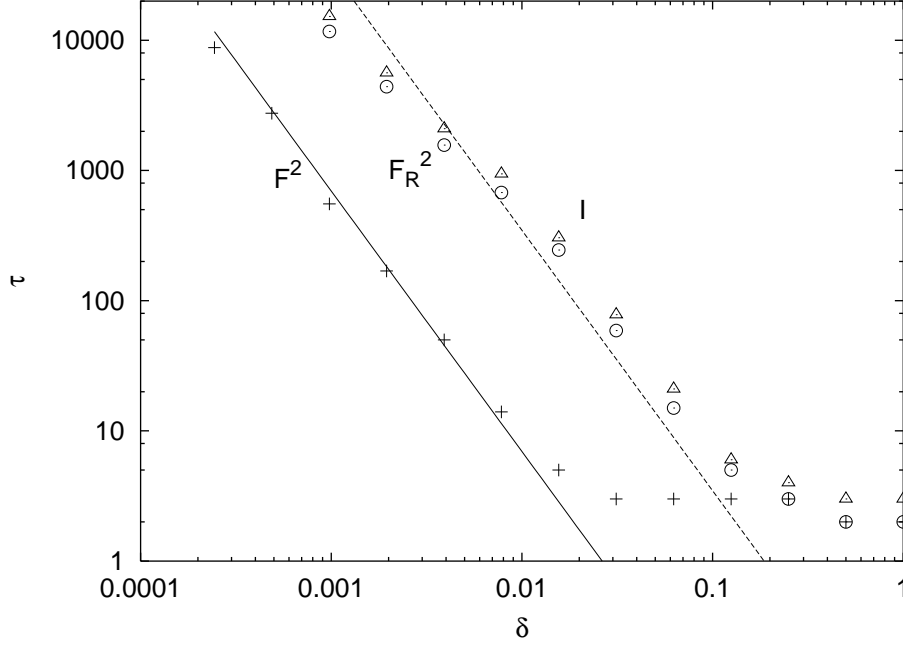


Figure 5.9: Times τ at which $F^2(t)$, $F_R^2(t)$, $I(t)$ fall to level 0.37 for different δ and fast chaotic environment. Symbols give the numerics and lines give the theoretical dependence of τ . All is for $S = 100$. For other parameters see text.

Here, we will focus on a different situation where the integral of systems correlation function converges, i.e. the dynamics of the central system is mixing. We will additionally assume the average “position” V_c to be zero $\overline{\langle V_c \rangle} = 0$. The transport coefficient of the central system σ_c is then

$$\sigma_c := \lim_{t \rightarrow \infty} \langle \Sigma_c^2(t) \rangle / 2t, \quad \Sigma_c(t) = \int_0^t V_c(\xi) d\xi. \quad (5.65)$$

The expressions for $S_F(t)$, $S_P(t)$ (5.28) and $S_R(t)$ (5.58) are independent of time and can be simplified to

$$\begin{aligned} S_F &= 2\sigma_c \bar{C}_e \\ S_R &= 2\sigma_c \bar{C}_e \\ S_P &= 2\sigma_c \left\{ \bar{C}_e - \overline{\langle V_e \rangle}^2 \right\}. \end{aligned} \quad (5.66)$$

Note that now the reduced fidelity $F_R(t)$ decays on the same time scale as the fidelity $F(t)$. This must be contrasted to the case of a fast mixing environment (5.59), where $F_R(t)$ decayed on the same time scale as the purity. If the initial state of the environment $\rho_e(0)$ is a coherent state, then purity will decay on a $1/\hbar$ times longer time scale than fidelity or reduced fidelity. On the other hand, for a random initial state of the environment, the average force $\langle V_e \rangle = 0$ vanishes, and all three quantities decay on the same time scale.

For the purpose of numerical experiment we chose $V_c = S_z/S$, and $V_e = S_z^2/S^2$ in order to have a less trivial situation of non-vanishing average force $\langle V_e \rangle$. The initial condition is again $(\vartheta, \varphi)_{c,e} = (\pi/\sqrt{3}, \pi/\sqrt{2})$ and the parameters are $J = 200$, $\alpha_c = 30$, $\gamma_c = \pi/7$ and $\alpha_e = 0$, $\gamma_e = \pi/2.1$ and the perturbation strength $\delta = 6 \cdot 10^{-4}$. By choosing the explicitly solvable case $\alpha_e = 0$ we can calculate \bar{C}_e and $\overline{\langle V_e \rangle}^2$, say for the simple case of a $\pi/2$ rotation, $\gamma_e = \pi/2$,

$$\bar{C}_e = \frac{1}{4}(1 - y_e^2)^2 + \frac{1}{4S}(-3y_e^4 + 2y_e^2 + 1) + \mathcal{O}(1/S^2)$$

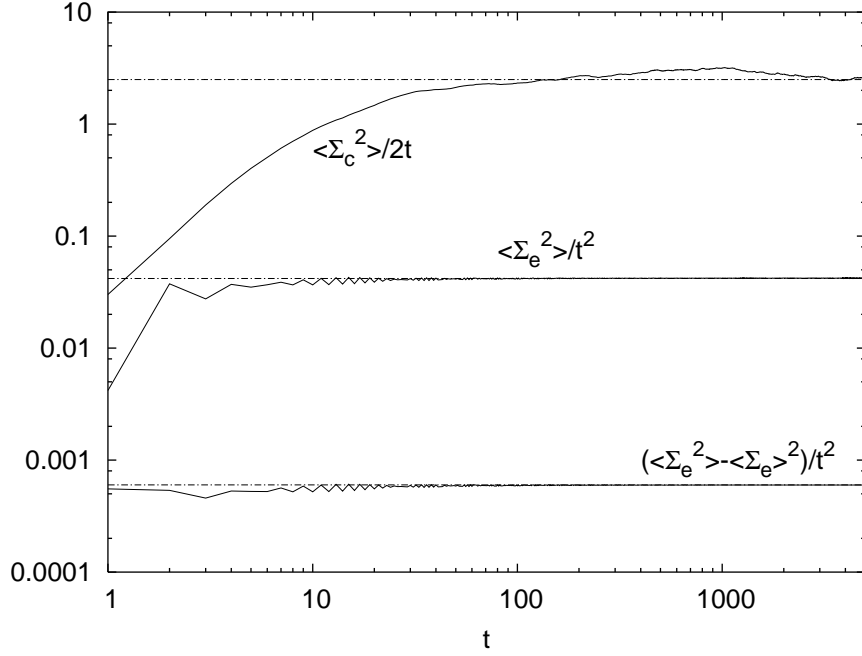


Figure 5.10: Correlation sums occurring in (5.66) (solid curves) for $S = 200$. The top chain line gives the best fit for σ_c and the two lower chain lines give theoretical time averaged correlation functions for the environment (5.67). All is for a fast regular environment. See text for details.

$$\bar{C}_e - \overline{\langle V_e \rangle}^2 = \frac{1}{2S} y_e^2 (1 - y_e^2) + \frac{1}{16S^2} (11y_e^4 - 11y_e^2 + 2) + \mathcal{O}(1/S^3). \quad (5.67)$$

For our parameters we have $y_{c,e} = 0.772$ giving $\bar{C}_e = 0.0407$ and $\bar{C}_e - \overline{\langle V_e \rangle}^2 = 0.120/S$. The values of these coefficients are shown in Figure 5.10 (lower two dotted lines) and nicely agree with the numerics. In Figure 5.11 we can observe the exponential decay of fidelity and reduced fidelity on the same time scale (both curves almost overlap) and the decay of the purity on a $1/\hbar$ longer time scale. For longer times purity decay is again algebraic. In Figure 5.12 we show dependence of the decay times on δ . The dependence for purity is quite interesting. If one looks at the time the purity falls to 0.99 one has agreement with linear response (by definition). But if one looks at the purity level 0.37, they don't agree as well, meaning that the shape of purity decay may change (not only the scale) as one varies δ or \hbar . On the other hand, this may also be simply a finite size effect.

5.5 Freeze in a Harmonic Oscillator

Previously we have discussed the so called freeze of fidelity in regular systems having a non-singular derivative of the unperturbed frequencies, $\Omega = \partial\omega/\partial\mathbf{j} \neq 0$. In the present section we will consider the case of a harmonic oscillator, for which $\Omega = 0$ and the theory explained in Section 4.2 can not be used. For the sake of numerical demonstration we will use a Jaynes-Cummings model (see Section 2.1.2) with the perturbation in the G' parameter, i.e. the only case not explained in Section 5.3.2. The initial state will be a product of coherent state for a spin and an oscillator. The perturbation will be

$$V = \frac{\hbar}{\sqrt{2S}} (a^+ S_+ + a S_-) = [\delta G']. \quad (5.68)$$

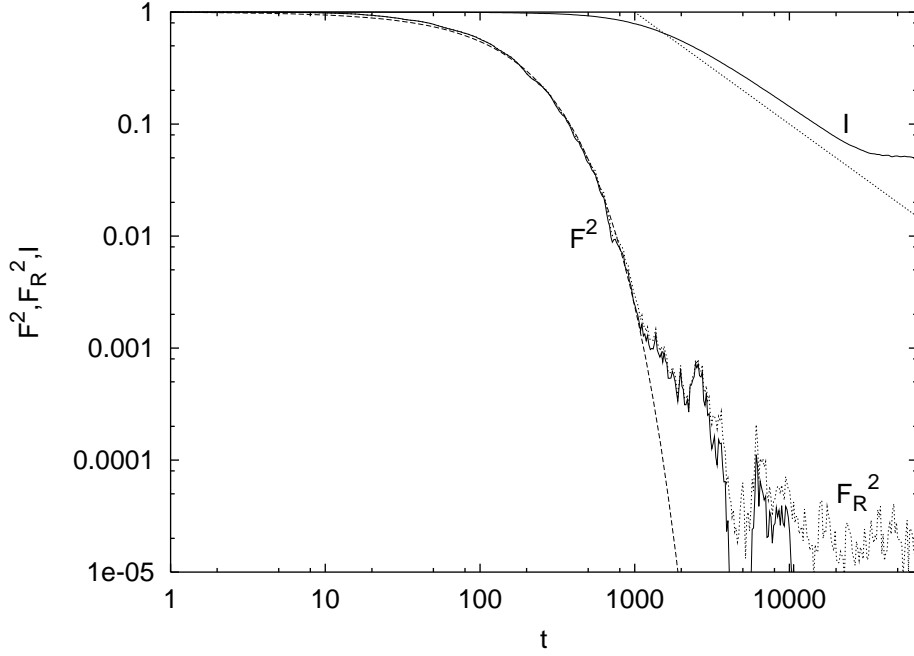


Figure 5.11: Decay of $F^2(t)$, $F_R^2(t)$ and $I(t)$ for fast regular environment. The dashed line is the exponential function with the exponent given by a product of σ_c and \bar{C}_e (5.66). The straight dotted line has slope -1 . See text for details.

Provided we have $G' = 0$ for the unperturbed system the correlation function has a zero time average regardless of other parameters. This is a simple consequence of the symmetries as the perturbation is a “counter-rotating” term, while the unperturbed Hamiltonian has only a “co-rotating” term. Due to the symmetry the perturbation is residual. The fact that the perturbation is residual has nothing to do with the perturbation G' breaking integrability. For instance, if we make a perturbation in G' and any other parameter at the same time, we will have a perturbation that breaks integrability but is not residual.

Because we want to study the case of $\Omega = 0$, we choose $G = 0$ so the unperturbed Hamiltonian,

$$H_0 = \hbar\omega a^+ a + \hbar\varepsilon S_z, \quad (5.69)$$

is uncoupled. As a consequence purity fidelity equals purity. Residual perturbation can be written as a time derivative of another operator W (4.6), which is in our case

$$V := \frac{i}{\hbar}[H_0, W] = \frac{dW}{dt}, \quad W = \frac{i\hbar}{\sqrt{2S}(\omega + \varepsilon)} (a^+ S_+ - a S_-). \quad (5.70)$$

The echo operator can than be written as

$$M_\delta(t) = \exp \left\{ -\frac{i}{\hbar} \left(\{W(t) - W(0)\} \delta + \frac{1}{2} \Gamma(t) \delta^2 + \dots \right) \right\}, \quad (5.71)$$

with $\Gamma(t)$ given by

$$\begin{aligned} \Gamma(t) &:= \int_0^t R(\tau) d\tau - \frac{i}{\hbar} [W(0), W(t)], \\ R &:= \frac{i}{\hbar} [W, \frac{dW}{dt}] = \frac{\hbar^2}{(\omega + \varepsilon)} (\mathbf{S}^2 - S_z^2 - S_z - 2a^+ a S_z). \end{aligned} \quad (5.72)$$

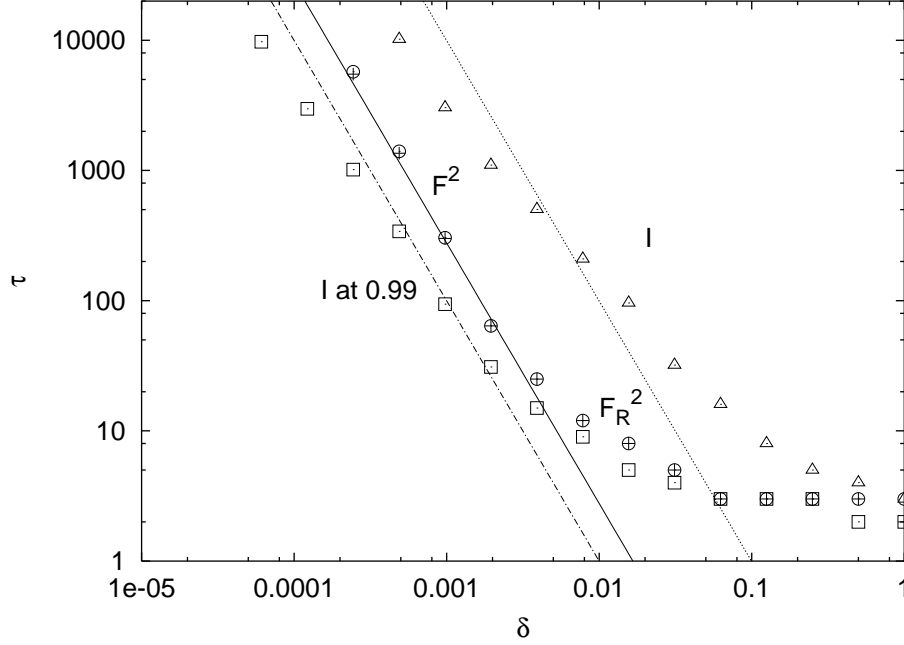


Figure 5.12: Times τ at which $F^2(t)$ (pluses), $F_R^2(t)$ (circles) and $I(t)$ (triangles) fall to level 0.37, and times τ when $I(t)$ falls to 0.99 (squares) for varying δ and fast regular environment. Symbols are the numerics and lines give theoretical dependences of τ . Everything is for $S = 100$.

For the semiclassical calculations we will also need the classical limits of W and R . Introducing canonical action angle variables for the spin (i.e. “central”) system,

$$\hbar S_z \rightarrow j_c = \cos \vartheta, \quad \hbar S_{\pm} \rightarrow \sqrt{1 - j_c^2} e^{\pm i\theta_c}, \quad \theta_c = \varphi, \quad (5.73)$$

and for the oscillator (“environment”),

$$a \rightarrow \frac{i}{\sqrt{2\hbar}} \sqrt{2j_e} e^{-i\theta_e}, \quad j_e = |\alpha|^2/S, \quad (5.74)$$

the classical Hamiltonian reads

$$h_0 = \boldsymbol{\omega} \cdot \mathbf{j}, \quad \boldsymbol{\omega} = (\varepsilon, \omega), \quad \mathbf{j} = (j_c, j_e). \quad (5.75)$$

The classical limits w of W and r of R are

$$\begin{aligned} w &= -\frac{\sqrt{2j_e(1-j_c^2)}}{\omega + \varepsilon} \cos(\theta_c + \theta_e) \\ r &= \frac{1}{\omega + \varepsilon} (1 - j_c^2 - 2j_c j_e). \end{aligned} \quad (5.76)$$

5.5.1 The Plateau

The height of the plateau is given by the expectation value of the echo operator

$$F_{\text{plat}} = |\langle \exp(-i\delta\{W(t) - W(0)\}/\hbar) \rangle|^2. \quad (5.77)$$

For a harmonic oscillator one has to evaluate this expression explicitly and can not use time averaging as has been done for a general unperturbed dynamics in Section 4.2. We immediately

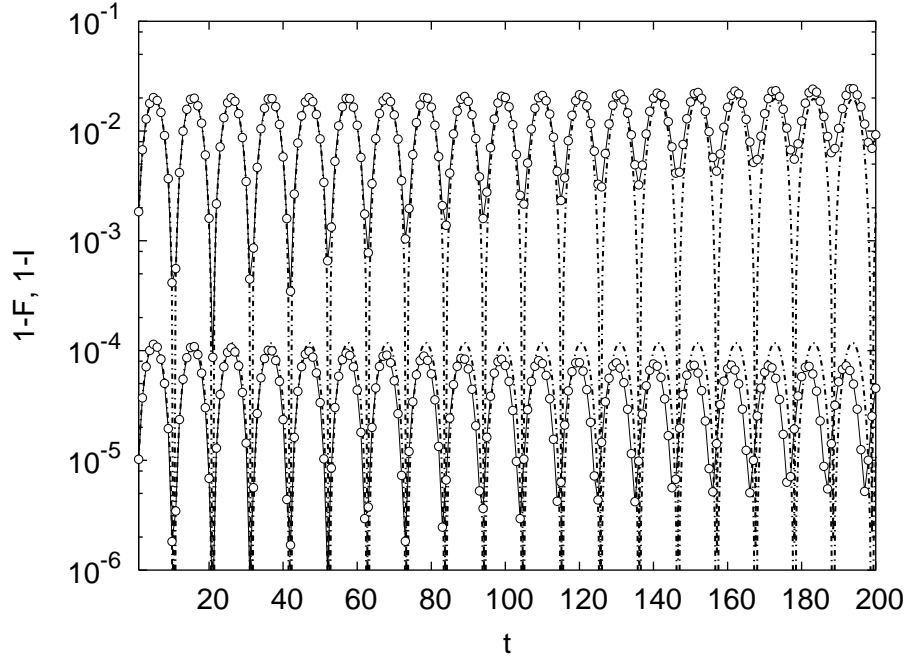


Figure 5.13: The plateau $1 - F(t)$ (upper symbols) and $1 - I(t)$ (lower symbols) for $S = 50$ and coherent initial state. Perturbation of strength $\delta = 0.01$ is in G' , $\omega = \varepsilon = 0.3$, $G = 0$, $\alpha = 1.15$. Chain lines represent the theory (5.87, 5.88) and circles full numerical simulations.

see, that the leading semiclassical order will vanish for coherent initial states. We would get $|\exp(-i\delta s(\mathbf{j}^*, \boldsymbol{\theta}^*, t)/\hbar)|^2 = 1$, where we denoted

$$s(\mathbf{j}, \boldsymbol{\theta}, t) := w(\mathbf{j}, \boldsymbol{\theta} + \boldsymbol{\omega}t) - w(\mathbf{j}, \boldsymbol{\theta}). \quad (5.78)$$

Recall that in case of $\Omega \neq 0$ this leading order already gave a nonzero contribution. Here though, we have to calculate the next order. For coherent initial states this is easily done using the stationary phase method, i.e. expanding the phase around the position of the packet to lowest order. The calculation is actually very similar to the calculation of the fidelity decay for coherent initial state and non-residual perturbations. Expansion of the phase gives

$$s(\mathbf{j}, \boldsymbol{\theta}, t) = s(\mathbf{j}^*, \boldsymbol{\theta}^*, t) + \mathbf{s}' \cdot (\mathbf{j} - \mathbf{j}^*, \boldsymbol{\theta} - \boldsymbol{\theta}^*) + \dots, \quad (5.79)$$

with

$$\mathbf{s}' := \left(\frac{\partial s(\mathbf{j}^*, \boldsymbol{\theta}^*, t)}{\partial \mathbf{j}}, \frac{\partial s(\mathbf{j}^*, \boldsymbol{\theta}^*, t)}{\partial \boldsymbol{\theta}} \right). \quad (5.80)$$

Note that now $s(\mathbf{j}, \boldsymbol{\theta}, t)$ depends also on the angles and therefore the ASI method cannot be used directly. Instead, we will use the *classical* averaging over the initial Gaussian distribution in a *phase space*. We will replace the quantum expectation value with the classical average. Using the compact notation $\mathbf{x} := (\mathbf{j}, \boldsymbol{\theta}) = (\mathbf{j}_c, \mathbf{j}_e, \boldsymbol{\theta}_c, \boldsymbol{\theta}_e)$, we can write the classical density corresponding to the coherent initial state as

$$\rho(\mathbf{x}; \mathbf{x}^*) = \left(\frac{2}{\pi\hbar} \right)^d \sqrt{\det D} \exp(-(\mathbf{x} - \mathbf{x}^*) \cdot D(\mathbf{x} - \mathbf{x}^*)/\hbar), \quad (5.81)$$

with \mathbf{x}^* being the position of the initial packet and a matrix D (of size $2d \times 2d$) determining the squeezing of the initial packet in $d = d_c + d_e$ degrees of freedom system. The above classical

density is normalised as $\int \rho d\mathbf{x} = 1$. For our choice of the initial state being a product of a spin coherent state (2.28) and an oscillator coherent state (2.31) the matrix D is diagonal with elements

$$D_{11} = \frac{1}{1 - j_c^2}, \quad D_{22} = \frac{1}{2j_e}, \quad D_{33} = 1 - j_c^2, \quad D_{44} = 2j_e. \quad (5.82)$$

The fidelity plateau is now calculated as

$$F_{\text{plat}} = \left| \int d\mathbf{x} \rho(\mathbf{x}; 0) \exp(-i\delta \mathbf{s}' \cdot \mathbf{x}/\hbar) \right|^2, \quad (5.83)$$

resulting in a Gaussian function

$$F_{\text{plat}}^{\text{CIS}} = \exp\left(-\frac{\delta^2}{\hbar} \nu_{\text{har}}\right), \quad \nu_{\text{har}} := \frac{1}{2} \mathbf{s}' \cdot D^{-1} \mathbf{s}'. \quad (5.84)$$

Note that the result is formally very similar to the expression for the fidelity decay for a non-residual perturbation (3.36). Linear response expansion of the plateau is of course $F_{\text{plat}}^{\text{CIS}} = 1 - \frac{\delta^2}{\hbar} \nu_{\text{har}}$ and so the plateau for a harmonic oscillator is by factor $1/\hbar$ *higher* than for general systems (4.62). Beyond linear response though, the plateau will decay faster (i.e. as a Gaussian) for a harmonic oscillator than for systems with $\Omega \neq 0$ where the asymptotic decay of the plateau was a power law (e.g. $1/(\delta S)$ for the numerical model used in Section 4.2).

For our Jaynes-Cummings model we have

$$s(\mathbf{j}, \boldsymbol{\theta}, t) = 2 \sin\left(\frac{\omega + \varepsilon}{2} t\right) \frac{\sqrt{2j_e(1 - j_c^2)}}{\omega + \varepsilon} \sin\left(\theta_c + \theta_e + t \frac{\omega + \varepsilon}{2}\right). \quad (5.85)$$

The coefficient ν_{har} is then

$$\nu_{\text{har}} = \frac{2}{(\omega + \varepsilon)^2} \sin^2\left(\frac{\omega + \varepsilon}{2} t\right) \left\{ (1 - j_c^2) + 2j_e \left[j_c^2 + (1 - j_c^2) \cos^2\left(\theta_c + \theta_e + t \frac{\omega + \varepsilon}{2}\right) \right] \right\}. \quad (5.86)$$

The same ν_{har} would be obtained from the quantum calculation of the second moment of $\Sigma(t)$.

Results of the numerical calculation are shown in Figure 5.13. The initial packet was at $(\vartheta, \varphi) = (1, 1)$ and $\alpha = 1.15$, giving actions $j_c = 0.54$ and $j_e = 0.026$ and angles $\theta_c = 1$ and $\theta_e = \pi/2$. Because $j_e \ll j_c$ we can neglect the second term in ν_{har} and get

$$1 - F_{\text{plat}}^{\text{CIS}} = 3.93 \delta^2 S \sin^2(0.3t). \quad (5.87)$$

The agreement of this theoretical prediction with numerics can be seen in Figure 5.13.

For the reduced fidelity and the purity one can go through similar calculations. We will just list the linear response result obtained from the quantum expectation values,

$$\begin{aligned} 1 - F_{\text{R}} &= \delta^2 S \frac{2}{(\omega + \varepsilon)^2} \sin^2\left(\frac{\omega + \varepsilon}{2} t\right) 2j_e \left[j_c^2 + (1 - j_c^2) \cos^2\left(\theta_c + \theta_e + t \frac{\omega + \varepsilon}{2}\right) \right] \\ 1 - I &= \delta^2 \frac{2}{(\omega + \varepsilon)^2} \sin^2\left(\frac{\omega + \varepsilon}{2} t\right) (1 - j_c)^2. \end{aligned} \quad (5.88)$$

Theory for the purity shown in Figure 5.13 also agrees well with numerics. The purity plateau for coherent initial states is \hbar -independent, just as the whole decay of purity.

5.5.2 Beyond the Plateau

After a sufficiently long time, when the second term $\Gamma(t)$ becomes important in the echo operator (5.71), the decay will be determined by the operator R . As our R is non-residual, we can use the theory for general perturbations, just using a “renormalised” perturbation strength $\delta^2/2$. The fidelity and the reduced fidelity will decay as Gaussians, with the decay times given by \bar{C} (5.20) and \bar{C}_R (5.21), respectively, while the decay of the purity in our 1 + 1 degrees of freedom system will be $I(t) = 1/\sqrt{1 + u(\delta t)^2}$ (5.42), with $u = 4\bar{C}_P/\hbar^2$ (5.24). For our simple example, the average \bar{r} is equal to r and the derivatives occurring in the expressions for \bar{C} ’s are

$$\frac{\partial \bar{r}}{\partial j_c} = -\frac{2}{\omega + \varepsilon}(j_c + j_e), \quad \frac{\partial \bar{r}}{\partial j_e} = -\frac{2}{\omega + \varepsilon}j_c, \quad \frac{\partial^2 \bar{r}}{\partial j_c \partial j_e} = -\frac{2}{\omega + \varepsilon}. \quad (5.89)$$

Taking into account that the squeezing parameters for coherent initial states are $\Lambda_c = 1/(1 - j_c^2)$ and for an oscillator $\Lambda_e = 1/(2j_e)$, we obtain

$$\begin{aligned} \bar{C} &= \hbar \frac{2}{(\omega + \varepsilon)^2} \left\{ (j_c + j_e)^2 (1 - j_c^2) + 2j_e^2 j_e \right\} \\ \bar{C}_R &= \hbar \frac{2}{(\omega + \varepsilon)^2} (j_c + j_e)^2 (1 - j_c^2) \\ \bar{C}_P &= \hbar^2 \frac{2}{(\omega + \varepsilon)^2} (1 - j_c^2) j_e. \end{aligned} \quad (5.90)$$

This then immediately gives the fidelity decay (4.66), the reduced fidelity (5.44) and the purity (5.42),

$$F(t) = \exp(-\delta^4 S^2 \bar{C} t^2 / 4), \quad F_R(t) = \exp(-\delta^4 S^2 \bar{C}_R t^2 / 4), \quad I(t) = \frac{1}{\sqrt{1 + \bar{C}_P S^2 \delta^4 t^2}}. \quad (5.91)$$

Note the \hbar -independent decay of purity.

In Figure 5.14 we show numerical results for the Jaynes-Cummings model with spin size $S = 1/\hbar = 50$ and a coherent initial state placed at $(\vartheta, \varphi) = (1, 1)$ and $\alpha = 1.15$, giving actions $j_c = 0.54$ and $j_e = 0.026$. The perturbation is $V = [\delta G']$ of strength $\delta = 0.01$, while the parameters of the unperturbed Hamiltonian are $\omega = \varepsilon = 0.3$, $G = 0$. The average correlation functions (5.90) are $\bar{C}S = 1.35$, $\bar{C}_R S = 1.26$ and $\bar{C}_P S^2 = 0.10$. For clarity we show in the figure only the fidelity and the purity as the reduced fidelity would almost overlap with the fidelity. This theoretical values are then used to compare with numerics. Agreement is excellent. We also show a numerical calculation of the classical fidelity (symbols). One can see that for a *harmonic oscillator* and a *residual* perturbation the classical fidelity *agrees* with the quantum one. Recall, that for a *residual* perturbation and a general unperturbed system, i.e. having $\Omega \neq 0$, the classical fidelity followed the quantum only up to $t_1 \propto \sqrt{1/\hbar}$ time. For harmonic oscillators though, the quantum fidelity is equal to the classical despite the perturbation being residual. Purity can also be calculated purely classically. The classical purity can be defined as

$$I_{cl} := \int d\mathbf{x}_c \rho_c^2(t), \quad \rho_c(t) := \int d\mathbf{x}_e \rho(t), \quad (5.92)$$

with $\rho(t)$ being the classical density at time t , i.e. $\rho(t) = \rho(\phi^{-t}(\mathbf{x}); \mathbf{x}^*)$ with $\phi(\mathbf{x})$ being the Hamiltonian flow in phase space[†]. Such classical purity (linear entropy) has been used before (Wehrl, 1978; Angelo *et al.*, 2004). For our system and perturbation the integrals in (5.92) are Gaussian and the result is *the same* as the one obtained from the quantum definition of purity (5.91).

[†]Here the density has to be square normalised, $\int d\mathbf{x} \rho^2 = 1$.

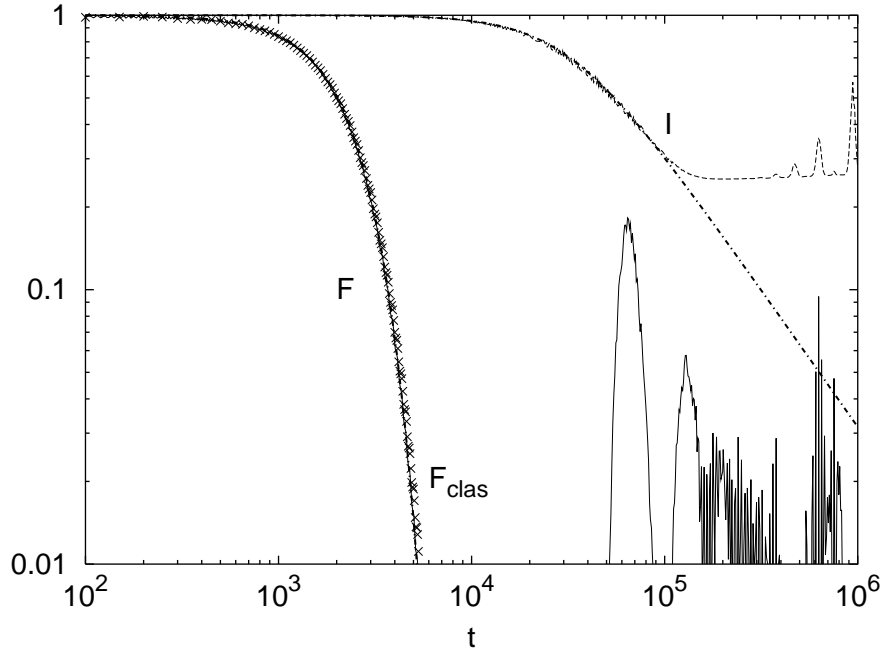


Figure 5.14: Long time fidelity and purity decay for the same data as in Figure 5.13. The theoretical decay for purity (chain curve)(5.91), agrees with the numerical $I(t)$ until the asymptotic plateau is reached. Similarly, theory for the fidelity overlaps with the numerics. Symbols show the numerical result for classical fidelity which in this case agrees with the quantum fidelity.

5.6 Decoherence for Cat States

In this section we want to study decoherence for macroscopic superpositions of states, the so-called Schrödinger cat states. We would like to demonstrate the accelerated decoherence for macroscopic superpositions, without resorting to any effective master equation description. The goal is to show that if we start with the initial state of the central system in the superposition of two macroscopically separated states $|\tau_1\rangle$ and $|\tau_2\rangle$, the decoherence (decay of purity) is much faster than if we start with a single state $|\tau_1\rangle$ of the central system.

We can explain the accelerated purity decay for cat states using our results for the reduced fidelity decay for coherent initial states. Decoherence of a cat state will cause the reduced density matrix to evolve from a coherent superposition of two packets at the beginning to a mixture of two packets after the decoherence time t_{dec} ,

$$\rho_c(0) \sim \frac{1}{2} (|\tau_1\rangle\langle\tau_1| + |\tau_2\rangle\langle\tau_2| + |\tau_1\rangle\langle\tau_2| + |\tau_2\rangle\langle\tau_1|) \xrightarrow{t_{\text{dec}}} \frac{1}{2} (|\tau_1\rangle\langle\tau_1| + |\tau_2\rangle\langle\tau_2|), \quad (5.93)$$

The purity $I(t)$ of the initial coherent state is $I(0) = 1$ while the purity of the final state is $I(t_{\text{dec}}) = 1/2$, if the states $|\tau_1\rangle$ and $|\tau_2\rangle$ are orthogonal.

Let us suppose that the initial state is a product state of the coherent state of the environment $|\alpha\rangle$ and a cat state of the central system, i.e. a superposition of two coherent states $|\tau_1\rangle$ and $|\tau_2\rangle$,

$$|\psi(0)\rangle = \frac{1}{\sqrt{2}} (|\tau_1\rangle + |\tau_2\rangle) \otimes |\alpha\rangle. \quad (5.94)$$

We will assume that we are in a regular regime, for which the decay of purity of individual product coherent states has been derived before (5.41) and was seen to decay on a \hbar -independent

time scale $t_d \sim 1/\delta$, where δ is a coupling strength between the central system and the environment. For times smaller than the decoherence time of individual coherent states t_d , the initial cat state (5.94) will evolve into a superposition of product states,

$$|\psi(t)\rangle \approx |\chi_1\rangle \otimes |\beta_1\rangle + |\chi_2\rangle \otimes |\beta_2\rangle, \quad (5.95)$$

where we used the notation $|\chi_1\rangle \otimes |\beta_1\rangle \approx U(t)|\tau_1\rangle \otimes |\alpha\rangle$ and $|\chi_2\rangle \otimes |\beta_2\rangle \approx U(t)R_c|\tau_1\rangle \otimes |\alpha\rangle$, where for the second state we have written $|\tau_2\rangle =: R_c|\tau_1\rangle$ with some unitary matrix R_c . Note that the propagator $U(t)$ has a coupling of strength δ between the two subsystems. The second state can therefore be thought of to be obtained from the same initial state $|\tau_1\rangle \otimes |\alpha\rangle$ under a slightly different, perturbed evolution $U_\delta(t) := U(t)R_c$. The coherences in the reduced matrix (off diagonal elements in ρ_c) of the evolved state (5.95) are proportional to the overlap $\langle\beta_1|\beta_2\rangle$. The square of the overlap $\langle\beta_1|\beta_2\rangle$ is in fact the overlap of two reduced density matrices, one obtained with the unperturbed evolution $U(t)$ and the other with the perturbed one $U_\delta(t)$. Because the final states $|\beta_{1,2}\rangle$ as well as the perturbed evolution $U_\delta(t)$ depend on the initial states of the central system $|\tau_{1,2}\rangle$, the square of the overlap is nothing but the reduced fidelity[‡] of the environment[§]. The decay of coherences and therefore of the purity will be given by the reduced fidelity of a product coherent initial state $|\tau_1\rangle \otimes |\alpha\rangle$. As we have seen before (5.44), the \bar{C}_R for a coherent state in a regular regime is $\bar{C}_R = \frac{1}{2}\hbar(\bar{\mathbf{v}}'_e \cdot \Lambda_e^{-1}\bar{\mathbf{v}}'_e)$ giving the reduced fidelity decay $\exp(-l^2\bar{C}_R t^2/\hbar^2)$, which in turn determines the decay of coherences and therefore also purity decay. Here the perturbation strength l depends on the unitary matrix R_c , i.e. on the “distance” between the initial states $|\tau_{1,2}\rangle$ of the central system, as well as on $U(t)$. This perturbation strength l is of course different than the coupling δ of the evolution $U(t)$. For instance, in the simple case of $|\tau_2\rangle$ being a space shifted packet $|\tau_1\rangle$, $|\tau_2\rangle = e^{-ixp/\hbar}|\tau_1\rangle$, the perturbation strength is proportional to the distance x between the two states. As the coupling δ causes decoherence of individual packets on a time scale $t_d \sim 1/\delta$ while the decoherence of the cat state happens on the decay time scale of the reduced fidelity $t_{\text{dec}} \sim \sqrt{\hbar}/l$, it is sufficient to have $l > \delta\sqrt{\hbar}$ in order to obtain faster decoherence for cat states. The separation l of the two packets constituting the cat state has to scale only as $l \sim \sqrt{\hbar}$ and therefore does not have to be macroscopically large in the semiclassical limit. For an environment with many degrees of freedom d_e , and if derivatives $\bar{\mathbf{v}}'_e$ are all nonzero, \bar{C}_R will be proportional to d_e^2 . The reduced fidelity for the central system on the other hand will have \bar{C}_R proportional to d_c^2 and so if $d_e \gg d_c$, the reduced fidelity of the environment will decay faster than the reduced fidelity of the central system. Therefore, at the decoherence time t_{dec} we will still have $|\chi_{1,2}\rangle \approx |\tau_{1,2}\rangle$, justifying the decoherence scenario (5.93). For cat states we therefore have $\bar{C}_P \propto \hbar$ instead of $\bar{C}_P \propto \hbar^2$ as for a single coherent state, resulting in an accelerated decoherence.

Of course, the above argumentation is by no means a strict proof but is just a simple illustration of how an accelerated decoherence arises. An argumentation using the fidelity has been used by Karkuszewski *et al.* (2002), but without realizing the key role played by the time scales of purity and reduced fidelity decays. To repeat, several ingredients were needed: (i) the dynamics was assumed to be regular, (ii) for the reduced fidelity of product coherent states we have $\bar{C}_R \propto \hbar$, (iii) the purity of constituent product coherent states decays on much longer \hbar -independent time scale (i.e. $\bar{C}_P \propto \hbar^2$) and approximation (5.95) was possible, (iv) furthermore, if $d_e \gg d_c$ the resulting decohered states $|\chi\rangle$ are still approximately equal to the initial states $|\tau\rangle$ of the central system as the reduced fidelity decay is faster for the environment than for the central system. All this together enabled us to “derive” a faster decoherence decay for macroscopic cat states.

[‡] Actually we used a slightly different definition of the reduced fidelity as an overlap of the initial and the echo state.

[§] In general the states $|\beta_{1,2}\rangle$ can not be obtained by a Hamiltonian evolution on the environmental subspace alone.

For chaotic dynamics and times longer than the Ehrenfest time $\sim \ln \hbar$ we have seen that fidelity, reduced fidelity and purity all decay on the same time scale irrespective of the initial state. A natural question arises: How does decoherence of macroscopic superposition in chaotic system behave? Actually, decoherence for macroscopic superpositions is so fast, that it happens on time scales *shorter* than any dynamical scale of the system (Braun *et al.*, 2001; Strunz *et al.*, 2003; Strunz & Haake, 2003). It therefore happens on an “instantaneous” time scale on which *every* system behaves as a regular one (i.e. no decay of correlation functions). The chaoticity therefore has no influence on decoherence of macroscopic superpositions.

Numerical Example

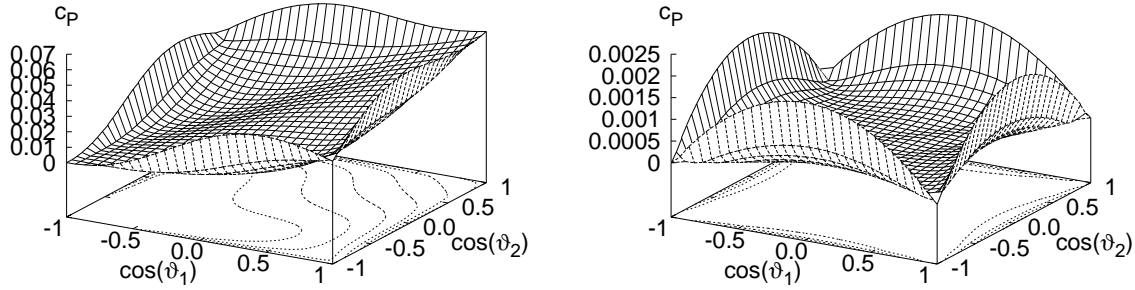


Figure 5.15: Dependence of \bar{C}_P (Eq. 5.99, exact expression) for the cat state (5.96) on the position angles of two constituent coherent packets. We have take $\varphi_1 = \varphi_2 = 1$ and $S = 4$ (left figure) and $S = 64$ (right figure).

We take a Jaynes-Cummings model with the unperturbed Hamiltonian $H_0 = \hbar\omega a^\dagger a + \varepsilon \hbar S_z$ and the perturbation in the coupling G of strenght δ , $V = [\delta G]$. Purity fidelity is then equal to the purity which will be used as a measure of decoherence. The initial state will be a product state of a coherent state $|\alpha\rangle$ for the oscillator acting as an environment and the superposition of two coherent packets for the spin,

$$|\psi(0)\rangle_c \propto |\tau_1\rangle + |\tau_2\rangle. \quad (5.96)$$

The Heisenberg evolution is simple, so that the integral of perturbation $\Sigma(t)$ is

$$\Sigma(t) = \frac{2\hbar}{\Delta\sqrt{2S}} \sin\left(\frac{t\Delta}{2}\right) \left\{ e^{-it\Delta/2} a^\dagger S_- + e^{it\Delta/2} a S_+ \right\}, \quad (5.97)$$

where $\Delta := \varepsilon - \omega$ is a detuning. From now on we set $\Delta = 0$ in order to have a non vanishing \bar{C}_P . As we take a coherent oscillator initial state, the expectations over oscillator space in correlation function sum (5.17) can be explicitly made and one ends up with the very neat result

$$\bar{C}_P = \frac{1}{2S^3} \{ \langle S_+ S_- \rangle - \langle S_+ \rangle \langle S_- \rangle \}, \quad (5.98)$$

where now the expectation values are only over a *spin state*, e.g. the cat state (5.96) or any other. A similar result has been obtained before trough a master equation approach to decoherence, see for instance (Benedict & Czirjak, 1999; Földi *et al.*, 2001). Our result though has quite different perspective as it was derived directly from the Hamiltonian dynamics without

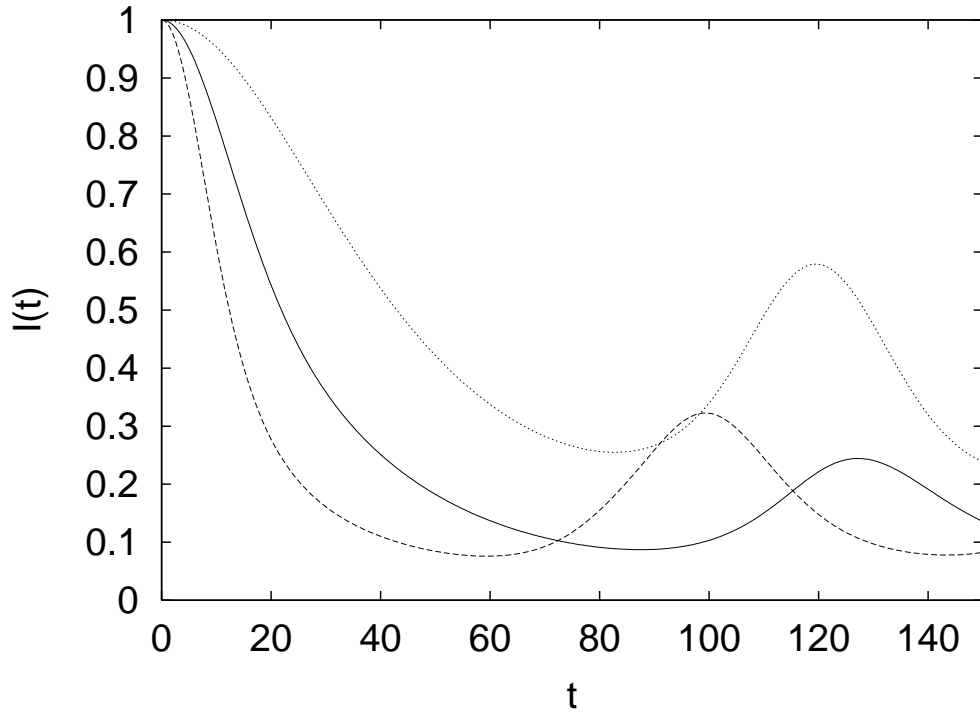


Figure 5.16: The purity decay for a random spin initial state (fastest decaying curve), Schrödinger cat state (middle curve) and coherent state (slowest decaying curve). The oscillator initial state is always a coherent state with $\alpha = 1.15$. The parameters of the Jaynes-Cummings model are $\omega = \varepsilon = 0.3$, $G = G' = 0$ and the perturbation is in G (i.e. in the coupling) with $\delta = 0.02$, $S = 20$. The cat state consists of two coherent SU(2) packets at $(\vartheta, \varphi) = (1, 1)$ and $(0, 1)$. The theoretical decay times $\tau = \hbar/\delta\sqrt{2\bar{C}_P}$ are $\tau = 46, 26$ and 13 for the coherent state, the cat state and the random state, respectively. \bar{C}_P for the coherent state has been calculated according to the theoretical formula in Figure 5.6, for the cat state according to (5.99) and for a random state using (5.100).

any resort to a Markovian description of the reduced dynamics or to dissipation. The calculation of \bar{C}_P (5.98) for a cat state (5.96) using formulas from Appendix B is straightforward although tedious, with the exact but considerably involved result. Rather than showing the whole result, we concentrate on the leading order in $1/S$ (i.e. \hbar) which will dictate the decay in the semiclassical limit and therefore will also govern the decoherence of macroscopic superpositions. The result is

$$\bar{C}_P = \frac{l^2}{8S} + \mathcal{O}(\hbar^2), \quad l^2 := \sin^2 \vartheta_1 + \sin^2 \vartheta_2 - 2 \sin \vartheta_1 \sin \vartheta_2 \cos(\varphi_1 - \varphi_2). \quad (5.99)$$

The l in the above expression has an interesting geometrical interpretation: it is a distance between the projections of positions of the two coherent states to the \mathbf{x} - \mathbf{y} plane. There is indeed a faster decoherence for cat states than for a single coherent state. For a cat state $\bar{C}_P \propto \hbar = 1/S$ whereas we had $\bar{C}_P \propto \hbar^2$ for a single coherent packet. The exact dependence of \bar{C}_P on the position of both packets in a cat state can be seen in Figure 5.15. The accelerated decoherence can be seen as the increasing of \bar{C}_P away from the diagonal ($\vartheta_1 \neq \vartheta_2$) for $S = 64$, where the exact result for \bar{C}_P can be approximated by the leading order expression (5.99). Note that due to symmetry there is a slow decoherence for states with $\vartheta_1 + \vartheta_2 = \pi$ despite of the fact that this leads to a macroscopic superpositions. Linear response decay time of purity

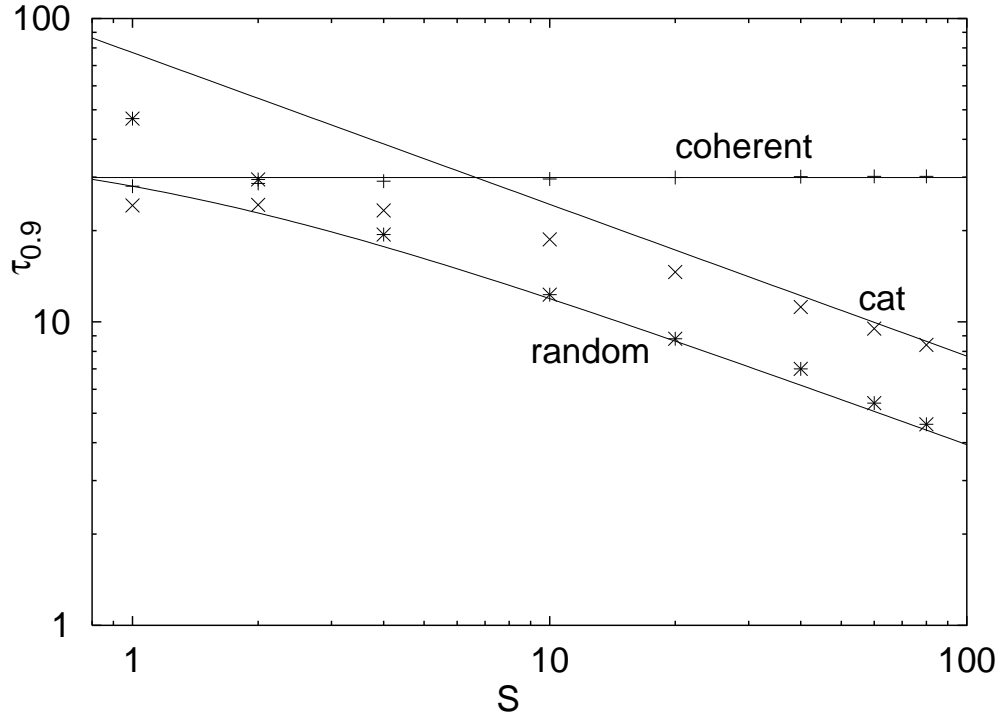


Figure 5.17: Dependence of numerically determined decay times of purity on S ($= 1/\hbar$) for a random spin initial state, a Schrödinger cat state and a coherent state. The perturbation strength is $\delta = 0.01$ while all other parameters are the same as for Figure 5.16. Theoretical decay times $\tau = \hbar/\delta\sqrt{2\bar{C}_P}$ are shown with full lines.

for macroscopic superpositions is therefore (5.99) $t_{\text{dec}} = 2\sqrt{\hbar}/(\delta l)$, while the decay time for individual coherent packets is (using \bar{C}_P from Figure 5.6) $t_d = 1/(\sqrt{2}\cos^2(\vartheta/2)\delta)$. We get an accelerated decoherence, $t_{\text{dec}} \ll t_d$, for $l \gg \sqrt{8\hbar}\cos^2(\vartheta/2)$.

For random initial state of a spin and a coherent packet for an oscillator we can calculate \bar{C}_P using the expression (5.98) and get

$$\bar{C}_P = \frac{S+1}{3S^2}, \quad \text{random spin i.c..} \quad (5.100)$$

Again we have $\bar{C}_P \propto \hbar$, just like for cat states, but with a smaller prefactor. If we had a random state on the whole Hilbert space, i.e. also for an oscillator, we would have $\bar{C}_P \propto \hbar^0$. Therefore, the decoherence rate for a cat state is *between* the decoherence rate of a single packet and the decoherence rate for a random state.

The accelerated decoherence can be seen in Figure 5.16 where we show numerically calculated purity decays for all three different initial spin states. Revivals of purity on a classical time scale $\sim 1/\delta$ due to integrability of unperturbed Hamiltonian can also be seen. This revivals will be absent in a general non-integrable Hamiltonian. To further illustrate the scaling of decay times with S we show in Figure 5.17 numerically calculated decay times in which the purity decays to level 0.9 for all three different initial states, coherent, cat state and random state of a spin, while the oscillator is initially always in the same coherent state.

Chapter 6

Application: Quantum Computation

In theory, there is no difference between theory and practice. In practice, there is no relationship between theory and practice.

—Anonymous

Quantum information theory is relatively recent, for a review see (Nielsen & Chuang, 2001; Steane, 1998; Ekert & Josza, 1996). Its beginnings go back to '80 and in recent years theoretical concepts have been demonstrated in experiments. While quantum cryptography, a method of provably secure communication, is already commercially available, quantum computation on the other hand is still limited to small laboratory experiments.

In order to perform quantum computation you obviously need a quantum computer. A quantum computer can be considered as a many-body system of n elementary two-level quantum systems — called *qubits*. The union of all n qubits is called a quantum register $|r\rangle$. The size of the Hilbert space \mathcal{N} and therefore the number of different states of a register grows with the number of qubits as $\mathcal{N} = 2^n$. Quantum computation then consists of the following steps:

- Load the data for the quantum computation in the initial state of the quantum register $|r\rangle$, resulting in a general superposition of \mathcal{N} basis states.
- Then perform the actual computation, represented by a unitary transformation U . As U acts on an exponentially large space it is usually decomposed into simpler units $U = U_T \cdots U_2 U_1$. Such sequence of T elementary one-qubit and two-qubit *quantum gates* U_t , $t = 1, 2, \dots, T$ is called a *quantum algorithm*.
- Finally, we read out the result of the computation by performing measurements on the qubits of the final register state $U|r\rangle$.

A quantum algorithm is called *efficient* if the number of needed elementary gates T grows with at most *polynomial* rate in $n = \log_2 \mathcal{N}$, and only in this case it can generally be expected to outperform the best classical algorithm. At present only few efficient quantum algorithms are known, perhaps the most generally useful being the Quantum Fourier Transformation (QFT) (Shor, 1994; Coppersmith, 1994) which will also be the subject of our study.

There are two major obstacles for performing practical quantum computation. First, there is the problem of *decoherence* (Chuang *et al.*, 1995) resulting from an unavoidable generally *time-dependent* perturbation due to the coupling between the qubits and the environment. If the perturbation couples only a small number of qubits at a time then such errors can be

eliminated at the expense of extra qubits by *quantum error correcting codes* (Steane, 1996a; Calderbank & Shor, 1996; Steane, 1996b), for another approach see (Tian & Lloyd, 2000). Second, even if one knows an efficient error correcting code or assumes that quantum computer is ideally decoupled from the environment, there will typically exist small *unknown* or *uncontrollable* residual interaction among the qubits which one may describe by a general *static* perturbation. Therefore, understanding the *stability* of quantum algorithms with respect to various types of perturbations is an important problem, for some results on this topic see (Miquel *et al.*, 1996, 1997; Gea-Banacloche, 1998, 1999, 2000; Song & Shepelyansky, 2001; Georgeot & Shepelyansky, 2000; Berman *et al.*, 2001, 2002a,b; Celardo *et al.*, 2003).

6.1 General Framework

Let us perturb the t -th quantum gate by a perturbation* generated by V_t ,

$$U_t^\delta := \exp(-i\delta V_t)U_t. \quad (6.1)$$

We set $\hbar = 1$ and use the superscript δ to denote a perturbed gate and the subscript t to denote a discrete time index, i.e. a gate number. We allow for different perturbations V_t at different gates. The perturbed algorithm is simply a product of perturbed gates, $U^\delta = U_T^\delta \cdots U_1^\delta$. Fidelity will again serve as a measure of stability and we have

$$F(T) = |\langle M_\delta(t) \rangle|^2, \quad M_\delta := U(-T)U^\delta(T), \quad (6.2)$$

with $U(t) := U_t \cdots U_1$ and similarly for $U^\delta(t)$. For our generally time dependent perturbation the echo operator equals to

$$M_\delta = e^{-i\delta V_T(T)} \cdots e^{-i\delta V_2(2)} e^{-i\delta V_1(1)}, \quad (6.3)$$

where $V_t(t) := U^\dagger(t)V_tU(t)$ is the perturbation of t -th gate V_t propagated with the unperturbed gates $U(t) = U_t \cdots U_1$. Beware that $V_t(t)$ is time dependent due to two reasons, one is due to the interaction picture (time in parentheses) and the second is that the perturbation itself is explicitly time dependent, i.e. different perturbation for different gate (time as a subscript). In quantum computation one is usually interested in initial states containing a maximum amount of information, thereby being close to random states. With this in view, we take the initial state average to be a trace over the whole Hilbert space,

$$\langle \bullet \rangle := \frac{1}{\mathcal{N}} \text{tr}(\bullet). \quad (6.4)$$

By this prescription we study the average fidelity over the whole Hilbert space. Without sacrificing generality we furthermore assume the average perturbation to be traceless, $\sum_{t=1}^T \text{tr} V_t = 0$. Trace of the average perturbation only changes the phase of the fidelity amplitude and has therefore no influence on the fidelity (i.e. probability). The linear response expansion of the fidelity then reads

$$F(T) = 1 - \delta^2 \sum_{t,t'=1}^T C(t,t'), \quad (6.5)$$

with the correlation function

$$C(t,t') := \frac{1}{\mathcal{N}} \text{tr}[V_t(t)V_{t'}(t')]. \quad (6.6)$$

*It is expected that the computation is stable only when the evolution is close to unitary.

Here we used the fact that the average trace vanishes so the term $\langle \Sigma(t) \rangle$ is zero. Decomposition of a given quantum algorithm U into quantum gates is by no means unique. An interesting question then is, given perturbations V_t , which form of the algorithm has the highest fidelity, i.e. is the most stable? We will see that the standard QFT algorithm can be rewritten in a non trivial way so that it becomes more stable against static perturbations. The guiding principle in the construction of this new algorithm will be to study the correlation function (6.5) and trying to minimise its sum.

6.1.1 Time Dependent Perturbations

If our perturbation V_t is time dependent, i.e. we have different perturbations on different gates, then the decay of correlation function will not only depend on the unperturbed dynamics, but also on how strong these perturbations are correlated at different gates. Let us have a closer look at one extreme example. If the perturbation V_t is an *uncorrelated noise*, as it would be in the case of coupling to an *ideal heath bath*, then the matrix elements of V_t may be assumed to be *Gaussian random* variables which are uncorrelated in time,

$$\langle V_{jk}(t)V_{lm}(t') \rangle_{\text{noise}} = \frac{1}{\mathcal{N}} \delta_{jm} \delta_{kl} \delta_{tt'}. \quad (6.7)$$

Hence one finds $\langle C(t, t') \rangle_{\text{noise}} = \delta_{tt'}$, where we have averaged over noise. In fact the average of the product in M_δ (6.3) equals to the product of the average and yields the noise-averaged fidelity

$$\langle F(T) \rangle_{\text{noise}} = \exp(-\delta^2 T), \quad (6.8)$$

which is *independent* of the quantum algorithm U . This result is completely general provided that the correlation time of the perturbation is *smaller* than the duration of a single gate. On the other hand, for a *static* perturbation $V_t \equiv V$ one may expect slower correlation decay, depending on the 'regularity' of the evolution operator U , and hence faster decay of fidelity. Importantly, note that in a physical situation, where perturbation is expected to be a combination $V_t = V_{\text{static}} + V_{\text{noise}}(t)$, the fidelity drop due to a static component is expected to *dominate* long-time quantum computation $T \rightarrow \infty$ (i.e. large number of qubits n) over the noise component, as soon as the quantum algorithm exhibits long time correlations of the operator V_{static} . If $V_{\text{static}} = 0$ is zero, the quantum computation can be stabilised by making "adiabatically" slow evolution of gates. In the following we will focus exclusively on the static perturbations being the worst ones.

6.2 Quantum Fourier Transformation

We will consider Quantum Fourier Transformation algorithm (QFT) and will consider its stability against static random perturbations. The perturbation $V_t \equiv V$ will be a random hermitian matrix from a Gaussian unitary ensemble (GUE). Gaussian unitary ensemble is invariant under unitary transformations and the matrix elements in an arbitrary basis are independent random Gaussian variables (Mehta, 1991). Due to hermitian symmetry they are real on the diagonal and complex off-diagonal. The GUE matrices can be used to model quantum statistical properties of classically chaotic Hamiltonians and have been first applied to studies of nuclear resonances. Second moments of a GUE matrix V are normalised as

$$\langle V_{jk}V_{lm} \rangle_{\text{GUE}} = \delta_{jm} \delta_{kl} / \mathcal{N}, \quad (6.9)$$

where the averaging is done over a GUE ensemble.

Let us briefly describe the QFT algorithm. Basis qubit states in a Hilbert space of dimension $\mathcal{N} = 2^n$ will be denoted by $|k\rangle$, $k = 0, \dots, 2^n - 1$. The unitary matrix U_{QFT} performs the following transformation on a state with expansion coefficients x_k

$$U_{\text{QFT}}\left(\sum_{k=0}^{\mathcal{N}-1} x_k |k\rangle\right) = \sum_{k=0}^{\mathcal{N}-1} \tilde{x}_k |k\rangle, \quad (6.10)$$

where $\tilde{x}_k = \frac{1}{\sqrt{\mathcal{N}}} \sum_{j=0}^{\mathcal{N}-1} \exp(2\pi i j k / \mathcal{N}) x_j$. The resulting expansion coefficients \tilde{x}_k are *Fourier transformed* input coefficients x_k . The “dynamics” of the QFT is decomposed into three kinds of unitary gates: One-qubit gates A_j acting on j -th qubit

$$A_j = \frac{1}{\sqrt{2}} \begin{pmatrix} 1 & 1 \\ 1 & -1 \end{pmatrix}, \quad (6.11)$$

where the basis is ordered as $(|0\rangle, |1\rangle)$, diagonal two-qubit gates $B_{jk} = \text{diag}\{1, 1, 1, \exp(i\theta_{jk})\}$, with $\theta_{jk} = \pi/2^{k-j}$, and transposition gates T_{jk} which interchange the j -th and k -th qubit, $T_{jk}|\dots j \dots k \dots\rangle = |\dots k \dots j \dots\rangle$. There are n A-gates, $n(n-1)/2$ B-gates and $[n/2]$ transposition gates, where $[x]$ is the integer part of x . The total number of gates for the algorithm is therefore $T = [n(n+2)/2]$. For instance, in the case of $n = 4$ we have a sequence of $T = 12$ gates (time runs from right to left)

$$U_{\text{QFT}} = T_{03} T_{12} A_0 B_{01} B_{02} B_{03} A_1 B_{12} B_{13} A_2 B_{23} A_3. \quad (6.12)$$

For the GUE perturbation we can average the correlation function $C(t, t')$ (6.6) over the GUE ensemble, resulting in

$$\langle C(t, t') \rangle_{\text{GUE}} = \left| \frac{1}{\mathcal{N}} \text{tr} U(t, t') \right|^2, \quad (6.13)$$

where $U(t, t')$ is the unperturbed propagator from gate $t' + 1$ to t , $U(t, t') := U_t \cdots U_{t'+1}$ with the convention $U(t, t) \equiv \mathbb{1}$. Averaging over the GUE is done only to ease analytical calculation and to yield a quantity that is independent of a particular realization of the perturbation. Qualitatively similar (numerical) results are obtained without the averaging.

We have calculated the correlator $\langle C(t, t') \rangle$ for the QFT (6.13) which is shown in the right Figure 6.1. One can clearly see square red plateaus on the diagonal due to blocks of successive B-gates. Similar square plateaus can also be seen off diagonal (from orange, yellow to green), so the correlation function has a staircase-like structure, with the A-gates responsible for the drops and B-gates responsible for the flat regions in between. This can be easily understood. For “distant” qubits $k - j \gg 1$ the gates B_{jk} are close to the identity and therefore cannot reduce the correlator. This slow correlation decay results in the correlation sum

$$\nu := \sum_{t, t'=1}^T C(t, t'), \quad (6.14)$$

being proportional to $\nu \propto n^3$ (sum of the first n squares) as compared to the theoretical minimum $\nu \propto T \propto n^2$.

In view of this, we will now try to rewrite the QFT with a goal to achieve a smaller correlation sum, hopefully $\nu \propto n^2$. From (6.13) we learn that the gates that are *traceless* (e.g. A-gates) reduce the correlator very efficiently. In the plain QFT algorithm (6.12) we have $n - 1$ blocks of B-gates, where in each block all B-gates act on the same first qubit, say j . In each such block, we propose to replace B_{jk} with a new gate $G_{jk} = R_{jk}^\dagger B_{jk}$, where a unitary gate R_{jk} will

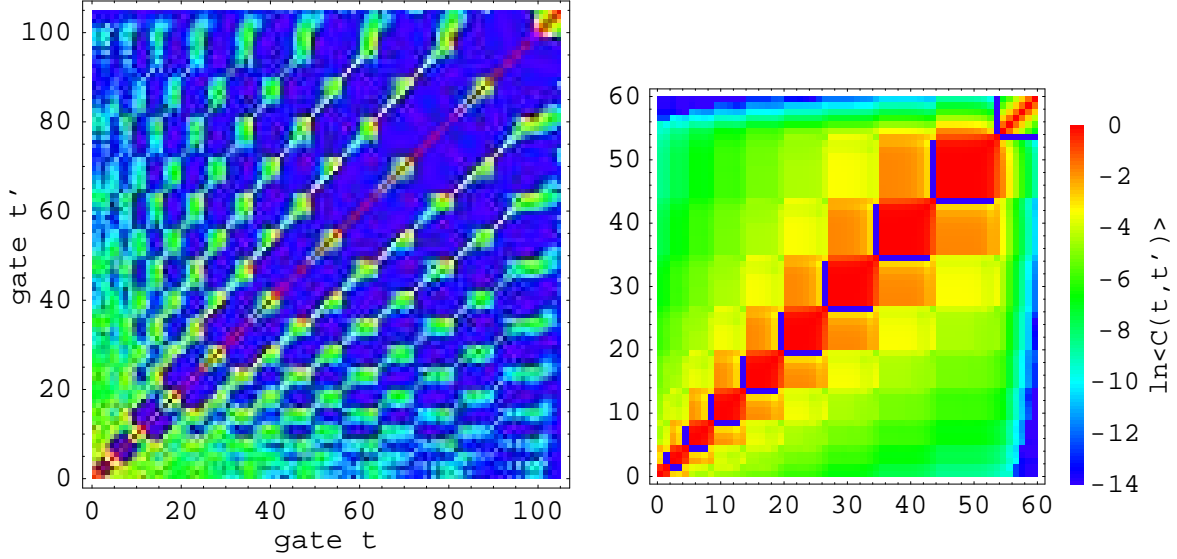


Figure 6.1: Correlation functions $\langle C(t, t') \rangle_{\text{GUE}}$ (6.13) for $n = 10$ qubits and static GUE perturbation. The right figure shows the standard QFT (6.12) with $T = 60$, while the left figure shows the IQFT with $T = 105$ gates. Colour represents the size of elements in a log-scale from red (e^{-0}) to blue (e^{-14} and less).

be chosen so as to commute with all diagonal gates B_{jl} in the block, whereas at the end of the block we will insert R_{jk} in order to “annihilate” R_{jk}^\dagger so as to preserve the evolution matrix of a whole block. The unitarity condition $R_{jk}^\dagger R_{jk} = 1$ and $[R_{jk}, B_{jl}] = 0$ for all j, k, l leaves us with a 6 parametric set of matrices R_{jk} . By further enforcing $\text{tr} R_{jk} = 0$ in order to maximally reduce the correlator, we end up with 4 free real parameters in R_{jk} . One of the simplest choices, that turned out to be as suitable as any other, is the following

$$R_{jk} = \begin{pmatrix} 0 & 0 & -1 & 0 \\ 0 & 1 & 0 & 0 \\ 1 & 0 & 0 & 0 \\ 0 & 0 & 0 & -1 \end{pmatrix}, \quad (6.15)$$

with the basis states $(|jk\rangle)$ ordered as $(00, 10, 01, 11)$. The R gate can be compactly written as $R_{jk}|\dots a_j \dots b_k \dots\rangle = (-1)^{b_k}|\dots a_j \dots (\bar{a}_j \oplus b_k) \dots\rangle$, where \oplus is an addition modulo 2, bar denotes a negation and a_j, b_k are 0 or 1. Furthermore, we find that R-gates also commute among themselves, $[R_{jk}, R_{jl}] = 0$, which enables us to write a sequence of R-gates whichever way we like, e.g. in the same order as a sequence of G’s, so that pairs of gates G_{jk}, R_{jk} operating on the same pair of qubits (j, k) , whose product is a *bad gate* B_{jk} , are never neighbouring. This is best illustrated by an example. For instance, the block $B_{01}B_{02}B_{03}$ will be replaced by $R_{01}R_{02}R_{03}R_{01}^\dagger B_{01}R_{02}^\dagger B_{02}R_{03}^\dagger B_{03} = R_{01}R_{02}R_{03}G_{01}G_{02}G_{03}$. This is how we construct an *improved quantum Fourier transform algorithm* (IQFT). For the IQFT we need one additional type of gate, instead of diagonal B-gates, we use nondiagonal ones R and G. To illustrate the obvious general procedure we write out the whole IQFT algorithm for $n = 4$ qubits (compare with (6.12))

$$U_{\text{IQFT}} = T_{03}T_{12}A_0R_{01}R_{02}R_{03}G_{01}G_{02}G_{03}A_1R_{12}R_{13}G_{12}G_{13}A_2R_{23}G_{23}A_3. \quad (6.16)$$

Such IQFT algorithm consists in total of $T = [n(2n+1)/2]$ gates (note that it does not pay off to replace a block with a single B gate as we have done, so we could safely leave $B_{23} \equiv R_{23}G_{23}$). The correlation function for the IQFT algorithm is shown on the left of Figure 6.1. Almost all off-diagonal correlations are greatly reduced (to the level $\propto 1/\mathcal{N}^2$), leaving us only with a dominant

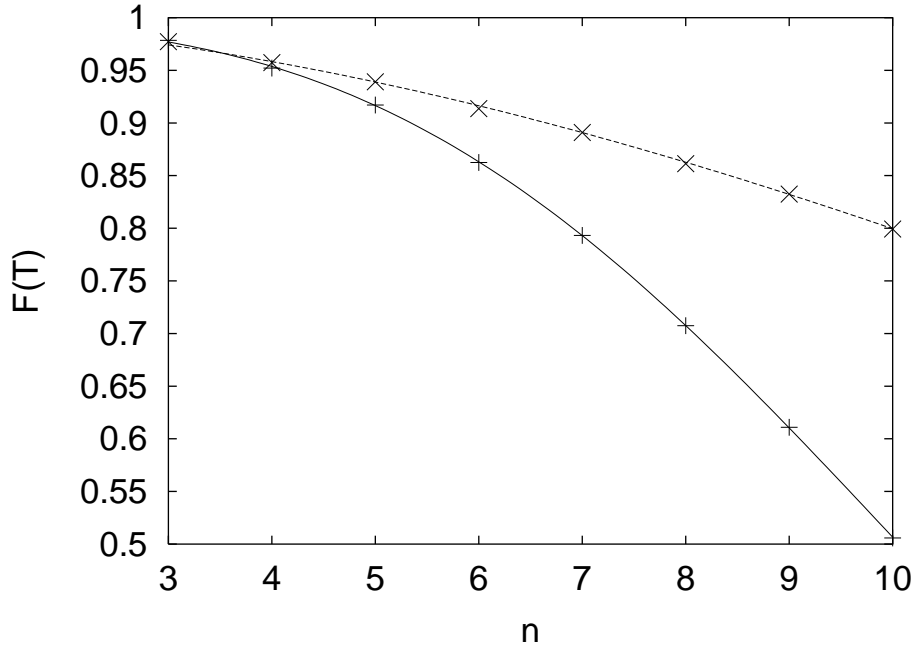


Figure 6.2: Dependence of the fidelity $F(T)$ on the number of qubits n for the QFT (pluses) and the IQFT algorithms (crosses), for fixed $\delta = 0.04$. Numerical averaging over 50 GUE realizations is performed. The full curve is $\exp(-\delta^2\{0.47n^3 - 0.76n^2 + 2.90n\})$ and the dashed one $\exp(-\delta^2\{1.22n^2 + 1.78n\})$. For $n = 10$ the trace is approximated by an average over 200 Gaussian random register states.

diagonal. If we would have only diagonal elements, the fidelity would be $F(T) = 1 - \delta^2 T$, (as in the case of noisy perturbation or decoherence, however, with a different physical meaning of the strength scale δ) where the number of gates scales as $T \propto n^2$. From Figure 6.1 it is clear that we have a very fast correlation decay for the IQFT. Studying the scaling with n , the correlation sum ν has decreased from $\nu \propto n^3$ to $\nu \propto n^2$. To further illustrate this, we have numerically calculated fidelity by simulating the quantum algorithm and applying the perturbation $\exp(-i\delta V)$ at each gate. The results are shown in Figure 6.2 where one can see much faster decay of the fidelity for the QFT than for the IQFT. Note that the IQFT has higher fidelity despite the perturbation being applied $\sim n^2$ times for the IQFT and only $\sim n^2/2$ times for the QFT. As we have argued before, the sum of 2-point correlator (6.5) gives us only the first nontrivial order in the δ -expansion. For dynamical systems, being either integrable or mixing and ergodic, we have shown in previous chapters that also higher orders of the fidelity can approximately be written as simple powers of the correlation sum ν , so that the fidelity has the simple form

$$F(T) \approx \exp(-\nu\delta^2). \quad (6.17)$$

Although quantum algorithm is quite inhomogeneous in time, we may still hope that $\exp(-\nu\delta^2)$ is a reasonable approximation of the fidelity also to higher orders in δ . This is in fact the case as can be seen in Figure 6.3. Note also that the leading coefficient in the exponent for the IQFT fidelity, $\lim_{n \rightarrow \infty} \nu/n^2 = 1.22$, is close to the theoretical minimum of 1. As the definition of what is a fundamental single gate is somehow arbitrary, the problem of minimising the sum ν depends on a given technical realization of gates and the nature of the perturbation V for an experimental setup. It has been shown (Celardo *et al.*, 2003), that the IQFT algorithm improves stability against GUE perturbations also for a more realistic model of a quantum

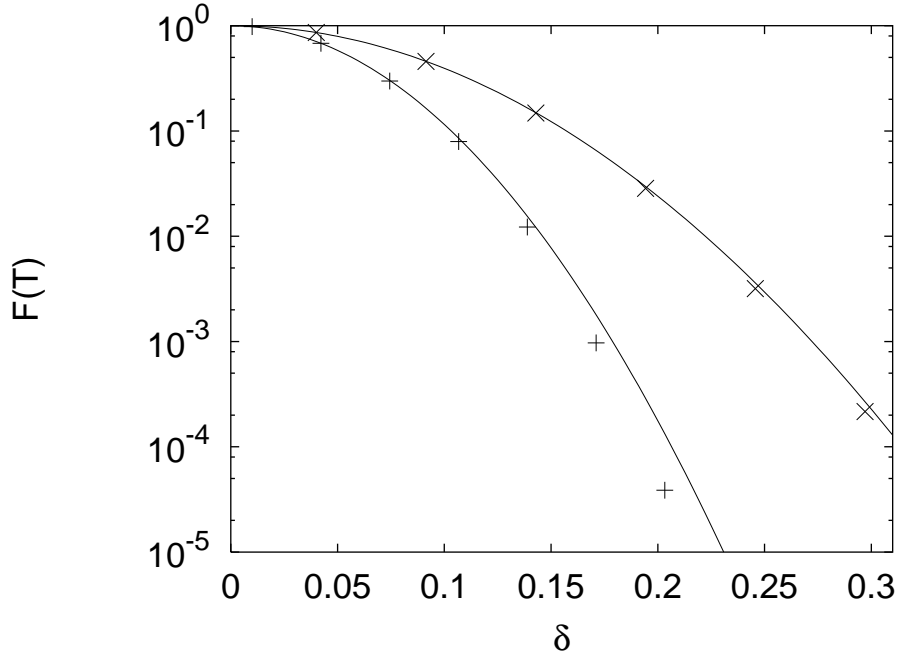


Figure 6.3: Dependence of the fidelity $F(T)$ on δ for the QFT (pluses) and the IQFT (crosses), for fixed $n = 8$. Solid curves are functions $\exp(-\nu\delta^2)$ (see text) with ν calculated analytically (6.13) and equal to $\nu = 216$ for the QFT and 93.2 for the IQFT.

computer, namely for an Ising quantum computer.

We should mention that the optimisation becomes harder if we consider *few-body* (e.g. two-body) random perturbation. This is connected with the fact that quantum gates are two-body operators and can perform only a very limited set of rotations on a full Hilbert space and consequently have a limited capability of reducing correlation function in a single step. For such errors the fidelity will typically decay with the square of the number of errors T (i.e. gates), like $\sim \exp(-\delta^2 T^2)$, that is the same as for regular systems, see also (Gea-Banacloche, 2000) for a similar result. This means that the very fact that the algorithm is efficient, having a polynomial number of gates, makes it very hard to reduce the correlation function and therefore causes a fast fidelity decay. However, our simple approach based on n -body random matrices seems reasonable, if the errors due to unwanted few-body qubit interactions can be eliminated by other methods.

Chapter 7

Conclusion

I hate quotations. Tell me what you know.

—Ralph Waldo Emerson

We have studied the decay of quantum fidelity, of reduced fidelity and of purity in quantum systems. We considered two extreme cases of system's dynamics, mixing and regular. The dependence on the initial conditions, in particular for a random and coherent initial state, and the influence of the perturbation type on quantum stability has been analysed.

For a *general* type of *perturbation*, having a nonzero diagonal matrix elements in the eigenbasis of the unperturbed system, i.e. having a nonzero time average, the fidelity decay depends on the mixing properties of system dynamics. For *mixing systems* in the Fermi golden rule regime fidelity decay is exponential, with the decay time given by the transport coefficient, which is in turn the integral of the correlation function of the perturbation. The decay time scales with Planck's constant and with the perturbations strength as $\tau_m \sim \hbar^2/\delta^2$. In this regime quantum fidelity decay is much slower than classical fidelity decay and moreover, it will in general be the *slower the more chaotic* the corresponding classical system is. This surprising result does not violate the quantum-classical correspondence though, as for large perturbation strengths, in the so called Lyapunov regime, quantum fidelity agrees with classical fidelity. Whether we observe the quantum or the classical behaviour depends on the order of two noncommuting limits, namely the semiclassical limit of vanishing Planck constant $\hbar \rightarrow 0$ and the limit of vanishing perturbation strength $\delta \rightarrow 0$. For sufficiently long times fidelity decay in mixing systems does not depend on the initial state. In *regular systems* and for perturbations with a nonzero time average the fidelity decay for wave packets is governed by a ballistic separation of the packets. For coherent initial states the resulting decay is Gaussian with the decay time scaling as $\tau_r \sim \sqrt{\hbar}/\delta$, and can be for sufficiently small perturbations *smaller* than for chaotic systems. For random initial states in a regular regime quantum fidelity decays according to a power law, $F \sim (\hbar/\delta t)^d$ in d degrees of freedom system. In regular systems we also considered the decay averaged over random positions of the initial coherent state, resulting in an algebraic decay but with the power being system specific. By a semiclassical method we theoretically calculated all decay times in both cases of regular and mixing dynamics in terms of classical quantities only, despite the fact that the quantum and the classical fidelity do not agree for mixing systems.

The quantum fidelity decay is markedly different for perturbations with a *zero time average*, which can be written as a time derivative of another operator. For such perturbations fidelity freezes at a constant plateau regardless of the dynamics and starts to again decay only after a much longer time, scaling as $\sim 1/\delta$. This freezing is a pure quantum phenomenon as the correspondence with classical fidelity ends before the plateau starts and classical fidelity decays

much faster. The only exception where the classical fidelity also exhibits freezing and agrees with quantum fidelity is for a harmonic oscillator, for which the plateau is higher than for other systems. We explicitly calculate the plateau value for mixing and regular dynamics and coherent and random initial states. For mixing dynamics a universal relation holds between the plateau $F_{\text{plat}}^{\text{RIS}}$ for random and $F_{\text{plat}}^{\text{CIS}}$ for coherent states, $(F_{\text{plat}}^{\text{CIS}})^2 = F_{\text{plat}}^{\text{RIS}}$. In the linear response regime the scaling of the plateau is $1 - F_{\text{plat}} \sim \delta^2/\hbar^2$ regardless of the dynamics. The asymptotic decay of fidelity after the plateau ends is also theoretically calculated in terms of a “renormalised” perturbation with strength $\delta^2/2$. For regular systems this long time Gaussian decay happens on a time scale $\sim \sqrt{\hbar}/\delta^2$ for coherent initial states whereas it is power law with the prefactor scaling as $\sim \hbar/\delta^2$ for random initial states. For mixing dynamics the long time decay does not depend on the initial state and is exponential with the decay time $\sim \hbar^2/\delta^4$ or Gaussian with the decay time $\sim \hbar^{1-d/2}/\delta^2$. The crossover from the exponential to the Gaussian decay happens at the Heisenberg time. For one dimensional regular systems we also explain echo resonances, a sudden revivals of fidelity.

We also study composite systems, composed of a central system and an environment, and connect the decay of purity with the decay of reduced fidelity. We prove a rigorous inequality between the fidelity (characterising the stability of the whole system), the reduced fidelity (characterising the stability of the central system) and the purity (characterising the entanglement). For *mixing systems* fidelity, reduced fidelity and purity all decay on the same time scale. For *regular systems* though, reduced fidelity has a Gaussian decay for coherent states whereas purity decays on an \hbar independent time scale. We explicitly calculate the purity decay and the power of the asymptotic algebraic decay depends on the perturbation and can range between 1 and d_c , the d_c being number of degrees of freedom of the central system. All decay constants are explicitly calculated. We also discuss an interesting case where the time scales of the central system and the environment are vastly different and one can use averaging over the faster system to simplify the theory. Decoherence for macroscopic superpositions of coherent states is derived and shown to be faster than for a single coherent state.

Finally, we show an application of fidelity theory. By “randomising” the quantum Fourier transform algorithm we are able to make it more resistant against random perturbations from the environment.

Appendix A

Spin Wigner functions

The Wigner function enables us to represent the quantum density matrices in a phase space and thereby compare it with the classical probability densities. If we have a one particle quantum system, described by a canonical pair $[\hat{q}, \hat{p}] = i\hbar$, the Wigner function W_ρ of a quantum state given by a density matrix $\hat{\rho}$ is

$$W_\rho(q, p) := \frac{1}{2\pi\hbar} \int dx \langle q - x | \rho | q + x \rangle \exp(-i2px/\hbar), \quad (\text{A.1})$$

if $|x\rangle$ is an eigenstate of operator \hat{q} with an eigenvalue x . In this appendix we will use a hat for quantum operators. For spin state such a definition can not be used as the Hilbert space has different structure due to $SU(2)$ commutation relations of spin operators.

We would like to obtain a Weyl symbol of an arbitrary operator \hat{A} acting on a Hilbert space of size $2S + 1$, i.e. on a state space of spin of size S . In the special case when the operator \hat{A} is equal to a density matrix, the resulting Weyl symbol is called a Wigner function. Such functions have been first proposed by Agarwal (1981). The Weyl symbol $W_A(\vartheta, \varphi)$ will be a function of coordinates on a sphere. Furthermore, we would like the standard trace dot product for operators to carry over to Weyl symbols, i.e. we demand that the following equality should hold

$$\text{tr}(\hat{A}, \hat{B}^\dagger) = \int W_A W_B^* d\Omega, \quad (\text{A.2})$$

with $d\Omega = d\varphi \sin \vartheta d\vartheta$. Spherical harmonic functions Y_l^m constitute an orthonormal basis on a sphere,

$$\int Y_l^m Y_{l'}^{m'}{}^* d\Omega = \delta_{ll'} \delta_{mm'}, \quad (\text{A.3})$$

and so we can expand the Weyl symbol over Y_l^m . On the other hand, an arbitrary operator \hat{A} can be in turn expanded over *multipole operators* \hat{T}_l^m forming an orthogonal basis in the Hilbert space of operators,

$$\text{tr}(\hat{T}_l^m \hat{T}_{l'}^{m'\dagger}) = \delta_{ll'} \delta_{mm'}. \quad (\text{A.4})$$

Therefore we can write the operator \hat{A} as

$$\hat{A} := \sum_{l=0}^{2S} \sum_{m=-l}^l a_{lm} \hat{T}_l^m, \quad a_{lm} = \text{tr}(\hat{A} \hat{T}_l^{m\dagger}). \quad (\text{A.5})$$

From this and the orthogonality property of Y_l^m we immediately see that the Weyl symbol defined as

$$W_A(\vartheta, \varphi) := \sum_{l=0}^{2S} \sum_{m=-l}^l a_{lm} Y_l^m(\vartheta, \varphi), \quad (\text{A.6})$$

will satisfy dot property (A.2) we demanded. The coefficients a_{lm} can be calculated using the explicit form of the multipole operators

$$\hat{T}_l^m := \sum_{q=-S}^S (-1)^{S-m-q} \sqrt{2l+1} \begin{pmatrix} S & l & S \\ -m-q & m & q \end{pmatrix} |m+q\rangle\langle q|, \quad (\text{A.7})$$

with $\begin{pmatrix} S & l & S \\ -m-q & m & q \end{pmatrix}$ being the Wigner $3j$ symbol.

The spin Wigner function for a state represented by a density matrix $\hat{\rho}$ is obtained by taking $\hat{A} = \hat{\rho}$ in the above formulas. As the density matrix is a Hermitian operator, the resulting Wigner function is real. In the case of two pure states, $\rho_1 = |\psi_1\rangle\langle\psi_1|$, $\rho_2 = |\psi_2\rangle\langle\psi_2|$ the dot condition gives simply

$$|\langle\psi_1|\psi_2\rangle|^2 = \int W_{\rho_1} W_{\rho_2} d\Omega. \quad (\text{A.8})$$

For examples of Wigner functions of some simple states see e.g. (Dowling *et al.* , 1994).

Appendix B

Coherent State Expectation Values

Boson coherent states

Expectation values of expressions involving creation and annihilation operators a^+ and a for a harmonic oscillator coherent state $|\alpha\rangle$ are frequently needed. Using the definition of $|\alpha\rangle$ (2.30) it is easy to show the following equality

$$\langle\alpha|g(a^+)f(a)|\alpha\rangle = g(\alpha^*)f(\alpha), \quad (\text{B.1})$$

with two polynomials g and f . Let $p(a, a^+)$ be some polynomial function and by $:p(a, a^+):$ we will denote a polynomial in a *normal* order which can be obtained from $p(a, a^+)$ by using the commutation relation $[a, a^+] = 1$ to bring all terms involving a^+ to the left of terms with a . For instance, $:aa^+ := a^+a + 1$. Then we can write the expectation value of an arbitrary polynomial as

$$\langle\alpha|p(a, a^+)|\alpha\rangle = \langle\alpha| :p(a, a^+) : |\alpha\rangle = :p(\alpha, \alpha^*) : . \quad (\text{B.2})$$

Spin coherent states

For spin coherent states formulas are a bit more complicated due to different group structure. The easiest systematic method for the calculation of expectation values of polynomials in operators $S_{x,y,z}$ in coherent state $|\vartheta^*, \varphi^*\rangle$ (2.26) is using generating function formalism (Arecchi *et al.*, 1972). For brevity let us denote a spin coherent state with a complex parameter $\tau := e^{i\varphi^*} \tan(\vartheta^*/2)$, i.e. $|\tau\rangle := |\vartheta^*, \varphi^*\rangle$. The following expression holds,

$$\langle\tau_1|S_+^a S_z^b S_-^c|\tau_2\rangle = \left\{ \left(\frac{\partial}{\partial\xi}\right)^a \left(\frac{\partial}{\partial\eta}\right)^b \left(\frac{\partial}{\partial\zeta}\right)^c X(\xi, \eta, \zeta) \right\}_{\xi=\eta=\zeta=0}, \quad (\text{B.3})$$

where

$$X(\xi, \eta, \zeta) := \langle\tau_1|e^{\xi S_+} e^{\eta S_z} e^{\zeta S_-}|\tau_2\rangle = \frac{\left\{e^{\eta/2} + e^{-\eta/2}(\tau_1^* + \xi)(\tau_2 + \zeta)\right\}^{2S}}{(1 + |\tau_1|^2)^S(1 + |\tau_2|^2)^S} e^{i(\varphi_1^* - \varphi_2^*)S}. \quad (\text{B.4})$$

This formula, together with the commutation relations, can be used to calculate some of the lowest powers

$$\begin{aligned} \langle\tau|S_z|\tau\rangle &= Sz \\ \langle\tau|S_z^2|\tau\rangle &= S^2 z^2 + \frac{S}{2}(1 - z^2) \\ \langle\tau|S_z^3|\tau\rangle &= S^3 z^3 + \frac{3S^2}{2}z(1 - z^2) - \frac{S}{2}z(1 - z^2) \\ \langle\tau|S_z^4|\tau\rangle &= S^4 z^4 + 3S^3 z^2(1 - z^2) + \frac{S^2}{4}(11z^4 - 14z^2 + 3) + \frac{S}{4}(-3z^4 + 4z^2 - 1), \end{aligned} \quad (\text{B.5})$$

where $z = \cos \vartheta^*$. The expressions for other spin operators S_y and S_x are obtained by replacing z with y or x on the right hand side, respectively. Some other useful expectation values are

$$\begin{aligned}\langle \tau | S_+ S_- | \tau \rangle &= S^2(1 - z^2) + \frac{S}{2}(1 + z)^2 \\ \langle \tau | S_- S_+ | \tau \rangle &= S^2(1 - z^2) + \frac{S}{2}(1 - z)^2.\end{aligned}\tag{B.6}$$

Bibliography

- ADAMOV, YURI, GORNYI, IGOR V., & MIRLIN, ALEXANDER D. 2003. Loschmidt echo and Lyapunov exponent in a quantum disordered system. *Phys. Rev. E*, **67**, 056217.
- AGARWAL, GIRISH S. 1981. Relation between atomic coherent-state representation, state multipoles, and generalized phase-space distributions. *Phys. Rev. A*, **24**, 2889–2896.
- ALICKI, ROBERT, MAKOWIEC, DANUTA, & MIKLASZEWSKI, WIESŁAW. 1996. Quantum Chaos in Terms of Entropy for a Periodically Kicked Top. *Phys. Rev. Lett.*, **77**, 838–841.
- ANDERSEN, MIKKEL F., KAPLAN, ARIEL, & DAVIDSON, NIR. 2003. Echo spectroscopy and quantum stability of trapped atoms. *Phys. Rev. Lett.*, **90**, 023001.
- ANGELO, RENATO M., VITIELLO, SILVIO A., DE AGUIAR, MARCUS A. M., & FURUYA, KYOKO. 2004. *Quantum linear mutual information and classical correlations in globally pure bipartite systems*. preprint quant-ph/0402091.
- ARAKI, HUZIHIO, & LIEB, ELLIOTT H. 1970. Entropy Inequalities. *Commun. Math. Phys.*, **18**, 160–170.
- ARECCHI, FORTUNATO T., COURTENS, ERIC, GILMORE, ROBERT, & THOMAS, HARRY. 1972. Atomic Coherent States in Quantum Optics. *Phys. Rev. A*, **6**, 2211–2237.
- BALLENTINE, LESLIE E., & ZIBIN, JAMES P. 1996. Classical state sensitivity from quantum mechanics. *Phys. Rev. A*, **54**, 3813–3819.
- BANDYOPADHYAY, JAYENDRA N., & LAKSHMINARAYAN, ARUL. 2002a. Entanglement production in coupled chaotic systems: Case of the kicked tops. *Phys. Rev. E*, **69**, 016201.
- BANDYOPADHYAY, JAYENDRA N., & LAKSHMINARAYAN, ARUL. 2002b. Testing Statistical Bounds on Entanglement Using Quantum Chaos. *Phys. Rev. Lett.*, **89**, 060402.
- BENEDICT, MIHALY G., & CZIRJAK, ATTILA. 1999. Wigner functions, squeezing properties, and slow decoherence of a mesoscopic superpositions of two-level atoms. *Phys. Rev. A*, **60**, 4034.
- BENENTI, GIULIANO, & CASATI, GIULIO. 2002. Quantum-classical correspondence in perturbed chaotic systems. *Phys. Rev. E*, **65**, 066205.
- BENENTI, GIULIANO, CASATI, GIULIO, MONTANGERO, SIMONE, & SHEPELYANSKY, DIMA L. 2002. Eigenstates of an operating quantum computer: hypersensitivity to static imperfection. *Eur. Phys. J. D*, **20**, 293–296.
- BENENTI, GIULIANO, CASATI, GIULIO, & VEBLE, GREGOR. 2003a. Decay of the classical Loschmidt echo in integrable systems. *Phys. Rev. E*, **68**, 036212.

- BENENTI, GIULIANO, CASATI, GIULIO, & VEBLE, GREGOR. 2003b. Stability of classical chaotic motion under a system's perturbations. *Phys. Rev. E*, **67**, 055202(R).
- BENENTI, GIULIANO, CASATI, GIULIO, & MONTANGERO, SIMONE. 2003c. Stability of quantum computation in the presence of imperfections. *Int. J. Mod. Phys. B*, **17**, 3932–3946.
- BERMAN, GENNADY P., & ZASLAVSKY, GEORGE M. 1978. Condition of stochasticity in quantum nonlinear systems. *Physica A*, **91**, 450–460.
- BERMAN, GENNADY P., BORGONOV, FAUSTO, IZRAILEV, FELIX M., & TSIFRINOVICH, VLADIMIR I. 2001. Delocalization border and onset of chaos in a model of quantum computation. *Phys. Rev. E*, **64**, 056226.
- BERMAN, GENNADY P., BORGONOV, FAUSTO, IZRAILEV, FELIX M., & TSIFRINOVICH, VLADIMIR I. 2002a. Avoiding quantum chaos in quantum computation. *Phys. Rev. E*, **65**, 015204(R).
- BERMAN, GENNADY P., BORGONOV, FAUSTO, CELARDO, GIUSEPPE L., IZRAILEV, FELIX M., & KAMENEV, DMITRY I. 2002b. Dynamical fidelity of a solid-state quantum computation. *Phys. Rev. E*, **66**, 056206.
- BERRY, MICHAEL V. 1977. Semi-classical mechanics in phase space: a study of Wigner's function. *Phil. Trans. R. Soc. A*, **287**, 237–271.
- BETTELLI, STEFANO. 2004. A quantitative model for the effective decoherence of a quantum computer with imperfect unitary operations. *Phys. Rev. A*, **69**, 042310.
- BOLTZMANN, LUDWIG. 1872. Weitere Studien über das Wärmegleichgewicht unter Gasmolekülen. *Sitzungsberichte der Akademie der Wissenschaften, Wien, II*, **66**, 275–370. [for an English translation see Brush (1966)].
- BOLTZMANN, LUDWIG. 1877. Über die Beziehung eines allgemeine mechanischen Satzes zum zweiten Hauptsatze der Warmetheorie. *Sitzungsberichte der Akademie der Wissenschaften, Wien, II*, **75**, 67–73. [for an English translation see Brush (1966)].
- BRAUN, D, HAAKE, FRITZ, & STRUNZ, WALTER T. 2001. Universality of decoherence. *Phys. Rev. Lett.*, **86**, 2913.
- BRAUN, PETR A., & SAVICHEV, V. I. 1996. The influence of higher-order anharmonic corrections to the energy spectrum on the evolution of quantum wavepackets. *J. Phys. B*, **29**, L329.
- BRESLIN, JOHN K., & MILBURN, GERARD J. 1999. Sensitivity to measurement errors in quantum kicked top. *Phys. Rev. A*, **59**, 1781–1787.
- BRUSH, STEPHEN G. 1966. *Kinetic Theory, Vol. 2, Irreversible processes*. Oxford: Pergamon Press.
- CALDERBANK, ROBERT A., & SHOR, PETER W. 1996. Good quantum error-correcting codes exist. *Phys. Rev. A*, **54**, 1098–1105.
- CASATI, GIULIO, CHIRIKOV, BORIS V., GUARNERI, ITALO, & SHEPELYANSKY, DIMA L. 1986. Dynamical Stability of Quantum "Chaotic" Motion in a Hydrogen Atom. *Phys. Rev. Lett.*, **56**, 2437–2440.

- CELARDO, GIUSEPPE L., PINEDA, CARLOS, & ŽNIDARIČ, MARKO. 2003. *Stability of the quantum Fourier transformation on the Ising quantum computer*. preprint quant-ph/0310163.
- CERCIGNANI, CARLO. 1998. *Ludwig Boltzmann: The Man Who Trusted Atoms*. Oxford: Oxford University Press.
- CERRUTI, NICHOLAS R., & TOMSOVIC, STEVEN. 2002. Sensitivity of Wave Field Evolution and Manifold Stability in Chaotic Systems. *Phys. Rev. Lett.*, **88**, 054103.
- CERRUTI, NICHOLAS R., & TOMSOVIC, STEVEN. 2003a. *Corrigendum: A Uniform Approximation for the Fidelity in Chaotic Systems*. *J. Phys. A*, **36**, 11915–11916.
- CERRUTI, NICHOLAS R., & TOMSOVIC, STEVEN. 2003b. A Uniform Approximation for the Fidelity in Chaotic Systems. *J. Phys. A*, **36**, 3451–3465.
- CHUANG, ISAAC L., LAFLAMME, RAYMOND, SHORE, PETER W., & ZUREK, WOJCIECH H. 1995. Quantum computers, factoring, and decoherence. *Science*, **270**, 1633–1635.
- COHEN, DORON. 1999. Quantum Dissipation due to the Interaction with Chaotic Degrees of Freedom and the Correspondence Principle. *Phys. Rev. Lett.*, **82**, 4951.
- COHEN, DORON. 2000. Chaos and energy spreading for time-dependent hamiltonians, and the various regimes in the theory of quantum dissipation. *Ann. Phys. (NY)*, **283**, 175–231.
- COHEN, DORON, & KOTTOS, TSAMPIKOS. 2000. Quantum-Mechanical Nonperturbative Response of Driven Chaotic Mesoscopic Systems. *Phys. Rev. Lett.*, **85**, 4839.
- COPPERSMITH, DON. 1994. *An Approximate Fourier Transform Useful in Quantum Factoring*. IBM Research Report RC 19642.
- CUCCHIETTI, FERDINANDO M., PASTAWSKI, HORACIO M., & WISNIACKI, DIEGO A. 2002a. Decoherence as decay of the Loschmidt echo in a Lorentz gas. *Phys. Rev. E*, **65**, 045206(R).
- CUCCHIETTI, FERNANDO M., LEWENKOPF, CAIO H., MUCCIOLO, EDUARDO R., PASTAWSKI, HORACIO M., & VALLEJOS, RAUL O. 2002b. Measuring the Lyapunov exponent using quantum mechanics. *Phys. Rev. E*, **65**, 046209.
- CUCCHIETTI, FERNANDO M., DALVIT, DIEGO A. R., PAZ, JUAN P., & ZUREK, WOJCIECH H. 2003a. Decoherence and the Loschmidt Echo. *Phys. Rev. Lett.*, **91**, 210403.
- CUCCHIETTI, FERNANDO M., PASTAWSKI, HORACIO M., & JALABERT, RODOLFO A. 2003b. *Universality of the Lyapunov regime for the Loschmidt echo*. preprint cond-mat/0307752.
- DEMKOWICZ-DOBZAŃSKI, RAFAŁ, & KUŚ, MAREK. 2004. *Global entangling properties of the coupled kicked tops*. preprint quant-ph/0403232.
- DOWLING, JONATHAN P., AGARWAL, GIRISH S., & SCHLEICH, WOLFGANG P. 1994. Wigner distribution of a general angular-momentum state: Application to a collection of two-level atoms. *Phys. Rev. A*, **49**, 4101–4109.
- ECKHARDT, BRUNO. 2003. Echoes in classical dynamical systems. *J. Phys. A*, **36**, 371–380.
- EKERT, ARTHUR, & JOSZA, RICHARD. 1996. Quantum computation and Shor’s factoring algorithm. *Rev. Mod. Phys.*, **68**, 733–753.

- EMERSON, JOSEPH, WEINSTEIN, YAAKOV S., LLOYD, SETH, & CORY, DAVID. 2002. Fidelity decay as an efficient indicator of quantum chaos. *Phys. Rev. Lett.*, **89**, 284102.
- FÖLDI, PETER, CZIRJAK, ATTILA, & BENEDICT, MIHALY G. 2001. Rapid and slow decoherence in conjunction with dissipation in a system of two-level atoms. *Phys. Rev. A*, **63**, 033807.
- FEINGOLD, MARIO, & PERES, ASHER. 1986. Distribution of matrix elements of chaotic systems. *Phys. Rev. A*, **34**, 591–595.
- FEINGOLD, MARIO, LEITNER, DAVID M., & PIRO, ORESTE. 1989. Semiclassical structure of Hamiltonians. *Phys. Rev. A*, **39**, 6507–6514.
- FEYNMAN, RICHARD P. 1982. Simulating Physics with Computers. *Int. J. Theor. Phys.*, **21**, 467–488.
- FISHMAN, SHMUEL, GREMPPEL, D R., & PRANGE, R E. 1982. Chaos, Quantum Recurrences, and Anderson Localization. *Phys. Rev. Lett.*, **49**, 509–512.
- FOX, RONALD F., & ELSTON, TIMOTHY C. 1994. Chaos and a quantum-classical correspondence in the kicked top. *Phys. Rev. E*, **50**, 2553–2563.
- FRAHM, KLAUS M., FLECKINGER, ROBERT, & SHEPELYANSKY, DIMA L. 2004. Quantum chaos and random matrix theory for fidelity decay in quantum computations with static imperfections. *Eur. Phys. J. D*, **29**, 139.
- FUJISAKI, HIROSHI, MIYADERA, TAKAYUKI, & TANAKA, ATUSHI. 2003. Dynamical aspects of quantum entanglement for weakly coupled kicked tops. *Phys. Rev. E*, **67**, 066201.
- GARDINER, SIMON A., CIRAC, IGNACIO J., & ZOLLER, PETER. 1997. Quantum Chaos in an Ion Trap: The Delta-Kicked Harmonic Oscillator. *Phys. Rev. Lett.*, **79**, 4790–4793.
- GARDINER, SIMON A., CIRAC, IGNACIO J., & ZOLLER, PETER. 1998. Erratum: Quantum Chaos in an Ion Trap: The Delta-Kicked Harmonic Oscillator. *Phys. Rev. Lett.*, **80**, 2968.
- GEA-BANACLOCHE, JULIO. 1998. Qubit-qubit interaction in quantum computers. *Phys. Rev. A*, **57**, R1–R4.
- GEA-BANACLOCHE, JULIO. 1999. Qubit-qubit interaction in quantum computers. II. Adder algorithm with diagonal and off-diagonal interactions. *Phys. Rev. A*, **60**, 185–193.
- GEA-BANACLOCHE, JULIO. 2000. Error correction for mutually interacting qubits. *Phys. Rev. A*, **62**, 062313.
- GEORGEOT, BERTRAND, & SHEPELYANSKY, DIMA L. 2000. Quantum chaos border for quantum computing. *Phys. Rev. E*, **62**, 3504–3507.
- GONG, JIANGBIN, & BRUMER, PAUL. 2003a. Chaos and quantum-classical correspondence via phase-space distribution functions. *Phys. Rev. A*, **68**, 062103.
- GONG, JIANGBIN, & BRUMER, PAUL. 2003b. Intrinsic decoherence dynamics in smooth Hamiltonian systems: Quantum-classical correspondence. *Phys. Rev. A*, **68**, 022101.
- GONG, JIANGBIN, & BRUMER, PAUL. 2003c. When is Quantum Decoherence Dynamics Classical? *Phys. Rev. Lett.*, **90**, 050420.

- GORIN, THOMAS, & SELIGMAN, THOMAS H. 2002. A random matrix approach to decoherence. *J. Opt. B*, **4**, S386–S392.
- GORIN, THOMAS, & SELIGMAN, THOMAS H. 2003. Decoherence in chaotic and integrable systems: a random matrix approach. *Phys. Lett. A*, **309**, 61.
- GORIN, THOMAS, PROSEN, TOMAŽ, & SELIGMAN, THOMAS H. 2004. A random matrix formulation of fidelity decay. *New J. Phys.*, **6**, 19.
- GREMPPEL, D R., PRANGE, R E., & FISHMAN, SHMUEL. 1984. Quantum dynamics of a nonintegrable system. *Phys. Rev. A*, **29**, 1639–1647.
- HAAKE, FRITZ. 1991. *Quantum Signatures of Chaos*. Berlin: Springer Verlag. [2nd enlarged Edition 2000].
- HAAKE, FRITZ. 2000. Can the kicked top be realized? *J. Mod. Opt.*, **47**, 2883–2890.
- HAAKE, FRITZ, KUŚ, MAREK, & SCHARF, RAINER. 1987. Classical and Quantum Chaos for a Kicked Top. *Z. Phys. B*, **65**, 381.
- HAHN, ERWIN L. 1950. Spin Echoes. *Phys. Rev.*, **80**, 580–594.
- HELLER, ERIC J. 1991. Wave packet Dynamics and Quantum Chaology. In: VOROS, A., ZINN-JUSTIN, J., & GIANNONI, M. J. (eds), *Chaos and Quantum Physics*. Proc. Les Houches Summer School, Session LII 1989. Amsterdam: North-Holland.
- HILLER, MORITZ, KOTTOS, TSAMPIKOS, COHEN, DORON, & GEISEL, THEO. 2004. Quantum Reversibility: Is there an Echo? *Phys. Rev. Lett.*, **92**, 010401.
- HORVAT, MARTIN, & PROSEN, TOMAŽ. 2003. Wigner function statistics in classically chaotic systems. *J. Phys. A*, **36**, 4015–4034.
- IOMIN, ALEXANDER. 2003. *Loschmidt echo for a chaotic oscillator*. preprint nlin.CD/0312018.
- IZRAILEV, FELIX M., & CASTAÑEDA-MENDOZA, A. 2004. *Entropy production and fidelity for quantum many-body systems with noise*. preprint quant-ph/0403097.
- JACQUOD, PHILIPPE. 2004. Semiclassical Time Evolution of the Reduced Density Matrix and Dynamically Assisted Generation of Entanglement for Bipartite Quantum Systems. *Phys. Rev. Lett.*, **92**, 150403.
- JACQUOD, PHILIPPE, SILVESTROV, PETER G., & BEENAKKER, CARLO W. J. 2001. Golden rule decay versus Lyapunov decay of the quantum Loschmidt echo. *Phys. Rev. E*, **64**, 055203(R).
- JACQUOD, PHILIPPE, ADAGIDELI, INANC, & BEENAKKER, CARLO W. J. 2002. Decay of the Loschmidt Echo for Quantum States with Sub-Planck-Scale Structures. *Phys. Rev. Lett.*, **89**, 154103.
- JACQUOD, PHILIPPE, ADAGIDELI, INANC, & BEENAKKER, CARLO W. J. 2003. Anomalous power law of quantum reversibility for classically regular systems. *Europhys. Lett.*, **61**, 729–735.
- JALABERT, RODOLFO A., & PASTAWSKI, HORACIO M. 2001. Environment-Independent Decoherence Rate in Classically Chaotic Systems. *Phys. Rev. Lett.*, **86**, 2490.

- JAYNES, EDWIN T., & CUMMINGS, FREDERICK W. 1963. Comparison of Quantum and Semi-classical Radiation Theory with Application to the Beam Maser. *Proc. IEEE*, **51**, 89–109.
- JORDAN, ANDREW, & SREDNICKI, MARK. 2001. *Sub-Planck Structure, Decoherence, and Many-Body Environments*. preprint quant-ph/0112139.
- JOZSA, RICHARD. 1994. Fidelity for mixed quantum states. *J. Mod. Opt.*, **41**(12), 2315–2323.
- KÜBLER, O., & ZEH, DIETER H. 1973. Dynamics of Quantum Correlations. *Ann. Phys. (N.Y.)*, **76**, 405–418.
- KAPLAN, LEV. 2002. Quantization ambiguity, ergodicity and semiclassics. *New J. Phys.*, **4**, 90.
- KARKUSZEWSKI, ZBYSZEK P., JARZYNSKI, CHRISTOPHER, & ZUREK, WOJCIECH H. 2002. Quantum Chaotic Environments, the Butterfly Effect, and Decoherence. *Phys. Rev. Lett.*, **89**, 170405.
- KIM, JI IL, NEMES, M. C., DE TOLEDO PIZA, ANTONIO F. R., & BORGES, H. E. 1996. Perturbative Expansion for Coherence Loss. *Phys. Rev. Lett.*, **77**, 207.
- KOLOVSKY, ANDREY R. 1994. Number of degrees of freedom for a thermostat. *Phys. Rev. E*, **50**, 3569–3576.
- LEBOWITZ, JOEL L. 1999. Microscopic Origins of Irreversible Macroscopic Behavior. *Physica A*, **263**, 516–527.
- LEICHTLE, CLEMENS, AVERBUKH, ILYA SH., & SCHLEICH, WOLFGANG P. 1996. Multilevel quantum beats: An analytical approach. *Phys. Rev. A*, **54**, 5299.
- LEVSTEIN, PATRICIA R., USAJ, GONZALO, & PASTAWSKI, HORACIO M. 1998. Attenuation of polarization echoes in nuclear magnetic resonance: A study of the emergence of dynamical irreversibility in many-body quantum systems. *J. Chem. Phys.*, **108**, 2718–2724.
- LOMBARDI, MAURICIO, & SELIGMAN, THOMAS H. 1993. Universal and nonuniversal statistical properties of levels and intensities for chaotic Rydberg molecules. *Phys. Rev. A*, **47**, 3571–3586.
- LOSCHMIDT, JOSEF. 1876. Über den Zustand des Wärmegleichgewichtes eines Systems von Körpern mit Rücksicht auf die Schwerkraft. *Sitzungsberichte der Akademie der Wissenschaften, Wien, II*, **73**, 128–142.
- MEHTA, MADAN L. 1991. *Random Matrices and the Statistical Theory of Spectra*. New York: Academic Press.
- MEYSTRE, PIERRE, & SARGENT III, MURRAY. 1990. *Elements of Quantum Optics*. Berlin: Springer.
- MILLER, PAUL A, & SARKAR, SARBEN. 1999. Signatures of chaos in the entanglement of two kicked tops. *Phys. Rev. E*, **60**, 1542–1550.
- MIQUEL, CÉSAR, PAZ, JUAN P., & PERAZZO, ROBERTO. 1996. Factoring in a dissipative quantum computer. *Phys. Rev. A*, **54**, 2605–2613.
- MIQUEL, CÉSAR, PAZ, JUAN P., & ZUREK, WOJCIECH H. 1997. Quantum Computation with Phase Drift Errors. *Phys. Rev. Lett.*, **78**, 3971.

- NIELSEN, MICHAEL A., & CHUANG, ISAAC L. 2001. *Quantum Computation and Quantum Information*. Cambridge: Cambridge University Press.
- PASTAWSKI, HORACIO M., LEVSTEIN, PATRICIA R., & USAJ, GONZALO. 1995. Quantum Dynamical Echoes in the Spin Diffusion in Mesoscopic Systems. *Phys. Rev. Lett.*, **75**, 4310–4313.
- PASTAWSKI, HORACIO M., LEVSTEIN, PATRICIA R., USAJ, GONZALO, RAYA, JESUS, & HIRSCHINGER, JÉRÔME. 2000. A nuclear magnetic resonance answer to the Boltzmann-Loschmidt controversy? *Physica A*, **283**, 166–170.
- PENROSE, ROGER. 1989. *The Emperor's New Mind*. Oxford: Oxford University Press.
- PERES, ASHER. 1984. Stability of quantum motion in chaotic and regular systems. *Phys. Rev. A*, **30**, 1610–1615. [see also book Peres (1995)].
- PERES, ASHER. 1995. *Quantum Theory: Concepts and methods*. Dordrecht: Kluwer.
- PROSEN, TOMAŽ. 1994. Statistical properties of matrix elements in a Hamilton system between integrability and chaos. *Ann. Phys.*, **235**, 115–164.
- PROSEN, TOMAŽ. 2002. General relation between quantum ergodicity and fidelity of quantum dynamics. *Phys. Rev. E*, **65**, 036208.
- PROSEN, TOMAŽ, & ROBNIK, MARKO. 1993. Distribution and fluctuation properties of transition probabilities in a system between integrability and chaos. *J. Phys. A*, **26**, L319–L326.
- PROSEN, TOMAŽ, & SELIGMAN, THOMAS H. 2002. Decoherence of spin echoes. *J. Phys. A*, **35**, 4707–4727.
- PROSEN, TOMAŽ, & ŽNIDARIČ, MARKO. 2001. Can quantum chaos enhance the stability of quantum computation? *J. Phys. A*, **34**, L681–L687.
- PROSEN, TOMAŽ, & ŽNIDARIČ, MARKO. 2002. Stability of quantum motion and correlation decay. *J. Phys. A*, **35**, 1455–1481.
- PROSEN, TOMAŽ, & ŽNIDARIČ, MARKO. 2003a. <http://chaos.fiz.uni-lj.si/papers/freeze>.
- PROSEN, TOMAŽ, & ŽNIDARIČ, MARKO. 2003b. Quantum freeze of fidelity decay for a class of integrable dynamics. *New J. Phys.*, **5**, 109.
- PROSEN, TOMAŽ, & ŽNIDARIČ, MARKO. 2004. *Quantum freeze of fidelity decay for chaotic dynamics*. preprint quant-ph/0401142.
- PROSEN, TOMAŽ, SELIGMAN, THOMAS H., & ŽNIDARIČ, MARKO. 2003a. Estimation of purity in terms of correlation functions. *Phys. Rev. A*, **67**, 062108.
- PROSEN, TOMAŽ, SELIGMAN, THOMAS H., & ŽNIDARIČ, MARKO. 2003b. Evolution of entanglement under echo dynamics. *Phys. Rev. A*, **67**, 042112.
- PROSEN, TOMAŽ, SELIGMAN, THOMAS H., & ŽNIDARIČ, MARKO. 2003c. Theory of quantum Loschmidt echoes. *Prog. Theor. Phys. Suppl.*, **150**, 200–228.
- RHIM, WON-KYU, PINES, ALEXANDER, & WAUGH, JOHN S. 1970. Violation of the Spin-Temperature Hypothesis. *Phys. Rev. Lett.*, **25**, 218–220.

- ROSSINI, DAVIDE, BENENTI, GIULIANO, & CASATI, GIULIO. 2003. *Entanglement Echoes in Quantum Computation*. preprint quant-ph/0309146.
- SANKARANARAYANAN, R., & LAKSHMINARAYAN, ARUL. 2003. Recurrence of fidelity in nearly integrable systems. *Phys. Rev. E*, **68**, 036216.
- SCHÄFER, RUDI, GORIN, THOMAS, SELIGMAN, THOMAS H., & STÖCKMANN, HANS-JÜRGEN. 2003. Correlation function of scattering matrix elements in microwave cavities with strong absorption. *J. Phys. A*, **36**, 3289–3302. *Also private communication*.
- SCHACK, RÜDIGER, & CAVES, CARLTON M. 1992. *Information and Entropy in the Baker's Map*. *Phys. Rev. Lett.*, **69**, 3413.
- SCHACK, RÜDIGER, & CAVES, CARLTON M. 1993. *Hypersensitivity to Perturbations in the Quantum Baker's Map*. *Phys. Rev. Lett.*, **71**, 525.
- SCHACK, RÜDIGER, & CAVES, CARLTON M. 1996. *Information-theoretic characterization of quantum chaos*. *Phys. Rev. E*, **53**, 3257–3270.
- SCHLUNK, SOPHIE, D'ARCY, MICHAEL B., GARDINER, SIMON A., CASSETTARI, DONATELLA, GODUN, RACHEL M., & SUMMY, GIL S. 2003. *Signatures of Quantum Stability in a Classically Chaotic System*. *Phys. Rev. Lett.*, **90**, 054101.
- SCOTT, ANDREW J., & CAVES, CARLTON M. 2003. *Entangling power of the quantum baker's map*. *J. Phys. A*, **36**, 9553.
- SHACK, RUDIGER, D'ARIANO, MAURO G., & CAVES, CARLTON M. 1994. *Hypersensitivity to perturbations in the quantum kicked top*. *Phys. Rev. E*, **50**, 972–987.
- SHEPELYANSKY, DIMA L. 1983. *Some statistical properties of simple classically stochastic quantum systems*. *Physica D*, **8**, 208–222.
- SHOR, PETER W. 1994. *Algorithms for quantum computation: discrete logarithms and factoring*. Pages 124–134 of: *Proc. 35th Symp. on Foundations of Computer Science*.
- SILVESTROV, PETER G., TWORZYDŁO, JAKUB, & BEENAKKER, CARLO W. J. 2003. *Hypersensitivity to perturbations of quantum-chaotic wave-packet dynamics*. *Phys. Rev. E*, **67**, 025204(R).
- SONG, PIL HUN, & SHEPELYANSKY, DIMA L. 2001. *Quantum computing of quantum chaos and imperfection effects*. *Phys. Rev. Lett.*, **86**, 2162.
- STÖCKMANN, HANS-JÜRGEN. 1999. *Quantum chaos: an introduction*. *Cambridge: Cambridge University Press*.
- STEANE, ANDREW. 1996a. *Error correcting codes in quantum theory*. *Phys. Rev. Lett.*, **77**, 793–797.
- STEANE, ANDREW. 1996b. *Multiple particle interference and quantum error correction*. *Phil. Trans. R. Soc. A*, **452**, 2551.
- STEANE, ANDREW. 1998. *Quantum Computing*. *Rep. Prog. Phys.*, **61**, 117–173.
- STRUNZ, WALTER T., & HAAKE, FRITZ. 2003. *Decoherence scenarios from microscopic to macroscopic superpositions*. *Phys. Rev. A*, **67**, 022102.

- STRUNZ, WALTER T., HAAKE, FRITZ, & BRAUN, DANIEL. 2003. *Universality of decoherence for macroscopic quantum superpositions*. Phys. Rev. A, **67**, 022101.
- TANAKA, ATUSHI, FUJISAKI, HIROSHI, & MIYADERA, TAKAYUKI. 2002. *Saturation of the production of quantum entanglement between weakly coupled mapping systems in a strongly chaotic region*. Phys. Rev. E, **66**, 045201(R).
- TAVIS, MICHAEL, & CUMMINGS, FREDERICK W. 1968. *Exact Solution for an N-Molecule-Radiation-Field Hamiltonian*. Phys. Rev., **170**, 379–384.
- TEGMARK, MAX, & WHEELER, JOHN ARCHIBALD. 2001. *100 Years of Quantum Mysteries*. Sci. Am., **284**(2), 68–75.
- TERRANELO, MARCELLO, & SHEPELYANSKY, DIMA L. 2003. *Imperfection effects for multiple application of the quantum wavelet transform*. Phys. Rev. Lett., **90**, 257902.
- THOMPSON, WILLIAM. 1874. *The Kinetic Theory of the Dissipation of Energy*. Proceedings of the Royal Society of Edinburgh, **8**, 325–334. [reprinted in Brush (1966)].
- TIAN, LIN, & LLOYD, SETH. 2000. *Resonant cancellation of off-resonant effects in a multilevel qubit*. Phys. Rev. A, **62**, 050301.
- UHLMANN, ARMIN. 1976. *The "transition probability" in the state space of A^* -algebra*. Rep. Math. Phys., **9**, 273–279.
- USAJ, GONZALO, PASTAWSKI, HORACIO M., & LEVSTEIN, PATRICIA R. 1998. *Gaussian to Exponential Crossover in the Attenuation of Polarization Echoes in NMR*. Mol. Phys., **95**, 1229.
- VANÍČEK, JIŘÍ, & HELLER, ERIC J. 2003. *Semiclassical evaluation of quantum fidelity*. Phys. Rev. E, **68**, 056208.
- VEBLE, GREGOR, & PROSEN, TOMAŽ. 2004. *Faster Than Lyapunov decays of the Classical Loschmidt Echo*. Phys. Rev. Lett., **92**, 034101.
- WANG, WEN-GE, & LI, BAOWEN. 2002. *Crossover of quantum Loschmidt echo from golden-rule decay to perturbation-independent decay*. Phys. Rev. E, **66**, 056208.
- WANG, WEN-GE, CASATI, GIULIO, & LI, BAOWEN. 2004. *Stability of quantum motion: Beyond Fermi-golden-rule and Lyapunov decay*. Phys. Rev. E, **69**, 025201(R).
- WEHRL, ALFRED. 1978. *General properties of entropy*. Rev. Mod. Phys., **50**, 221–260.
- WEINSTEIN, YAAKOV S., LLOYD, SETH, & TSALLIS, CONSTANTINO. 2002a. *Border between Regular and Chaotic Quantum Dynamics*. Phys. Rev. Lett., **89**, 214101.
- WEINSTEIN, YAAKOV S., LLOYD, SETH, EMERSON, JOSEPH, & CORY, DAVID G. 2002b. *Experimental Implementation of the Quantum Baker's Map*. Phys. Rev. Lett., **89**, 157902.
- WEINSTEIN, YAAKOV S., EMERSON, JOSEPH V., LLOYD, SETH, & CORY, DAVID G. 2002c. *Fidelity Decay Saturation Level for Initial Eigenstates*. preprint quant-ph/0210063.
- WILKINSON, MICHAEL. 1987. *A semiclassical sum-rule for matrix elements of classically chaotic systems*. J. Phys. A, **20**, 2415–2423.

- WISNIACKI, DIEGO A. 2003. *Short time decay of the Loschmidt echo*. Phys. Rev. E, **67**, 016205.
- WISNIACKI, DIEGO A., & COHEN, DORON. 2002. *Quantum irreversibility, perturbation independent decay, and the parametric theory of the local density of states*. Phys. Rev. E, **66**, 046209.
- WISNIACKI, DIEGO A., VERGINI, EDUARDO G., PASTAWSKI, HORACIO M., & CUCCHIETTI, FERNANDO M. 2002. *Sensitivity to perturbations in a quantum chaotic billiard*. Phys. Rev. E, **65**, 055206(R).
- ZHANG, SHANMIN, MEIER, BEAT H., & ERNST, RICHARD R. 1992. *Polarization echoes in NMR*. Phys. Rev. Lett, **69**, 2149–2151.
- ZUREK, WOJCIECH H. 1991. *Decoherence and the transition from quantum to classical*. Phys. Today, **44**(10), 36–44.
- ŽNIDARIČ, MARKO, & PROSEN, TOMAŽ. 2003. *Fidelity and purity decay in weakly coupled composite systems*. J. Phys. A, **36**, 2463–2481.